

**Enantiomere Erkennungsmechanismen von Cyclodextrinen: Ein NMR spektroskopischer und gaschromatographischer Ansatz zur Evaluierung der Rolle der Kavität bei enantioselektiven Wechselwirkungen. Anwendung von „Acyclodextrinen“ in Enantiodiskriminierungsexperimenten**

**Enantiorecognition mechanism of cyclodextrins: an NMR spectroscopic and gas-chromatographic approach to evaluate the role of the cavity in the enantioselective interactions. Applications of “acyclodextrins” in enantiodiscrimination experiments**

DISSERTATION

der Fakultät für Chemie und Pharmazie  
der Eberhard-Karls-Universität Tübingen  
zur Erlangung des Grades eines Doktors  
der Naturwissenschaften

2006

vorgelegt von  
GIUSEPPE SICOLI

Tag der mündlichen Prüfung:

26. Januar 2006

Dekan:

Prof. Dr. S. Laufer

1. Berichterstatter:

Prof. Dr. V. Schurig

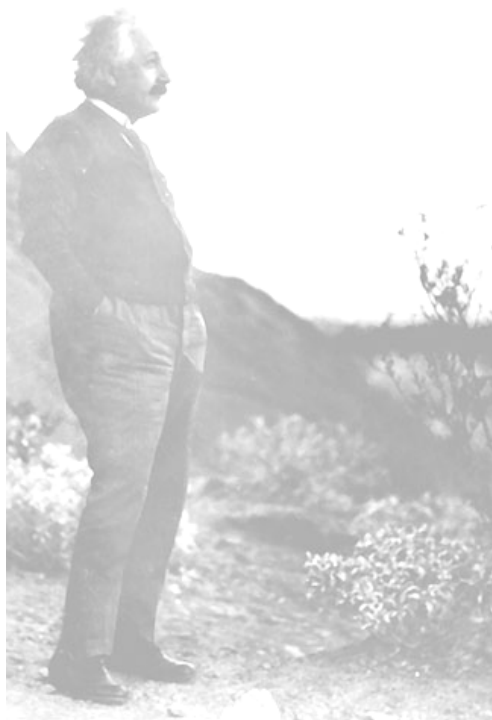
2. Berichterstatter:

Prof. Dr. K. Albert

3. Berichterstatter:

Prof. Dr. W. Lindner, Wien

Die vorliegende Arbeit wurde unter der Leitung von Prof. Dr. Volker Schurig im Zeitraum von November 2002 bis November 2005 am Institut für Organische Chemie der Eberhard-Karls-Universität Tübingen durchgeführt.



*What I see in Nature is a magnificent structure that we can comprehend only very imperfectly, and that must fill a thinking person with a feeling of humility. This is a genuinely religious feeling that has nothing to do with mysticism.*

Albert Einstein (1879-1955)



I wish to thank my supervisor Prof. Dr. Volker Schurig for the extremely interesting discussions about the fascinating world of chirality. I would like to thank all my colleagues for their continuous assistance.

I also wish to thank the “Graduiertenkolleg – Chemie in Interphasen” for the financial support of my Ph. D.



## Index





Index.....	I
Abbreviations.....	VII
Summary.....	1
Introduction.....	7
<b>1. Enantiorecognition mechanism by cyclic and acyclic dextrins: an overview.....</b>	<b>13</b>
1.1. Enantiodiscrimination in solution.....	15
1.2. NMR spectroscopic and CE studies of enantiorecognition.....	15
1.3. Computational studies of cyclodextrins and their derivatives.....	18
1.4 Ability of acyclic oligosaccharides to form complexes and their use for chiral separation.....	20
1.5. Enantioselective gas chromatography.....	29
1.5.1. CSPs based on amino acid derivatives.....	30
1.5.2. CSPs based on cyclodextrin derivatives.....	30
1.6. Enantioseparation of amino acid derivatives, saturated hydrocarbons, halogenomethanes and chlorinated/fluorinated ethers (inhalation anaesthetics).....	32
1.7. Enantiorecognition mechanism in gas chromatography involving modified cyclodextrins.....	37
<b>2. Results and discussion; Part I: Synthesis and characterization of cyclic and acyclic dextrin derivatives.....</b>	<b>39</b>
2.1. Introduction.....	41
2.2. Linear dextrins derived from cyclodextrins.....	42
2.3. Synthesis and characterization of acetyl/TBDMS cyclic and acyclic dextrins by NMR spectroscopy.....	43
2.3.1. Heptakis(2,3-di- <i>O</i> -acetyl-6- <i>O</i> - <i>tert</i> -butyldimethylsilyl)- $\beta$ -cyclodextrin <b>5</b> .....	46
2.3.2. Heptakis[(2,3-di- <i>O</i> ,4''- <i>O</i> )-acetyl-(1'- <i>O</i> ,6- <i>O</i> )- <i>tert</i> -butyldimethylsilyl]-maltoheptaose ( <b>10</b> ).....	49
2.3.3. Octakis[(2,3-di- <i>O</i> ,4''- <i>O</i> )-acetyl-(1'- <i>O</i> ,6- <i>O</i> - <i>tert</i> -butyldimethylsilyl)]maltooctaose ( <b>12</b> ).....	53
2.3.4. Tris[(2,3-di- <i>O</i> ,4''- <i>O</i> )-acetyl-(1'- <i>O</i> ,6- <i>O</i> )- <i>tert</i> -butyldimethylsilyl]-maltotriose ( <b>14</b> ).....	53
2.3.5. (2,3,4-tri- <i>O</i> -acetyl-1,6-di- <i>O</i> - <i>tert</i> -butyldimethylsilyl)- <i>D</i> -glucose ( <b>16</b> ) and (2,3,4-tri- <i>O</i> -acetyl-1,6-di- <i>O</i> - <i>tert</i> -butyldimethylsilyl)- <i>L</i> -glucose ( <b>18</b> ).....	54
2.4. Synthesis of per- <i>O</i> -methyl- <i>D</i> -maltoheptaose ( <b>19</b> ).....	55

2.5. Synthesis of <i>D</i> -maltoheptaose bonded to a polydimethylsiloxane <i>via</i> an undecenyl spacer.....	57
2.6. Synthesis of acyclic ‘Lipodex E’ ( <b>28</b> ).....	60
2.7. Molecular modeling analysis.....	62
<b>3. Results and discussion; Part II: Enantiorecognition by NMR spectroscopy in solution</b> .....	65
3.1. Introduction.....	67
3.2. Enantiodiscrimination of halogenated compounds.....	68
3.2.1. Enantiodiscrimination of ‘compound B’ by CD 7 ( <b>5</b> ).....	71
3.3. Preliminary study of ‘acyclodextrins’ in solution.....	85
<b>4. Results and discussion; Part III: Enantioseparation by gas chromatography</b> .....	91
4.1. Introduction.....	93
4.2. Enantioseparation of halogenated anaesthetics and ‘compound B’.....	93
4.3. Enantioseparation of $\alpha$ -amino acid derivatives.....	96
4.4. Further enantioseparation of various derivatized and underivatized compounds.....	98
4.5. How does the degree of oligomerization in acyclic dextrins affect the enantioselectivity.....	108
4.6. Preliminary study on acyclic dextrins with different derivatization patterns.....	113
4.7. Enantioseparation of saturated aliphatic hydrocarbons.....	118
4.8. Thermodynamic data obtained from retention increment <i>R'</i> analysis.....	122
<b>Conclusions</b> .....	125
<b>Experimental section</b> .....	131
Materials and Methods.....	133
Heptakis(2,3-di- <i>O</i> -acetyl-6- <i>O</i> - <i>tert</i> -butyldimethylsilyl)- $\beta$ -cyclodextrin ( <b>5</b> ).....	134
Hexakis(2,3-di- <i>O</i> -acetyl-6- <i>O</i> - <i>tert</i> -butyldimethylsilyl)- $\alpha$ -cyclodextrin ( <b>4</b> ).....	134
Octakis(2,3-di- <i>O</i> -acetyl-6- <i>O</i> - <i>tert</i> -butyldimethylsilyl)- $\gamma$ -cyclodextrin ( <b>6</b> ).....	134
Heptakis[(1'- <i>O</i> ,6- <i>O</i> )- <i>tert</i> -butyldimethylsilyl]-maltoheptaose ( <b>9</b> ).....	135
Heptakis[(2,3-di- <i>O</i> ,4''- <i>O</i> )-acetyl-(1'- <i>O</i> ,6- <i>O</i> )- <i>tert</i> -butyldimethylsilyl]-maltoheptaose ( <b>10</b> ).....	135
Octakis[(1'- <i>O</i> ,6- <i>O</i> )- <i>tert</i> -butyldimethylsilyl]-maltooctaose ( <b>11</b> ).....	136
Octakis[(2,3-di- <i>O</i> ,4''- <i>O</i> )-acetyl-(1'- <i>O</i> ,6- <i>O</i> )- <i>tert</i> -butyldimethylsilyl]-maltooctaose ( <b>12</b> ).....	136

Tris[(1'- <i>O</i> ,6- <i>O</i> )- <i>tert</i> -butyldimethylsilyl]-maltotriose ( <b>13</b> ).....	137
Tris[(2,3-di- <i>O</i> ,4''- <i>O</i> )-acetyl-(1'- <i>O</i> ,6- <i>O</i> )- <i>tert</i> -butyldimethylsilyl]-maltotriose ( <b>14</b> ).....	137
1,6-di- <i>O</i> - <i>tert</i> -butyldimethylsilyl- <i>D</i> -glucose ( <b>15</b> ).....	137
(2,3,4-tri- <i>O</i> -acetyl-1,6-di- <i>O</i> - <i>tert</i> -butyldimethylsilyl)- <i>D</i> -glucose ( <b>16</b> ).....	138
1,6-di- <i>O</i> - <i>tert</i> -butyldimethylsilyl- <i>L</i> -glucose ( <b>17</b> ).....	138
(2,3,4-tri- <i>O</i> -acetyl-1,6-di- <i>O</i> - <i>tert</i> -butyldimethylsilyl)- <i>L</i> -glucose ( <b>18</b> ).....	138
Per- <i>O</i> -methyl- <i>D</i> -maltoheptaose ( <b>19</b> ).....	139
<i>N</i> -(1-methanesulfonyl)-benzotriazole ( <b>21</b> ).....	139
<i>N</i> -undecenoylbenzotriazole ( <b>23</b> ).....	139
10-Undecenoylhydrazide ( <b>24</b> ).....	140
<i>D</i> -maltoheptaosyl-10-undecenoylhydrazone ( <b>25</b> ).....	140
Per- <i>O</i> -methyl- <i>D</i> -maltoheptaosyl-10-undecenoylhydrazone ( <b>26</b> ).....	140
Chemical bonding of per- <i>O</i> -methyl- <i>D</i> -maltoheptaosyl-10-undecenoylhydrazone <b>26</b> to hydridomethyldimethylsiloxane copolymer.....	141
Octakis[(3- <i>O</i> ,4''- <i>O</i> )-butanoyl-(1'- <i>O</i> ,2,6-di- <i>O</i> )- <i>n</i> -pentyl]-maltooctaose ( <b>28</b> ).....	141
<b>Appendix</b> .....	143
<b>References</b> .....	159



**Abbreviations and Symbols**

Ac	Acetyl
AGT	Aminoglutethimide
BR	Bilirubin-IX
CCC	Couter Current Chromatography
CD	Cyclodextrin
CE	Capillary Electrophoresis
CSA	Chiral Solvating Agent
CSP	Chiral Stationary Phase
CZE	Capillary Zone Electrophoresis
DMF	Dimethylformamide
DMSO	Dimethylsulfoxide
DOSY	Diffusion Ordered Spectroscopy
ECD	Electron Capture Detection
ESI	Electro Spray Ionization
GC	Gas Chromatography
HPLC	High Performance Liquid Chromatography
HFB	Heptafluorobutanoyl
GC	Gas Chromatography
gCOSY	gradient-CORrelation Spectroscopy
gHMQC	gradient-Heteronuclear Multiple Quantum Coherence
gHMBC	gradient-Heteronuclear Multiple Bond Coherence
gHSQC	gradient-Heteronuclear Single Quantum Correlation
i.d.	Inner diameter
ISC	Induced Shift Complexation
ITP	Isotachopheresis
Lipodex E	Octakis(3- <i>O</i> -butanoyl-2,6-di- <i>O</i> - <i>n</i> -pentyl)- $\gamma$ -cyclodextrin
MM-FF	Merck Molecular-Force Field
MS	Mass Spectrometry
NMR	Nuclear Magnetic Resonance
NOE	Nuclear Overhauser Effect
PFP	Pentafluoropropionyl
PGSE	Pulsed Gradient Spin Echo
ROESY	Rotating-frame Overhauser Enhancement Spectroscopy

*Abbreviations*

SFC	Supercritical Fluid Chromatography
TBDMSCI	<i>tert</i> -Butyldimethylsilyl chloride
TFA	Trifluoroacetyl
TLC	Thin-Layer Chromatography
TOCSY	TOTAL Correlation Spectroscopy
$R'$	Retention increment
$k$	Retention factor
$\alpha$	Enantioseparation factor
$R_s$	Resolution

*amino acids abbreviations*

Ala	Alanine
Abu	2-Aminobutanoic acid
Asp	Aspartic acid
Isoleu	Isoleucine
Met	Methionine
Norval	Norvaline
Pro	Proline
Ser	Serine
<sup>t</sup> BuLeu	<i>tert</i> -Butyl leucine
Thr	Threonine
Val	Valine

## Summary





*On the role of outside vs. inside interactions for the enantiorecognition by cyclodextrins: conventional mechanism and novel insights*

Native and derivatized cyclodextrins represent versatile chiral selectors for the separation of enantiomers by chromatographic and electromigratory methods. However, the underlying mechanisms of enantiorecognition are still poorly understood. While the presence of a cavity and inclusion therein is often thought to be of prime importance for enantioseparation of racemic analytes it is conceivable that this effect can be complemented, or even overridden, by interaction of analytes with the external surface of cyclodextrins. To probe the importance of the molecular inclusion mechanism, linear dextrin derivatives - devoid of a true cavity (figure S1) - have been synthesized and compared with their cyclic analogues with regard to their properties as chiral selectors for enantioselective gas chromatography.

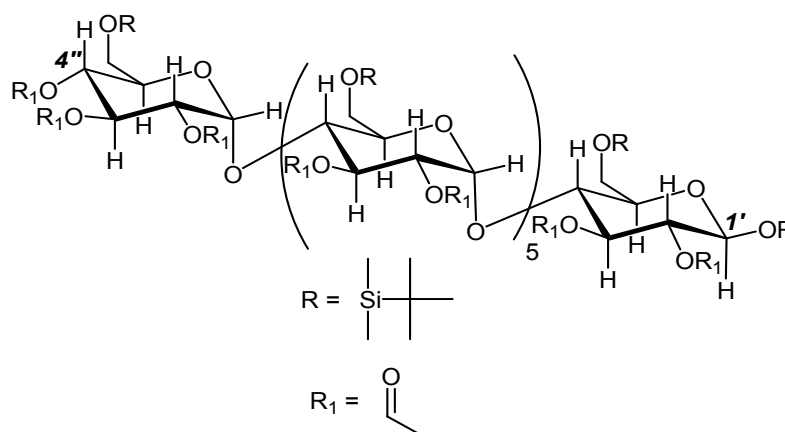


**Figure S1.** Structure of heptakis[(2,3-di-*O*,4''-*O*)-acetyl-(1'-*O*,6-*O*)-*tert*-butyldimethylsilyl]-maltoheptaose.

Via the comparison of cyclic and acyclic dextrins (cyclodextrins *versus* ‘acyclodextrins’) it is demonstrated that the existence of a cavity is not a prerequisite to enantiorecognition. Thus, the well known gas-chromatographic selector heptakis(2,3-di-*O*-acetyl-6-*O*-*tert*-butyldimethylsilyl)- $\beta$ -cyclodextrin has been compared with the corresponding linear derivative heptakis[(2,3-di-*O*,4''-*O*)-acetyl-(1'-*O*,6-*O*)-*tert*-butyldimethylsilyl]-maltoheptaose and a complementary enantioseparation ability for  $\alpha$ -amino acid derivatives (*N*-trifluoroacetyl-*O*-methyl/ethyl-esters) and racemic halogenated compounds was observed. In several cases, the acyclic chiral stationary phase (CSP) was even more enantioselective than the cyclic CSP. While it is conceivable that the maltoheptaose derivative could still form a “pseudo cavity” which is responsible for the observed enantiorecognition, this is certainly not

Summary

the case with the maltotriose and glucose derivatives (figure S2), these molecules being too small to be able to form a cavity or a turn of a helical conformation.

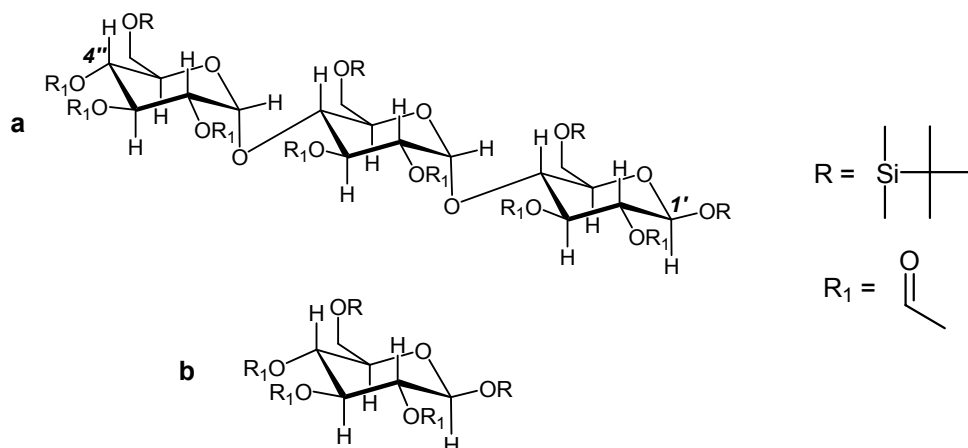


**Figure S2.** Structure of tris[(2,3-di-*O*,4''-*O*)-(1'-*O*,6-*O*)-*tert*-butyldimethylsilylacetyl]-maltotriose (a) and (2,3,4-tri-*O*-acetyl-1,6-di-*O*-*tert*-butyldimethylsilyl)-*D*-glucose (b).

Surprisingly, even on the single building block comprising cyclodextrins and linear dextrans, *i.e.*,  $\alpha$ -2,3,4-tri-*O*-acetyl-1,6-di-*O*-*tert*-butyldimethylsilyl-*D*-glucose, the enantiomers of some  $\alpha$ -amino acid derivatives and racemic halogenated compounds could be separated by gas chromatography. Whereas cyclodextrins are available only in the *D* form, the linear counterparts can readily be synthesized in the *D* and *L* form, which is of interest for peak inversion scenarios in the chromatographic analysis of non-racemic mixtures. For those gas-chromatographic separations obtained on the single glucose units (*D* and *L*) the influence of the cavity must obviously be excluded in explaining the enantioselective process.

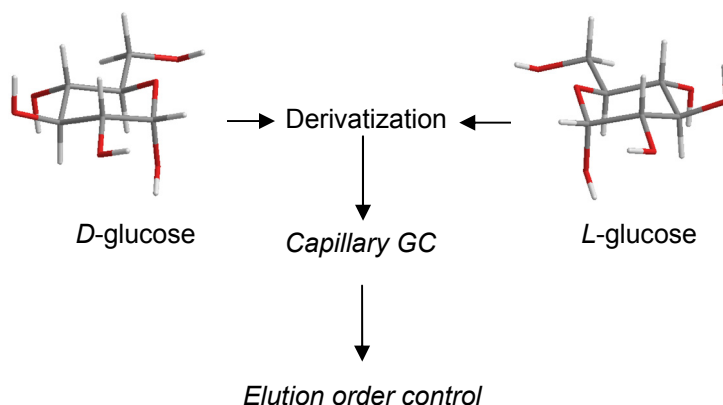


**Figure S3.** Schematic representation of a versatile application of *D*- and *L*-glucose derivatives for enantioselective gas chromatography.

These unexpected enantioseparations prove the existence of enantioselective interactions with the outer surface of the selector. As mentioned before, the ready access to unnatural *L*-maltooligomers represents a novel and important tool in the field of enantioselective gas chromatography due to the possibility to tune the elution order of the enantiomers (figure S3). Subtle changes both in the structure of the racemic analytes and in the nature of the functional groups of the modified cyclodextrins affected significantly the enantioselective ability of the selectors. Thus, the common idea to rationalize the enantioselective recognition through a general mechanism by cyclodextrins must be revisited.

#### *Enantioselective recognition mechanism by NMR spectroscopic studies*

The controversial role of the inclusion phenomenon by cyclodextrins has also been verified by NMR studies in solution, where investigations were focused on the enantioselective recognition process and on the conformation of the derivatized chiral selector. In this respect, derivatized cyclodextrins differ strongly from the native macrocycles. Due to the distortion of the glucose units and their tilting across the glycosidic linkages, the conformation of modified  $\alpha$ -,  $\beta$ - and  $\gamma$ -cyclodextrin selectors are often significantly different from a classical torus shaped structure and the diameter of the cavity is markedly affected by derivatization.

Thus, the functional groups on the two rims of cyclodextrins play an important role in the complexation step as demonstrated in this work for the enantiodiscrimination of 'compound B' by heptakis(2,3-di-*O*-acetyl-6-*O*-*tert*-butyldimethylsilyl)- $\beta$ -cyclodextrin (figure S4).

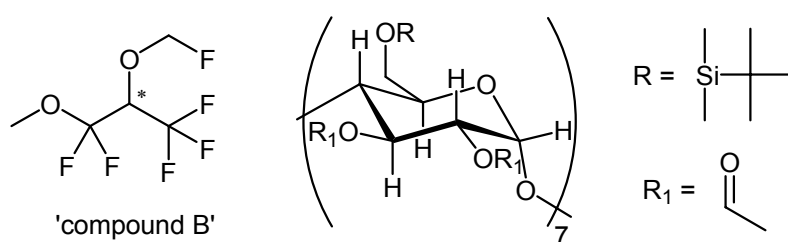


**Figure S4.** Structure of 1,1,1,3,3-pentafluoro-2-(fluoromethoxy)-3-methoxypropane ('compound B') and heptakis(2,3-di-*O*-acetyl-6-*O*-*tert*-butyldimethylsilyl)- $\beta$ -cyclodextrin.

According to the NMR studies, the chiral diether is juxtaposed preferentially in the chiral environment formed by two adjacent glucose units and this is indeed a suitable region responsible for enantioselective interactions.

*The yet unchallenged role of the cavity in the enantioseparation process of racemic hydrocarbons*

In the case of apolar racemic analytes such as saturated aliphatic hydrocarbons, the inclusion process still appears to be the driving force for enantioselectivity on the well established selector Chirasil- $\beta$ -Dex, since no enantioseparation is observed on the acyclic counterpart of linear permethylated maltoheptaose (both as the diluted and supported CSP).

However, in many cases, e.g. for the per-*O*-methylated  $\beta$ -cyclodextrin, the role of the cavity is not very well understood. Thus, the application of linear selectors as novel CSP represents a comparable tool to determine whether an inclusion phenomenon is present or absent with the established cyclic selectors.

Furthermore, the size of the cavity cannot be the sole parameter in rationalizing the enantioselectivity because the nature of the functional groups on the two rims plays a key role for the overall structure by modifying the cavity size and by directing the enantioselectivity towards the external surface of the macrocycles.

## Introduction



## History of cyclodextrins

Cyclodextrins (CDs) are cyclic oligosaccharides consisting of six ( $\alpha$ -cyclodextrin), seven ( $\beta$ -cyclodextrin), eight ( $\gamma$ -cyclodextrin) or more glucopyranose units linked by  $\alpha$ -(1,4) bonds. They are also known as cycloamyloses, cyclomaltoheptaose (i.e.,  $\beta$ -CD), and Schardinger dextrins.<sup>1a</sup> CDs are formed by an intramolecular transglycosylation reaction via degradation of starch by the cyclodextrin glucotransferase (CGTase) enzyme.<sup>2</sup> In figure 1 a cartoon resembling a “doughnut  $\beta$ -cyclodextrin” is shown. CDs were discovered in 1891, when during a *Bacillus amylobacter* digestion of starch, in addition to reducing dextrans, “...there is formed in very small amount (about 3 g/kg of starch) a carbohydrate which forms beautiful radiate crystals after a few weeks in the alcohol from which the dextrans were precipitated... having the composition represented by a multiple of the formula  $(C_6H_{10}O_3) \cdot 3H_2O$ ...”<sup>1a</sup> According to subsequent studies, Villiers in 1891 probably used impure cultures and the cyclodextrins were produced by contamination with *Bacillus macerans*. Villiers named his crystalline product ‘cellulosine’. In 1903, Schardinger was able to isolate two crystalline products, dextrans A and B, which were described with regard to their lack of reducing power.<sup>1b</sup>

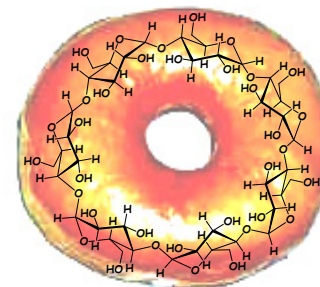


**Figure 1.** ‘Doughnut cyclodextrin’ where a classic cavity is shown.

In 1904,<sup>1c</sup> Schardinger isolated a new organism (isolated strains of bacteria) which was capable to produce acetone and ethanol from sugar and starch-containing plant material. In 1911,<sup>1d</sup> he described that this strain, called *Bacillus macerans*, also produces large amounts of crystalline dextrans (25-30%) from starch.<sup>2</sup> Schardinger named his crystalline products ‘crystallised dextrin  $\alpha$ ’ and ‘crystallised dextrin  $\beta$ ’. It took until 1935 before  $\gamma$ -dextrin was isolated. Several fractionation schemes for the production of cyclodextrins were also developed.<sup>3</sup> At that time the structures of these compounds were still uncertain, but in 1942 the structures of  $\alpha$  and  $\beta$ -cyclodextrin were determined by X-ray crystallography.<sup>4</sup> In 1948, the X-ray structure of  $\gamma$ -cyclodextrin was established and it was recognized that CDs can form inclusion complexes.<sup>5</sup> In 1961, evidence for the existence of  $\delta$ -,  $\zeta$ -,  $\xi$ - and even  $\eta$ -cyclodextrin (9-12 glucose units) was provided.<sup>6</sup> From the X-ray structural analysis cyclodextrins show a truncated cone shaped structure where the secondary hydroxyl groups (on C<sub>2</sub> and C<sub>3</sub>) are located on the wider edge and primary hydroxyl groups (on C<sub>6</sub>) on the narrower edge, while the apolar H<sub>3</sub> and H<sub>5</sub> hydrogens and ether-like oxygens reside on the inside of the torus-like molecules. As a result, a molecule with a hydrophilic exterior, which leads to solubility in

water, and an apolar cavity (figure 2), which provides a hydrophobic matrix, is described as a ‘micro heterogeneous environment’.<sup>7</sup>

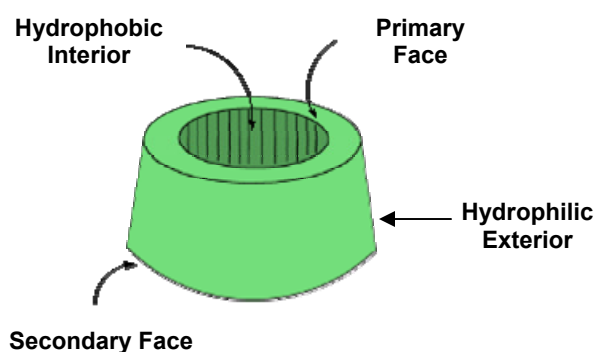


**Figure 2.** Schematic representation of the hydrophobic and hydrophilic regions of cyclodextrins.

As a result of the presence of a cavity, cyclodextrins are able to form inclusion complexes with a wide variety of hydrophobic guest molecules. One or two guest molecules can be entrapped by one, two or three cyclodextrins. The three different hydroxyl groups can be derivatized in order to modify the properties and even the shape of cyclodextrins,<sup>8</sup> so that a broad spectrum of applications is achieved.<sup>9</sup>

### **Properties and applications of cyclodextrins**

Several studies of the conformation of cyclodextrins in solution are supported by a large number of solid state crystal structure studies. Cyclodextrins crystallise in two main types of crystal packing, i.e., channel structures and cage structures depending on the type of cyclodextrin and also on the guest compound, if present. These crystal structures show that cyclodextrins (especially native cyclodextrins) adopt the expected cyclic structure with the glucopyranose units in the  ${}^4C_1$  chair conformation. Furthermore, studies with native linear maltohexaoses (G6), which form an antiparallel double helix, indicate that  $\alpha$ -cyclodextrin (CD6) is the form in which the steric strain due to the cyclization is the least while  $\gamma$ -cyclodextrin is the most strained.<sup>2</sup> Apart from the native cyclodextrins, many cyclodextrin derivatives have been synthesized. These derivatives usually are produced by aminations, esterification or etherification of the primary and secondary hydroxyl groups. Depending on the substituent, the solubility of a cyclodextrin derivative is usually different from that of its parent cyclodextrin. Derivatization almost always alters the hydrophobic cavity volume and these modifications can also improve solubility, stability against light or oxygen, and help to control the physical and chemical properties of guest molecules.<sup>1e</sup>



Annually, cyclodextrins are the subject of almost 1000 research articles and scientific abstracts, mainly dealing with drugs and drug-related products. In addition, numerous inventions involving cyclodextrins have been described (over 1000 patents or patent applications in the past five years). From a regulatory standpoint, monographs on  $\beta$ -cyclodextrin, in which the regulatory aspect is predominant, are already available in both the US Pharmacopeia/National Formulary (USP 23/NF 18, 1995) and the European Pharmacopeia (3<sup>rd</sup> ed., 1997). A monograph on 2-hydroxypropyl- $\beta$ -cyclodextrin is in preparation for the US Pharmacopeia/National Formulary, and various monographs for cyclodextrins are included in compendial sources, e.g. the *Handbook of Pharmaceutical Excipients*.<sup>10</sup> Thus, more than one century after their discovery cyclodextrins are now accepted as 'new' pharmaceutical excipients.

The most notable feature of cyclodextrins (native or derivatized) is, as mentioned before, their ability to form inclusion host-guest complexes with a very wide range of solid, liquid and gaseous compounds by molecular complexation.<sup>11</sup> In these complexes a guest molecule is held within the cavity of the cyclodextrin host molecule.<sup>12</sup> Complex formation requires a suitable fit between the host cavity and the guest molecule.<sup>13</sup> The lipophilic cavity of cyclodextrins provides a microenvironment into which appropriately sized non-polar moieties can enter to form inclusion complexes.<sup>14</sup> No covalent bonds are broken or formed during formation of the inclusion complex.<sup>15</sup>

The binding of guest molecules within the host cyclodextrin is not fixed or permanent but rather a dynamic equilibrium. Complexes can be formed either in solution or in the crystalline state and water is typically the solvent of choice. Inclusion complexation can also be accomplished in a co-solvent system and in the presence of any non-aqueous solvent. A variety of molecules are amenable to molecular inclusion in cyclodextrins including straight or branched chain aliphatics, aldehydes, ketones, alcohols, organic acids, fatty acids, aromatics, polar amino acids, hydroxy- and keto-acids and amines, irrespective of their state of aggregation (gas, liquid, solid).

As a result of these typical complexation properties, native and derivatized cyclodextrins can be applied for:

- stabilization of light- or oxygen-sensitive substances;<sup>16</sup>
- modification of the chemical reactivity of guest molecules;<sup>17</sup>
- improvement of solubility of substances;<sup>18</sup>
- protection of substances against degradation by microorganisms;<sup>19</sup>
- masking of undesired odour and taste;<sup>20</sup>

- attenuation of pigments or the colour of substances.<sup>11</sup>

The complexation properties displayed by native and derivatized cyclodextrins have led to their extensive use in separation science, where they have been shown to discriminate between functional groups, homologues and positional isomers and enantiomers.<sup>18</sup> Much attention has been paid to the use of cyclodextrins for chiral recognition in capillary electrophoresis (CE),<sup>21</sup> liquid chromatography (LC),<sup>22</sup> gas chromatography (GC, *see also* chapter I for ‘enantioselective gas chromatography’)<sup>23</sup> and supercritical fluid chromatography (SFC);<sup>24</sup> but more exotic applications of cyclodextrins in separation methods, including gel electrophoresis, isotachopheresis (ITP),<sup>25-26</sup> isoelectric focussing, preparative scale electrophoretic techniques, thin-layer chromatography (TLC),<sup>27</sup> electrochemically modulated liquid chromatography, use of monolithic media in liquid chromatography, microdialysis, separation on hollow fibers, foam flotation enrichment, solid- and liquid-phase extractions, countercurrent chromatography (CCC),<sup>28-29</sup> separation through liquid and composite membranes and cyclodextrin application in molecular imprinted polymers have also been described.<sup>30-31</sup>

For all these applications, a variety of different chiral recognition mechanisms have been proposed (*see also* chapter I for ‘chiral recognition mechanism by cyclodextrins’) but nonetheless the mechanism of chiral complexation is still not very well understood.<sup>32</sup>

When considering these quite disparate techniques, one should bear in mind that large differences can be observed in the complexation characteristics of cyclodextrins in solution (aqueous media or organic solvents) and in the solid phase. Critical comparisons among different techniques may give insight into the mechanism of chiral recognition and allow the rational planning of the synthesis of new cyclodextrin modifications with enhanced selectivity towards particular analytes.

## Chapter I

Enantiorecognition by cyclic and acyclic dextrins: an overview



### 1.1. Enantiodiscrimination in solution

In solution, native or partially derivatized cyclodextrins adopt a toroidal conformation with a hydrophobic inner surface, because all hydroxyl groups are located outside the cavity of the molecule.<sup>33</sup> For this reason, hydrocarbon segments of many organic compounds readily occupy the inner cavity to form inclusion compounds with CDs.<sup>34</sup> Cyclodextrins can be involved in both hydrophobic and polar interactions as well as in hydrogen bonding with sorbed molecules and it is this amphoteric character which explains the broad spectrum of action of CDs as chiral selectors.

The stability of an inclusion complex depends substantially on the degree of hydrophobicity and steric compatibility between the guest and the host (CD) molecules. It was experimentally found by HPLC studies that compounds bearing one aromatic ring (for example, benzene) have a size suitable for  $\alpha$ -CD (CD6), compounds with two fused aromatic rings (for example, naphthalene) are suited to the inclusion with  $\beta$ -CD (CD7), and compounds such as substituted pyrenes are suitable for the inclusion with  $\gamma$ -CD (CD8).<sup>35</sup> The presence of one or several polar groups in the guest molecule is favourable for hydrogen bonding with the hydroxyl groups of native CDs. When racemic selectands are involved, the enantioselectivity of complex formation is determined by Gibbs free energy difference between the inclusion complexes of the enantiomers. In most cases studied the enantiomers contained an aromatic ring (often more than one ring).<sup>36</sup>

Most of the published experimental data demonstrate that the size of the  $\beta$ -CD cavity is appropriate for the enantioseparation of a broad spectrum of racemic compounds, including those relevant for pharmaceutical industry.<sup>37</sup> Moreover, it should be noted that the guest molecule need not be completely located inside the CD cavity. Thus, examples of the separation of enantiomers containing three or four aromatic rings on  $\beta$ -CD have also been reported.<sup>38</sup> It is sufficient if the guest molecule is only partially located within the cavity and forms an inclusion complex.

Substituted CDs with various functional groups have been used. The presence of such groups provides additional enantioselective interactions between the guest and the surface, which allows one to extend substantially the spectrum of racemates being separated.

### 1.2. NMR spectroscopic and CE studies of enantiorecognition

The application of NMR spectroscopy for a better understanding of enantioselective CD-guest interactions has a quite long history. The technique provided the very first evidence of inclusion complex formation between CDs and guest molecules in solution in 1970. Over the

last 30 years it has provided very useful information on the stoichiometry,<sup>39</sup> the binding constants, the structure, Gibbs free energy, enthalpy, entropy and dynamics of CD guest complexes (see also chapter III and appendix for further details about these techniques).<sup>40</sup> Studies on the combined application of CE and NMR spectroscopy for a better understanding of the binding and enantiomer recognition ability of chiral analytes by CDs have been published since 1992.<sup>41</sup> These studies include a correlation between the magnitude and pattern of signal splitting in <sup>1</sup>H-NMR,<sup>42</sup> <sup>13</sup>C-NMR<sup>43</sup> and <sup>19</sup>F-NMR<sup>44</sup> spectra on the one hand and enantioseparations in CE on the other hand, as investigations on stoichiometry,<sup>45</sup> binding constants,<sup>46</sup> structure and dynamics<sup>47</sup> of CD-guest complexes related to CE enantioseparations.

The NMR spectroscopic pattern of CD-guest complexes may provide preliminary information on the extent of enantioselectivity, as well as the involvement of different groups of both the guest and host molecules in the intermolecular complex formation. In some interesting cases where the elution order of an enantiomeric pair are reversed in the chromatographic separation on different CDs, the following questions arise:<sup>48</sup>

1. Are there any apparent structural differences, which may be responsible for the reversal of the elution order?
2. Are there additional instrumental techniques available, or is the selected technique adequate in order to detect these changes on the molecular level?
3. Do we possess reliable techniques at present in order to accurately determine the intermolecular forces based on the structure of a diastereomeric complex? Do these techniques allow a correct identification of the forces responsible for chiral recognition? Can these calculations be performed accurately enough in order to distinguish very small free energy differences (commonly far less than 1 kcal·mol<sup>-1</sup>) between the two diastereomeric complexes?

Up to now, NMR spectroscopic analysis combined with CE analysis<sup>43</sup> has been successful in determining which segments of the guest are interacting with the host selector. However, even when clear information about differences in the interactions of native  $\alpha$ -,  $\beta$ - and  $\gamma$ -CD with chiral analytes are observed (i.e. inclusion through the wider or narrower rim), there is not an exhaustive explanation about the mechanism which differentiate the two enantiomers.<sup>49</sup> Indeed, at present it is difficult even with very sophisticated powerful NMR techniques to define the structure and dynamics of the complexes with sufficient accuracy.

In addition to their applications in HPLC and CE studies, native and derivatized cyclodextrins have also been extensively applied as Chiral Solvating Agents (CSAs)<sup>50</sup> for NMR

spectroscopy in solution. Here they play an important role in the development of direct, rapid and reliable methods for the determination in solution of the enantiomeric compositions of chiral analytes, complementing GC, HPLC and CE chromatographic techniques. Furthermore, the chemical shift nonequivalence of enantiomers in the presence of the chiral CSA has been attributed to at least two, probably mutually dependent contributions which are related to the stability and geometry of the resulting association complexes.<sup>51e-f</sup> The association constants of the diastereomers formed between the enantiomers and CSA vary giving rise to different induced shifts (*stability*) and the diastereotopic nuclei reside in different spatial environments (*geometry*).

Thus, permethylated cyclodextrins have proved to be highly effective in the NMR enantiodiscrimination of substrates devoid of hydrogen bond donor functional groups, such as trisubstituted allenes and aromatic hydrocarbons.<sup>51a-d</sup>

Benzylated and benzoylated cyclodextrins, readily soluble in chloroform, were reported for the NMR enantiodiscrimination of 3,5-dinitrobenzoyl derivatives of  $\alpha$ -amino acids, amines, alcohols.<sup>52</sup> Carbamoylated cyclodextrins, which were used in the chromatographic area, were also applied for the NMR spectroscopic analysis of chiral polar substrates.<sup>53</sup> In the case of heptakis[2,3,6-tri-*O*-(2,3-dimethylphenylcarbamoyl)]- $\beta$ -cyclodextrin, for example, no intermolecular dipolar interactions with internal protons of the cyclodextrin derivative were detected in the mixture containing either one of the enantiomers of *N*-(3,5-dinitrobenzoyl)-alanine-*O*-methyl ester, so that only  $\pi$ - $\pi$  interactions between the 3,5-dinitrophenyl and 3,5-dimethylphenyl moieties are involved in the formation of the diastereomeric complexes. Moreover, in the case of the (*S*)-enantiomer such interaction involves all the three kinds of carbamate groups (on the 2-, 3- and 6-position), while in the case of the (*R*)-enantiomer only the primary site interacts with the analyte (figure 1.1).<sup>53</sup> This work represents one of the few examples where only external enantio-recognition occurs applying cyclodextrin derivatives as chiral selectors.<sup>53</sup>

Applying two mixed methylated/carbamoylated  $\beta$ -cyclodextrins heptakis[2,3-di-*O*-methyl-6-*O*-(3,5-dimethylphenylcarbamoyl)]- $\beta$ -cyclodextrin and heptakis[6-*O*-methyl-2,3-di-*O*-(3,5-dimethylphenylcarbamoyl)]- $\beta$ -cyclodextrin as CSAs for NMR spectroscopy it was possible to combine the enantiodiscriminative properties of the corresponding fully permethylated and percarbamoylated cyclodextrins and, hence, to enhance their versatility for the analysis both of apolar and polar substrates.<sup>54</sup> The enantio-recognition mechanism proposed for all these selectors does not involve the inclusion phenomenon.

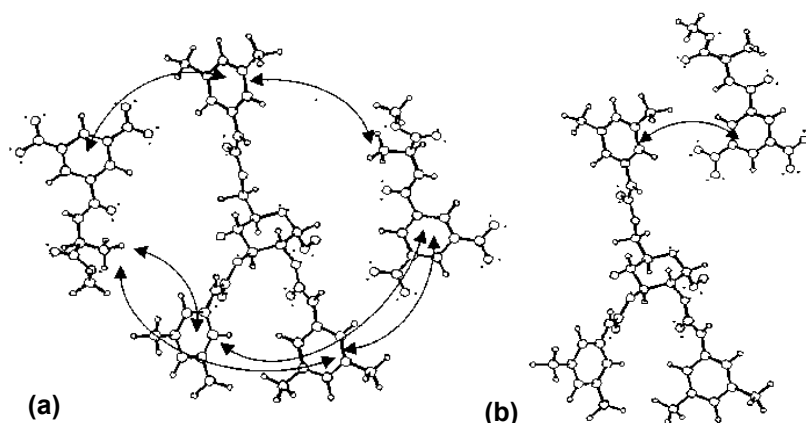


**Figure 1.1.** Schematic representation derived from NOEs detected in the two diastereomeric complexes formed by (a) (*S*)- and (b) (*R*)-enantiomer of *N*-(3,5-dinitrophenyl)-alanine-*O*-methyl ester and heptakis[2,3,6-tri-*O*-(3,5-dimethylphenylcarbamoyl)]- $\beta$ -cyclodextrin.<sup>53</sup>

### 1.3. Computational studies of cyclodextrins and their derivatives

Computational chemistry ('molecular modeling') has been applied in the area of cyclodextrins, although somewhat limited.<sup>55</sup> The reason for this is the fact that cyclodextrins are relatively large, flexible molecules that are often used in aqueous environments. This renders computations either prohibitive or, as is often the case, forces one to make so many assumptions and impose so many restrictions that the results become unrealistic. The size of cyclodextrins and their derivatives makes applications of quantum mechanics difficult even when symmetry conditions are imposed. Lipkowitz *et al.*<sup>56</sup> attempted to overcome these difficulties and to extend these studies from free cyclodextrins to their inclusion complexes, focussing on four important considerations:

- (1) Which regions of cyclodextrins and their derivatives are responsible for complexation? Do analytes always prefer to bind at the wider rim, as is found in many examples of aqueous guest binding from NMR measurements,<sup>57</sup> or at the narrower rim?
- (2) What are the intermolecular forces holding the complexes together? Are these forces predominantly weak van der Waals forces or more powerful electrostatic forces? Moreover, what percentage of the interaction energy can be attributed to each?
- (3) Which intermolecular forces are primarily responsible for enantiorecognition? Are these the same forces that hold the complexes together or are they different? What proportion of the total enantiorecognition can be attributed to the short-range dispersion forces and which from the long-range electrostatic interactions?



(4) What region at the cyclodextrin is inherently the most enantiodiscriminating? Although the entire cyclodextrin is chiral, there are probably regions in or around the cyclodextrin that discriminate enantiomers better than others. This is an important aspect of chiral discrimination which is often overlooked. If, for example, the preferred binding site of a cyclodextrin is inside the cavity, but the most discriminating region is outside, one could expect diminished ability in chiral discrimination.

In the case of heptakis(2,3,6-tri-*O*-methyl)- $\beta$ -cyclodextrin, for example, the “principle of maximum chiral discrimination” was established.<sup>56</sup> In order to answer the question of where the guest molecule is most likely to be found, molecular mechanics mimicing the enantio-recognition of this selector towards certain guest molecules were applied, whereby the time-averaged CD's center of mass was placed at the origin of a Cartesian coordinate system, which in turn was placed on a three-dimensional grid. These calculations indicated that all the guests prefer to bind within the interior of the CD cavity. The reason for this behaviour is that interior binding is stabilized by the macrocycle, which collapses around these small guests, thus maximizing van der Waals' forces (in contrast to exterior binding).

It is always difficult to detect which forces are responsible for enantioselective complexation because the total energy of a diastereomeric complex comprises both intramolecular energies and intermolecular energies. Differential intermolecular forces between each enantiomer and its complex with cyclodextrin have been evaluated, by comparing the averaged intermolecular van der Waals energy for the *R* enantiomer with that of the *S* enantiomer of selected substrates<sup>55</sup> and determining whether this energy difference is greater or smaller in magnitude than the corresponding electrostatic values. According to studies carried out by Lipkowitz,<sup>55</sup> although the preferring binding sites have been located inside the cyclodextrin cavity, the most discriminating regions of the host molecule have not been identified. Thus, the complexation phenomena and in particular the enantio-recognition of CDs still remains a challenge for computational studies.

In addition to the comparison among the different techniques mentioned above, it should be pointed out the cyclodextrins usually have the ability to include hydrophobic guest molecules in their cavity, as reported for the first time by Cramer and Dietsche.<sup>58</sup> However, the need to apply the three-point rule,<sup>59</sup> the three-point binding (Ogston)<sup>60</sup> and the lock-and-key mechanism (Fischer)<sup>61</sup> to the enantio-recognition by cyclodextrins (native and fully derivatized) must be considered.<sup>62</sup>

## 1.4. Ability of linear dextrans to form molecular complexes and their use for chiral separations

### *Capillary zone electrophoresis*

While it is well known that cyclic CDs are able to include various organic compounds in their cavity, the ability of linear dextrans to form molecular complexes has scarcely been recognized. However, it is known that the  $\alpha$ -1,4-linked linear glucose polymer, amylose, the helical structure of which has been proved by X-ray analysis, forms complexes with various alcohols. Kano *et al.*<sup>63</sup> found that underivatized  $\alpha$ -1,4-linked oligosaccharides such as maltohexaose (G6) and/or maltoheptaose (G7), which represent approximately one turn of an amylose helix, form complexes with different organic compounds. Thus, according to the authors, linear oligomers of glucose are also expected to act as guest molecules which may discriminate between the enantiomers of the guest molecules. Minor enantioseparation of a binaphthyl derivative (BNC, table 1.1) was achieved by capillary zone electrophoresis (CZE) by using linear dextrans (Gn) as chiral selectors (figure 1.2).<sup>64</sup>

**Table 1.1.** Enantioseparation of ( $\pm$ )-BNC (0.1 M) by CZE at 17-18  $\mu$ A using linear dextrans (0.4 M) as selectors.<sup>64</sup>

linear dextrin	voltage (kV)	$t_0$ (min)	$t_1$ (min)	$t_2$ (min)	$\alpha$
G2	8	9.6	26.4 ( <i>S</i> )	26.8 ( <i>R</i> )	1.02
G3	10	9.2	23.6 ( <i>S</i> )	25.0 ( <i>R</i> )	1.10
G4	11	10.6	27.0 ( <i>S</i> )	27.9 ( <i>R</i> )	1.09
G5	13	12.0	29.8 ( <i>S</i> )	29.8 ( <i>R</i> )	1.00
G6	21	13.8	32.2 ( <i>R</i> )	32.7 ( <i>S</i> )	1.03
G7	22	17.8	60.3 ( <i>R</i> )	63.7 ( <i>S</i> )	1.08

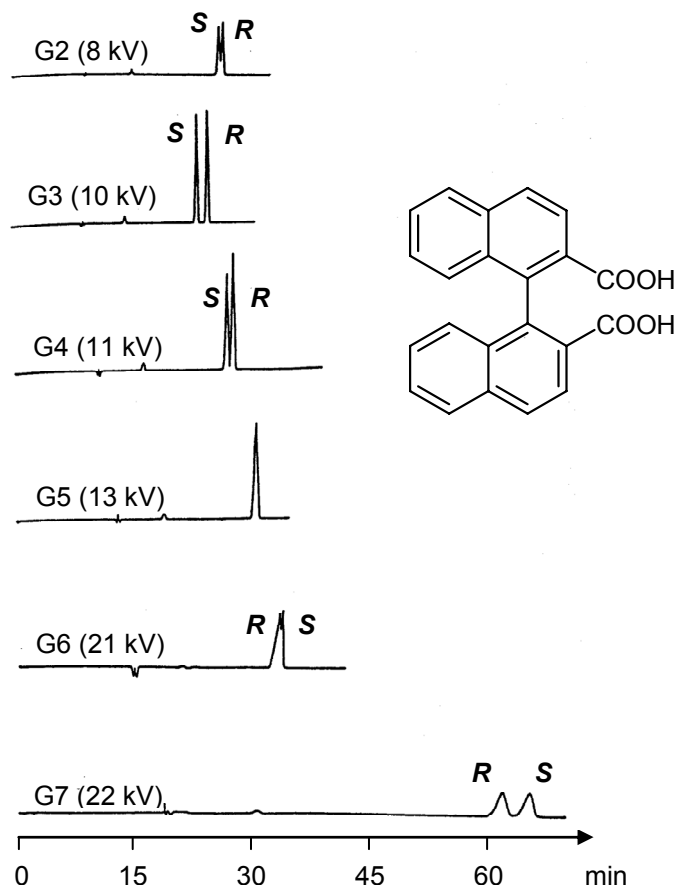


**Figure 1.2.** Electropherograms of ( $\pm$ )-BNC (0.1 mM) obtained by CZE using 0.04 M carbonate buffer (pH 9-9.5) containing Gn (0.4 M); current 17-18  $\mu$ A, detection wavelength 225 nm.<sup>64</sup>

Except for the case of G5, baseline or partial enantioseparation of BNC was achieved by all linear dextrans. An opposite elution order has been observed increasing the degree of oligomerisation: with G2, G3 and G4, the (*S*)-enantiomer eluted first whereas with G6 and G7 the (*R*)-enantiomer eluted first.

In their work the authors took into account the MM-MD calculations for Gn, which were carried out in water. The most stable structures derived from the calculations are shown in figure 1.3. The maltoheptaose (G7) is calculated to describe a complete turn of a helix which is in good agreement with the result of the X-ray analysis.

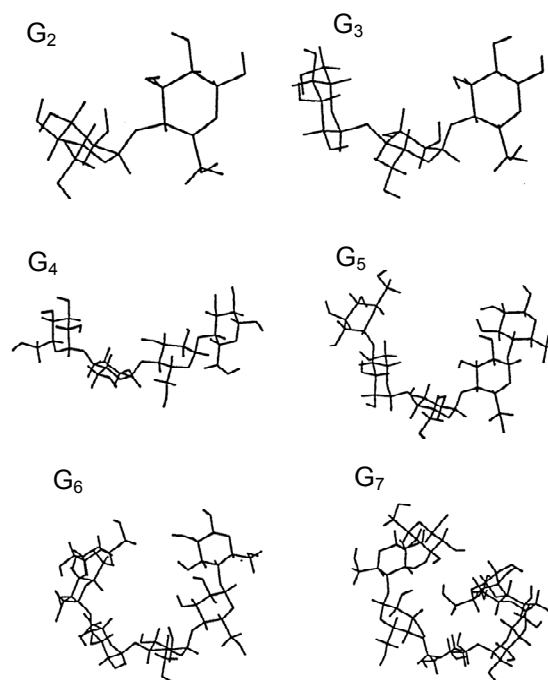


**Figure 1.3.** Optimized structures of  $G_n$  in water obtained by the MM-MD calculations.<sup>64</sup>

Another example of enantioseparation by linear dextrans is the recognition of the helicity of 1,12-dimethylbenzo[*c*]phenanthrene-5,8-dicarboxylic acid (figure 1.4), in CZE.<sup>65</sup>

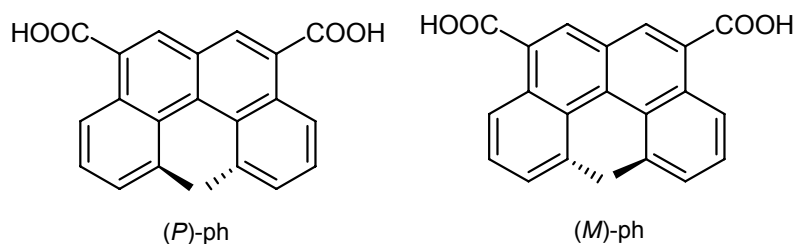


**Figure 1.4.** Structure of (*P*)- and (*M*)-1,12-dimethylbenzo[*c*]phenanthrene-5,8-dicarboxylic acid (ph).<sup>65</sup>

The results are summarized in table 1.2. From the table, it is apparent that the difference in stability of the two diastereomeric complexes increases with increasing the molecular weight of the oligosaccharide Gn.

Indeed, no peak separation was observed when G1, G2 and G3 were used, while baseline enantioseparation was obtained with G4, G5, G6 as chiral selectors. Although the question of enantio-recognition by acyclic oligosaccharides would appear to be very important in connection with the biological role of oligosaccharides at the cell surface, little attention has hitherto been paid to the enantio-recognition ability of linear dextrans.

**Table 1.2.** Enantioseparation of ( $\pm$ )-ph by CZE using Gn as chiral selector.<sup>a</sup>

saccharide	$t_1$ (min)	$t_2$ (min)	$\alpha$
G1	26.4 ( <i>S</i> )	26.8 ( <i>R</i> )	1.02
G2	23.6 ( <i>S</i> )	25.0 ( <i>R</i> )	1.10
G3	27.0 ( <i>S</i> )	27.9 ( <i>R</i> )	1.09
G4	29.8 ( <i>S</i> )	29.8 ( <i>R</i> )	1.00
G5	32.2 ( <i>R</i> )	32.7 ( <i>S</i> )	1.03
G6	60.3 ( <i>R</i> )	63.7 ( <i>S</i> )	1.08
G7	60.3 ( <i>R</i> )	63.7 ( <i>S</i> )	1.08

<sup>a</sup>  $4 \times 10^{-4}$  M, [Gn] = 0.01 M, buffer solution: 0.033 M phosphate buffer at pH 8.0; applied voltage: 15.2 kV, current: 40  $\mu$ A.<sup>65</sup>

Khaledi *et al.*<sup>66</sup> obtained the enantioseparation of selected racemic compounds by capillary zone electrophoresis using a mixture of cyclic and acyclic dextrans, produced by degradation of starch by enzymatic hydrolysis (figure 1.5)

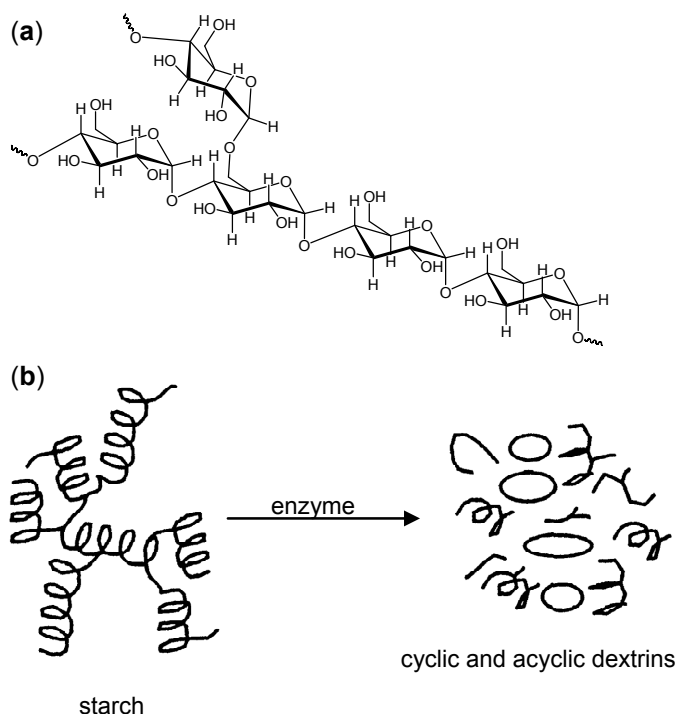
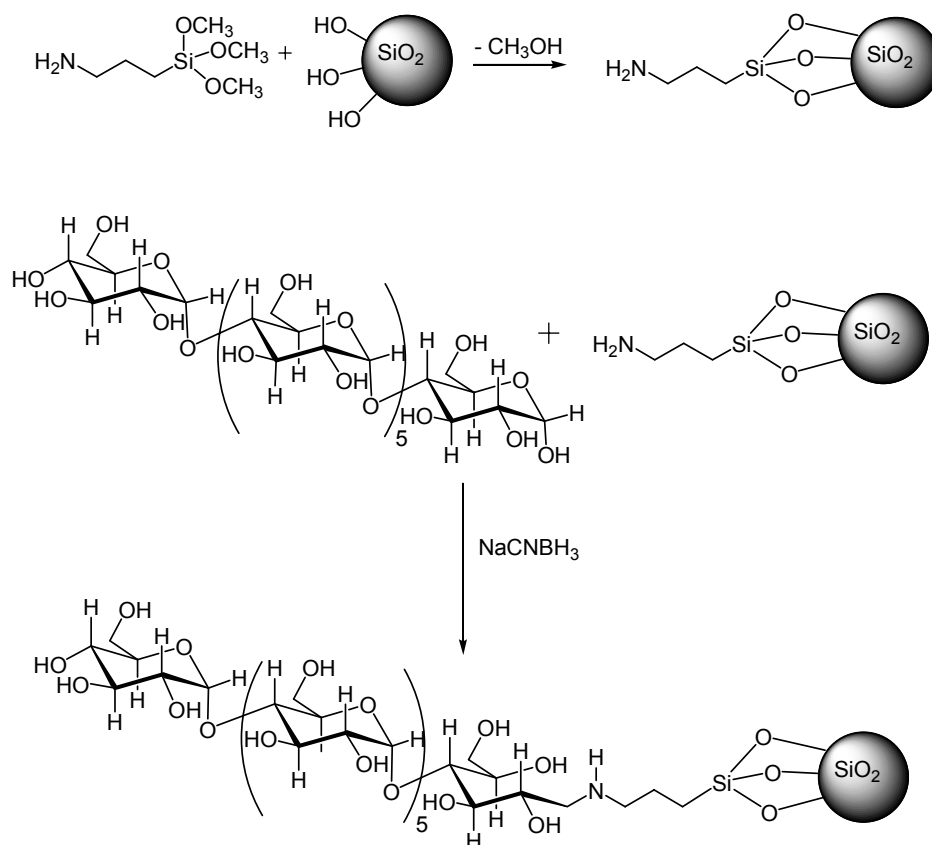


**Figure 1.5.** Chemical structure of starch (a) and schematic degradation of starch to a mixture of cyclic and acyclic dextrans by enzymatic hydrolysis (b).<sup>66</sup>

According to the authors, the conformation of linear dextrans in aqueous solution is a flexible random coil which consists of extended helical segments connected by deformed non-helical segments.<sup>66</sup> Thus, the enantioseparation of non-steroidal antiinflammatory drugs (e.g., flurbiprofen, suprofen, indoprofen, ibuprofen and fenoprofen), in addition to acidic racemic compounds including warfarin and sulfinpyrazone and some dansylated amino acids were resolved by using the buffer electrolytes containing the mixture mentioned above.<sup>66</sup> The major difference between cyclic and acyclic dextrans is that while native cyclodextrans are constrained to the well known “doughnut” conformation with little intramolecular flexibility, linear dextrans in solution have considerable conformational mobility. However, the application of the above mentioned mixture (figure 1.5) implies the difficulty to rationalize which kind of mechanism for the enantio-recognition is involved and which is the selector mainly responsible for the enantio-recognition.

*Linear dextrans in HPLC analysis*

Native maltoheptaose (G7) was also attached to the solid support of the silica surface according to the synthetic procedure shown in figure 1.6.<sup>67</sup>

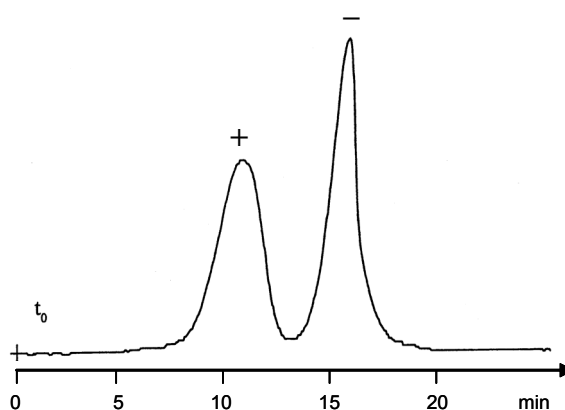


**Figure 1.6.** Synthesis of maltoheptaose (G7) functionalized silica particles *via* reductive amination with  $\text{NaCNBH}_3$ .<sup>66</sup>

The most simple way to graft maltoheptaose to amino functionalized silica particles is *via* reductive amination with  $\text{NaCNBH}_3$  to give maltoheptaose functionalized silica particles. This chiral stationary phase was used in HPLC and compared with the commonly used amylose modified silica. Enantiodiscrimination is quite good in most cases (table 1.3) and does not depend much on the chain length of the grafted oligosaccharides. This must be due to the fact that only those segments of the chains which constitute the top of the surface are in contact with the liquid phase and therefore only these molecules interact to form diastereomeric complexes. In table 1.3 the enantioseparation factors  $\alpha$  of various chiral molecules on supported maltoheptaose and amylose are reported and in figure 1.7 the enantioseparation of Tröger's base on the former is shown.

**Table 1.3.** Enantioseparation factor  $\alpha$  of racemic mixtures on maltoheptaose and amylose functionalized silicagels.<sup>66</sup>

saccharide	maltoheptaose	amylose
Tröger's base	1.72	1.80
camphor	1.64	1.64
menthol	1.40	1.49
isoborneol	1.32	1.40
mandelic acid	1.40	1.40
tryptophane	1.28	1.29

**Figure 1.7.** Enantioseparation of Tröger's base on maltoheptaose functionalized silicagel (UV detection).<sup>66</sup>

#### *Linear dextrans in enantioselective gas chromatography*

In addition to the well known properties for enantioseparation of amylose derivatives (per-*n*-pentylated or per-*n*-butylcarbamate amylose)<sup>67-68</sup> in enantioselective gas chromatography, Vigh *et al.*<sup>69</sup> used corn syrup polysaccharides as chiral stationary phase. Corn syrup is a mixture of mono-, di-, tri- and oligosaccharides with an average reducing sugar content of 34-38 Dextrose Equivalent (DE). After the derivatization (*n*-pentyl/trifluoroacetyl) the syrup becomes a viscous liquid which can be used as a chiral stationary phase without dilution in polysiloxane. The low enantioseparations achieved by this phase suggest that competitive and opposite effects are present during the enantiorecognition process.

#### *Linear dextrans in NMR spectroscopic studies in solution*

In addition to the enantiorecognition mentioned above, there are other examples where an inclusion phenomenon does not seem to be a prerequisite for the formation of the host-guest

complex in cyclodextrins.<sup>69</sup> According to NMR spectroscopic studies, interactions between native cyclodextrins and carboxylate anions (figure 1.8) involved only the secondary OH groups at the 2- and 3-positions, while all the other signals of CD7, including the signals of the primary OH groups, were unaffected by  $p\text{-CH}_3\text{C}_6\text{H}_4\text{CO}_2^-$  (figure 1.9).

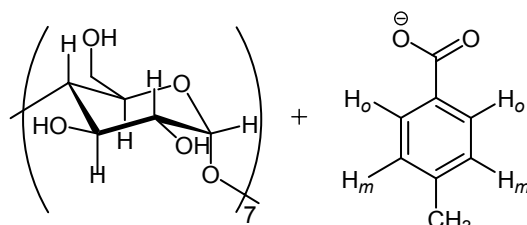


**Figure 1.8.** Structure of  $\beta$ -cyclodextrin (CD7) and carboxylate anion described by Kano *et al.*<sup>69</sup>

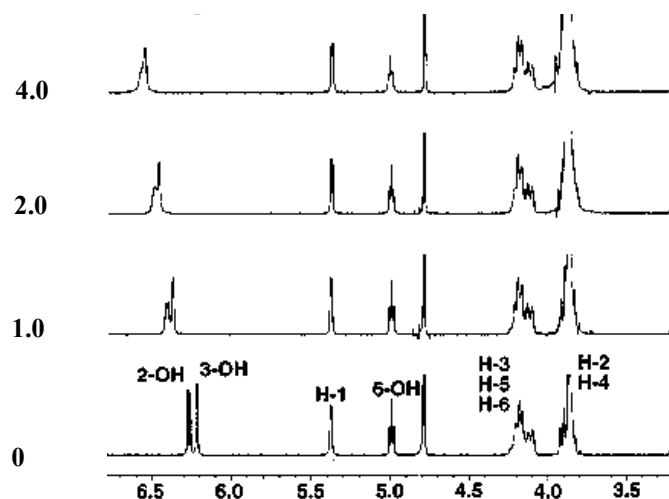


**Figure 1.9.**  $^1\text{H-NMR}$  spectra of CD7 (1 x 10<sup>-3</sup> M) in  $d_6$ -DMSO at 25 °C with increasing concentrations (x 10<sup>-3</sup> M) of  $p\text{-CH}_3\text{C}_6\text{H}_4\text{CO}_2\text{Na}$ .<sup>69</sup>

The *ortho* and *meta* protons of the guest molecule were only partially shifted to lower fields (due to the different binding constant) and no remarkable shift is observed for the methyl group in the *para* position (figure 1.10).

These results imply that no inclusion of the guest anion in the host cavity occurs and no hydrogen bonding between the  $\text{CO}_2^-$  group of the guest and the primary OH groups of the host takes place. The hydrogen bonding interaction between the secondary OH groups of the CD7 and the anionic guest obviously occurs outside the CD cavity.

The binding constants for complexation of  $p\text{-CH}_3\text{C}_6\text{H}_4\text{CO}_2^-$  with the dextrins (cyclic and acyclic, table 1.4) were determined by NMR titrations technique. In the case of



$p\text{-CH}_3\text{OC}_6\text{H}_4\text{CO}_2^-$ , a similar binding constant was determined with the CD7 and with G7 ( $1070\text{ M}^{-1}$  versus  $1020\text{ M}^{-1}$ ). Native G7, representing the open form of CD7, shows a slightly smaller  $K$  value as compared to CD7. This may be due to the more fluctuating nature of these acyclic oligosaccharides. The mechanism proposed by the authors is depicted in figure 1.11.<sup>69</sup>

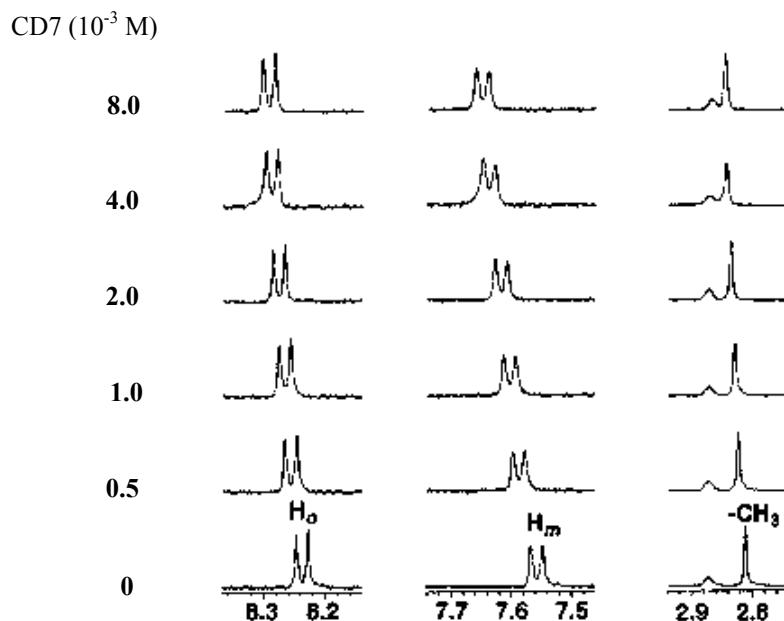


**Figure 1.10.** Effect increasing concentrations of CD7 on the  $^1\text{H}$ -NMR spectra of  $p\text{-CH}_3\text{C}_6\text{H}_4\text{CO}_2\text{Na}$  ( $1 \times 10^{-3}\text{ M}$ ) in  $d_6$ -DMSO at  $25\text{ }^\circ\text{C}$ .<sup>69</sup>

**Table 1.4.** Binding constants for complexation of carboxylate anions with CD and Gn in  $d_6$ -DMSO at  $25\text{ }^\circ\text{C}$

guest	host	$K$ ( $\text{M}^{-1}$ )
$p\text{-CH}_3\text{C}_6\text{H}_4\text{CO}_2\text{Na}$	CD6	$669 \pm 40$
$p\text{-CH}_3\text{C}_6\text{H}_4\text{CO}_2\text{Na}$	CD7	$792 \pm 45$
$p\text{-CH}_3\text{C}_6\text{H}_4\text{CO}_2\text{Na}$	CD8	$1300 \pm 60$
$p\text{-CH}_3\text{C}_6\text{H}_4\text{CO}_2\text{Na}$	G3	$297 \pm 19$
$p\text{-CH}_3\text{C}_6\text{H}_4\text{CO}_2\text{Na}$	G4	$349 \pm 19$
$p\text{-CH}_3\text{C}_6\text{H}_4\text{CO}_2\text{Na}$	G5	$476 \pm 27$
$p\text{-CH}_3\text{C}_6\text{H}_4\text{CO}_2\text{Na}$	G6	$542 \pm 43$
$p\text{-CH}_3\text{C}_6\text{H}_4\text{CO}_2\text{Na}$	G7	$679 \pm 36$
$p\text{-CH}_3\text{OC}_6\text{H}_4\text{CO}_2\text{Na}$	CD7	$1070 \pm 80$
$p\text{-O}_2\text{NC}_6\text{H}_4\text{CO}_2\text{Na}$	CD7	$151 \pm 10$
$p\text{-CH}_3\text{OC}_6\text{H}_4\text{CO}_2\text{Na}$	G7	$1020 \pm 100$
$p\text{-O}_2\text{NC}_6\text{H}_4\text{CO}_2\text{Na}$	G7	$173 \pm 16$

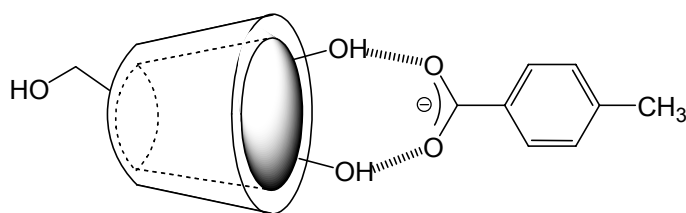


**Figure 1.11.** Structure of the hydrogen-bonded complex of CD7 and  $p\text{-CH}_3\text{C}_6\text{H}_4\text{CO}_2^-$  in  $d_6\text{-DMSO}$ .<sup>69</sup>

### *Linear dextrans in circular dichroism analysis*

Kano *et al.*<sup>63</sup> found that (4*Z*, 15*Z*)-bilirubin-IX (BR, a cytotoxic pigment observed in jaundice), which can assume enantiomeric conformations as *M*- and *P*-helices *via* intramolecular hydrogen binding is bound to maltose (G2), maltotriose (G3) and maltoheptaose (G7) to form diastereomeric BR complexes *via* hydrogen bonding between the  $\text{CO}_2^-$  groups of BR and the OH groups of the linear  $\alpha$ -1,4-linked dextrin (Gn). The circular dichroism spectral measurements of BR ( $5 \times 10^{-5}$  M) in aqueous saccharide solutions (pH 10.8 NaOH) are summarized in table 1.2. Two oligosaccharides involved in this study, *D*-glucose and heptakis(2,3,6-tri-*O*-methyl)- $\beta$ -cyclodextrin (CD7) (table 1.5) did not induce any circular dichroism signal, while all the other oligosaccharides display enantioselectivity towards BR enantiomers (table 1.5)

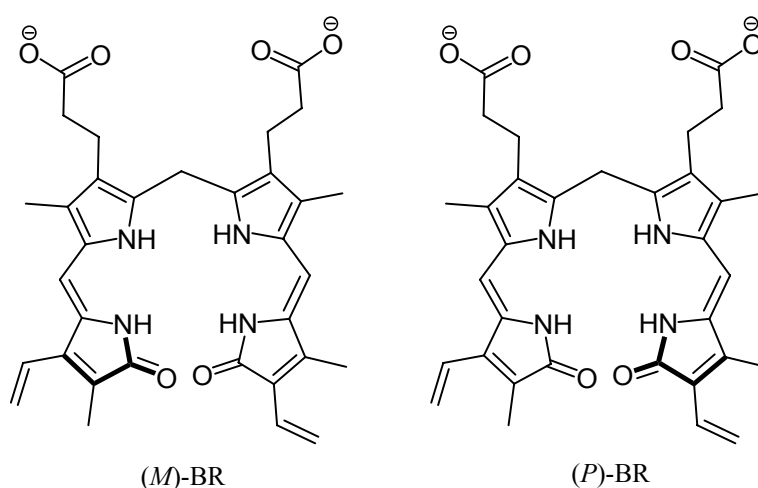


**Figure 1.12.** Enantiomeric conformers of (4*Z*, 15*Z*)-bilirubin-IX (BR).<sup>63</sup>

**Table 1.5.** C.d. spectral data for bilirubin in various saccharides solution at pH 10.8.<sup>63</sup>

saccharide	$\lambda_{\text{ext}}^1$ (nm)	$\Delta\epsilon_1$ (L mol <sup>-1</sup> cm <sup>-1</sup> )	$\lambda_{\text{ext}}^2$ (nm)	$\Delta\epsilon_2$ (L mol <sup>-1</sup> cm <sup>-1</sup> )
CD7 (0.01 M)	455	- 9.0	405	+ 5.1
CD7 (0.01 M)	455	- 10.4	405	+ 7.3
DM-CD7 (0.01M)	435	+ 1.8	378	- 2.1
TM-CD7 (0.01M)	no Cotton effect			
<i>D</i> -glucose (2.0 M)	no Cotton effect			
Maltose (0.1 M)	455	- 1.2	395	+ 0.6
Maltose (0.5 M)	455	- 2.1	400	+ 1.8
Maltose (1.0 M)	460	- 3.5	397	+ 2.4
Maltotriose (0.1 M)	455	- 3.6	402	+ 1.8
Maltoheptaose (0.01M)	458	- 5.5	408	+ 4.1
Cellobiose (0.1 M)	455	+ 7.6	405	- 4.8
Cellotetraose (0.025 M)	455	+ 1.5	408	- 0.9
Lactose (0.1 M)	455	- 7.3	405	+ 5.2
Gentobiose (0.1 M)	450	+ 1.5	<i>ca.</i> 400	<i>ca.</i> 0

All the findings described above for different analytical techniques prompt us to investigate the application of derivatized linear dextrans as novel chiral stationary phases for enantioselective gas chromatography (chapter IV), in order to probe the role of the presence or absence of a cavity in the enantiorecognition process. Thus, the present study involves the reaction of linear oligosaccharides (Gn) to form derivatives analogous to those of well established cyclodextrin selectors (CDn) (chapter II) and the direct comparison of the enantioselectivity of the cyclic with the corresponding acyclic selector (chapter IV).

### 1.5. Enantioselective gas chromatography

Since the pioneering work of Gil-Av, Feibush and Charles-Sigler in 1966,<sup>70</sup> rapid advances in the development and understanding of enantioseparations have made the analysis of many chiral compounds by enantioselective GC now a matter of routine. Compared to other chromatographic methods, chiral capillary GC combines the advantages of high efficiency, sensitivity and reproducibility.

Enantiomers can be separated either by direct or indirect methods using capillary GC. The indirect approach involves off-column derivatization with an enantiopure reagent, thus converting the enantiomers into diastereomers. These are then separated on an achiral GC

stationary phase.<sup>71</sup> The success of the direct GC separation of enantiomers relies on the use of chiral stationary phases (CSPs), which can rapidly and reversibly form transient diastereomers with the targeted chiral molecules.

According to the type of enantioselective interactions with chiral molecules, chiral selectors are currently classified into three major categories: (a) amino acid derivatives and diamides which are capable of hydrogen-bonding;<sup>72</sup> (b) chiral metal complexes which are prone to coordination;<sup>73</sup> (c) cyclodextrin (CD) derivatives which separate enantiomers by forming inclusion complex, dipole-dipole interactions, or other specific mechanism dependent on the CD derivative employed.<sup>74</sup> The chiral selectors have been used in the form of a neat liquid, as a solution in an achiral matrix (most commonly a polysiloxane) or were covalently bound to a polysiloxane (Chirasil-type).<sup>74</sup>

Among the three categories of chiral selectors, the importance of chiral metal complex stationary phases in enantioselective GC has diminished dramatically with the advent of CD derivatives as CSPs.

### 1.5.1. CSPs based on amino acid derivatives

Since Gil-Av et al. introduced *N*-trifluoroacetyl-*L*-isoleucine lauryl ester as the first CSP for enantioselective GC in 1966,<sup>70</sup> numerous hydrogen-bonding chiral selectors have been developed.<sup>72</sup> Among them, Chirasil-Val, which is prepared by covalently anchoring *L*-valine-*tert*-butylamide with random distribution along a polydimethylsiloxane, is one of the most successful and versatile GC-CSPs. In an attempt to expand the usefulness of hydrogen-bonding GC-CSPs, several new phases have been reported recently.<sup>75</sup> A highly ordered Chirasil-type GC phase, namely Chiral-Calix, was synthesized by covalently linking resorcinarenes, which have pendant *L*-valine-*tert*-butylamide moieties, to a dimethylpolysiloxane. Nevertheless, as compared to Chirasil-Val, Chiral-Calix did not demonstrate a significant improvement in enantioselectivity.<sup>76</sup>

### 1.5.2. CSPs based on cyclodextrin derivatives

In recent years, cyclodextrin derivatives have become the most popular chiral selectors for the direct enantiomeric GC separation of volatile racemates. Their applications include also such fields where other CSPs have previously been applied. For example, direct chiral GC separation of *N*-trifluoroacetyl-*O*-alkyl ester derivatives of amino acids can be accomplished on both modified cyclodextrins and on Chirasil-Val CSPs.<sup>77</sup> A large number of cyclodextrin-based GC CSPs differing in degree of oligomerization, type and site of derivatization have

been synthesized and proved to be useful in separating a large variety of chiral molecules.<sup>77</sup> Since their introduction in the late 80's, derivatized CD-CSPs have been used to separate a broad spectrum of chiral molecules with different geometries and functionalities, which are of great importance to the pharmaceutical,<sup>78</sup> agricultural,<sup>79</sup> food,<sup>80</sup> flavour and fragrance,<sup>81</sup> industries and environmental analysis.<sup>80</sup>

The enantioselectivity of CD-CSPs are greatly influenced by the cavity size and concentration of cyclodextrins ( $\alpha$ ,  $\beta$  or  $\gamma$ ) in the achiral matrix and by the type, degree and positions of substitution (2-, 3- and 6-position) of glucose units of CD. In some cases, the elution order of chiral molecule can be reversed by simply changing the size of the CDs.<sup>82</sup> It is believed that the type and the site of substitution is at least of equal importance.<sup>83</sup> For these reasons, small changes in the cyclodextrin composition can significantly influence the enantioselective properties of the CSP. Incomplete substitution reaction often yields a mixture of CD derivatives. Therefore, the synthesis of CD derivatives must be carefully controlled to give a material with unambiguous structure.<sup>84-85</sup> The products obtained must be completely characterized in order to avoid problems with the reproducibility of separation characteristics.<sup>86</sup> Subtle changes in the structure of the selector (figure 1.13)<sup>87-88</sup> may imply striking variations of enantioseparation patterns of racemic compounds. These CDs derivatives are able to separate a broad spectrum of chiral analytes, especially 2-pentyl acetate and its analogues. Simply the introduction of the methoxymethyl moiety (figure 1.13) leads to a significant increase in the resolution of many compounds compared to their separation on other CSPs.

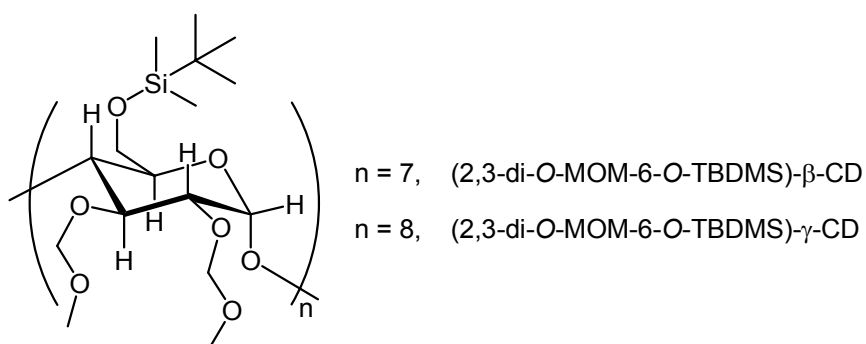


**Figure 1.13.** Structure of heptakis(2,3-di-*O*-methoxymethyl-6-*O*-*tert*-butyldimethylsilyl)- $\beta$ -cyclodextrin and octakis(2,3-di-*O*-methoxymethyl-6-*O*-*tert*-butyldimethylsilyl)- $\gamma$ -cyclodextrin.<sup>87-88</sup>

In the following sections, particular attention is focused on the enantioseparation of three important classes of chiral compounds: amino acid derivatives, saturated hydrocarbons,

halogenomethanes and chlorinated/fluorinated ethers (section 1.6). These molecules will be investigated in the course of the present work in order to evaluate the role of the cavity in the enantioseparation by cyclodextrin *via* comparative analysis with the new CSPs based on linear dextrin derivatives (chapter IV).

## 1.6 Enantioseparation of amino acid derivatives, saturated hydrocarbons, halogenomethanes and chlorinated/fluorinated ethers (inhalation anaesthetics)

### *Amino acid derivatives*

The enantioseparation of amino acids is of great importance for several studies concerning the search for optical activity in extraterrestrial space (such as comets or planets)<sup>89</sup> which has been proposed to help to understand the origin of homochirality in life.<sup>90-94</sup> The possible extraterrestrial provenance of homochirality finds strong support with the discovery of an enantiomeric excess of  $\alpha$ -amino acids in Murchison meteorite.<sup>95</sup> In order to obtain unequivocal results and to minimize the risk of contamination during laboratory analysis,<sup>96-98</sup> *in situ* measurements are the only way to get unaltered samples.<sup>99</sup>

Amino acids are usually derivatized according to the procedure illustrated in figure 1.14, which involves the formation of an alkyl ester ( $R_1 = \text{methyl-}, \text{ethyl-}$  or *isopropyl-*) followed by the acylation of the amino group ( $R_2 = \text{trifluoroacetyl-}, \text{pentafluoropropionyl-}$  or *heptafluorobutanoyl-*).

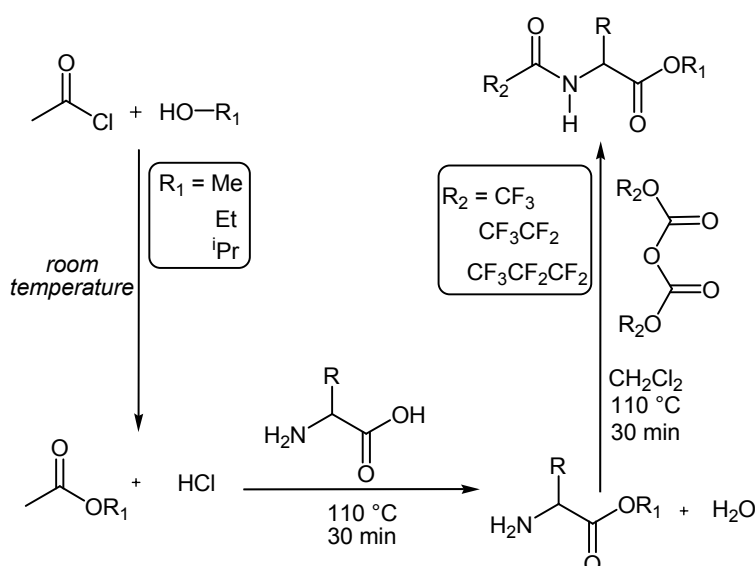


**Figure 1.14.** Sequential derivatization procedure for amino acids.

For amino acids derivatives, Chirasil-Val (*N*-propanoyl-*L*-valine-*tert*-butylamide linked to a polysiloxane matrix)<sup>72-73</sup> is the most thoroughly studied chiral selectors. It is capable of

separating all proteinogenic amino acid enantiomers in 25 minutes.<sup>100</sup> However, the enantiomers of proline are incompletely resolved.

Subsequently, different modified cyclodextrins have been used for the separation of amino acids. Among these are: Lipodex E (octakis(2,6-di-*O*-*n*-pentyl-3-*O*-butanoyl)- $\gamma$ -cyclodextrin),<sup>100</sup> heptakis(2,3-di-*O*-acetyl-6-*O*-*tert*-butyldimethylsilyl)- $\beta$ -cyclodextrin, heptakis(2,3-di-*O*-butanoyl-6-*O*-*tert*-butyldimethylsilyl)- $\beta$ -cyclodextrin, octakis(2,3-di-*O*-butyl-6-*O*-*tert*-butyldimethylsilyl)- $\gamma$ -cyclodextrin, octakis(2,6-di-*O*-*n*-pentyl-6-*O*-trifluoroacetyl)- $\gamma$ -cyclodextrin as well as many other CDs.<sup>101</sup> The enantioselectivity towards the amino acid derivatives is found to be dependent on the cavity size of the cyclodextrins and the nature of the functional groups on the 2-, 3- or 6-position. Differences in the residue bonded to the stereogenic carbon atom of the amino acids (R, figure 1.13), but also the nature of the derivatives, the ester group (R<sub>1</sub>, figure 1.14) and the perfluoroacyl group (R<sub>2</sub>, figure 1.14), are important in determining the enantioselectivity of the system. All these parameters have scarcely been rationalized in order to define a reasonable mechanism for the enantiorecognition of amino acid derivatives on cyclodextrin selectors.

#### *Chiral saturated hydrocarbons*

Apart from amino acids, various aliphatic hydrocarbons have also been detected in samples of meteorites (CI1 and CM2 chondrites) and their abundance in the interstellar medium is established. The formation of aliphatic hydrocarbons in the interstellar medium and in meteorites is still a subject of debate.<sup>102</sup> A Fischer-Tropsch (FTT) process was suggested, as well as interstellar photoreactions *via* alkyl radicals and the decomposition of hydrogen cyanide polymeric structures. In this context the biotic *versus* abiotic generation of chiral hydrocarbons was recently discussed.<sup>98</sup> Separation of enantiomers of chiral saturated hydrocarbons is a challenging problem since these molecules lack functional groups susceptible to derivatization into diastereomers which then could be easily separated by simple achiral chromatographic methods or differentiated by NMR techniques. Thus, the direct enantioseparation is a prerequisite for these compounds. For 20 years the enantiomeric separations of different tetraalkylmethanes, R<sub>1</sub>R<sub>2</sub>R<sub>3</sub>R<sub>4</sub> (R = alkyl) has been pursued. 3-Methylhexane (the smallest aliphatic hydrocarbon) was quantitatively separated into its enantiomers by a gas chromatographic method using a 50 m glass capillary column<sup>103</sup> coated with undiluted octakis(2,3-di-*O*-*n*-pentyl-6-*O*-methyl)- $\gamma$ -cyclodextrin. No significant improvements on the gas chromatographic enantioseparation of chiral saturated hydrocarbons

have been reported, with the only exception of the separation of 3-methylheptane and some homologues on permethylated  $\beta$ -cyclodextrin obtained by Meierhenrich *et al.* (figure 1.15).<sup>104</sup>

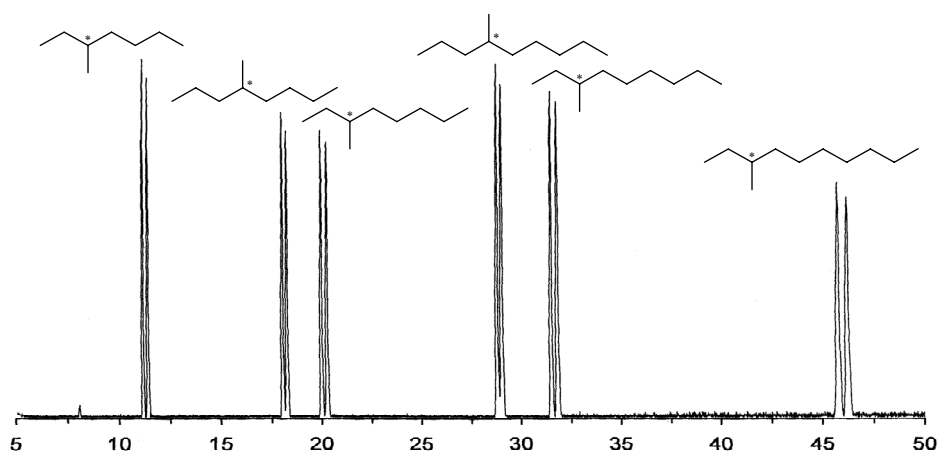


**Figure 1.15.** Gas chromatogram of resolved enantiomers of 3-methylheptane, 4-methyloctane, 3-methyloctane, 4-methylnonane, 3-methylnonane and 3-methyldecane separated on a capillary column coated with  $\beta$ -Chirasil-Dex. Column: 25 m x 0.25 mm (i.d.), film thickness 0.25  $\mu$ m. Split injection 1:50 at injector temperature of 230  $^{\circ}$ C, 1.3 mL/min constant flow of He as carrier gas, oven temperature program: 3 min 35  $^{\circ}$ C, 1  $^{\circ}$ C/min to 70  $^{\circ}$ C.<sup>104</sup>

#### *Halogenomethanes and chlorinated/fluorinated ethers (inhalation anaesthetics)*

Another difficult task for the CD-CSPs is the enantioseparation of five-atomic chiral molecules such as chlorofluorobromomethane (CHFCIBr) and chlorofluoroiodomethane (CHFCII), again due to the lack of a suitable functionality. Such molecules are of interest for parity violation (PV) measurements.<sup>105</sup> Parity violation energy differences has been suggested as the force driving the evolution of homochirality in terrestrial biopolymers ( the nearly exclusive selection of *L*-amino acids and *D*-monosaccharides) and remains a most controversial issue.<sup>106-108</sup> Recently, the synthesis of enantiomerically enriched CHFCII has been characterize by its gas chromatographic separation on octakis(3-*O*-butanoyl-2,6-di-*O*-*n*-pentyl)- $\gamma$ -cyclodextrin (CD8).<sup>109</sup> In a previous work the same CSP was applied for the enantioseparation of CHFCIBr.<sup>110</sup>

The inhalation anaesthetics shown in figure 1.16 contain a chiral center in a molecule that was obviously introduced unintentionally. Although such haloether anaesthetics are synthesized as racemic mixtures,<sup>111-114</sup> some progress has been made toward the synthesis of enantiomerically enriched materials. Thus it became important to monitor the enantiomeric purity of these materials. The enantioseparation of the anaesthetics desflurane, isoflurane,



enflurane and halothane has been successfully achieved on octakis(2,6-di-*O*-*n*-pentyl-3-*O*-butanoyl)- $\gamma$ -cyclodextrin (CD8) (Lipodex E) (figure 1.17).<sup>115</sup>

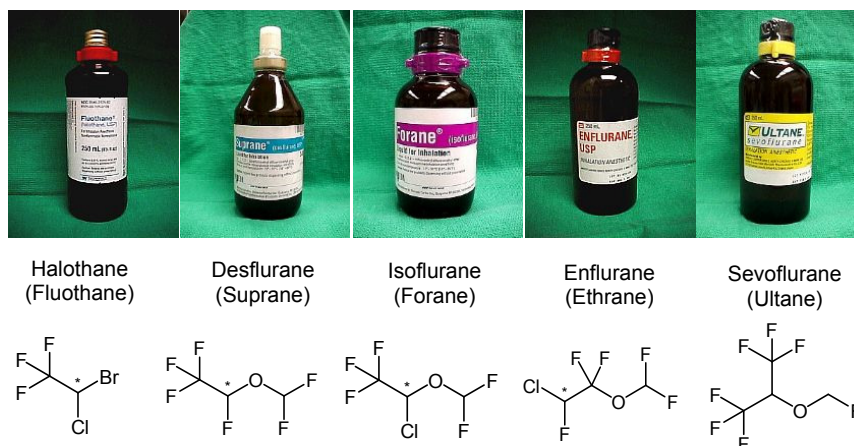


**Figure 1.16.** Structures of chiral halothane, desflurane, isoflurane, enflurane and achiral sevoflurane.

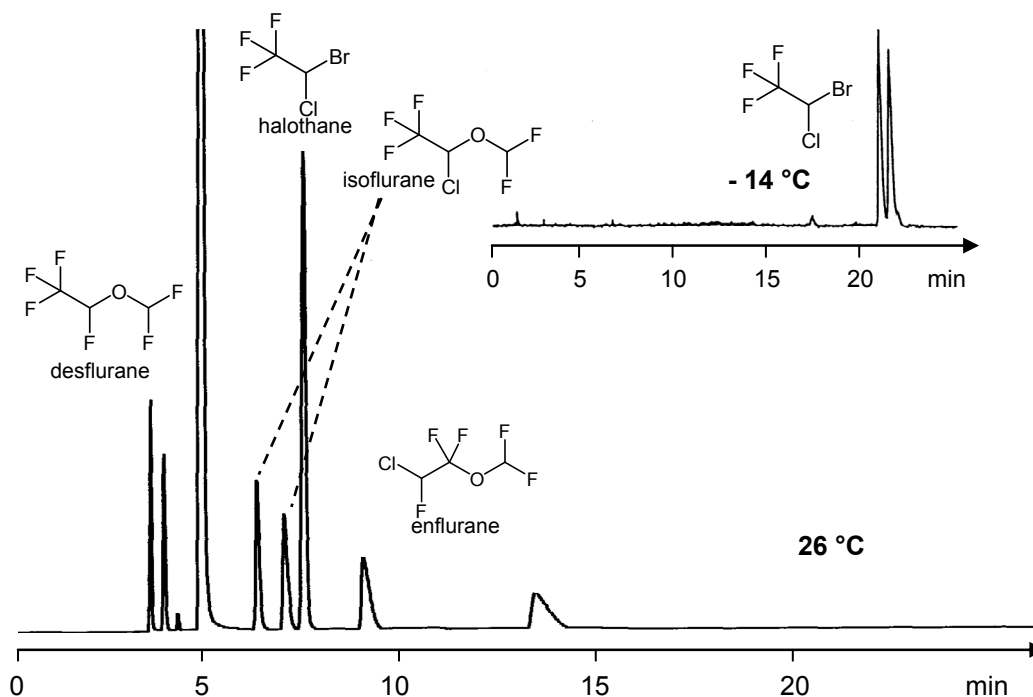


**Figure 1.17.** Gas-chromatographic enantioseparation of racemic desflurane, enflurane, isoflurane and halothane. Fused silica capillary column (25 m x 0.25 mm i.d.) coated with octakis(2,6-di-*O*-*n*-pentyl-3-*O*-butanoyl)- $\gamma$ -cyclodextrin in PS 255 (10 % w/w), film thickness 0.25  $\mu$ m, 35 kPa H<sub>2</sub>. Oven temperature 26 °C for the mixture; -14 °C for halothane.<sup>110</sup>

The achiral inhalation anaesthetic sevoflurane (figure 1.16) [(1,1,1,3,3,3,-hexafluoro-2-(fluoromethoxy)]-propane was introduced in Japan in the early 1990s and since 1995 it has been approved for use in several European countries and in the USA. It shows rapid induction

and recovery and it is non-irritant to the respiratory system.<sup>116</sup> Yet sevoflurane possesses two drawbacks, namely, metabolism that releases fluoride ions and base instability which renders it chemically active in the presence of soda lime and other carbon dioxide absorbents. When achiral sevoflurane is recycled during anaesthesia in a rebreathing circuit such as low-flow and closed-circuit anaesthesia, thereby passing through a carbon dioxide absorbent, two chemical degradation products are detected in small quantities.<sup>117</sup> The major degradation product 1,1,1,3,3-pentafluoro-2-(fluoromethoxy)-propene, known as ‘compound A’, is nephrotoxic in rats due to a  $\beta$ -lyase-dependent metabolism. The second observed degradation product, 1,1,1,3,3-pentafluoro-2-(fluoromethoxy)-3-methoxypropane (‘compound B’), is formed *in situ* by the reaction of methanol and compound A, according to the mechanism known in literature.<sup>117</sup>

This chiral molecule is produced in traces and its toxicity is low. Extremely high enantioselectivity was observed in the chiral separation of ‘compound B’ on the heptakis(2,3-di-*O*-acetyl-6-*O*-*tert*-butyldimethylsilyl)- $\beta$ -cyclodextrin (CD7) ( $\alpha = 4.1$  at 30 °C)<sup>118</sup> and on octakis(3-*O*-butanoyl-2,6-di-*O*-*n*-pentyl)- $\gamma$ -cyclodextrin (CD8) (Lipodex E,  $\alpha = 10$  at 26 °C),<sup>119</sup> as shown in figure 1.18.

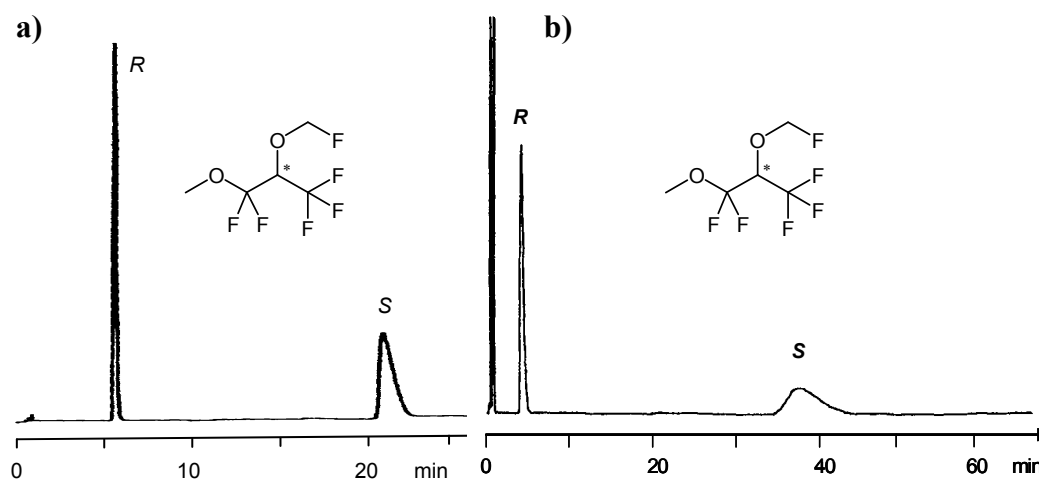


**Figure 1.18.** Gas-chromatographic enantioseparation of racemic ‘compound B’ on (a) heptakis(2,3-di-*O*-acetyl-6-*O*-*tert*-butyldimethylsilyl)- $\beta$ -cyclodextrin (CD7) 20 % in PS 86. Column: 10 m x 0.25 mm i.d., film thickness 0.25  $\mu$ m. Carrier gas 25 kPa H<sub>2</sub>; oven temperature 30 °C. On (b) octakis(2,6-di-*O*-*n*-pentyl-3-*O*-butanoyl)- $\gamma$ -cyclodextrin (CD8) (Lipodex E) 30 % in PS 255. Column: 5 m x 0.25 mm i.d., film thickness 0.25  $\mu$ m. Carrier gas 12 kPa H<sub>2</sub>; oven temperature 26 °C.<sup>118-119</sup>

Although these chiral selectors possess an extremely high enantioselectivity towards ‘compound B’, no information is yet available as to the enantiorecognition mechanism involved.

### 1.7. Enantiorecognition mechanism in gas chromatography involving modified cyclodextrins

Up to now, it is difficult to rationalize the prevalent enantiorecognition mechanism from gas-chromatographic studies. Earlier, most authors believed that the chiral recognition was solely the result of the formation of tight inclusion complexes. However, later it was found that relatively small molecules such as ( $\pm$ )-*cis*-pinane could be separated on derivatives of both  $\beta$ - as well as  $\gamma$ -CD.<sup>83,102</sup> Here and also in the case of the above mentioned enantioseparation of 3-methylhexane on octakis(2,3-di-*O-n*-pentyl-6-*O*-methyl)- $\gamma$ -CD,<sup>102</sup> it is hard to imagine the formation of an inclusion complex in its original meaning. Racemic analytes do probably enter the CD cavity but enantiorecognition is likely to take place by interactions with both the interior and the rim(s) of the CD rather than by the formation of tight complexes. The successful use of various cyclodextrin derivatives in gas chromatography should remind us that in derivatized cyclodextrins, protons involved in hydrogen bonding, which is the basis of the rigid and very well defined cyclic structure of native CDs, are no longer present. As a result CD derivatives take the form of a rather “flexible, elliptically distorted torus” as illustrated in figure 1.19.<sup>82</sup>

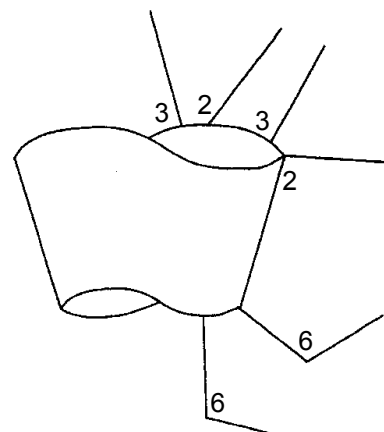


**Figure 1.19.** The elliptically distorted torus of derivatized  $\beta$ -cyclodextrin.<sup>82</sup>

The length and direction of the bonds within glucopyranose units differs from unit to unit and thereby there is a broad range of sites available for interaction with analytes. Several gas chromatographic applications of cyclodextrin derivatives suggest that different points of interaction are involved and this multi-modal process is still not very well understood.<sup>76</sup> Therefore, the proposed application of linear dextrin derivatives (Gn) as CSPs for enantioselective gas chromatography in the present work (chapter IV), represents a new tool to evaluate the role of the cavity for the enantiorecognition process by cyclodextrins. It will be pointed out that outside enantioselective forces may complement or even override the classical inclusion interaction.



## Chapter II

### Results and discussion: Part I

#### Synthesis and characterization of cyclic and acyclic dextrin derivatives



## 2.1. Introduction

Methods for the modification of cyclodextrins can be divided into three categories: (1) the “clever” method, where the specific properties of the cyclodextrins are exploited to get the desired product by the shortest possible route; (2) the “long” method, where a series of protection and deprotection steps have taken place in order to selectively substitute at the positions which would otherwise not be accessible; (3) the “sledgehammer” method, where the cyclodextrin is indiscriminately reacted to give a mixture of products, after which the desired product is painstakingly separated from by-products (usually other isomers and/or homologues) by chromatographic methods.<sup>9</sup> An example of the first category is the synthesis of 2-*O*-tosyl- $\beta$ -cyclodextrin by reacting cyclodextrin with *m*-nitrophenyl tosylate.<sup>120</sup> An example of the second category is the alkylation of the primary side,<sup>121</sup> which involves in sequence (1) protection of the primary sides with silyl groups, (2) protection of the secondary side with acetyl groups, (3) desilylation of the primary side, (4) reaction of the primary hydroxyl group with an appropriate alkyl halide, and finally (5) deprotection of the secondary side to give the desired product. In this strategy, each reaction is carefully chosen to give high yields. Furthermore, the product should be easily separable and purifiable. Yet, the overall yield of the final product is usually small. An example of the third category is ditosylation of the secondary side of cyclodextrin.<sup>122</sup> In this case, tosyl chloride is reacted with cyclodextrin to give a mixture of products which is then separated by reversed-phase HPLC. Given the choice between the three categories, one would always choose the first strategy because it is most productive and least difficult; however, a method of the first category is not always available when a modified cyclodextrin with a specific structure is needed. For instance, the well known persubstituted  $\beta$ -cyclodextrin carrying *tert*-butyldimethylsilyl groups on the primary side and the acetyl groups on the secondary side can, to date, only be synthesized by the multistep procedure (second method) and in this work the extension of this method to linear dextrans, in order to obtain the analogous mixed acetylated/silylated derivatives, is described.

The procedure for the preparation of the mixed acetyl/TBDMS derivatives is easy and efficient and the final purification is rapid. Such a synthesis stands in contrast to the preparation of other well known cyclodextrin derivatives such as Lipodex E [octakis(2,6-di-*O*-*n*-pentyl-3-*O*-butanoyl)- $\gamma$ -cyclodextrin], where the yield of the first reaction step (pentylation) is dramatically reduced by over-pentylation (yield ~ 25 %). Also the yield in the second step (acylation) step (~ 25 %) is depressed by the formation of a stable and undesired

complex between the final octakis(3-*O*-butanoyl-2,6-di-*O*-pentyl-)- $\gamma$ -cyclodextrin and the butyric acid formed in the reaction mixture.<sup>123, 75b</sup>

The practical and easy procedure of *tert*-butyldimethylsilylation followed by acetylation has been applied in this work to linear dextrans comprising either eight (G8), seven (G7) and three (G3) *D*-glucose units and to single *D*- and *L*-glucose (G1) in order to gain high yields and enable fast purification.

## 2.2. Linear dextrans derived from cyclodextrins

The synthesis of native linear maltoheptaose was carried out by Jicsinsky *et al.*,<sup>124</sup> and analogously by Farkas *et al.*<sup>125</sup> This procedure involves the one-pot acetylation and subsequent acetolysis of acetylated CD6, CD7 or CD8 in order to obtain the corresponding peracetylated maltohexaose (G6), maltoheptaose (G7) or maltooctaose (G8) respectively. Thus, according to the general procedure, FeCl<sub>3</sub>·6H<sub>2</sub>O is suspended in acetic anhydride and CD6, CD7 or CD8 is added in small portions under cooling (< 40 °C), and the reaction mixture is stirred vigorously for 2.5 h. The reaction temperature is raised to 70 °C and the mixture is stirred for another 3.5 h. The mixture is poured into water, the resulting crystalline product is filtered off, washed with water, dried and crystallized three times from EtOH to obtain (as in the case of CD7) the peracetylated maltoheptaose (G7) with a 9:1 ratio of the  $\alpha$  and  $\beta$  anomers. In order to synthesize the underivatized maltooligomers, the cleavage of the acetyl groups is carried out according to the standard procedure which involves the addition of a catalytic amount of MeONa (pH ca. 8) to a solution of the peracetylated maltooligomers in MeOH; the mixture is stirred for 24 h and, after neutralization with Amberlite IR 120 (H<sup>+</sup>) resin, the mixture is filtered and evaporated.

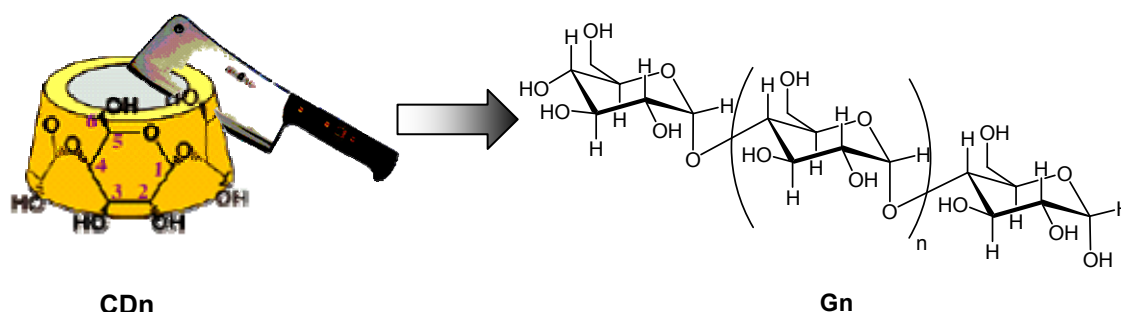


**Figure 2.1.** Schematic representation of the linear maltooligomer consisting of  $n$  glucose units. The native cyclodextrin (CD6, CD7 or CD8) is “cut” to obtain the corresponding linear system; for further details see reference 124. In this figure only the  $\alpha$ -anomer is shown.



The resulting foam is dissolved in a small amount of water and filtered on SM-113 (0.1  $\mu\text{m}$ ) membrane filter and then is lyophilised to obtain the native maltooligomers in 80-90% yield (figure 2.1).<sup>124</sup>

### 2.3. Synthesis and characterization of acetyl/TBDMS cyclic and acyclic dextrins by NMR spectroscopy

To characterize the cyclic and acyclic systems by NMR (in addition to elemental analysis and mass spectroscopy), the spectra of two known derivatives of the maltooligomers<sup>126c</sup> were taken into account in order to explain the different steps necessary to overcome the difficulties of the characterization which concerns especially the linear systems. Assignment of the various signals of the per-*O*-acetylated- $\beta$ -cyclodextrin (CD7) and per-*O*-acetylated maltoheptaose (G7) (figure 2.2) is simpler than of the acetylated/TBDMS derivatives which have been synthesized in this work, and the characterization of these two systems represents a significant aid for the elucidation of the structure of the multifunctional dextrins (acetyl/TBDMS).

In the case of the peracetylated CD7 (**1**), the  $C_7$ -symmetry is retained after the acetylation, so that only one set of signals is generated for the seven glucose units which form the macrocycle (figure 2.3). The same trend is observed for the cyclodextrins with different functional groups on the 2-, 3- and 6-OH sites.

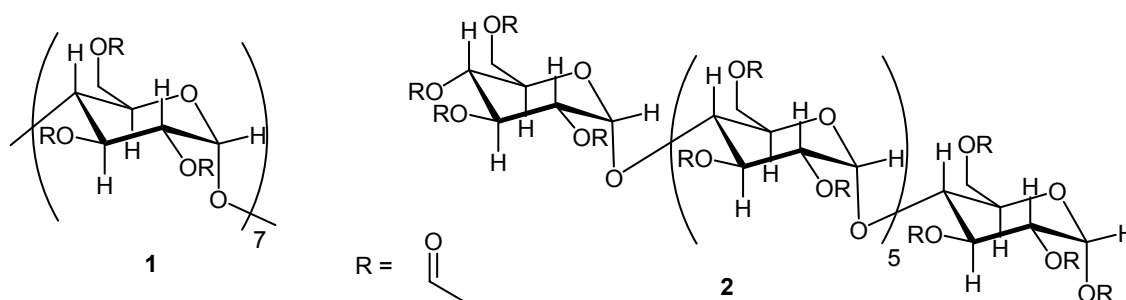


**Figure 2.2.** Structures of per-*O*-acetylated CD7 (**1**) and per-*O*-acetylated G7 (**2**).

On the contrary, in the case of the peracetylated G7 (**2**), Laignel *et al.*<sup>126c</sup> assigned the signals for the different glucose units, but the linear dextrin derivative does not allow a complete characterization for the single glucose units, as is described in the comparison shown in figure 2.4. These signals comprise the terminal  $\alpha$ -glucose unit ( $\alpha\text{-Glc}^I$ ), the glucose unit before this ( $\text{Glc}^{II}$ ), a set of the signal for three glucose units in the middle position ( $\text{Glc}_m$ ) and the last two

glucose units ( $\text{Glc}_{n-1}$  and  $\text{Glc}_n$ ), as shown in figure 2.5. The analysis started with the well separated anomeric doublets (H-1, 6.25 ppm), from which H-2 proton was assigned and from this, H-3, H-4, H-5 and H-6 for the reducing glucose end. In addition, the isolated H-4 at 5.05 ppm is assigned to the non-reducing end ( $\text{Glc}_n$ ) with its terminal acetyl ester on C-4''. These data are summed up in the table 2.1.

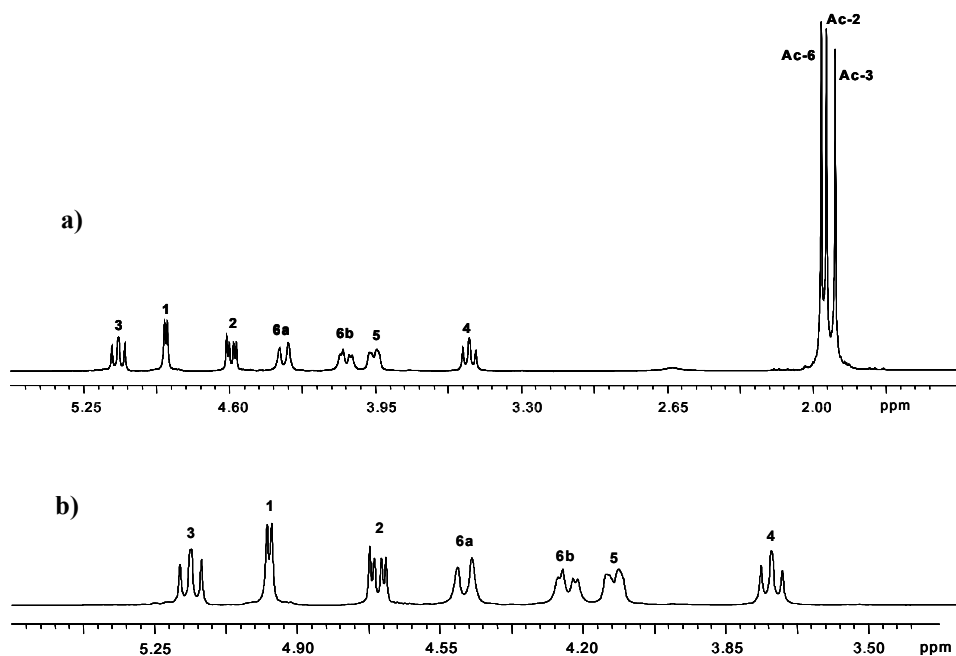


**Figure 2.3.**  $^1\text{H}$  NMR spectrum of peracetylated CD7 (**1**) (300 MHz,  $\text{CDCl}_3$ , 25 °C): (a) complete spectrum; (b) spectral region of glucose ring protons.

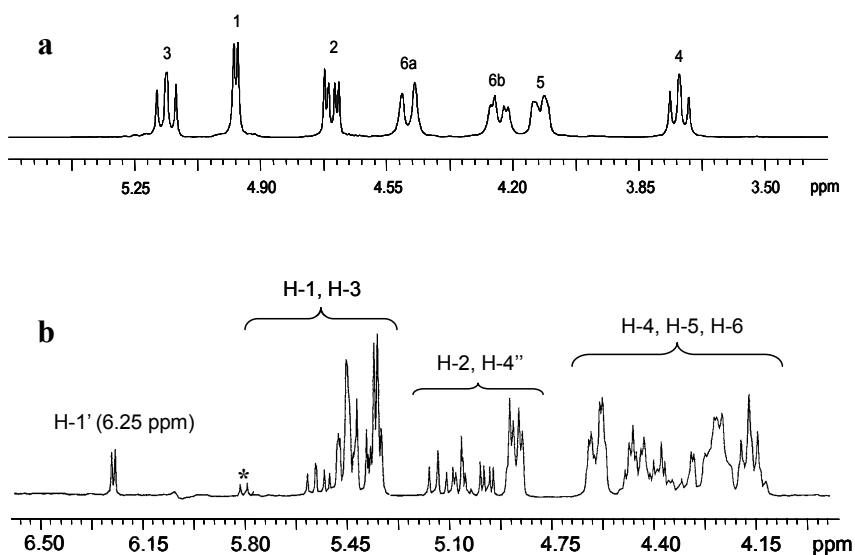


**Figure 2.4.** (a)  $^1\text{H}$  NMR spectrum regions of per-*O*-acetylated CD7 (**1**) (300 MHz,  $\text{CDCl}_3$ , 25 °C) and (b) per-*O*-acetylated G7 (**2**) (300 MHz,  $\text{CDCl}_3$ , 50 °C); (\*) H-1 for the  $\beta$ -anomer of **2**.

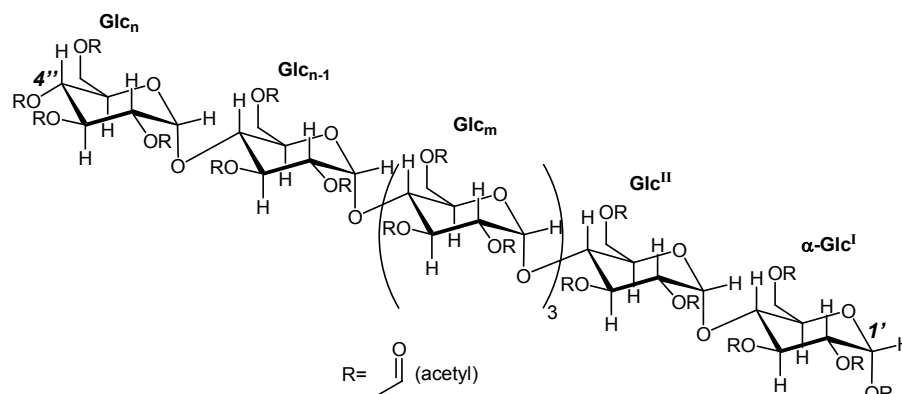


**Figure 2.5.** Assignment of the glucose units for the peracetylated maltoheptaose according to the chemical shifts summed up in table 2.1.

**Table 2.1.**  $^1\text{H}$  NMR data (ppm) for per-*O*-acetylated maltoheptaose **2** (protons of acetyl groups are omitted).

Protons	Residue				
	$\alpha\text{-Glc}^{\text{I}}$	$\text{Glc}^{\text{II}}$	$\text{Glc}_m$	$\text{Glc}_{n-1}$	$\text{Glc}_n$
H-1	<b>6.25</b>	5.31	5.28	5.27	5.36
H-2	4.96	4.75	4.75	4.75	4.86
H-3	5.50	5.42	5.39	5.38	5.35
H-4	4.00	3.90	3.90	3.89	<b>5.05</b>
H-5	4.10	4.02	4.00	3.96	3.96
H-6a	4.47	4.46	4.46	4.47	4.23
H-6b	4.30	4.32	4.32	4.21	4.09

Thus, by NMR spectroscopic two-dimensional analysis of the G7 (**2**), Laignel *et al.*<sup>126c</sup> have been able to assign the overlapped signals for most of the glucose units which form the linear dextrin, especially the terminal C-1' and C-4''.

Unfortunately, no further details are given about the ratio of the  $\alpha/\beta$  anomers, even if the doublet centered at 5.80 ppm in the case of the linear oligosaccharides can be assigned to an H-1 with  $J_{1,2}$  typical of a diaxial proton pair arrangement. Indicative of the strong predominance of the  $\alpha$  anomer, Laignel *et al.*<sup>126c</sup> did not make a characterization of this minor species in this work.<sup>126c</sup> Because of the strong predominance ( $\sim 95\%$ ) of the  $\alpha$  anomer, the authors took into account only this anomer.

In the present work, some more crowded systems are produced by the acyclic dextrins with the acetyl groups on the secondary OH-sites and the *tert*-butyldimethylsilyl groups on the primary OH-sites. In the subsequent paragraphs, when it is not specified, only the main

species is characterized. A direct analysis to confirm also the degree of the derivatization is to calculate (by integration of the signals) the ratio between the acetyl groups and the protons signal of the glucose unit. Moreover, the characterization for all the glucose units is focused on spectral regions for the H-1 protons, H-2, H-3, H-4, H-5 and H-6 protons.

### 2.3.1. Heptakis(2,3-di-*O*-acetyl-6-*O*-*tert*-butyldimethylsilyl)- $\beta$ -cyclodextrin (5)

The selective acetylation of 2- and 3-position of cyclodextrin is achieved through the “key intermediate” 6-*O*-*tert*-butyldimethylsilyl ether, which can be applied to the CD6, CD7 and CD8, to obtain the intermediates **3a-c**.<sup>127</sup> The desired compounds were obtained after complete acetylation of the 2- and 3-sites with acetic anhydride in pyridine at 100 °C for four hours (figure 2.6).

This compound shows a spectrum with all signals well separated, thus allowing a complete characterization (figure 2.7). The gCOSY technique was used in order to get information about the coupling in the glucose ring (figure 2.8).

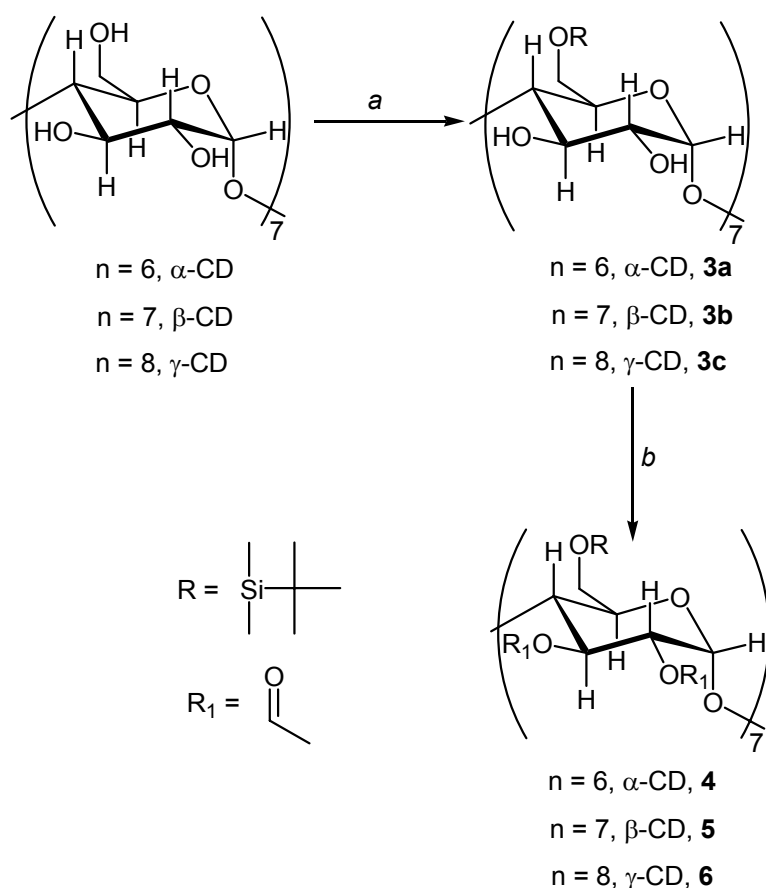


**Figure 2.6.** Synthesis of mixed acetyl/TBDMS cyclodextrins; (a) TBDMSCl, pyridine, r.t.; (b) Ac<sub>2</sub>O, pyridine, 100 °C.

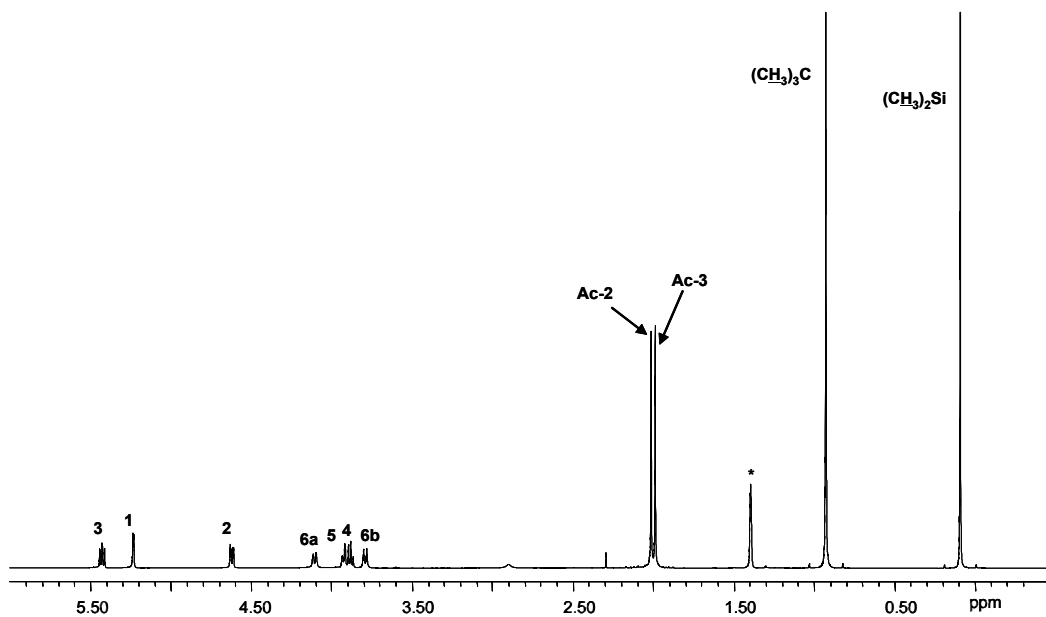


**Figure 2.7.**  $^1\text{H-NMR}$  spectrum of heptakis(2,3-di-*O*-acetyl-6-*O*-*tert*-butyldimethylsilyl)- $\beta$ -cyclodextrin (CD7) **5** (600 MHz,  $\text{C}_6\text{D}_{12}$ , 25 °C).

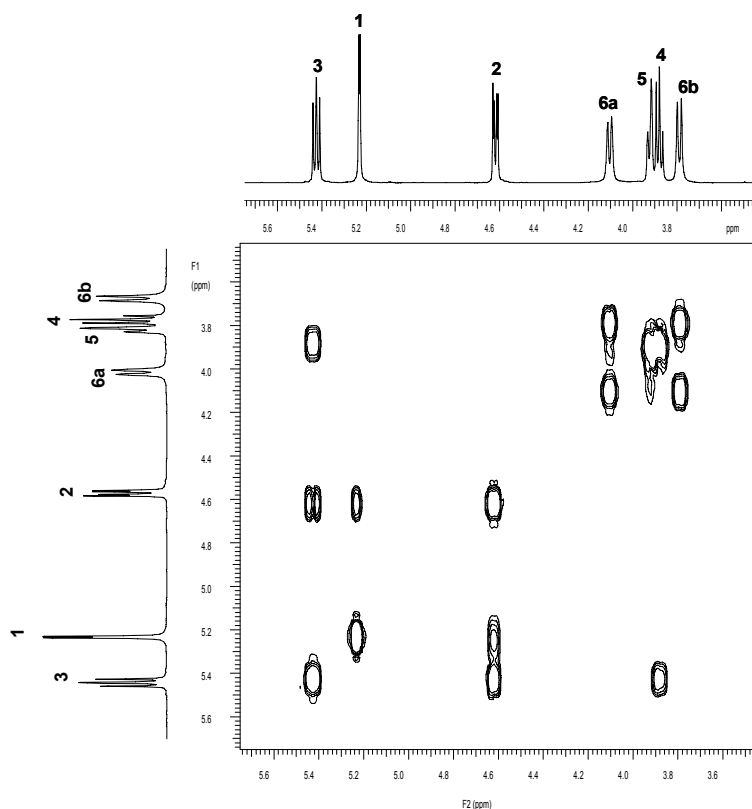


**Figure 2.8.** gCOSY map ( $\text{C}_6\text{D}_{12}$ , 25 °C) of CD7 (**5**).

The gHMQC (figure 2.9) and gHSQC (figure 2.10) allowed to characterize especially the acetyl groups, through long-range coupling with the proton in 2- and 3-positions. Thus, the

carbon atom of the carbonyl at 168.9 ppm is assigned to the acetyl group on the 2-site, while the carbonyl at 169.3 ppm to the acetyl on the 3-site.

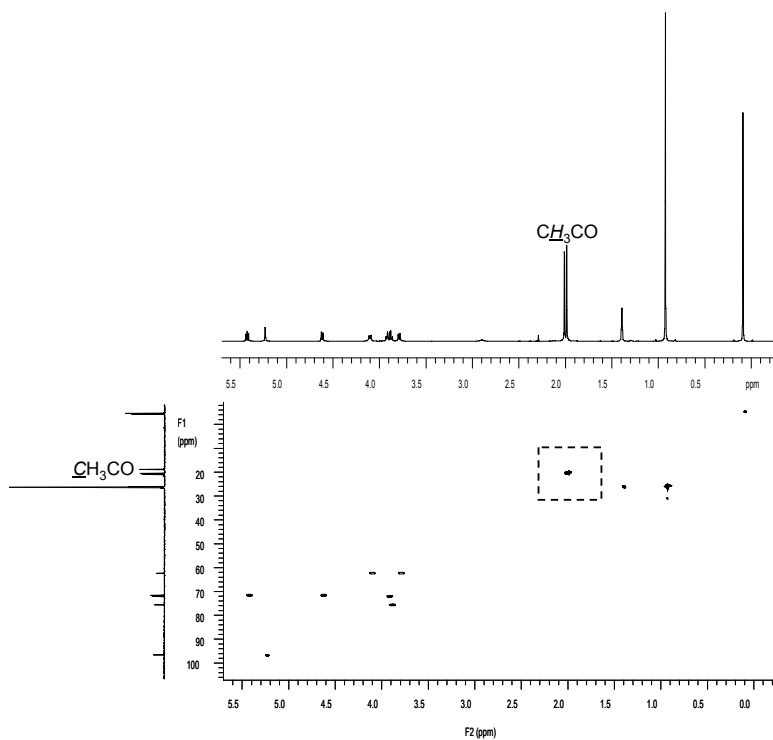


**Figure 2.9.** gHSQC of CD7 (**5**) ( $C_6D_{12}$ , 25 °C).

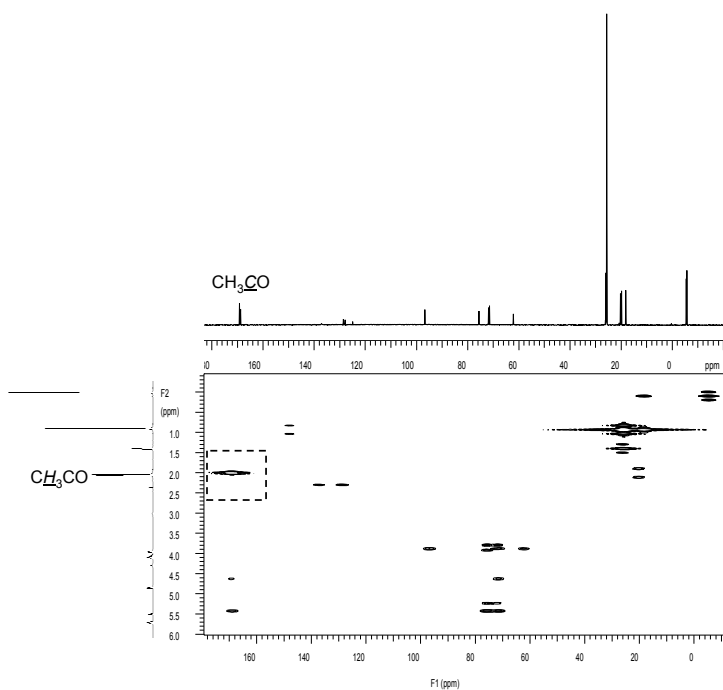


**Figure 2.10.** gHMBC of CD7 (**5**) ( $C_6D_{12}$ , 25 °C).

Analogously, the carbon atom of the methyl at 20 ppm is assigned to the 3-site and that at 20.3 ppm to the methyl at the 2-site. Both of these correlations were determined on the basis of the hetero-coupling with the protons at 1.99 and 2.01 ppm, respectively. For the complete assignment of the protons, see experimental section.

In addition to the above mentioned characterization for CD7 (**5**), complete assignment of the protons of the CD6 (**4**) and CD8 (**6**) has been carried out by one- and two-dimensional analysis (see experimental section).

In order to evaluate the influence of the nature of the functional group on the 2- and 3-sites, especially for the high enantioseparation of ‘compound B’ (see chapter I for the structure), another two  $\beta$ -cyclodextrin derivatives were synthesized, bearing the methyl and *n*-pentyl groups respectively on the wider rim of the macrocycle and the *tert*-butyldimethylsilyl bulky on the 6-sites (figure 2.11). For the details about synthesis and characterization of heptakis(2,3-di-*O*-methyl-6-*O*-*tert*-butyldimethylsilyl)- $\beta$ -cyclodextrin (**7**) and heptakis(2,3-di-*O*-*n*-pentyl-6-*O*-*tert*-butyldimethylsilyl)- $\beta$ -cyclodextrin (**8**), see reference 121.

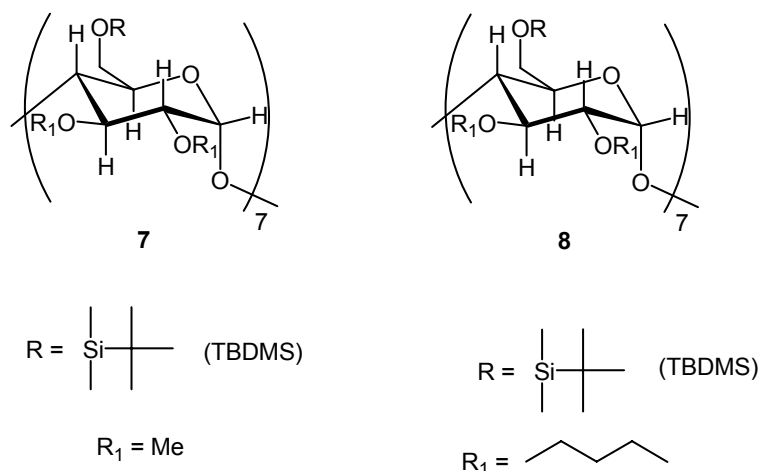


**Figure 2.11.** Structures of heptakis(2,3-di-*O*-methyl-6-*O*-*tert*-butyldimethylsilyl)- $\beta$ -cyclodextrin (**7**) and heptakis(2,3-di-*O*-*n*-pentyl-6-*O*-*tert*-butyldimethylsilyl)- $\beta$ -cyclodextrin (**8**).

### 2.3.2. Heptakis[(2,3-di-*O*,4''-*O*)-acetyl-(1'-*O*,6-*O*)-*tert*-butyldimethylsilyl]-maltoheptaose (**10**)

In the following sections the multistep procedure for the synthesis of dextrin derivatives is applied to the acyclic oligosaccharides, in order to obtain linear analogues of the well known cyclodextrins. As already mentioned above, only the spectral regions of selected protons will be shown in the following discussion of the characterization by NMR. The only complication in the preparation of G7 (**10**) (figure 2.12) is the presence of a mixture of two compounds, one

with an acetyl group on the anomeric center C1 and the other with a *tert*-butyldimethylsilyl group on the same terminal reducing end, due to the fact that in the first step of synthesis an excess of TBDMSCl is used.

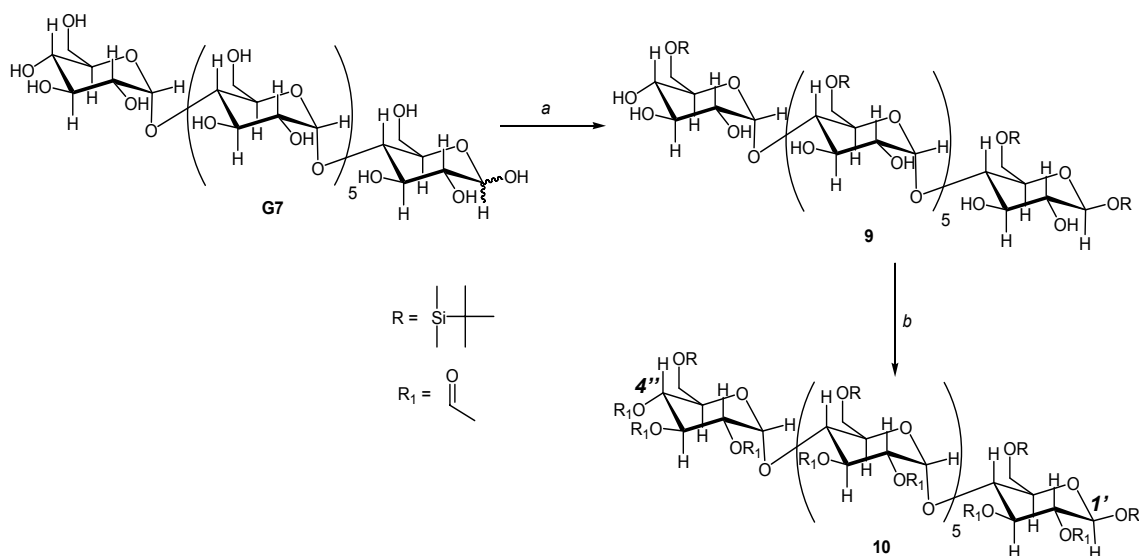


**Figure 2.12.** (a) TBDMSCl, pyridine, r.t.; (b) Ac<sub>2</sub>O, pyridine, 100 °C.

This ‘oversilylation’ is better demonstrated after the second step, the acetylation, which allows separation of both compounds by column chromatography. Due to the excess of the derivative with eight *tert*-butyldimethylsilyl groups (95:5) only this derivative will be characterized.

Because the presence of either a TBDMS group or an acetyl group on the reducing end C-1' has no influence on the enantioselectivity of the derivatives when applied as a chiral stationary phase for gas chromatography, no further details will be given for the minor species (i.e. with the terminal acetyl group on C-1'). Comparison of the theoretical (1:2.67) and experimental (1:2.64) ratio of acetyl/TBDMS protons groups confirms that eight acetyl groups are located at the primary hydroxyl groups (including the reducing C1' end) and 15 acetyl groups on the secondary hydroxyl groups (figure 2.13).

Due to the absence of the deshielded H-1, as in the case of the peracetylated G7 (2), it is concluded that on the anomeric C-1 is occupied by TBDMS (ether) rather than by an ester group (figure 2.13). Moreover it is possible to distinguish (and quantify by integration) three spectral regions related with *a*) protons H-1/H-3, *b*) protons H-2/H-4'' and *c*) H-4/H-5/H-6 protons (figure 2.14).



Integration of the different spectral regions confirmed the presence of an isolated proton H-4'' which is superimposed on the spectral region of H-2 protons but completely deshielded in comparison to the other H-4 protons of the remaining six glucose units.

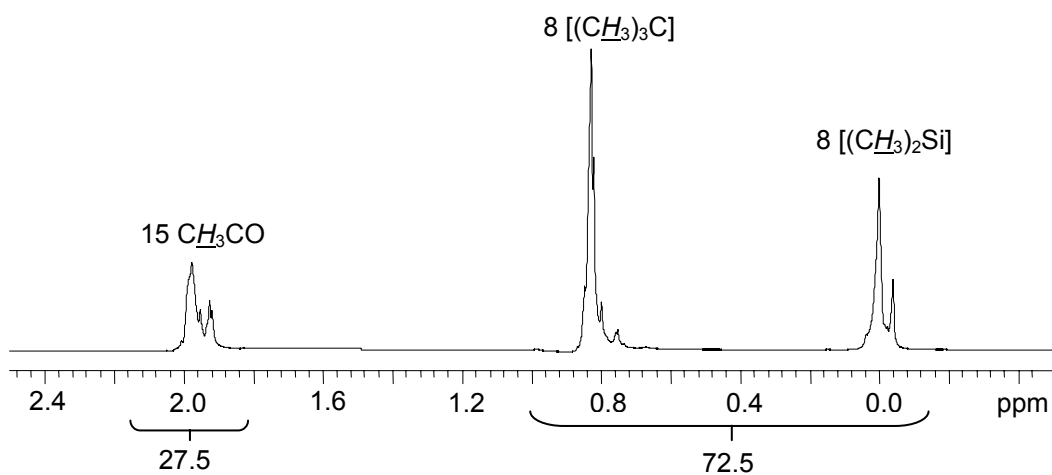


**Figure 2.13.**  $^1\text{H-NMR}$  spectral region of the acetyl and TBDMS groups for G7 (**10**) (400 MHz,  $\text{CDCl}_3$ , 25 °C).

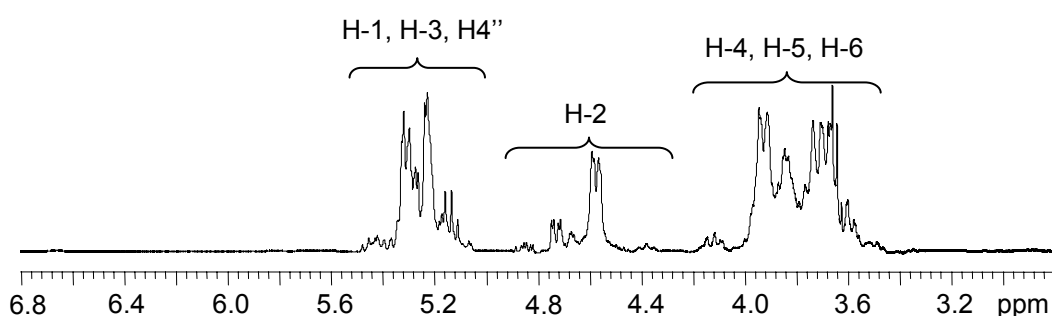


**Figure 2.14.**  $^1\text{H-NMR}$  spectral region of the protons of the glucose units for G7 (**10**) (400 MHz,  $\text{CDCl}_3$ , 25 °C). No isolated H-1 protons are observed at ca. 6 ppm.

For further information about the characterization of G7 (**10**), see experimental section. By column chromatography (toluene/*n*-hexane/ethanol, 5:4:1) it was possible to isolate also the minor species with seven *tert*-butyldimethylsilyl groups and 16 acetyl groups, as shown in figure 2.14. The theoretical ratio (1:2.19) of the *tert*-butyldimethylsilyl and acetyl groups is in very good agreement with the experimental ratio (1:2.15).

As with the main species, the different spectral regions of the minor product were determined by one- and two-dimensional NMR. In the case of compound **10**, the isolated doublet of proton H-1 at 6.21 ppm confirms the presence of an acetyl group on the terminal C-1' (figures 2.15 and 2.16). It is possible to tune the ratio of the acetyl/TDBMS groups by varying the excess of the *tert*-butyldimethylsilyl chloride which is used in the first step of this synthesis, in order to obtain intermediate **9** with a different ratio suitable for different applications.

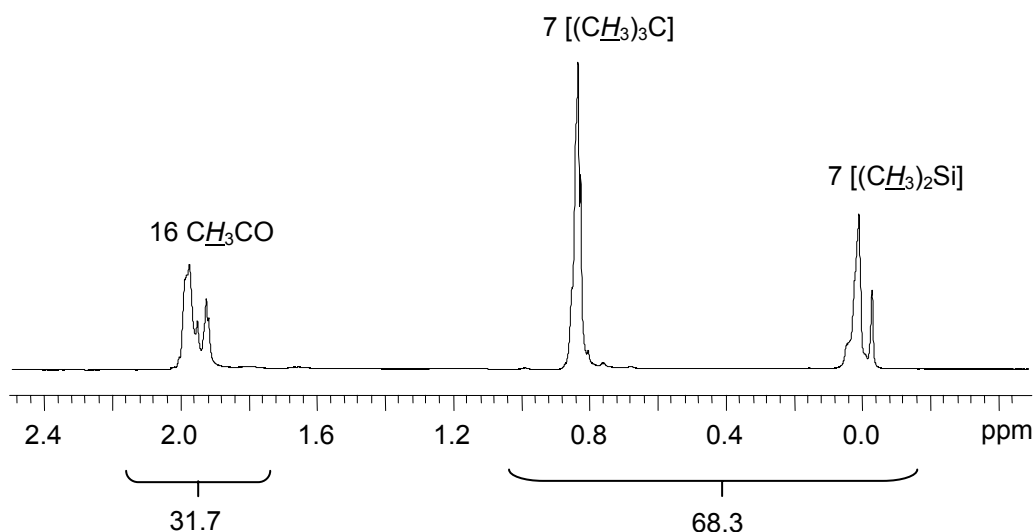


**Figure 2.15.**  $^1\text{H-NMR}$  spectral region of the acetyl and TDBMS groups for the selector **10** (400 MHz,  $\text{CDCl}_3$ , 25 °C).

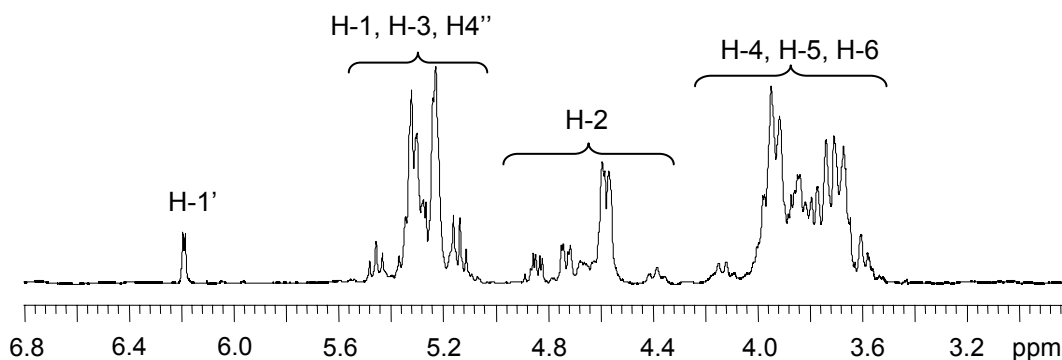


**Figure 2.16.**  $^1\text{H-NMR}$  spectral region of the protons of the glucose units for the selector G7 (**10**) (400 MHz,  $\text{CDCl}_3$ , 25 °C). An isolated H-1 proton is observed at ca. 6.21 ppm.

### 2.3.3. Octakis[(2,3-di-*O*,4''-*O*)-acetyl-(1'-*O*,6-*O*)-*tert*-butyldimethylsilyl]-maltooctaose (12)

The drawbacks encountered in the synthesis of G7 (**10**) are also observed in the preparation of the maltooctaose derivative (figure 2.17). 'Over-silylation' on the first step leads to the intermediate **11** bearing predominantly 9 and to a lesser extent 8 TBDMS ether groups. After acetylation it was possible to elucidate the final structure of G8 (**12**) (main species).

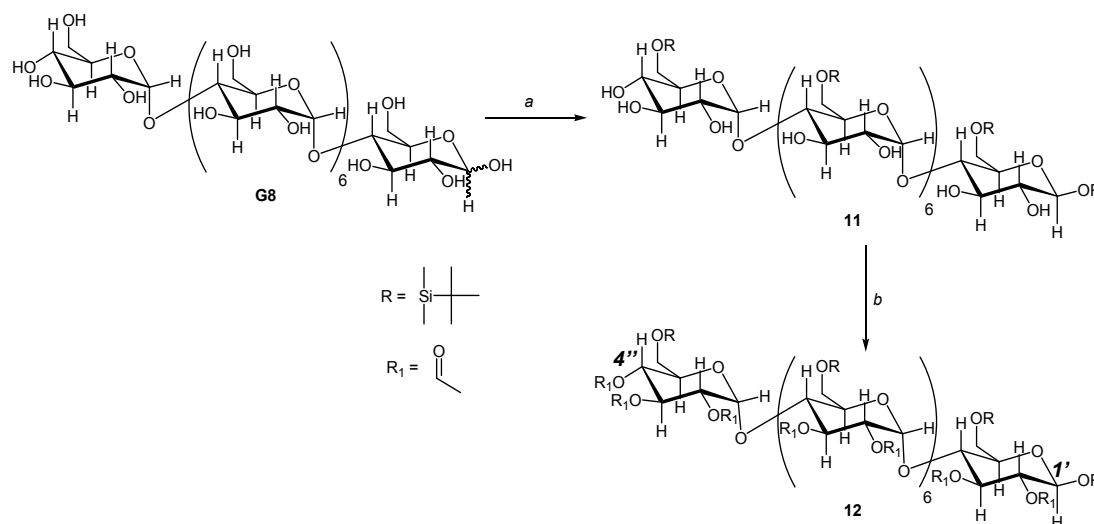


**Figure 2.17.** (a) TBDMSCl, pyridine, r.t.; (b) Ac<sub>2</sub>O, pyridine, 100 °C.

By column chromatography (toluene/*n*-hexane/ethanol, 6:3:1) the main species bearing nine TBDMS groups was isolated and characterized as described for compound G7 (**10**). For further details, see experimental section.<sup>a</sup>

### 2.3.4. Tris[(2,3-di-*O*,4''-*O*)-acetyl-(1'-*O*,6-*O*)-*tert*-butyldimethylsilyl]-maltotriose (14)

'Over-silylation' (due to the excess of TBDMSCl used for the preparation of the intermediate **13**) is a side effect also for the synthesis of the maltotriose derivative G3 (**14**). However, after the acetylation, the main species **14** characterized by four TBDMS ether groups and seven acetyl groups (figure 2.18) was isolated by column chromatography (*n*-hexane/EtOAc, 6:4). For all these derivatives, the overall yield is always quite high (more than 85 %) but the presence of two species reduced drastically the yield of the desired product.

<sup>a</sup> The  $\alpha/\beta$  ratio for the anomeric configuration was confirmed by measuring the  $J_{1,2}$  coupling constants of the 'reducing end' for the selector G3 (**14**), *D*-G1 (**16**) and *L*-G1 (**18**). Unfortunately, for the G7 (**10**) and G8 (**12**) the  $J_{1,2}$  coupling constants of the 'reducing end' could not be measured because the anomeric proton is overlapped with the anomeric protons in the region 5.0 – 5.6 ppm. However, due to the analogous reactivity of the anomeric center, the prevailing  $\beta$ -configuration for the TBDMS-ether (main species) is expected for the linear dextrans with different degrees of oligomerization.

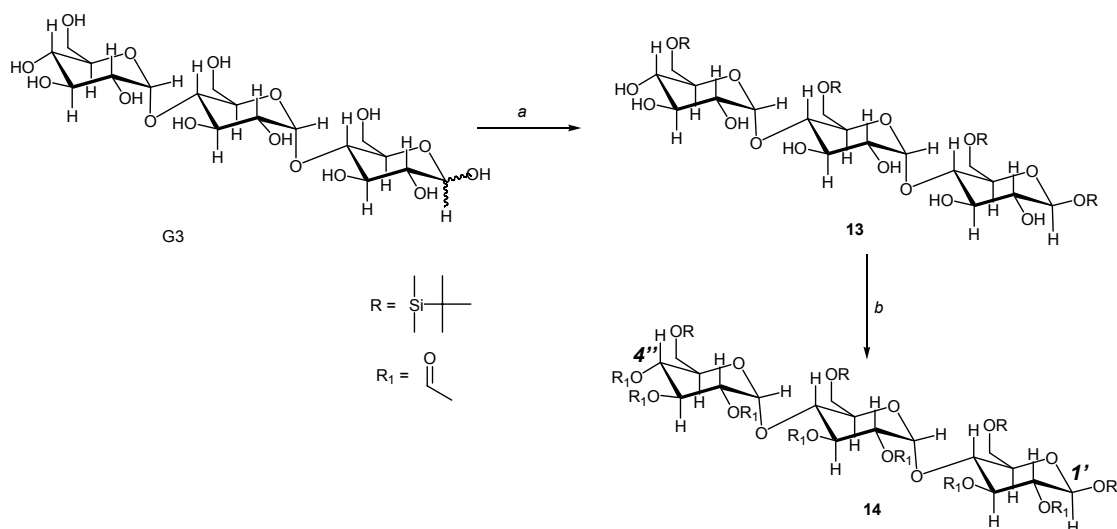


Figure 2.18. (a) TBDMSCl, pyridine, r.t.; (b) Ac<sub>2</sub>O, pyridine, 100 °C.

### 2.3.5. (2,3,4-tri-*O*-acetyl-1,6-di-*O*-*tert*-butyldimethylsilyl)-*D*-glucose (16) and (2,3,4-tri-*O*-acetyl-1,6-di-*O*-*tert*-butyldimethylsilyl)-*L*-glucose (18)

Finally, silylation followed by acetylation of *D*- and *L*-glucose led to compounds **16** and **18**, respectively, as depicted in figures 2.19 and 2.20.

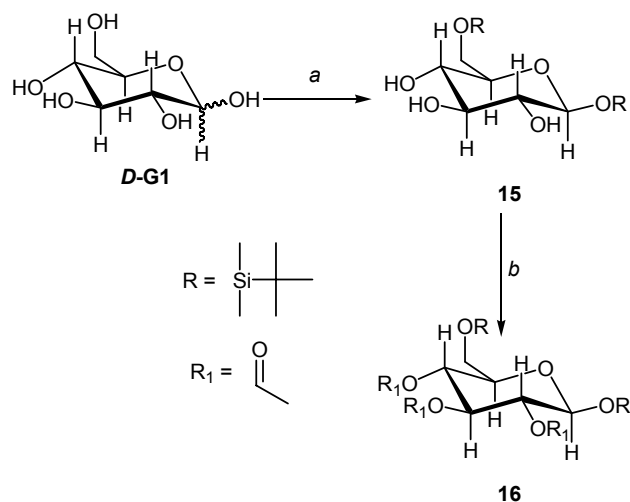
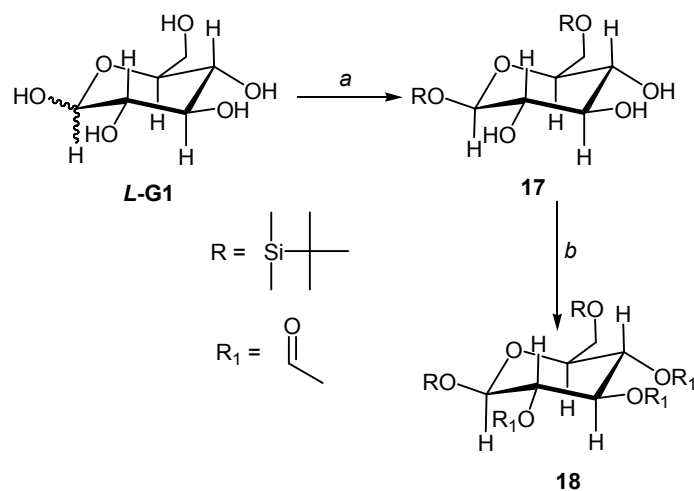


Figure 2.19. (a) TBDMSCl, pyridine, r.t.; (b) Ac<sub>2</sub>O, pyridine, 100 °C.

The first step of the reaction yields a *tert*-butyldimethylsilyl ether moiety on both C-6 and on the anomeric C-1, when applying the standard procedure which involve a slight excess of

TBDMSCl. After the acetylation of the OH-2, OH-3 and OH-4, the desired 1,6-di-*O-tert*-butyldimethylsilyl-2,3,4-tri-*O*-acetyl)- $\alpha$ -*D*-glucose (**16**) and (1,6-di-*O-tert*-butyldimethylsilyl-2,3,4-tri-*O*-acetyl)- $\alpha$ -*L*-glucose (**18**) were obtained.



**Figure 2.20.** (a) TBDMSCl, pyridine, r.t.; (b) Ac<sub>2</sub>O, pyridine, 100 °C.

#### 2.4. Synthesis of per-*O*-methyl-*D*-maltoheptaose (**19**)

A versatile cyclodextrin derivative applied as chiral selector in enantioselective GC is the permethylated  $\beta$ -cyclodextrin,<sup>73e</sup> which was synthesized according to an established procedure for the methylation of cyclodextrins. Methylation of hydroxyl groups is commonly carried out using strong bases such as sodium hydride or potassium *tert*-butoxide in dipolar aprotic solvents. Using methyl iodide in *N,N*-dimethylformamide, the reaction rate increases in the order silver oxide < barium hydroxide < sodium hydride as the basic reagent, but complete methylation is not achieved.<sup>128</sup>

Because of the different reactivity of the cyclic and acyclic dextrans, the standard procedure for the methylation of cyclodextrin with sodium hydride/methyl iodide in *N,N*-dimethylformamide could not be applied. These reagents caused the degradation of the native maltoheptaose (G7). As is known for the permethylation of the *D*-glucose,<sup>128</sup> a larger excess of sodium hydroxide (figure 2.21) and an optimal base/solvent ratio (2-3 mmol of sodium hydroxide per mL of methyl sulfoxide, figure 2.22), as well as an optimum ratio of methyl iodide/replaceable H (which is usually 3-5 mol of methyl iodide per mol of replaceable H, figure 2.23) leads to a complete methylation in a minimum of time.

Based on the results obtained for glucose (G1), finely powdered hydroxide was added with continuous stirring to the solution of the maltoheptaose G7 sample in dimethyl sulfoxide,

followed by the addition of a larger amount of methyl iodide, in order to obtain the desired compound **19** (figure 2.24), which was purified by column chromatography (AcOEt/methanol 9:1).

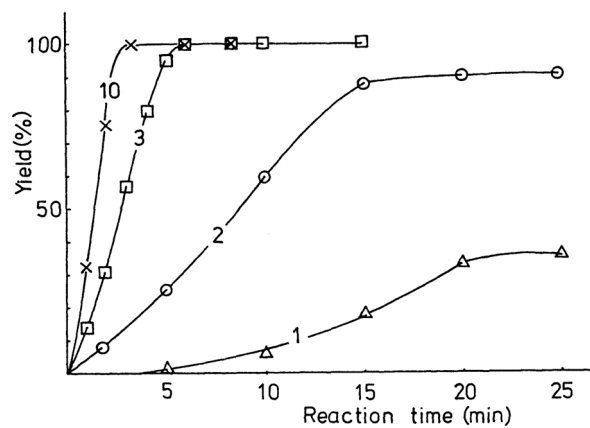


**Figure 2.21.** Methylation of *D*-glucose at various (1-10) equivalents of sodium hydroxide per mol of replaceable H (2 mmol of NaOH/mL of DMSO).<sup>127</sup>

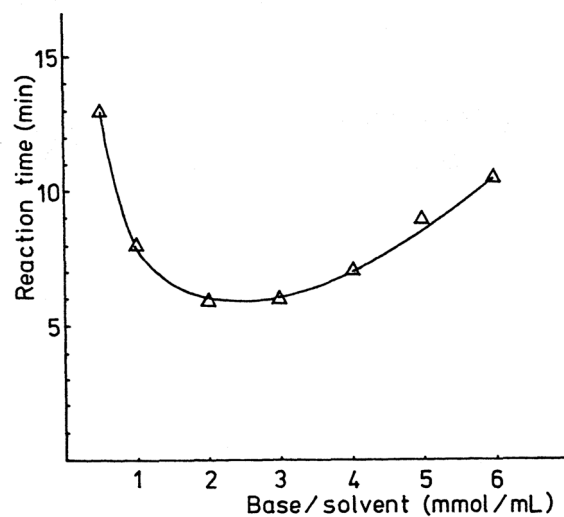


**Figure 2.22.** The reaction time for the permethylation of *D*-glucose as a function of the NaOH/DMSO ratio (mmol/mL) (3 equivalents of NaOH per mol of replaceable H).<sup>127</sup>

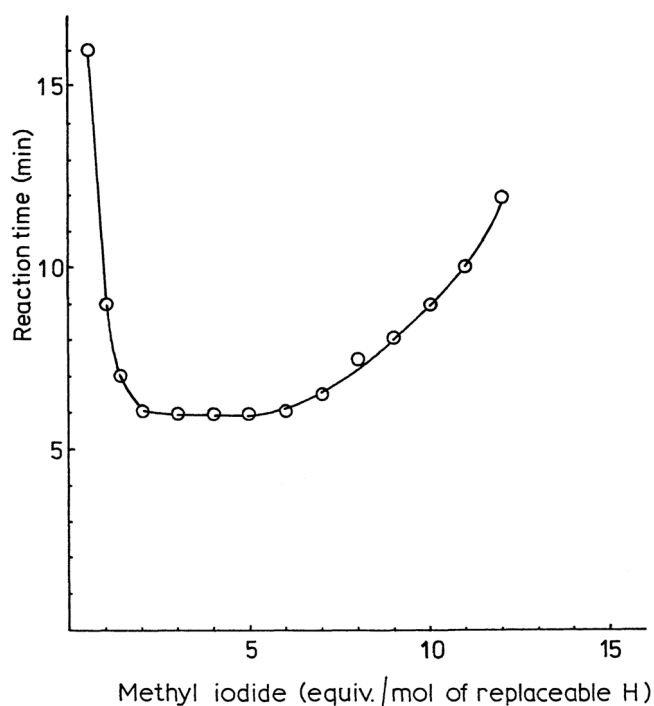


**Figure 2.23.** The dependence of the reaction time for the permethylation of *D*-glucose on the amount of methyl iodide (3 equivalents of NaOH per mol of replaceable H, 2 mmol of NaOH/mL of DMSO).<sup>127</sup>

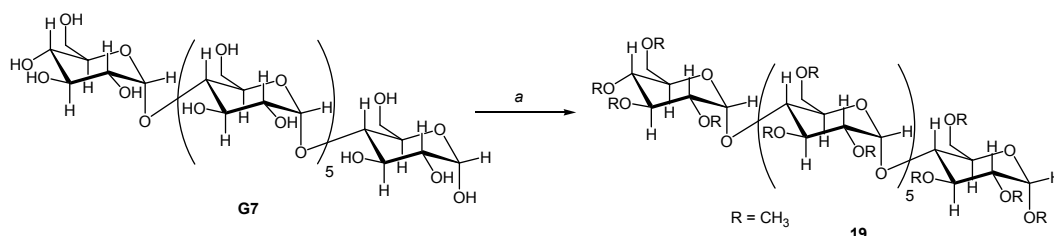


**Figure 2.24.** (a) NaOH, DMSO, MeI, 0 °C, then r.t.

## 2.5. Synthesis of *D*-maltoheptaose bonded to a polydimethylsiloxane *via* an undecenyl spacer

In order to compare the chiral selector diluted in a polysiloxane matrix with one linked to polydimethylsiloxane, a modified permethylated maltoheptaose has been synthesized. The linker of this linear dextrin derivative was obtained from an  $\omega$ -unsaturated carboxylic acid by conversion to the corresponding hydrazide.<sup>129</sup> A suitable reagent for this synthesis of the desired hydrazide is *N*-acylbenzotriazole,<sup>130</sup> which is converted to the corresponding hydrazide by treatment with anhydrous hydrazine in THF. The *N*-acylbenzotriazole was

synthesized by reaction of 1-(methansulfonyl)benzotriazole with  $\omega$ -unsaturated carboxylic acid (figure 2.25).<sup>131</sup>

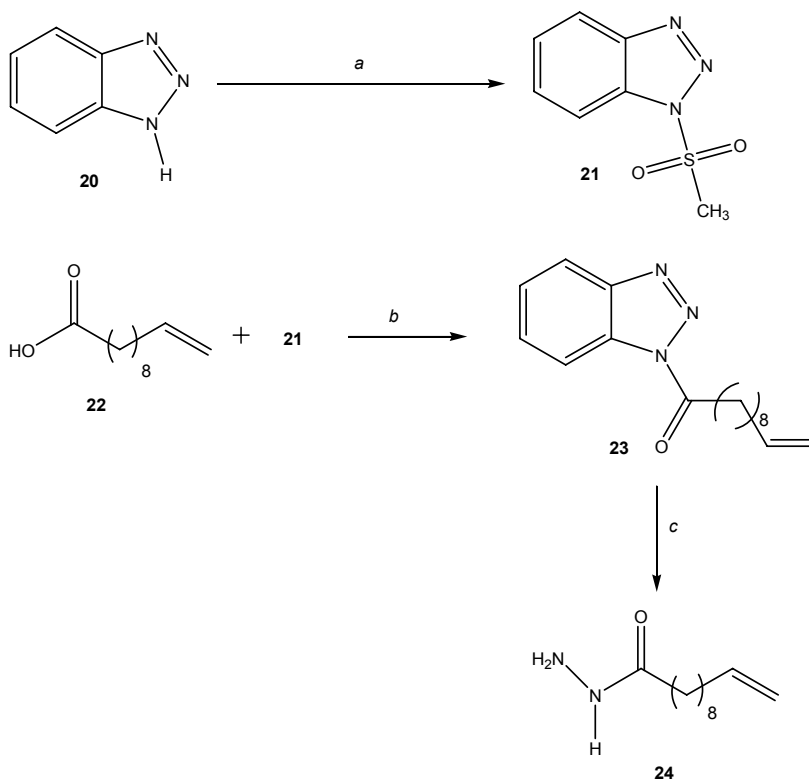


**Figure 2.25.** (a)  $CH_3SO_2Cl$ , Pyridine/toluene, 0 °C, then r.t.; (b)  $Et_3N$ , THF, reflux; (c)  $N_2H_4$ , THF, r.t.

The linear maltoheptaose was then coupled with the hydrazide (figure 2.26) and finally methylated by the established procedure using methyl iodide/dimethyl sulfoxide/sodium hydroxide (MeI/DMSO/NaOH), as shown in figure 2.27, in order to obtain the selector G7 (**26**).<sup>73</sup>

As in the case of the  $\beta$ -cyclodextrin, the bonding reaction illustrated in figure 2.28 was monitored by the disappearance of the signals of the double bond of the undecenyl-spacer in compound **26**, which is depicted in figure 2.29



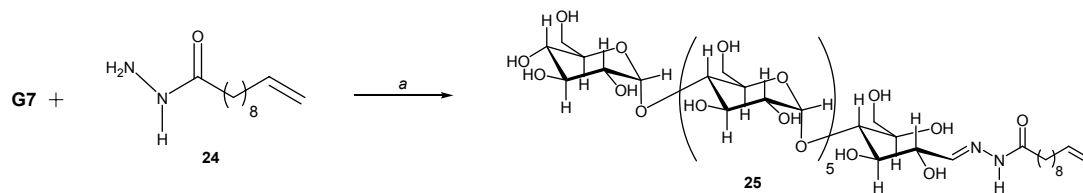


Figure 2.26. (a) Pyridine, 60 °C, 48 h.

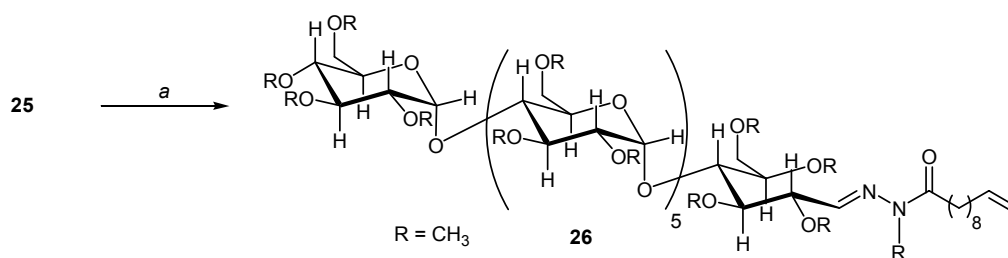
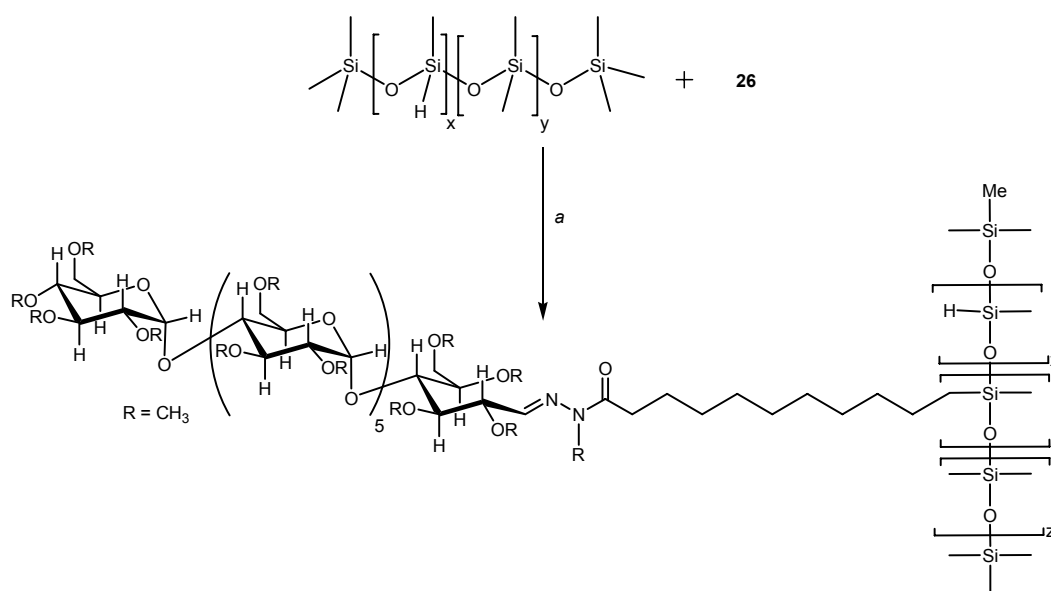
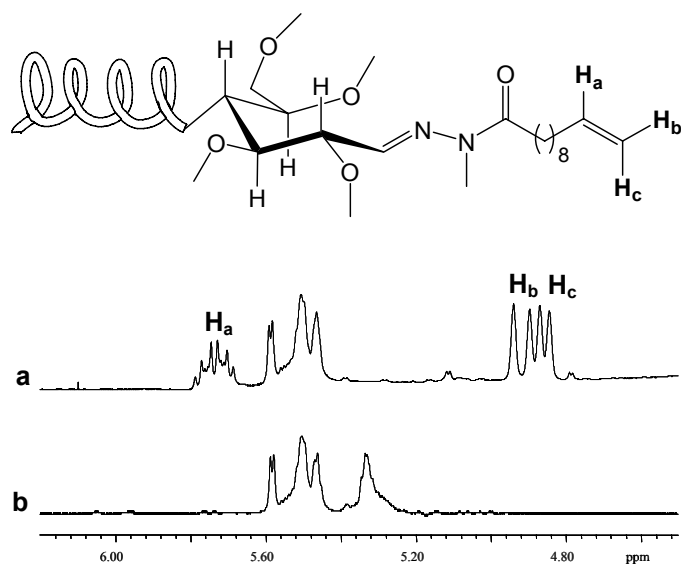


Figure 2.27. (a) NaOH, DMSO, MeI, 0 °C, then r.t.

Figure 2.28. (a) H<sub>2</sub>PtCl<sub>6</sub>, toluene, reflux, 24 h.



**Figure 2.29.** Maltoheptaose derivative **26** before (a) and after (b) the reaction of hydrosilylation with  $\text{H}_2\text{PtCl}_6$  as catalyst.

## 2.6. Synthesis of acyclic ‘Lipodex E’

A preliminary study on linear dextrin derivatives was focused also on the ‘acyclic Lipodex E’, named octakis[(3-*O*,-4’’*O*)-butanoyl-(1’-*O*,2,6-di-*O*)-*n*-pentyl]-maltooctaose G8 (**28**), which was synthesized according to the multistep procedure formed by pentylation carried out with *n*-pentyl bromide in dry DMSO followed by acylation with butyric anhydride in dry pyridine, as in the case of the Lipodex E (figure 2.30).<sup>73, 132</sup>

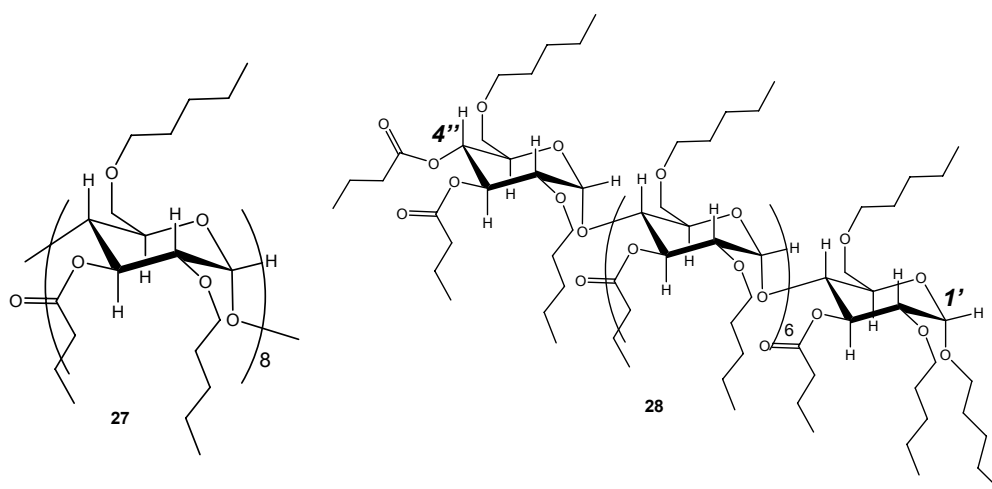


**Figure 2.30.** Structure of cyclic (**27**) Lipodex E, octakis(3-*O*-butanoyl-2,6-di-*O*)- $\gamma$ -cyclodextrin and acyclic (**28**) octakis[(3-*O*,-4’’*O*)-butanoyl-(1’-*O*,2,6-di-*O*)-*n*-pentyl]-maltooctaose. In this figure only the  $\alpha$ -anomer of **28** is shown.

The ratio of the different peaks allowed to evaluate the amount of the various species by determining the degree of substitution (DS). The structure depicted in figure 2.30 corresponds to the acyclic Lipodex E with an additional *n*-pentyl group on the terminal reducing end C-1' (it is due to the high reactivity of the anomeric OH-group and to the over-pentylation which occurs in the first step of the reaction) and a butanoyl group on the non-reducing terminal end C-4''.

In figure 2.31 a glucose unit of **28** is shown with methyl and methylene protons for the *n*-pentyl (*a-e*, *f-l*) and butanoyl (*m-n*) substituents. As in the case of the selector **10** it is possible to exclude a butanoyl (an acyl group in general) on the terminal C-1' because an isolated downshielded proton H1 is not observed at 6.0-6.5 ppm. However, the desired compound **28** (with 17 pentyl and 9 butanoyl groups), after purification still shows traces of a compound with higher degree of pentylation (see experimental section for further details). The methylene protons (CH<sub>2</sub>)-*e*,*l* (figure 2.33) on the 6-positions (pentyl ethers) are downfield shielded in the region of the proton of glucose rings, as confirmed by TOCSY analysis (figure 2.33), in addition to the assignment of the other methylene protons obtained by gHSQC analysis (figure 2.32).

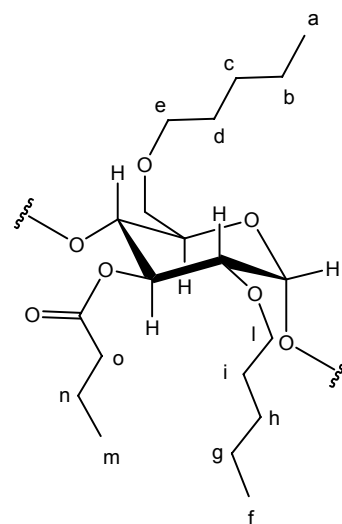


**Figure 2.31.** Glucose unit of compound **28**.

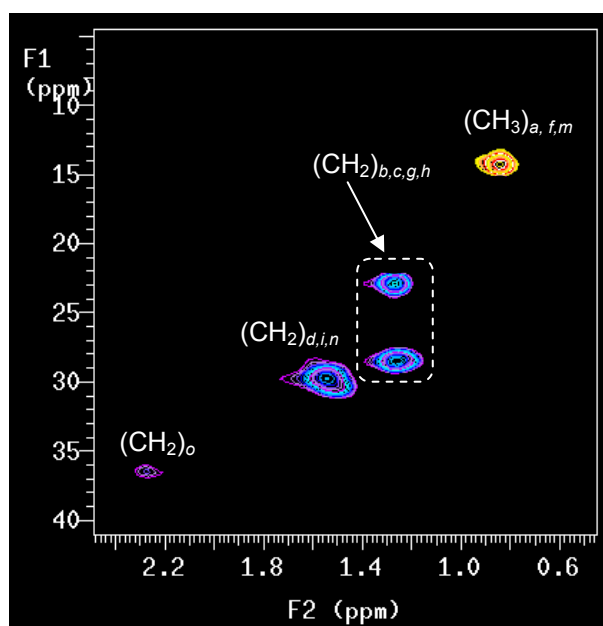


**Figure 2.32.** Spectral region of the gHSQC map of the 'acyclic Lipodex E' (**28**) corresponding to the methylene and methyl protons of the pentyl and butanoyl functional groups; by their integration (on the <sup>1</sup>H-NMR spectrum) it was possible to establish the ratio *n*-pentyl/butanoyl groups).

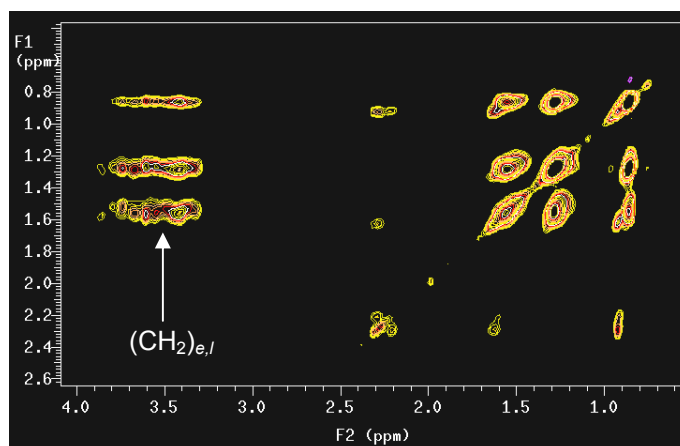


**Figure 2.32.** Spectral region of the TOCSY map of the ‘acyclic Lipodex E’ (**28**); corresponding to the methylene and methyl protons of the *n*-pentyl and butanoyl functional groups; the methylene protons of the downfield shielded (CH<sub>2</sub>)-e are shown.

The same side-effect which occurs during the synthesis of Lipodex E, where the per-*O*-*n*-pentyl- $\gamma$ -cyclodextrin is also synthesized, reduces in this case the yield of the desired product as well.

## 2.7. Molecular modeling analysis

In order to complement the synthesis and the NMR spectroscopic characterization of the cyclic and acyclic selectors, molecular modeling studies have been performed for some compounds described above.

Force field-based molecular modeling is routinely applied to examine molecular conformations, molecular motion and intermolecular interactions, such as those in a ligand-receptor complex.<sup>133</sup> Most of force field methods in widespread use for macromolecular systems are based on harmonic bond, stretching and angle bending, Fourier series of torsional energetics and Coulomb plus Lennard-Jones terms for intermolecular and intramolecular non-bonded interactions.<sup>134</sup> Anharmonic and cross-terms may be added.<sup>135</sup> The non-bonded interactions are represented by Coulomb plus Lennard-Jones terms in the equation 2.1, where  $E_{n.b.}$  represent the energy for non-bonded interactions between all pairs of atoms ( $i < j$ ) separated by three or more bonds.

$$E_{n.b.} = \sum_i \sum_j [q_i q_j e^2 / r_{ij} + 4\epsilon_{ij} (\sigma_{ij}^{12} / r_{ij}^{12} - \sigma_{ij}^6 / r_{ij}^6)] f_{ij} \quad (2.1.)$$

Here the first part of the equation represents the electrostatic term and the second the van der Waals terms.

The energetics for bond stretching and angle bending are represented by equations 2.2 and 2.3

$$E_{\text{bond}} = \sum_{\text{bonds}} K_r (r - r_{eq})^2 \quad (2.2)$$

$$E_{\text{angle}} = \sum_{\text{angles}} K_{\theta} (\theta - \theta_{eq})^2 \quad (2.3)$$

The last intramolecular term is for the torsional energy (eq. 2.4) where  $\phi_i$  is the dihedral angle,  $V_1$  and  $V_2$  and  $V_3$  are the coefficients in the Fourier series and  $f_1$ ,  $f_2$  and  $f_3$  are phase angles.

$$E_{\text{torsion}} = \sum_i \{ V_1^i/2 [1 + \cos(\phi_i + f_1)] + V_2^i/2 [1 + \cos(2\phi_i + f_2)] + V_3^i/2 [1 + \cos(3\phi_i + f_3)] \} \quad (2.4)$$

In order to derive a lowest energetic structure, the fitting procedures are applied to equation 2.5:

$$E(\phi) = E_{\text{bound}}(\phi) + E_{\text{angle}}(\phi) + E_{\text{n.b.}}(\phi) + E_{\text{torsion}}(\phi) \quad (2.5)$$

Thus, according to the different contributions illustrated by the eqs. 2.1-2.5, MMFF (Merck Molecular Force Field) calculations were performed on heptakis[(1'-*O*,6-*O*)-*tert*-butyldimethylsilyl-(2,3-di-*O*,4''-*O*)-acetyl]-maltoheptaose (**10**), on tris[(1'-*O*,6-*O*)-*tert*-butyldimethylsilyl-(2,3-di-*O*,4''-*O*)-acetyl]-maltotriose (**14**) and on per-*O*-methyl-*D*-maltoheptaose (**19**). For further details about the software used in these section, see reference 133. In figure 2.34 the optimized structures for the above mentioned linear dextrin derivatives are shown. In the case of the linear maltoheptaose derivatized as TBDMS-ether/acetyl-ester (**10**) a 'pseudo-cavity' or a 'pocket' is still present for this structure, whereas such environment can be excluded in the case of the G3 (**14**).

Only an initial bend is formed in the case of per-*O*-methyl-*D*-maltoheptaose (**19**) but the overall structure is closer to a linear chain than to a cyclic arrangement characteristic of the per-*O*-methyl- $\beta$ -cyclodextrin (Chirasil- $\beta$ -Dex).

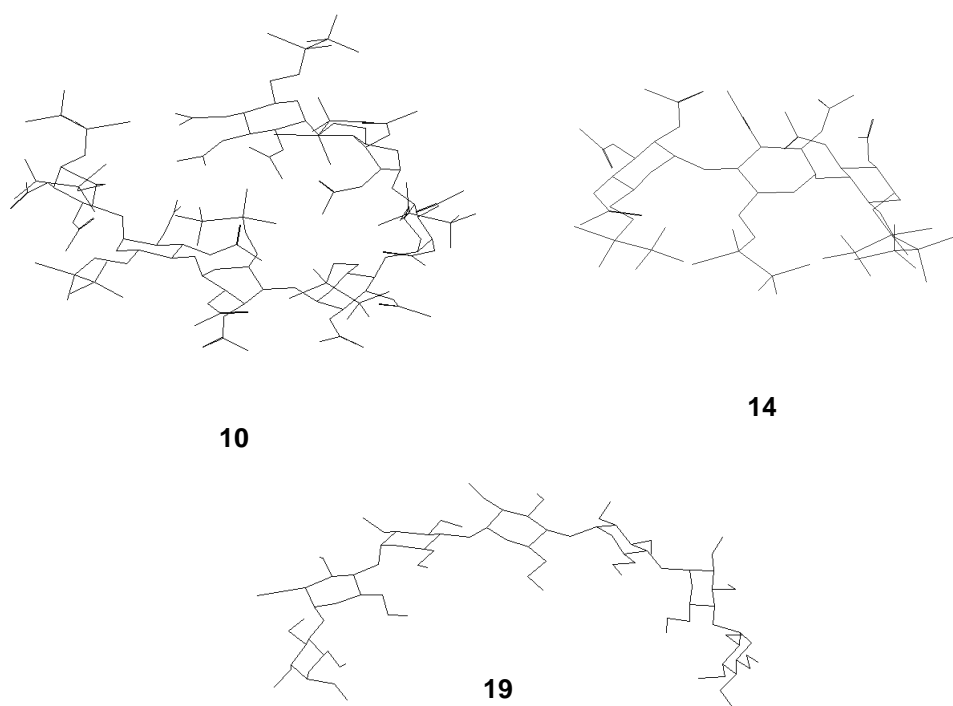


**Figure 2.34.** Optimized structures for the selector G7 (**10**), G3 (**14**) and G7 (**19**) by MMFF calculations. Hydrogen atoms are omitted for clarity.

## Chapter III

### Results and discussion: Part II

#### Enantiorecognition by NMR spectroscopy in solution





### 3.1. Introduction

Since the first report by Pirkle about the observation of chemical shift nonequivalence for enantiomeric nuclei in an enantiomerically pure solvent,<sup>50</sup> a great number of chiral solvating agents (CSAs)<sup>51</sup> have been introduced and have proved to be of great utility for the determination of the enantiomeric composition by NMR as well as for the correlation of the absolute configuration.<sup>52</sup> In many cases, an understanding of the mechanistic basis for the nonequivalence of enantiomeric (and enantiotopic) nuclei was achieved.<sup>53</sup> Furthermore, the versatility of cyclodextrin derivatives in enantioselective chromatography as chiral stationary phases (CSPs) and as CSAs has been complemented by systematic NMR spectroscopic studies in order to explain the enantiorecognition process.<sup>54</sup> The convenient synthesis of heptakis(2,3-di-*O*-acetyl-6-*O*-*tert*-butyldimethylsilyl)- $\beta$ -cyclodextrin (CD7) (**5**) (for the structure see chapter II) and the significant enantioseparation factor  $\alpha$  obtained for the perfluorodiether ‘compound B’ (chapter I)<sup>118</sup> suggested to test this cyclodextrin derivative as CSA for an NMR spectroscopic study in solution. Thus, the following enantiodiscrimination experiments include:

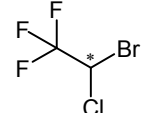
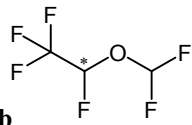
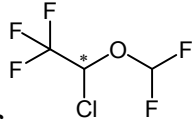
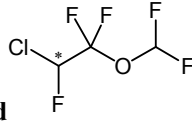
- (a) conformational analysis of the free chiral selector CD7 (**5**), since the derivatization often causes significant changes on the native classical truncated cone shape structure of cyclodextrins;
- (b) determination of association constants by diffusion NMR measurements (DOSY) for the diastereomeric complexes formed by CD7 (**5**) and selected racemic compounds;
- (c) analysis of NOEs detected in the diastereomeric complexes.

Indeed, the aim of this study is to pinpoint the regions of a representative cyclodextrin derivative (CD7 (**5**), for the structure see chapter II) which are responsible for the enantiorecognition process. A detailed study about the enantioselective interactions which occur between the *cyclic* selector CD7 (**5**) and the enantiomers of ‘compound B’ led to the development of *acyclic* chiral selectors. Thus, a preliminary NMR study of G7 (**10**) in solution (section 3.3) is reported and an extensive application of G7 (**10**) as novel chiral stationary phase for enantioselective gas chromatography is described in chapter IV.

In the appendix further details about the Diffusion Ordered Spectroscopy (DOSY) are furnished, in order to provide a better understanding of the association studies reported in the subsequent section 3.2.

### 3.2. Enantiodiscrimination of halogenated compounds

The previous use of octakis(3-*O*-butanoyl-2,6-di-*O*-*n*-pentyl)- $\gamma$ -cyclodextrin (Lipodex E)<sup>136</sup> as chiral solvating agent (CSA) for the enantiodiscrimination of halogenated ethers was extended in this work to heptakis(2,3-di-*O*-acetyl-6-*O*-*tert*-butyldimethylsilyl)- $\beta$ -cyclodextrin CD7 (**5**). This selector is able to produce remarkable chemical shift nonequivalences towards the halogenated anaesthetics **3a-3c**, as summarized in table 3.1. These enantiodiscrimination measurements were carried out in the apolar solvent *n*-hexane-*d*<sub>14</sub> or cyclohexane-*d*<sub>12</sub>, where the competition with the analyte molecule in the formation of the complex is significantly reduced. In figure 3.1 the chemical shift non-equivalence measurements are depicted for the enantiodiscrimination of desflurane **3b**. The chemical shift nonequivalences increase by decreasing the temperature (table 3.1) and the selector **5** exhibits enantio recognition towards all the CH and CHF<sub>2</sub> groups of the halogenated anaesthetics.

<b>Table 3.1.</b> <sup>1</sup> H NMR (600 MHz, C <sub>6</sub> D <sub>14</sub> ) chemical shift nonequivalence $\Delta\delta^a$ data measured for racemic halogenated anaesthetics <b>3a-d</b> in the presence of CD7 ( <b>5</b> ).				
guest	$\Delta\delta$ (ppm)			
	25 °C		5 °C	
<b>3a</b> 	CH			CH
	0.033			0.040
<b>3b</b> 	CHF <sub>2</sub>	CH	CHF <sub>2</sub>	CH
	0.025	0.041	0.039	0.090
<b>3c</b> 	CHF <sub>2</sub>	CH	CHF <sub>2</sub>	CH
	0.038	0.07	0.061	0.010
<b>3d</b> 	CHF <sub>2</sub>	CH	CHF <sub>2</sub>	CH
	0.022	0.011	0.041	0.017

<sup>a</sup> $\Delta\delta = |\delta_S - \delta_R|$ , difference between the chemical shifts (ppm) of corresponding nuclei of the two enantiomers of **3a-d** in the presence of **5**

The versatility of the chiral selector CD7 (**5**) as CSA in solution is also confirmed by <sup>19</sup>F-NMR spectroscopic analysis carried out on the halogenated anaesthetics **3a-d** (table 3.2 and figure 3.2).

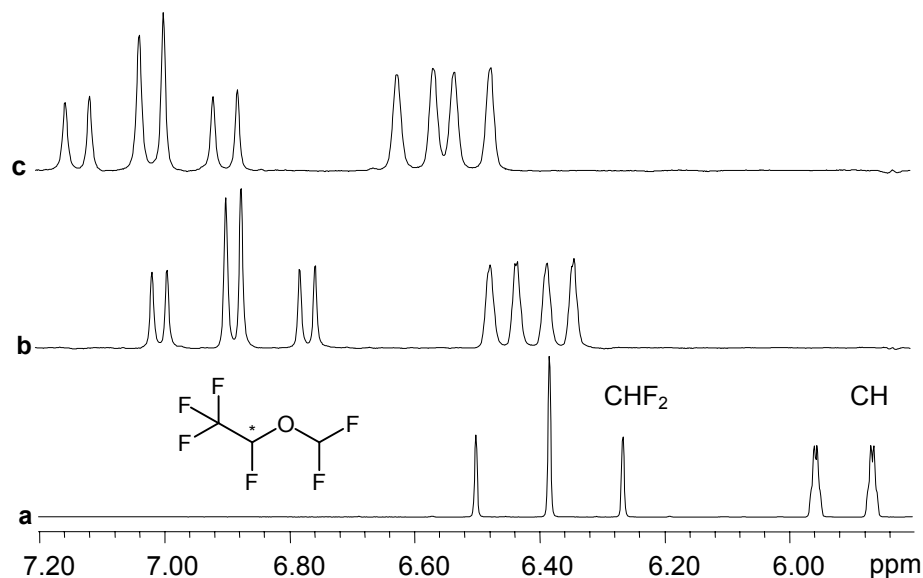


**Figure 3.1.**  $^1\text{H-NMR}$  (600 MHz,  $\text{C}_6\text{D}_{14}$ ) spectral regions corresponding to the protons of the CH-group and  $\text{CHF}_2$ -group of (a) pure racemic **3b** (60 mM, 25 °C), (b) equimolar mixture of racemic **3b** and **5** (60 mM, 25 °C), (c) equimolar mixture of racemic **3b** and **5** (60 mM, 5 °C).

**Table 3.2.**  $^{19}\text{F}$  NMR (282 MHz,  $\text{C}_6\text{D}_{14}$ , 25 °C) chemical shift nonequivalences  $\Delta\delta^a$  data measured for racemic halogenated anaesthetics **3a-d** in the presence of CD7 (**5**).

guest	$\Delta\delta$ (ppm)		
<b>3a</b> 	$\text{CF}_3$ 0.113		
<b>3b</b> 	$\text{CF}_3$ 0.186	$\text{CHF}_2$ n.d.	$\text{C}^*\text{F}$ n.d.
<b>3c</b> 	$\text{CF}_3$ 0.222	$\text{CHF}_2$ n.d.	
<b>3d</b> 	$\text{CF}$ 0.044	$\text{CHF}_2$ n.d.	$\text{CF}_2\text{C}^*$ n.d.

<sup>a</sup> $\Delta\delta = |\delta_S - \delta_R|$ , difference between the chemical shifts (ppm) of corresponding nuclei of the two enantiomers of **3a-d** in the presence of **5**; n.d. = not determined

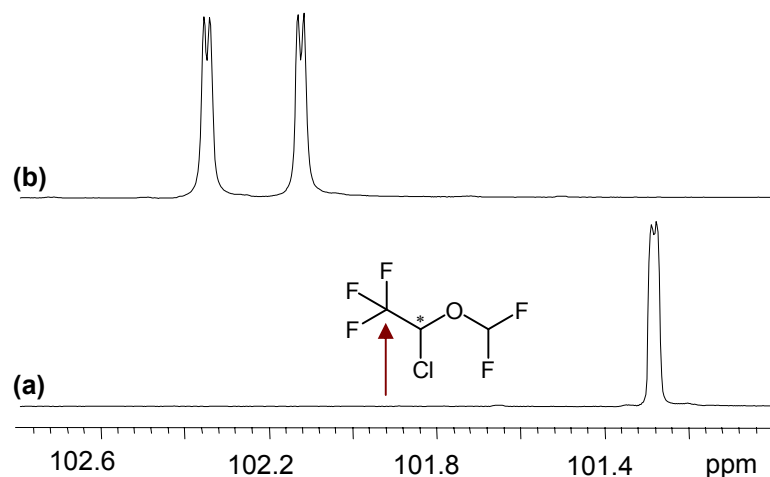


**Figure 3.2.**  $^{19}\text{F}$ -NMR (282 MHz,  $\text{C}_6\text{D}_{12}$ , 25 °C) spectral regions corresponding to the fluorine nuclei of the  $\text{CF}_3$ -group of (a) pure racemic **3d** (60 mM), (b) equimolar mixture of racemic **3d** and **5** (60 mM).

The strength of the enantioselective interaction of these anaesthetics with the selector **5** has been also measured by DOSY analysis, as shown in table 3.3, where the diffusion coefficient in the free (f) and in the bound (b) state is reported.

The diffusion constant depends on the size of the molecule:<sup>137-139</sup>

$$D = kT/6\pi\eta r \quad (3.1)$$

where  $k$  is the Boltzmann constant ( $1.380662 \times 10^{-23} \text{ J K}^{-1}$ ),  $T$  is the absolute temperature (K),  $\eta$  the dynamic viscosity (Pa·s) and  $r$  the radius of the molecule (m). In the case of non-spherical molecules,  $r$  is replaced by  $R_h$ , the hydrodynamic radius.

If the exchange between free and bound analyte is fast on the diffusion time scale ( $\sim 100$  ms), the diffusion parameter observed in the NMR experiment is a weighted average of the diffusion coefficients of bound ( $D_b$ ) and free ( $D_f$ ) analyte:

$$D_{\text{obs}} = X_b D_b + (1 - X_b) D_f \quad (3.2)$$

The fraction of bound analyte can be determined as:

$$X_b = \frac{D_{\text{obs}} - D_f}{D_b - D_f} \quad (3.3)$$

where  $D_{\text{obs}}$  is the measured diffusion coefficient of the analyte in the mixture.  $D_b$  is very likely to be equal to that of the cyclodextrin since the analyte is small compared to the cyclodextrin derivative and therefore global diffusion controlled by the cyclodextrin can be assumed.<sup>140</sup> (Since the analytes are small compared to cyclodextrin, we assume that  $D_b \approx D_{\text{CD}}$ , which lead to a slight overestimation of the determined value of  $X_b$ . The method can be applied to analytes of any size; if the size of the analyte is of the same order or bigger than that of the cyclodextrin, suitable approximations have to be made).

The fraction of the guest molecules ( $X_b$ ) bound to cyclodextrin is defined as:

$$X_b = [\text{G:CD}]/([\text{G}] + [\text{G:CD}]) \quad (3.4)$$

Combining the K equation ( $K = [\text{G:CD}]/[\text{G}] \cdot [\text{CD}]$ ) for a 1:1 complex (the stoichiometry of these complexes (1:1) was determined by the continuous variation method (Job plot))<sup>141</sup> with the equation 3.4:

$$X_b = K[\text{G}][\text{CD}]/([\text{G}] + K[\text{G}][\text{CD}])$$

$$X_b = K[\text{CD}]/(1 + K[\text{CD}]) \quad (3.5)$$

Therefore, measurements of diffusion coefficients of the analyte (G) in the absence ( $D_f$ ) and in the presence ( $D_{\text{obs}}$ ) of the cyclodextrin (CD) allowed to calculate the fraction of bound analyte  $X_b$ , which can be substituted in the equation 3.5.<sup>a</sup> Diffusion coefficient analysis became recently a fast and alternative method to the well established chemical shift ( $\delta$ ) titration method.<sup>141</sup> However, even the titration method can also be applied using as a variation parameter the diffusion coefficient instead of chemical shift.<sup>139</sup>

---

<sup>a</sup> By measuring the apparent diffusion constant of the guest molecules (G) and calculating the fraction of the bound guest molecules ( $X_b$ ) at different concentrations of cyclodextrin (CD) and plotting  $X_b$  versus [CD], K can be determined from fitting the data to eq. 3.5. However, a remarkable advantage of the diffusion measurements is the definition of all the parameters required in the equations mentioned above by a single experiment. Titrations are no longer required.

In figure 3.3 an example of a DOSY measurement is shown for the anaesthetic desflurane **3b** in presence of the CSA **5**.

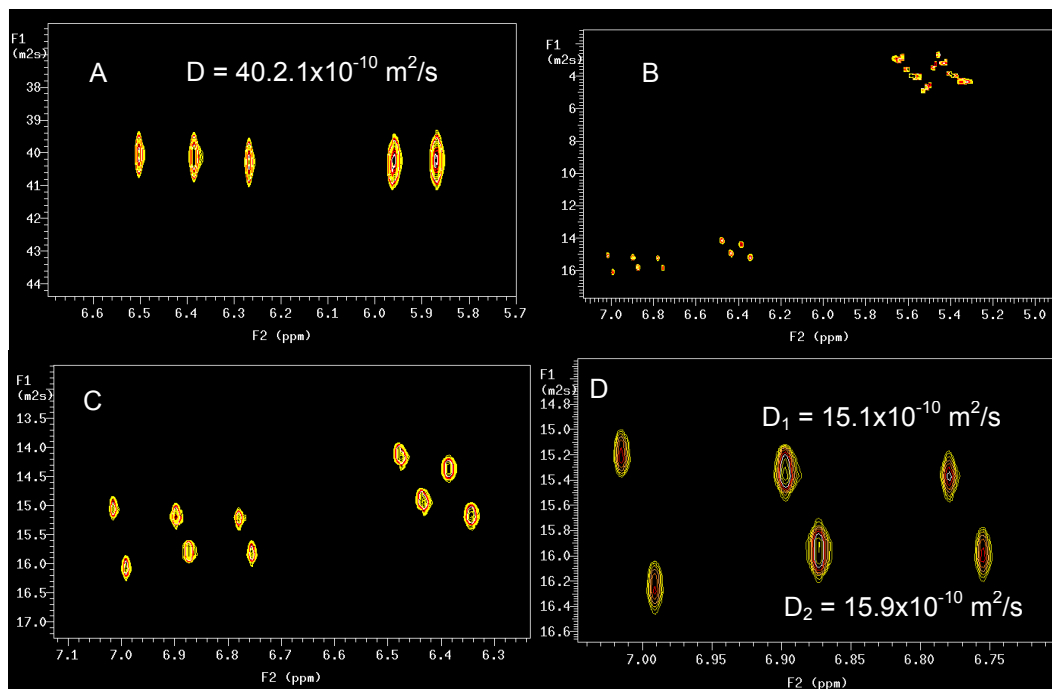


**Figure 3.3.** (A) DOSY experiment (25 °C) for desflurane **3b** in the free state and (B) in the presence of the CSA **5**; (C) spectral region of the desflurane protons CH and CHF<sub>2</sub>; (D) spectral region of the CHF<sub>2</sub> protons for the two enantiomers.

**Table 3.3.** Diffusion coefficients (**D**) (600 MHz, C<sub>6</sub>D<sub>14</sub>, 25 °C) and association constants (**K**) calculated for the complexes formed by the CSA **5** and the enantiomers of the anaesthetics **3a-d**.

guest	<b>D</b> (10 <sup>-10</sup> m <sup>2</sup> /s)	<b>K</b> (M <sup>-1</sup> )
<b>3a</b> <chem>BrC(Cl)(F)C(F)(F)F</chem>	$D_f = 38.3$	
	$D_b(S) = 20.6$	$K_S = 37.6$
	$D_b(R) = 22.5$	$K_R = 26.9$
<b>3b</b> <chem>FC(F)C(F)OC(F)F</chem>	$D_f = 40.2$	
	$D_b(S) = 15.1$	$K_S = 126.8$
	$D_b(R) = 15.9$	$K_R = 107.5$
<b>3c</b> <chem>ClC(F)C(F)OC(F)F</chem>	$D_f = 37.0$	
	$D_b(S) = 13.8$	$K_S = 136.9$
	$D_b(R) = 14.5$	$K_R = 117.6$
<b>3d</b> <chem>ClC(F)C(F)OC(F)F</chem>	$D_f = 37.4$	
	$D_b(S) = 17.5$	$K_S = 62.0$
	$D_b(R) = 18.2$	$K_R = 53.9$

The remarkable chemical shift nonequivalences can not be explained by the small differences of the association constants (table 3.3) for the diastereomeric complexes formed by CD7 (**5**)

and the enantiomers of racemic **3a-d**. Indeed, the chemical shift nonequivalence in the presence of the CSA can be defined as the result of two contributions which are related to the association constants (in these cases it gives a small contribution) and the geometry of the resulting diastereomeric complexes. Obviously the geometries of the diastereomeric complexes play a predominant role in the enantioselective process compared to thermodynamic stability differences. Such a distinction is even more pronounced in the enantiodiscrimination of 'compound B' described in the section 3.2.1.

### 3.2.1. Enantiodiscrimination of 'compound B' (**3e**) by CD7 (**5**)

Particular attention was focused on the enantiodiscrimination of 'compound B' **3e**,<sup>118-119</sup> which showed a remarkable enantioseparation in enantioselective gas chromatography (chapter I).

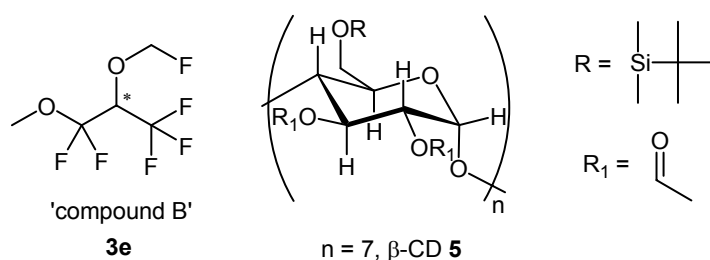


**Figure 3.4.** Structure of 'compound B' **3e** and the CD7 (**5**) used as CSA.

#### *Enantiodiscrimination measurements*

The (**5**) used as CSA produced significant proton chemical shift nonequivalences for racemic **3e**, revealing a strong enantioselectivity also in solution. Thus, the methoxy protons of racemic **3e** exhibited two sharp singlets at 3.57 ppm and 3.58 ppm (figure 3.5 b and table 3.4). Anisochrony measured for the methine resonances (figure 3.5 f) was even much larger (0.11 ppm). The methylene protons were also differentiated, but the signals were partially superimposed by proton resonances of the CSA **5**.

In a next step, the proton resonances of the isolated single (*R*)- and (*S*)-enantiomers of **3e**, obtained by enantioselective preparative GC, were measured in the presence of CD7 (**5**). It was established that the (*S*)-enantiomer of **3e** exhibits a larger downfield shift as compared to the (*R*)-enantiomer of **3e** (assignments in figure 3.5). This observation is in agreement with the GC experiment whereby the (*S*)-enantiomer of **3e** is eluted after the (*R*)-enantiomer on the selector **5**. A further increase of chemical shift nonequivalences could be obtained by

increasing the total concentration of **3e** and **5** in the 1:1 mixture (figures 3.5 d, h and table 3.3) and adding further equivalents of the CSA **5** (figure 3.5 c, g and table 3.3) and by lowering the temperature (table 3.4).

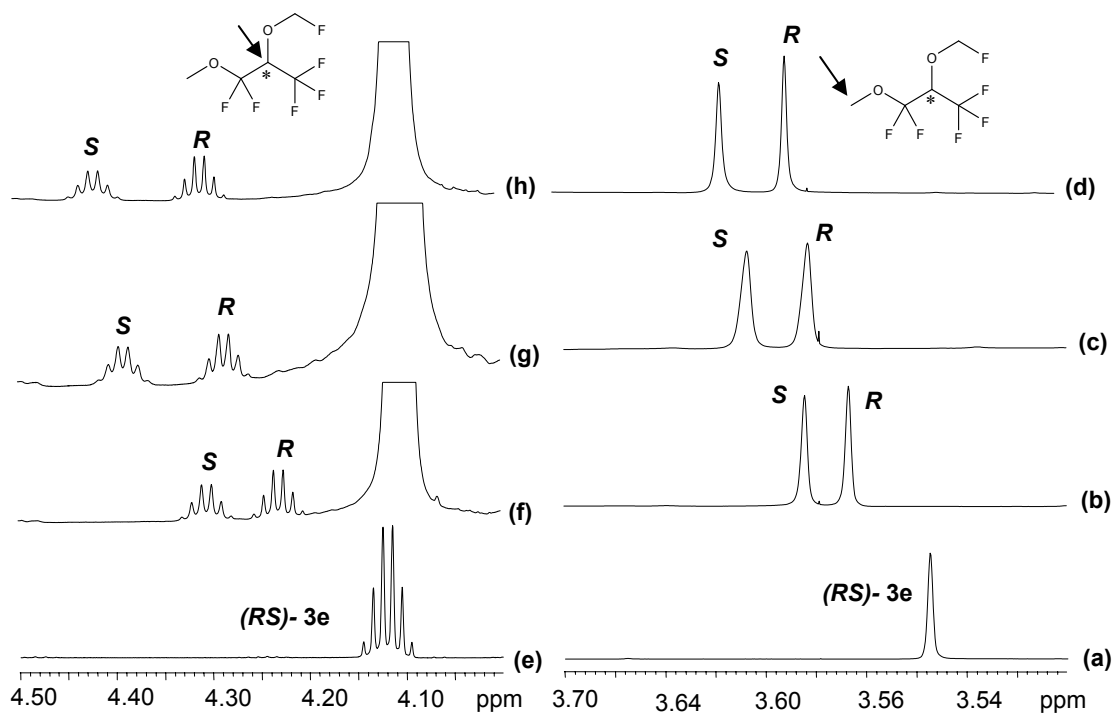


**Figure 3.5.**  $^1\text{H}$  NMR (600 MHz,  $\text{C}_6\text{D}_{12}$ , 25 °C) spectral regions corresponding to the protons of the  $\text{CH}_3\text{O}$ -group of (a) pure racemic **3e** (20 mM), (b) equimolar mixture of racemic **3e** and **4** (20 mM), (c) racemic **3e** (20 mM) and **5** (40 mM), (d) equimolar mixture of racemic **3e** and **5** (60 mM).  $^1\text{H}$  NMR (600 MHz,  $\text{C}_6\text{D}_{12}$ , 25 °C) spectral regions corresponding to the protons of the CH-group of (e) pure racemic **3e** (20 mM), (f) in presence of equimolar mixture of racemic **3e** and **5** (20 mM), (g) racemic **3e** (20 mM) and **3e** (40 mM), (h) equimolar mixture of racemic **3e** and **5** (60 mM).

**Table 3.4.**  $^1\text{H}$  NMR (600 MHz,  $\text{C}_6\text{D}_{12}$ , 25 °C) chemical shift nonequivalence  $\Delta\delta^a$  data measured for racemic **3e** in the presence of CD7 (**5**).

	<i>(RS)</i> - <b>3e</b> / <b>5</b> (1:1)		<i>(RS)</i> - <b>3e</b> / <b>5</b> (1:2)			
	20 mM		20 mM			
	25 °C	10 °C	25 °C	10 °C		
CH	0.074	0.142	0.111	0.176	0.105	0.171
$\text{OCH}_3$	0.018	0.032	0.026	0.041	0.024	0.039

<sup>a</sup> $\Delta\delta = |\delta_S - \delta_R|$ , difference between the chemical shifts (ppm) of corresponding nuclei of the two enantiomers of **3e** in the presence of **5**.



Anisochrony induced in the  $^{19}\text{F}$  nuclei (table 3.5) ranged from 0.21 ppm to 0.52 ppm for the 20 mM equimolar mixture of **3e** and **5** (1:1). It significantly increased for the 60 mM (1:1) equimolar mixture (0.30-0.72 ppm) and for the 20 mM (1:2) solution added by another equivalent of **5** (0.25-0.73 ppm). As in the case of proton nuclei, fluorine resonances of the two enantiomers were downfield shifted compared with pure **3e** and the (*S*)-enantiomer of **3e** is more shifted than the (*R*)-enantiomer (figure 3.6) in agreement with the GC experiment.

**Table 3.5.**  $^{19}\text{F}$  NMR (282 MHz,  $\text{C}_6\text{D}_{12}$ , 25 °C) chemical shift nonequivalence  $\Delta\delta^a$  data measured for racemic **3e** in the presence of  $\text{CD7 5}$ .

	20 mM		60mM
	1:1	1:2	1:1
$\text{CF}_3$	0.206	0.249	0.303
$\text{CF}_2$	0.363	0.514	0.520
	0.521	0.727	0.722
$\text{CH}_2\text{F}$	0.422	0.487	0.571

<sup>a</sup> $\Delta\delta = |\delta_S - \delta_R|$ , difference between the chemical shift (ppm) of corresponding nuclei of the two enantiomers of **3e** in the presence of **5**.

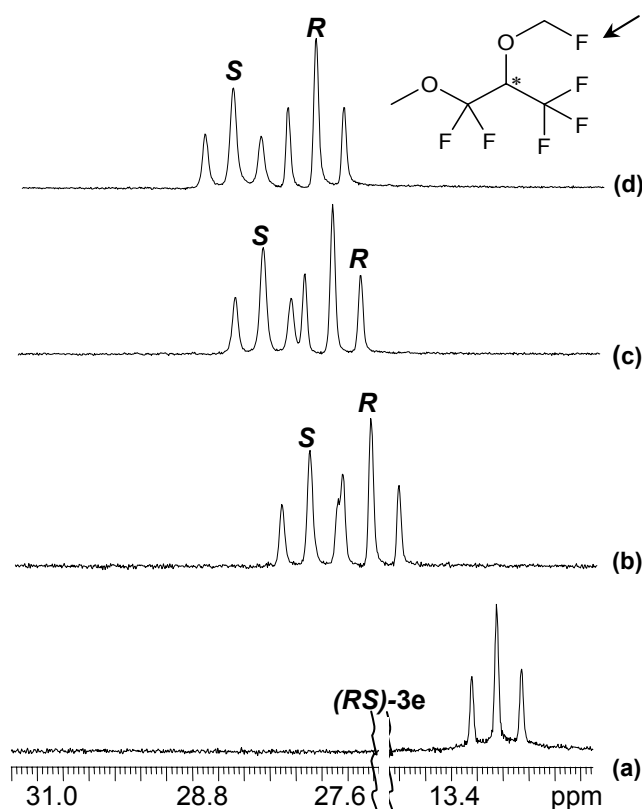


**Figure 3.6.**  $^{19}\text{F}$ -NMR (282 MHz,  $\text{C}_6\text{D}_{12}$ , 25 °C) spectral regions corresponding to the fluorine nuclei of the  $\text{CH}_2\text{F}$ -group of (a) pure racemic **3e** (20 mM), (b) equimolar mixture of racemic **3e** and **5** (20 mM) (c) racemic **3e** (20 mM) and the **5** (40 mM), (d) equimolar mixture of racemic **3e** and **5** (60 mM).

The first step to elucidate the enantioselective mechanism (in addition to the determination of the association constants) is to find out the conformation of the **CD7 (5)**, in order to detect some conformational changes compared to the truncated cone shape structure, typical of

underivatized cyclodextrins. Such conformational changes are usually kept after complex formation with the single enantiomer. Finally, the detection of the interactions between the CD7 (**5**) and the enantiomers of **3e** is furnished, based on the intermolecular NOEs observed for the diastereomeric complexes.

#### Determination of association constant

The association constants for the diastereomeric complexes formed by the enantiomers of **3e** and the CSA **5** were determined according to the method which takes into account the diffusion parameter  $D$ , as described in section 3.2.<sup>137-138</sup> The calculated values for the association constants are summarized in table 3.6.

<b>Table 3.6.</b> Diffusion coefficients $D$ ( $10^{-10}$ m <sup>2</sup> /s) of the analyte <b>3e</b> in the free and bound state, of the selector <b>5</b> ; molar fraction of the bound guest ( $X_b$ ) and association constants $K$ ( $M^{-1}$ ) calculated according to the equation 3.4.	
	$D$ ( $10^{-10}$ m <sup>2</sup> /s)
	$\beta$ -CD <b>5</b>
	1.28
$D_{RS-3e}$	$D-3e/5$
13.4 ( <i>RS</i> )	6.67 ( <i>R</i> )
	5.94 ( <i>S</i> )
	$X_b$
	0.56 ( <i>R</i> )
	0.62 ( <i>S</i> )
	$K$ ( $M^{-1}$ )
	48.2 ( <i>R</i> )
	71.6 ( <i>S</i> )

Indeed, in the case of association with CD7 (**5**) ( $71.6 M^{-1}$  for the *S*-**3e** and  $48.2 M^{-1}$  for *R*-**3e**) the association constants are small and such values are not typical of an inclusion complex.<sup>142</sup> This suggest an interaction mechanism which involves mainly the external surface of the selector.<sup>143</sup> The values of the association constants for the diastereomers formed by ‘compound B’ (**3e**) and the CD7 (**5**) confirm the presence of two contributions for the enantio-recognition. Thus, the diastereotopic nuclei of ‘compound B’ reside in different spatial environments (*geometry*) able to induce the high enantiodiscrimination in the case of the association with the CSA **5**, even if the value of the association constants are significantly small (*stability*).

#### Conformational analysis of the CSA **5**

The CD7 (**5**) exhibited significant enantiodiscrimination by GC and NMR towards the racemic ‘compound B’ (**3e**). Before analyzing the diastereomeric complexes formed between (*R*)-**3e** or (*S*)-**3e** and **5**, conformational features of CD7 (**5**) were investigated in order to detect expected changes on the structure of the native CD7 after derivatization, *e.g.*, by the bulky TBDMS group. Rotation of glucopyranose units about the glycosidic linkages and deviations of the glucopyranose rings from the common <sup>4</sup>C<sub>1</sub> chair conformation can be ascertained *via* the accurate analysis of *intra*- and *inter*unit interproton dipolar interactions detected in the

ROESY map ( $C_6D_{12}$ , 25 °C, mix 0.3 s), previously applied to other derivatized cyclodextrins.<sup>126</sup>

The relative intensities of H-1–H-4' (the apex indicates protons belonging to the unit adjacent to the one taken into consideration) and H-1–H-2 NOEs (figure 3.7 b) are diagnostic probes for intermolecular rotation occurring between two adjacent glucose units.

Thus, the C–H-1 and C–H-4' bonds of underivatized cyclodextrins are held coplanar by the strong network of attractive hydrogen bonding interactions between secondary hydroxyl groups, which renders the distance H-1–H-4' significantly shorter with respect to that of H-1–H-2.

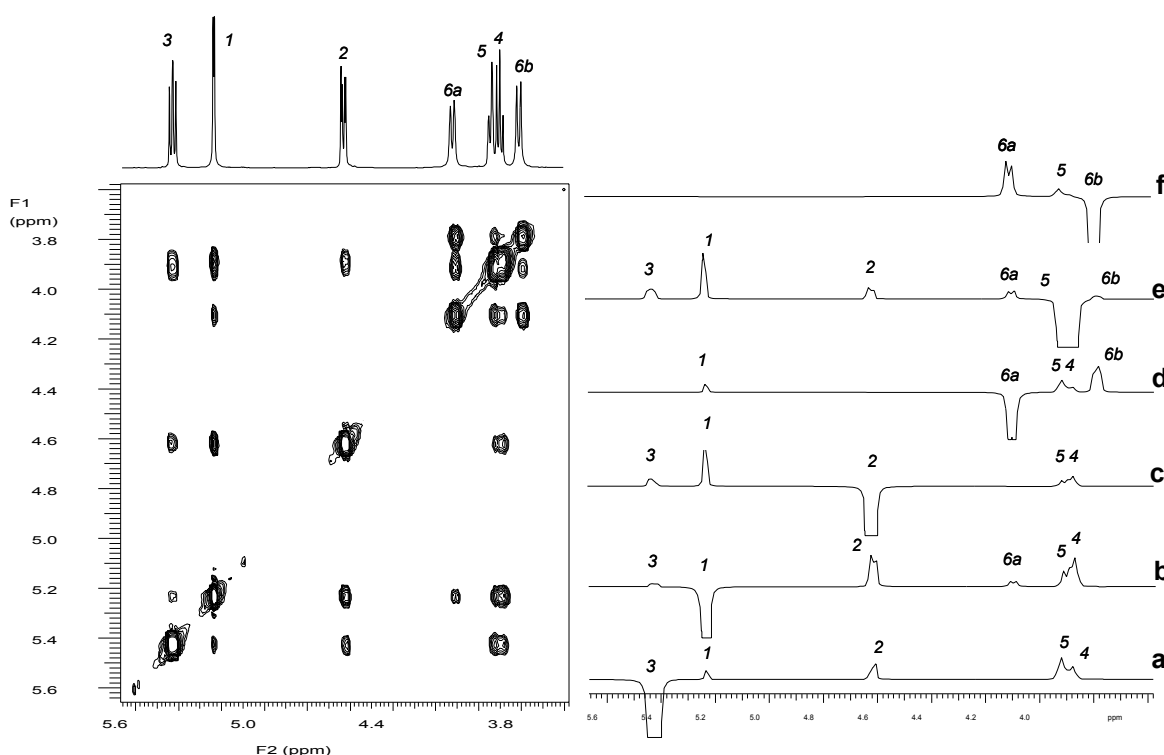


**Figure 3.7.** 2D ROESY (600 MHz,  $C_6D_{12}$ , 25 °C,  $\tau_m=0.3$  s) map of CD7 (**5**). Traces corresponding to the (a) H-3, (b) H-1, (c) H-2, (d) H-6a, (e) H-5 and H-4 and (f) H-6b protons.

In these cases, the *inter*NOE H-1–H-4' is more intense than the H-1–H-2 dipolar interaction. The intensities of the NOEs H-1–H-4' and H-1–H-2 of **5** (figure 3.7 b) were comparable, which reflects the lengthening of the *inter*unit H-1–H-4' distance with respect to the fixed *intra*unit H-1–H-2 caused by the rotation across the glycosidic linkages. Furthermore, clockwise and anticlockwise rotation of the units brings alternatively the proton H-1 of one unit in proximity of the internal protons H-3' and H-5' of the adjacent one and in the trace of the proton H-1 the corresponding NOEs were detected (figure 3.7 b).

Changes of the extent of prevalence of  ${}^4C_1$  chair conformers of the glucopyranose units in favour of different ones are revealed by *intraunit* NOEs between 1,2-diaxial protons, which are unexpected. Accordingly, in the trace of the proton H-2 (figure 3.7 c) not only the usual 1,2 axial-equatorial and 1,3-diaxial dipolar interactions with the H-1 and H-4 protons were respectively detected, but also an NOE with the internal proton H-3, which should be 1,2-diaxial with respect to it. However, the most interesting point is the analysis of the relative intensities of the *inter*NOEs H-2–H-4 and H-2–H-3, respectively, which not only were comparable to each other, but also were both smaller with respect to the H-2–H-1 one. Due to the fact that the 1,3-diaxial distance H-2–H-4 of the undistorted  ${}^4C_1$  chair is expected to be similar to the 1,2-axial-equatorial H-2–H-1 one and shorter relative to the 1,2-diaxial H-2–H-3 distance and taking into account that, in the fast exchange conditions, the observed effects are the average on all the glucopyranose rings, it can be concluded that some chair distortion must occur bringing the protons H-2 closer to the protons H-3 and lengthening the H-2–H-4 distances with respect to the H-2–H-1 ones. In figure 3.9 the different conformations for a single glucose units are shown, in addition to the clockwise rotation of two adjacent glucose units. Therefore, as previously reported for peracetylated  $\beta$ -cyclodextrin,<sup>126</sup> a significant population of skew conformers (figures 3.8 and 3.9,  ${}^0S_5$ ) must be present having the H-3, H-2 and H-4 protons inverted to the equatorial positions.

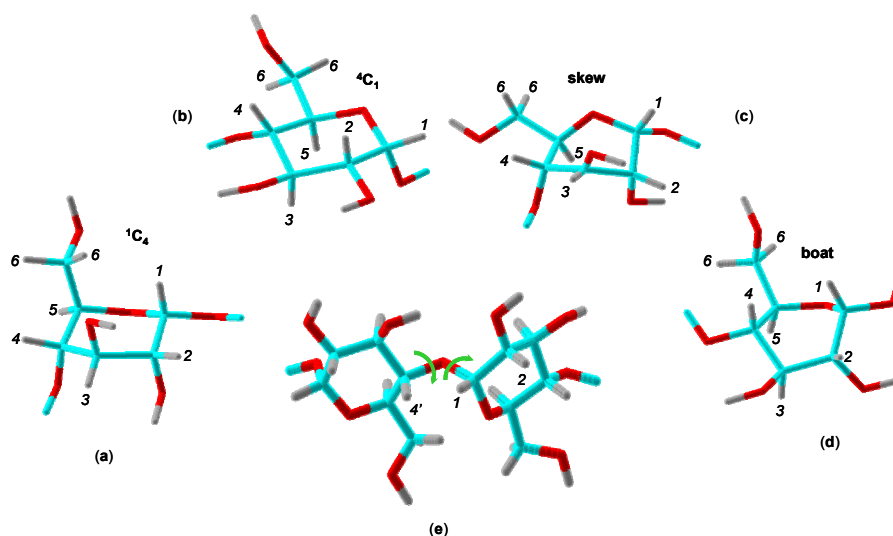


**Figure 3.8.** Conformation structures for a single glucose unit: (a)  ${}^1C_4$ , (b)  ${}^4C_1$ , (c) *skew*, (d) *boat*; (e) clockwise rotation of two adjacent glucose units.

In the trace of the proton H-3 (figure 3.7 a) the usual dipolar interaction with the internal proton H-5 is detected and also unusual dipolar interactions with the protons H-2 and H-4 are

evident. These last two changes are in agreement with the pseudo-equatorial arrangements of the protons H-2, H-3 and H-4.

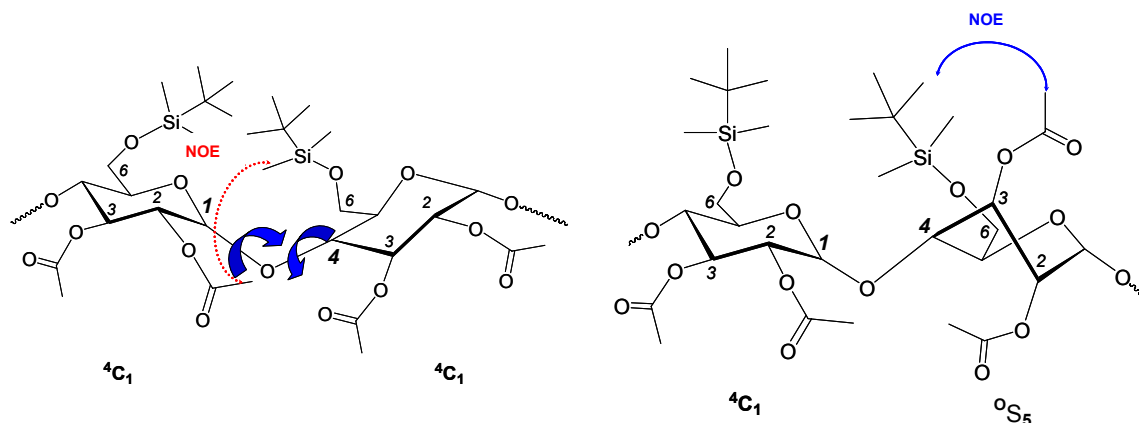


**Figure 3.9.** Schematic representation of *rotation* and *distortion* detected for the CD7 (**5**).

Other dipolar interactions support the above conclusion. In the skew conformers the 2-acetyl groups reside in an axial position close to the proton H-5 (figure 3.9) and the corresponding dipolar interaction, although weak, was clearly detected in the trace of the acetyl groups (figure 3.10 c).

Both conformational changes, *i.e.*, relative rotation and distortion, were confirmed by the *interNOEs* between the 6-(CH<sub>3</sub>)<sub>3</sub>C- and 6-(CH<sub>3</sub>)<sub>2</sub>Si-fragments and the 2- and 3-acetyl groups (figure 3.10). All the conformational changes mentioned above determine an overall structure for CD7 (**5**) which may be described by a flexible, elliptically distorted torus (see also chapter I) where the typical inclusion of an analyte is significantly obstructed.

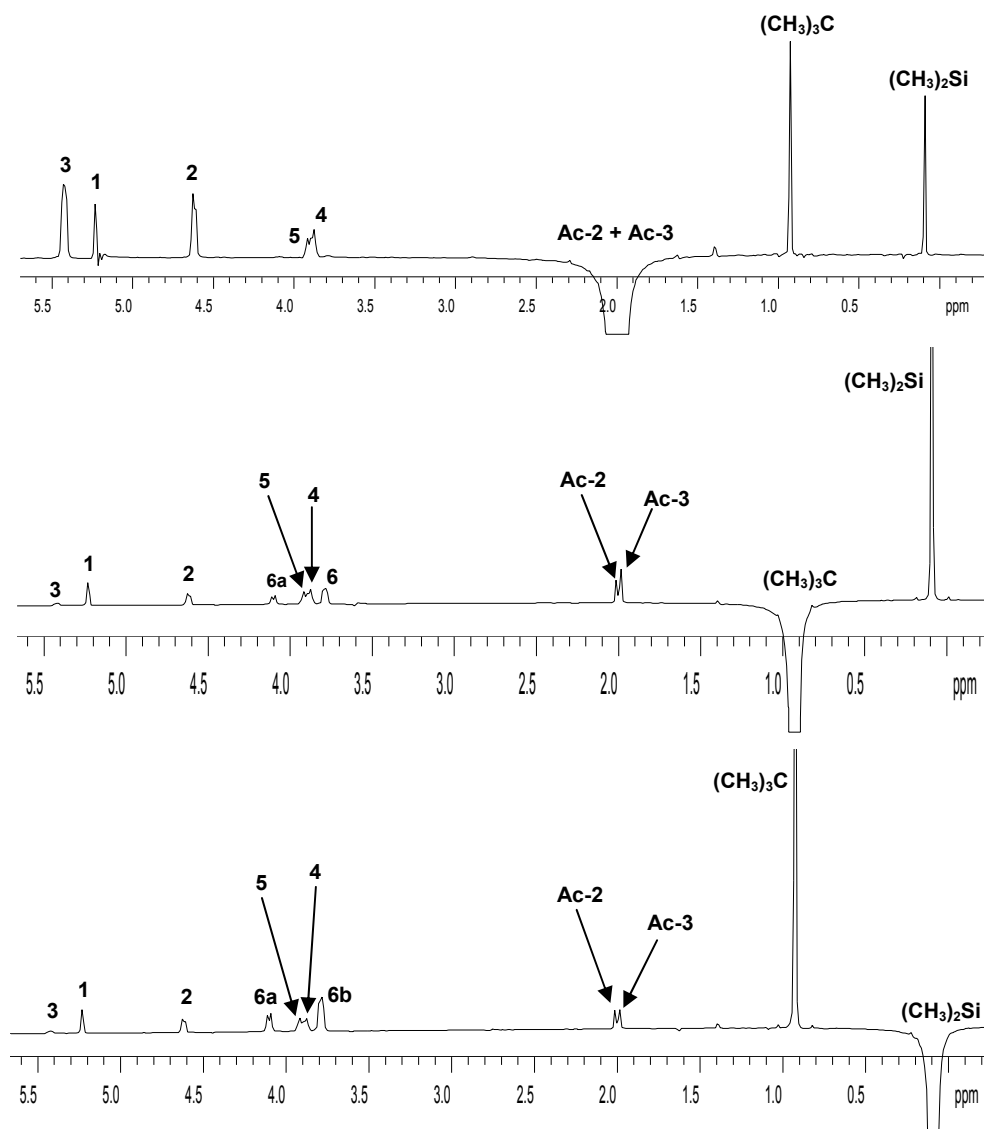


**Figure 3.10.** 2D ROESY (600 MHz,  $C_6D_{12}$ , 25 °C,  $\tau_m = 0.3$  s) analysis of CD7 (**5**). Traces corresponding to the protons of the methyl group of (a)  $SiMe_2$ , (b)  $SiMe_2$ , (c) Ac-2 and Ac-3.

The NOEs data were in very good agreement with the interproton distances calculated from the cross-relaxation terms  $\sigma_{ij}$  obtained by  $^1H$  mono- and biselective relaxation measurements. Indeed, in the initial rate approximation<sup>144</sup> the cross-relaxation term  $\sigma_{ij}$ , which describes the magnetization transfer between the proton pair  $ij$ , is a function of the reorientational correlation time  $\tau_c$  of the vector connecting the two spins  $i$  and  $j$  and of their distance  $r_{ij}$ . In the fast and slow motion regimes such parameter becomes a simple function of  $\tau_c$  and  $r_{ij}$ , as reported in equations 3.6 and 3.7:

$$\sigma_{ij} = 0.5\gamma^4\eta^2r_{ij}^{-6}\tau_c \quad \text{fast motion} \quad (3.6)$$

$$\sigma_{ij} = -0.1\gamma^4 \hbar^2 r_{ij}^{-6} \tau_c \text{ slow motion} \quad (3.7)$$

where  $\gamma$  is the proton gyromagnetic ratio and  $\hbar$  is the reduced Planck constant.

In the hypothesis of isotropic motion, the same reorientational time can be attributed to all the molecule and the ratio of the different  $\sigma_{ij}$  values are correlated to the ratios of the internuclear distances, as reported in equation 3.8:

$$\frac{\sigma_{ik}}{\sigma_{ij}} = \frac{r_{ij}^6}{r_{ik}^6} \quad (3.8)$$

The  $\sigma_{ij}$  parameters can be very simply calculated as differences between the biselective and monoselective relaxation rates for the proton pair  $ij$  (eq. 3.9).

$$\sigma_{ij} = R_{ij}^i - R^i \quad (3.9)$$

The monoselective relaxation rates  $R_{ij}^{\text{ms}}$  are obtained by selective inversion of the spin  $i$  leaving unperturbed the other protons, whereas the biselective ones  $R_{ij}^{\text{bs}}$  are measured following the recovery of the proton  $i$  in the time under simultaneous inversion of the sole spin  $j$ . Thus, being fixed and known the distance between another proton pair  $ik$ ,<sup>145</sup> the unknown value of the interproton distance can be calculated from the equation 3.8.

Thus, the monoselective relaxation rate of the proton H<sub>6a</sub> or H<sub>6b</sub> ( $R_{6a}^{\text{ms}}$ ) of **5** and their respective biselective relaxation rates ( $R_{6a6b}^{\text{bs}}$ ), which are listed in table 3.7, were measured. From their differences the cross-relaxation parameter ( $\sigma_{6a6b}$ ), corresponding to the fixed interproton distance of 1.78 Å,<sup>145</sup> were calculated.

**Table 3.7.** Measured mono- ( $R^i$ , s<sup>-1</sup>), biselective ( $R_{ij}^i$ , s<sup>-1</sup>) and cross-relaxation ( $\sigma_{ij}$ , s<sup>-1</sup>) rates for the protons of CD7 (**5**) (20 mM, C<sub>6</sub>D<sub>12</sub>, 25 °C) and calculated interproton distances ( $r_{ij}$ , Å).

ij	$R^i$ (s <sup>-1</sup> )	$R_{ij}^i$ (s <sup>-1</sup> )	$\sigma_{ij}$ (s <sup>-1</sup> )	$r_{ij}$ (Å)
6a6b	3.26	1.73	-1.53	1.78 <sup>(11)</sup>
12	1.60	1.22	-0.38	2.25
14'	1.60	1.19	-0.41	2.21
23	1.13	0.85	-0.28	2.62
34	0.95	0.76	-0.19	2.51

It should be noted that the cross-relaxation rate was negative, reflecting the slowing down of the molecular motion of the cyclodextrin due to the introduction of three groups on every unit. In the same way the  $\sigma_{ij}$  cross-relaxation terms of selected proton pairs collected in table 3.7 were calculated and, hence, by substituting *a*) these values, *b*) the fixed distance  $r_{6a6b}$  and *c*) its cross-relaxation rate  $\sigma_{6a6b}$  into the equation 3.7, the interproton distances  $r_{ij}$  were determined (table 3.7).

The distance  $r_{12}$  of 2.25 Å corresponded to the average value for two protons in an axial-equatorial spatial relationship, but its similarity to the distance H-1–H-4' (2.21 Å) reflected the tilting of the glucopyranose rings. Furthermore, the distances  $r_{23}$  (2.62 Å) and  $r_{34}$  (2.51 Å) were too short to be attributed to their 1,3-diaxial positions in the  ${}^4C_1$  chair conformation, according to the fact that derivatization of CD7 (**5**) generated a distortion which made the above distances shorter than they were in the  ${}^4C_1$  chair units conformers.

#### *Geometry of the association complexes between (R)-3e, (S)-3e and CD7 (5)*

In order to obtain information on the geometry of the diastereomeric complexes in solution, the 2D ROESY maps of equimolar solutions (*S*)-**3e**/**5** and (*R*)-**3e**/**5** were analysed. On the basis of the measured values of the association constants *K*, the equimolar concentration of 60 mM ( $C_6D_{12}$ , 25 °C) guaranteed the formation of detectable amounts of association complexes (see table 3.5 for the molar fraction of the bond analyte). The traces of the bidimensional maps were also compared with the monodimensional spectra obtained by 1D ROESY measurements (in figure 3.11 only the monodimensional measurements are reported).

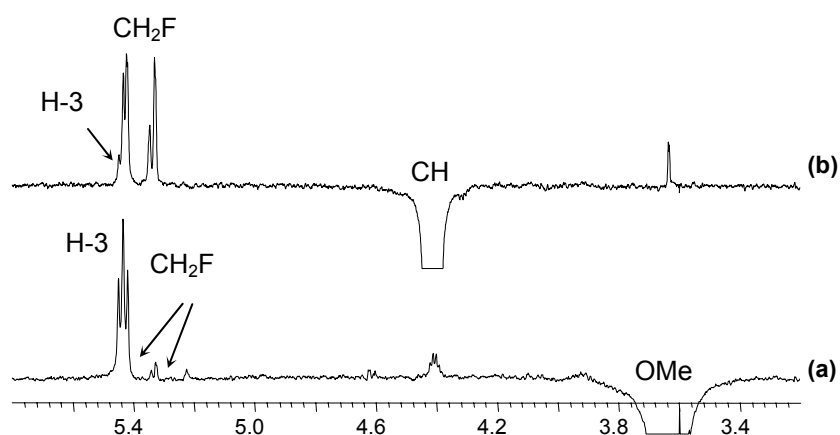


**Figure 3.11.** 1D ROESY (600 MHz,  $C_6D_{12}$ , 25 °C,  $\tau_m = 0.3$  s) spectra of an equimolar mixture of racemic **3e** and **5** (60 mM) corresponding to (a)  $CH_3O$ -protons and (b)  $CH$ -protons of **3e**.



According to this analysis, the conformation of **5** did not change after the association with (*R*)- or (*S*)-**3e**. Also the conformation of **3e** remained unchanged because also for the analyte the intramolecular NOEs detected for the free and bonded state are the same.

In both diastereomeric association complexes, the CH<sub>3</sub>O-group of the fluorinated diether **3e** is juxtaposed far away from the CH<sub>2</sub>F group whereas the CH-group is directed towards it, so that the molecule seems to be stretched out, with the CH<sub>3</sub>O-group far away from the CH<sub>2</sub>F-group. Thus, only the proton on the stereogenic center produced significant dipolar interaction with the CH<sub>2</sub>F group (figures 3.11 a and 3.11 b).

As far as the intermolecular NOEs are concerned, for both enantiomers of **3e** the CH<sub>3</sub>O-group of **3e** produced a very intense dipolar interaction with the inner H-3 proton (figure 3.11 a) lying on the wider internal diameter part of the cavity of the cyclodextrin.

No relevant intermolecular NOEs were detected between the CH<sub>3</sub>O-group and the inner H-5 proton belonging to the narrower internal diameter part of the cavity, as usually occur for total inclusion complexes, especially with native CD7. The CH-proton adjacent to the CH<sub>3</sub>O-group produced significantly lower NOEs on the H-3 proton (figure 3.11 b), but it was able to produce a higher NOE on the H-4 proton, located on the external surface of the cyclodextrin. Therefore, both enantiomers of **3e** undergo inclusion into the CD7 (**5**) only by their CH<sub>3</sub>O-group, but its penetration was not so deep (figure 3.12) to juxtapose it in the proximity of the internal proton H-5.

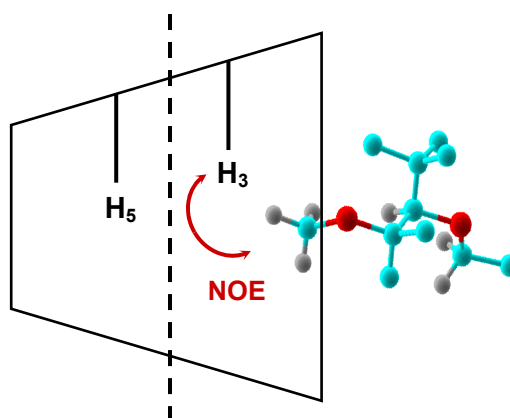


**Figure 3.12.** Schematic representation of the inclusion complex, where only a partial inclusion occurs.

In the traces of the 2D ROESY maps also significant intermolecular NOEs are detected among CH<sub>2</sub>F- protons of the enantiomers of **3e** and the silyl and acetyl substituents of CD7

(5) indicating that the CH<sub>2</sub>F (and hence the CF<sub>3</sub> group) must be directed towards the external surface bent at the acetyl and silyl groups (*vide supra*).

Therefore it can be concluded that both enantiomers of **3e** are partially included into **5** by their CH<sub>3</sub>O-groups from the wider internal diameter part of the cyclodextrin cavity with the CH-proton approaching the larger rim, while the CH<sub>2</sub>F- and CF<sub>3</sub>-groups interacted with the external surface. This geometrical arrangement may favour attractive fluorine-silicium interactions. Moreover, taking into account that the two enantiomers of **3e** seem to be included with a very similar geometry, the enantiodiscrimination should be determined mainly by diastereomeric interactions of the enantiomers with different stability between two *D*-glucopyranose units. This asymmetric region forces the CH<sub>2</sub>F and CF<sub>3</sub>-groups of **3e** to experience two different environments between the (*S*)-and (*R*)-enantiomers of **3e**. Entropic and enthalpic contributions to stability can only be ascertained *via* temperature dependent studies (figure 3.13).

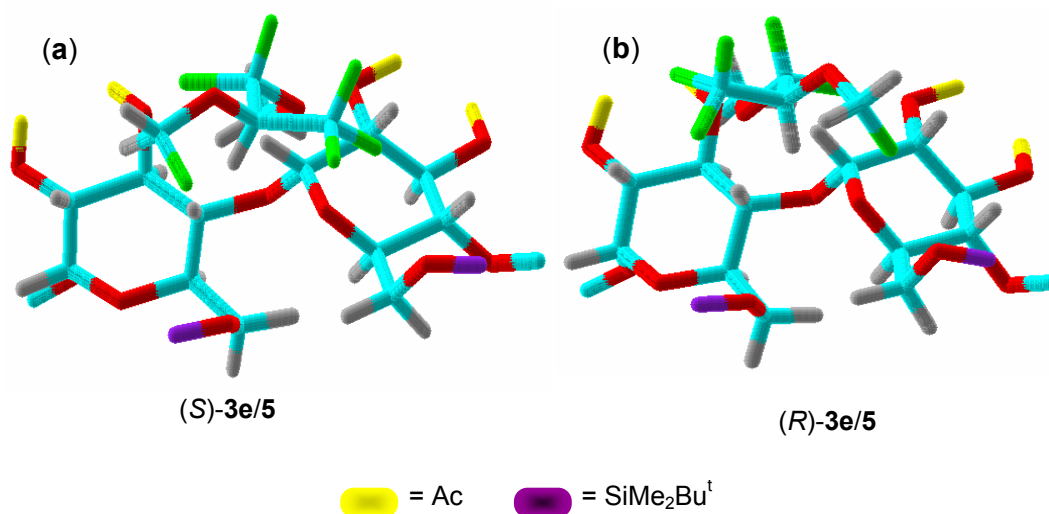


**Figure 3.13.** Schematic representation of the included enantiomers (*R*)-**3e** and (*S*)-**3e** close to two adjacent glucopyranose units of **5** (PCModel 6.0 program, MMx force field).

Furthermore, this merely “static interaction model” must be extended to a dynamic one, in which the fluorinated (*S*)-**3e** undergoes multiple fluorine-silicium stabilizing interactions which are stronger as compared to (*R*)-**3e**, explaining also its longer retention time in the GC separation, its larger association constant as well as the enhanced broadening of its resonances. It is important to underline that the NMR analysis in solution exhibits several limits in regard to a direct comparison with the gas-chromatographic results. The effect of the solvent, which reduces the interaction strength and competes with the analyte in the complex

formation, must be taken into account in order to justify the minor efficiency of the selectors in comparison to the gas phase. Moreover, in the gas chromatographic analysis, the chiral selector interacts with the highly diluted analyte by a high selector/selectand ratio, besides the continuous interaction which takes place across all the length of the column, while in solution such high ratios are not feasible.

The main interesting aspects described above can be summarized as follows:

- a) the enantioselective interaction is confined to a restricted (limited) region of the selector (the glycosidic linkage between two glucose units);
- b) the inclusion phenomenon is one of the multimodal processes involved in the complexation;
- c) in comparison to several enantiorecognition mechanisms, only two geometries of suitable diastereomeric complexes are proposed, in contrast to a multitude of hypotheses which characterizes other studies.

If the inclusion process is a step of the multimodal interaction which takes place in the enantiorecognition mechanism, is it possible to focus on the analysis of acyclic systems which have no cavity (or not a true cavity) in order to get information about the influence of the outside/inside interactions which might be involved in the complexation? Consequently, in chapter IV an extensive application of ‘acyclodextrins’ as chiral stationary phases for gas chromatography is furnished, while in section 3.3 a preliminary application of linear dextrans as CSA in solution is described.

### 3.3. Preliminary study of ‘acyclodextrins’ in solution

A preliminary study in solution indicates that even the open system heptakis[(2,3-di-*O*,4''-*O*)-acetyl-(1'-*O*,6-*O*)-*tert*-butyldimethylsilyl]-maltoheptaose G7 (**10**) is able to produce enantiodiscrimination, even if chemical shift nonequivalences are remarkably smaller as compared to those with the CD7 (**5**) (table 3.8).

The figure 3.14 shows the <sup>1</sup>H-NMR spectrum of a mixture (1:1) formed by ‘compound B’ and the derivatives CD7 (**5**) and G7 (**10**) (for the structure of these selectors and the racemic analyte see chapter II).

The above mentioned trend is observed also in the <sup>19</sup>F-NMR measurements (figure 3.15), where slight enantiodiscrimination is produced by the linear selector G7 (**10**) towards the perfluorodiether ‘compound B’. Moreover, as shown in figure 3.15, the chemical shift nonequivalences for the CH<sub>2</sub>F can be increased adding the chiral selector to the 1:1 mixture

(figure 3.15 c-f). However, the chemical shift nonequivalence is significantly lower than that obtained with the CD7 (**5**) (table 3.5).

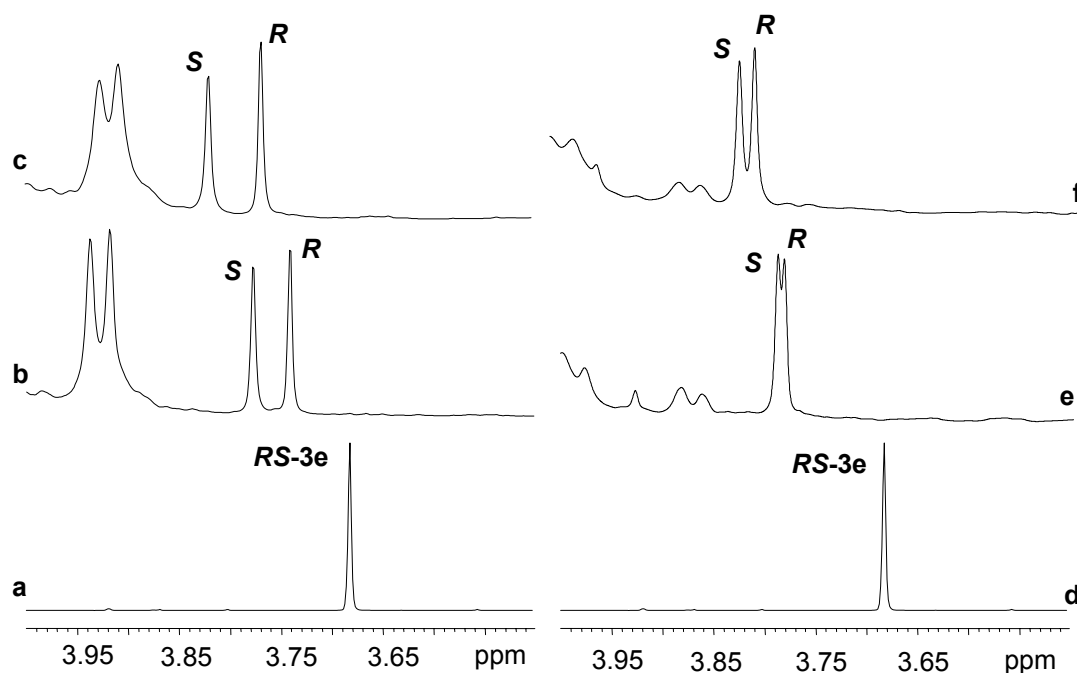


**Figure 3.14.** *Left:*  $^1\text{H}$ -NMR (600 MHz,  $\text{C}_6\text{D}_{14}$ ) spectral regions corresponding to the protons of the  $\text{CH}_3\text{O}$ -group of (a) pure racemic **3e** (60 mM, 25 °C), (b) equimolar mixture of racemic **3e** and **5** (60 mM, 25 °C), (c) equimolar mixture of racemic **3e** and **5** (60 mM, 5 °C). *Right:*  $^1\text{H}$  NMR (600 MHz,  $\text{C}_6\text{D}_{14}$ ) spectral regions corresponding to the protons of the  $\text{CH}_3\text{O}$ -group of (d) pure racemic **3e** (60 mM, 25 °C), (e) equimolar mixture of racemic **3e** and **10** (60 mM, 25 °C), (f) equimolar mixture of racemic **3e** and **10** (60 mM, 5 °C).

**Table 3.8.**  $^1\text{H}$  NMR (600 MHz,  $\text{C}_6\text{D}_{14}$ ) chemical shift nonequivalence  $\Delta\delta^a$  data measured for racemic ‘compound B’ **3e** in the presence of cyclic **5** and acyclic **10**.

<i>guest</i>	$\Delta\delta$ (ppm)			
	<i>RS-3e/5</i>		<i>RS-3e/10</i>	
	25 °C	5 °C	25 °C	5 °C
	CH	CH	CH	CH
	0.153	0.222	0.008	0.010
	OCH <sub>3</sub>	OCH <sub>3</sub>	OCH <sub>3</sub>	OCH <sub>3</sub>
	0.036	0.052	0.006	0.012

<sup>a</sup> $\Delta\delta = |\delta_S - \delta_R|$ , difference between the chemical shifts (ppm) of corresponding nuclei of the two enantiomers of **3e** in the presence of CD7 (**5**) and G7 (**10**).

The association constants for the diastereomeric complexes have been calculated by NMR diffusion analysis. Surprisingly the reduction of the diffusion coefficients in solution from the free to the bound state for ‘compound B’ is similar with the cyclic CD7 (**5**) and acyclic G7

(10) selectors and the values of the association constants are almost the same (figure 3.16 and table 3.9).

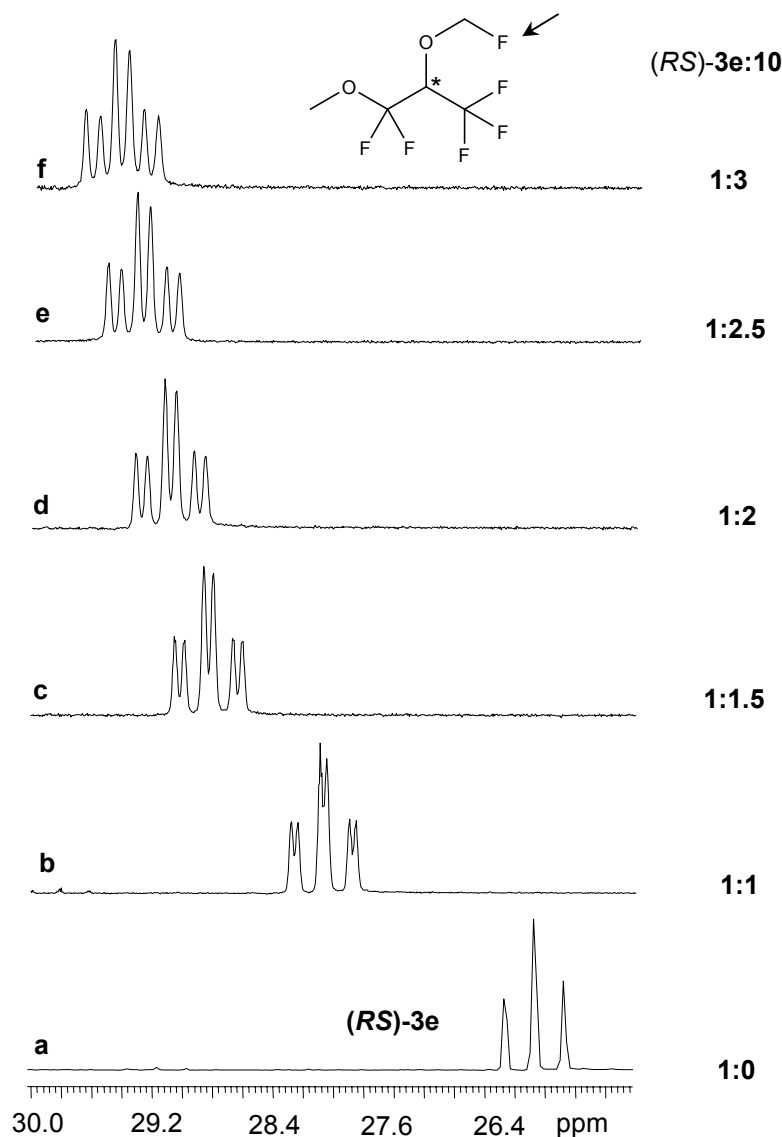


**Figure 3.15.**  $^{19}\text{F}$ -NMR (282 MHz,  $\text{C}_6\text{D}_{14}$ , 25 °C) spectral regions corresponding to the fluorine nuclei of the  $\text{CH}_2\text{F}$ -group of (a) pure racemic **3e** (60 mM), (b) 1:1 mixture of racemic **3e** and **10** (c) 1:1.5 mixture (d) 1:2 mixture (e) 1:2.5 mixture and (f) 1:3 mixture.

This comparison represents a very important example where the different geometries of the diastereomers plays a more decisive role than the differences of the association constants in the enantio-recognition process. Indeed the strength of the diastereomeric complexes is the same on the two selectors (the diffusion coefficient from the free to the bound state is equally reduced on the cyclic and linear dextrans) but their geometries exhibit reasonably a favourite

interactions on the CD7 (**5**) compared to the acyclic G7 (**10**), as confirmed by the high chemical shift nonequivalences produced by CD7 (**5**).

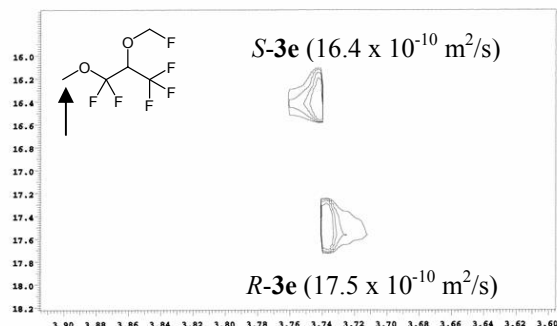


**Figure 3.16.** DOSY spectra for the racemic ‘compound B’ in presence of an equimolar amount of G7 (**10**). Spectral region (diffusion coefficients) corresponding to the methoxy groups.

**Table 3.9.** Diffusion coefficients  $D$  ( $10^{-10} \text{ m}^2/\text{s}$ ) in  $\text{C}_6\text{D}_{14}$  of the analyte **3e** in the free and bound state, of the CD7 (**5**) and G7 (**10**), molar fraction of the bound guest ( $X_b$ ) and association constants  $K$  ( $\text{M}^{-1}$ ) calculated according to the equation 3.4.

			$D$ ( $10^{-10} \text{ m}^2/\text{s}$ )	
			$\beta$ -CD ( <b>5</b> )	G7 ( <b>10</b> )
			4.35	3.65
$D_{RS-3e}$ (free)	$D-3e/5$	$D-3e/10$		
31.5	18.1 ( <i>R</i> )	17.5 ( <i>R</i> )		
	15.9 ( <i>S</i> )	16.4 ( <i>S</i> )		
			$X_b$	
			0.49 ( <i>R</i> )	0.50 ( <i>R</i> )
			0.58 ( <i>S</i> )	0.54 ( <i>S</i> )
			$K$ ( $\text{M}^{-1}$ )	
			32.2 ( <i>R</i> )	33.9 ( <i>R</i> )
			53.1 ( <i>S</i> )	43.1 ( <i>S</i> )

This kind of study will be a suitable tool in the future to understand the association of some other cyclodextrin derivatives, like Lipodex E [(3-*O*-butanoyl-2,6-di-*O*-pentyl)- $\gamma$ -cyclodextrin] (**27**, for the structure see chapter II), which in solution is also able to produce high chemical shift nonequivalences, as shown in figure 3.17. Indeed, CD8 (**27**) exhibits

chemical shift nonequivalences which are comparable with those obtained by CD7 (**5**) ( $\Delta\delta$ , OCH<sub>3</sub>, 25 °C, C<sub>6</sub>D<sub>12</sub>) = 0.094 ppm;  $\Delta\delta$  (CH, 25 °C, C<sub>6</sub>D<sub>12</sub>) = 0.391 ppm).

Moreover, the values of the association constants for the complexes formed by ‘compound B’ and Lipodex E are noteworthy very interesting due to their significant difference ( $K_S = 7646.4 \text{ M}^{-1}$  and  $K_R = 161.6 \text{ M}^{-1}$ ). The value of the  $K_S$  is typical of an inclusion complex, whilst in the case of *R*-enantiomer the low association might involve only an outside interaction. However, for these diastereomeric complexes a further analysis is required.

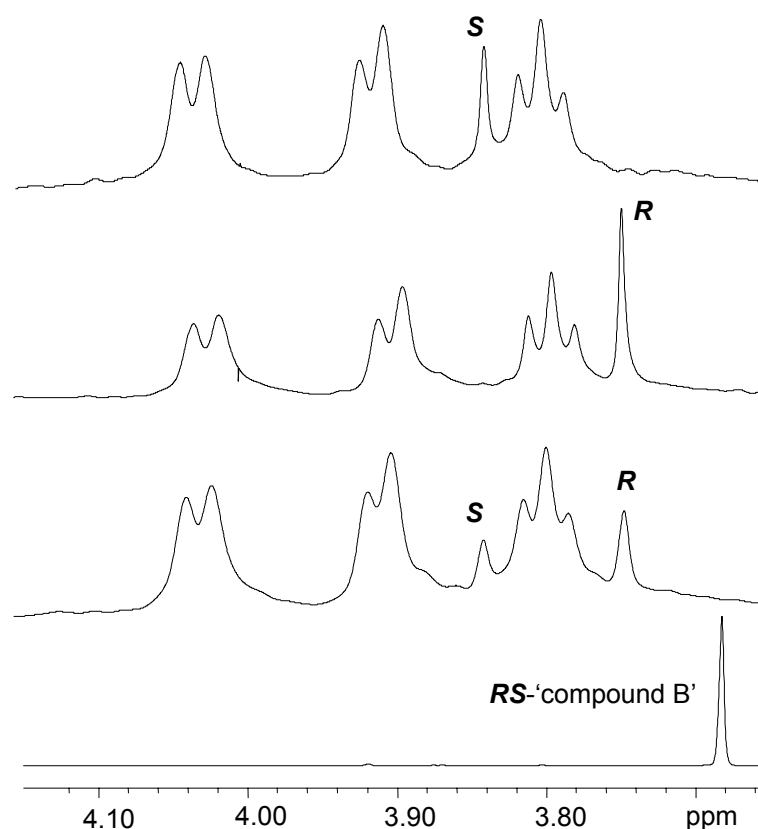


**Figure 3.17.** <sup>1</sup>H NMR (600 MHz, C<sub>6</sub>D<sub>14</sub>) spectral regions corresponding to the protons of the CH<sub>3</sub>O-group of (a) pure racemic **3e** (60 mM, 25 °C), (b) equimolar mixture of racemic **3e** and Lipodex E **27** (60 mM, 25 °C); (c) *R*-**3e** and Lipodex E (1:1, 60 mM, 25 °C); (d) *S*-**3e** and Lipodex E (1:1, 60 mM, 25 °C).

The proposed self-inclusion of the *n*-pentyl groups in solution seems to be established but the influence the cavity size for this CD8 (**27**) has not been explained.<sup>132</sup> As mentioned in chapter II CD8 (**27**) shows the highest enantioselectivity factor for ‘compound B’ but several aspects must still be studied in depth.<sup>118</sup>

Future studies will be focused on the attempt to verify the inclusion or the outside interaction for the analyte molecule in the association with the cyclodextrin selector, as shown in figure

3.18, in addition to the application of the acyclic G8 (**28**) as CSA for NMR spectroscopy in solution.



**Figure 3.18.** Schematic representation of the CD8 (**27**) with a self-included *n*-pentyl group and the guest analyte inside or outside the cavity.



## Chapter IV

### Results and discussion: Part III

#### Enantioseparation by gas chromatography



#### 4.1. Introduction

Because of the convenient preparation of the mixed silylated/acetylated cyclodextrins **4-6** (for their structures, see chapter III), the analogous linear dextrans comprising different number of glucose units (maltoheptaose G7, maltooctaose G8, maltotriose G3, *D*- and *L*-glucose G1) carrying the same functional groups were prepared yielding the new selectors **10**, **12**, **14**, **16** and **18** respectively (see chapter II for their structures).

Investigations with these derivatives were focused on an attempt to answer the key question “for which kind of cyclodextrin derivatives is the inclusion phenomenon the driving force of the enantioselectivity?” This question may be answered by applying the novel linear dextrin derivatives as chiral stationary phases (CSPs) for enantioselective gas chromatography. The application of acyclic dextrans as CSPs may also confirm the role of the functional groups of the derivatized cyclodextrins which strongly influences the structure of the macrocycles and markedly affects the cavity size of the  $\alpha$ -,  $\beta$ - and  $\gamma$ -congeners, in addition to their unpredictable behaviour as chiral selectors.

In this section a systematic comparison of cyclic and acyclic selectors is described, which will shed light on the role of the cavity in the enantioselectivity process. Thermodynamic data are also measured utilizing the concept of the retention increment  $R'$  for the enantioselectivity of different classes of compounds and, on the basis of these data, mechanisms of enantioselectivity are proposed. Most of the examples involve the comparison between heptakis(2,3-di-*O*-acetyl-6-*O*-*tert*-butyldimethylsilyl)- $\beta$ -cyclodextrin CD7 (**5**) and heptakis[(2,3-di-*O*,4''-*O*)-acetyl-(1'-*O*,6-*O*)-*tert*-butyldimethylsilyl]-maltoheptaose G7 (**10**). The effect of the number of glucose units in the oligosaccharides has been studied by comparing results from G7 (**10**) with those obtained from tris[(2,3-di-*O*,4''-*O*)-acetyl-(1'-*O*,6-*O*)-*tert*-butyldimethylsilyl]-maltotriose G3 (**14**) and the two chiral stationary phases based on single units (2,3,4-tri-*O*-acetyl-1,6-di-*O*-*tert*-butyldimethylsilyl)-*D*-glucose *D*-G1 (**16**) and (2,3,4-tri-*O*-acetyl-1,6-di-*O*-*tert*-butyldimethylsilyl)-*L*-glucose *L*-G1 (**18**).

#### 4.2. Enantioselectivity of halogenated anaesthetics and ‘compound B’

The role of molecular inclusion when utilizing cyclodextrin selectors cannot be ignored in examples of extreme enantioselectivities and their variation with the size of the cavity. For example, the unusually high enantioselectivity factor of  $\alpha = 4.1$  was observed for racemic 2-(fluoromethoxy)-3-methoxy-1,1,1,3,3-pentafluoropropane (‘compound B’, a decomposition product of the narcoticum sevoflurane, see also chapter II) on CD7 (**5**) (figure 4.1 a). The

separation factor drops to  $\alpha = 2.7$  for CD8 (**6**) and to  $\alpha =$  unity (no enantioseparation) for CD6 (**4**).

Surprisingly, 'compound B' is also separated on the corresponding maltoheptaose derivative G7 (**10**), although with markedly reduced enantioselectivity (figure 4.1 b). More interestingly, enantioselectivity is displayed by *acyclic* G7 (**10**) but not by *cyclic* CD6 (**4**) (table 4.1). It seems reasonable to explain the enantioseparation on the acyclic selector as a result of the existence of the 'semi-cavity' formed by the seven derivatized glucose units. Moreover, this hypothesis may shed light on the role of the external surface in the enantiorecognition in solution described in chapter III in the case of the cyclic CD7 (**5**), where the enantiorecognition was localized mainly between two adjacent glucose units and partial inclusion of 'compound B' was detected. Thus, the arrangement of the TBDMS and acetyl groups on the linear selector G7 (**10**) allows two enantiomers to be selectively bound on the external surface, but with diminished enantioselectivity.

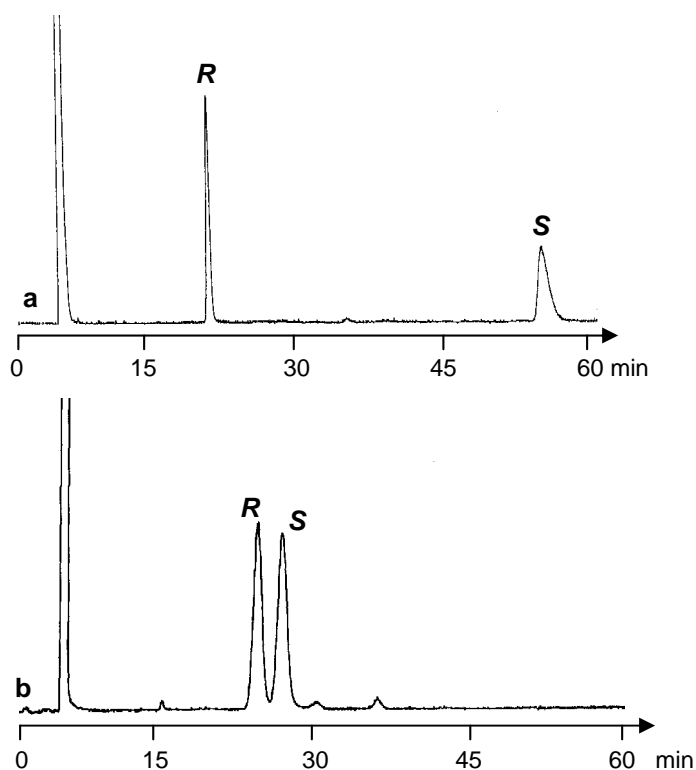


**Figure 4.1.** Gas-chromatographic separation of racemic 2-(fluoromethoxy)-3-methoxy-1,1,1,3,3-pentafluoropropane ('compound B') **3e** on CD7 (**5**) (a) and on G7 (**10**) (b) (each 20 % (w/w) in PS 86). Columns: 20 m x 0.25 mm i.d. fused-silica capillary, film thickness 0.25  $\mu\text{m}$ . Carrier gas: 30 kPa  $\text{H}_2$ ; oven temperature: 30  $^\circ\text{C}$ .

**Table 4.1.** Enantioseparation factor  $\alpha$  for ‘compound B’ (**3e**) on cyclic (**4-6**) and acyclic chiral selector (**10**) (for all the structures, see chapter II) at 30 °C.

	CD6 ( <b>4</b> )	CD7 ( <b>5</b> )	CD8 ( <b>6</b> )	G7 ( <b>10</b> )
<b>3e</b>	1.00	4.10	2.70	1.07

Thus, in the case of CD7 (**5**), the inclusion appears to be the driving force of enantioselectivity since it generates a higher enantioselectivity than does the corresponding acyclic G7 (**10**). However, the separation produced by G7 (**10**) suggests that the outside interactions also play an important role which may evolve as the “key interaction” for certain analytes of defined structures.

Further proof of the importance of the cavity for the enantioselectivity is provided by the separation of related halogenated anaesthetics (halothane **3a**, desflurane **3b**, enflurane **3c** and isoflurane **3d**, for structures see chapter III). Although the enantiomers of all chiral anaesthetics **3a-d** are separated on the cyclic CD7 (**5**) (figure 4.2), none are separated on the linear G7 (**10**).

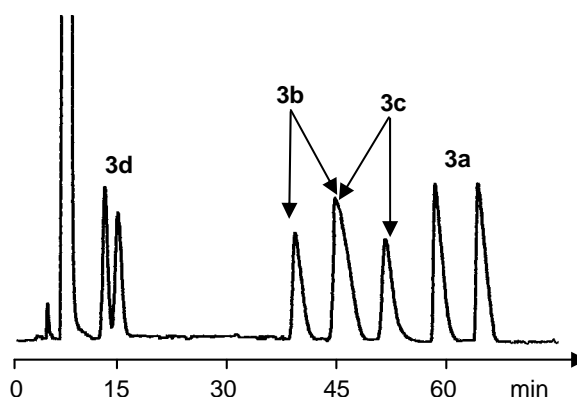


**Figure 4.2.** Gas-chromatographic separation of racemic halogenated anaesthetics on CD7 (**5**), 20 % (w/w) in PS 86; column: 25 m x 0.25 mm i.d. fused-silica capillary, film thickness 0.25  $\mu\text{m}$ . Carrier gas: 30 kPa  $\text{H}_2$ ; oven temperature: 30 °C. **3a**) halothane, **3b**) desflurane, **3c**) enflurane, **3d**) isoflurane; for structures see chapter III.

However, in order to demonstrate that not only the size of the cavity, but also the nature of the functional groups on the two rims of cyclodextrins plays a decisive role in the enantioselectivity, another two  $\beta$ -cyclodextrin derivatives, heptakis(2,3-di-*O*-methyl-6-*O*-*tert*-butyldimethylsilyl)- $\beta$ -cyclodextrin (**7**) and heptakis(2,3-di-*O*-*n*-pentyl-6-*O*-*tert*-butyldimethylsilyl)- $\beta$ -cyclodextrin (**8**) were investigated as chiral selectors for the enantioseparation of ‘compound B’ **3e** (figure 4.3).

The presence of an alkyl group (methyl or *n*-pentyl) on the 2- and 3-sites of the  $\beta$ -cyclodextrin instead of an acetyl group caused a significant reduction of the enantioseparation factor  $\alpha$ , as shown in figure 4.3 (for the structures of the selectors see chapter II). This is a very important proof about the strong influence of different functional groups on the overall structure of the native  $\beta$ -cyclodextrin: full derivatization not only modifies the conformation but may even influence the size of the cavity.

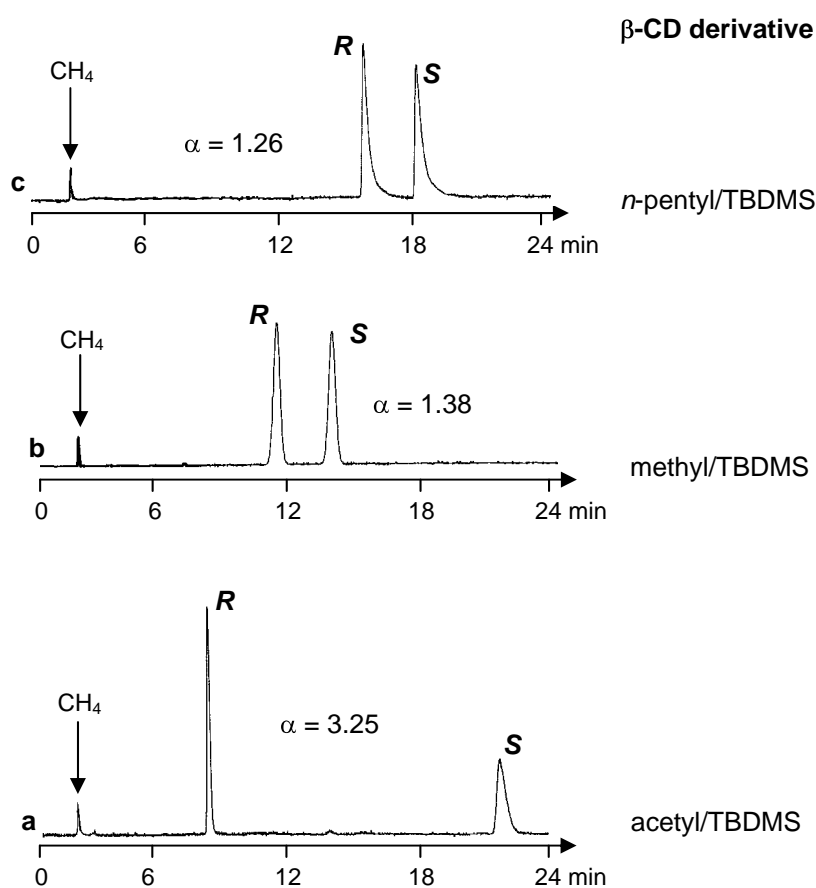


**Figure 4.3.** Gas-chromatographic separation of racemic 2-(fluoromethoxy)-3-methoxy-1,1,1,3,3-pentafluoropropane ('compound B') **3e** on (a) heptakis(2,3-di-*O*-acetyl-6-*O*-*tert*-butyldimethylsilyl)- $\beta$ -cyclodextrin (**5**), on (b) heptakis(2,3-di-*O*-methyl-6-*O*-*tert*-butyldimethylsilyl)- $\beta$ -cyclodextrin (**7**) and on (c) heptakis(2,3-di-*O*-pentyl-6-*O*-*tert*-butyldimethylsilyl)- $\beta$ -cyclodextrin (**8**) (each 20 % (w/w) in PS 86). Columns: 10 m x 0.25 mm i.d. fused-silica capillary, film thickness 0.25  $\mu$ m. Carrier gas: 40 kPa He; oven temperature: 30  $^{\circ}$ C.

#### 4.3. Enantioseparation of $\alpha$ -amino acid derivatives

Turning from halogenated compounds to amino acids derivatives, the results become more intriguing. As shown in figure 4.4, the racemic *N*-trifluoroacetyl-*O*-methyl esters of  $\alpha$ -amino

acids could both be separated on the cyclic CD7 (**5**) and on the analogous linear dextrin counterpart G7 (**10**) using optimized temperature programs. The similar enantioseparation for the alanine (**Ala**) derivative and the difference of the elution order for the *tert*-butyl leucine (**<sup>t</sup>BuLeu**) and norvaline (**Norval**) derivatives on the two selectors should be noted. All five amino acid derivatives showed higher enantioseparation factors  $\alpha$  on the cyclic CD7 (**5**) than on the acyclic analogue G7 (**10**) (table 4.2). The retention factors  $k$  of the enantiomers are quite different between CD7 (**5**) and G7 (**10**) and in all separations, *D*-enantiomers are eluted after *L*-enantiomers.

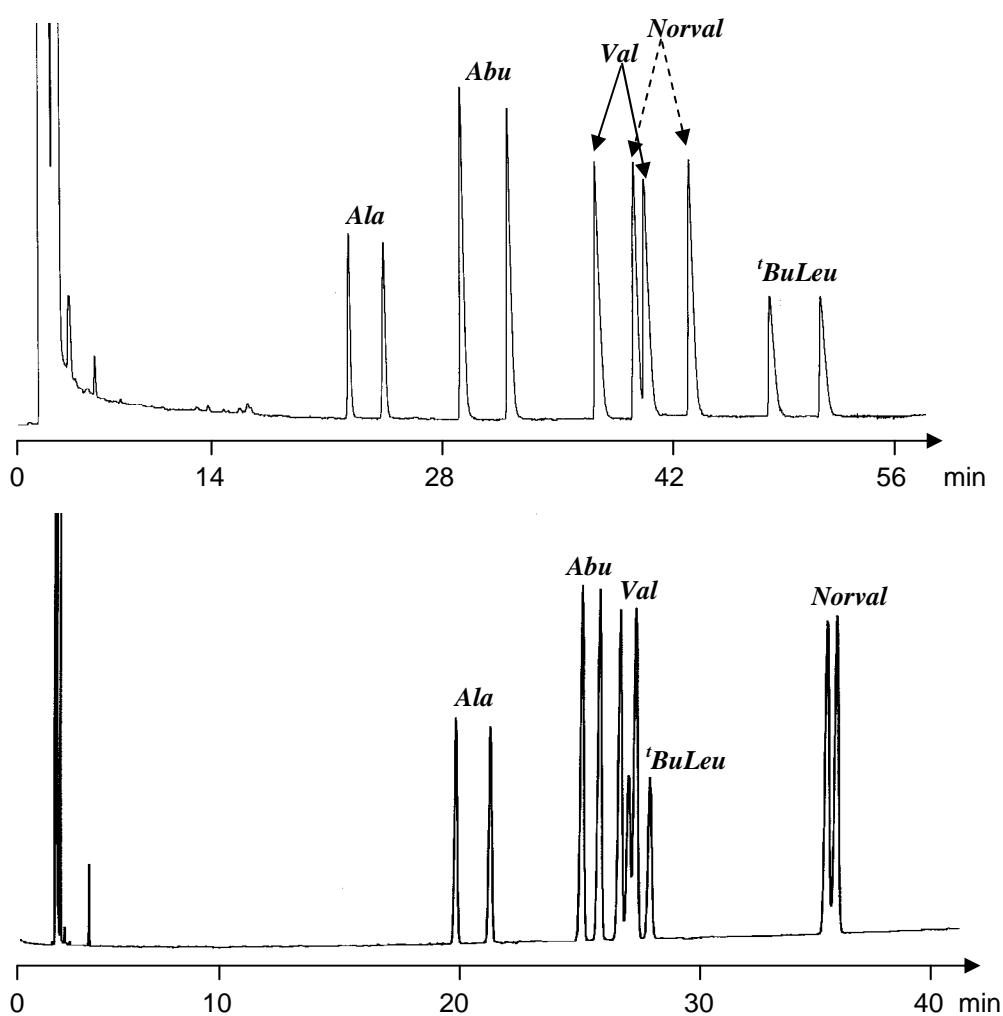


**Figure 4.4.** Gas-chromatographic separation of racemic *N*-trifluoroacetyl-*O*-methyl esters of  $\alpha$ -amino acids on CD7 (**5**) (*top*) and on G7 (**10**) (*bottom*) (each 20 % (w/w) in PS 86). Columns: 20 m x 0.25 mm i.d. fused-silica capillary, film thickness 0.25  $\mu$ m. Carrier gas: 80 kPa H<sub>2</sub>; oven temperature: 90 °C (5 min), temperature program to 120 °C, 0.5 °C/min (*top*); carrier gas: 50 kPa H<sub>2</sub>; oven temperature: 80 °C (5 min), temperature program to 120 °C, 0.5 °C/min. (*bottom*).

More striking differences are observed for the separation of the racemic *N*-trifluoroacetyl-*O*-ethyl esters of  $\alpha$ -amino acids. Whereas the enantioselectivity is higher for alanine (**Ala**) on cyclic CD7 (**5**) as compared to acyclic G7 (**10**) (table 4.3), only the two diastereomers of isoleucine (**IsoLeu**) are separated on cyclic CD7 (**5**) (figure 4.5 a). However, they are further resolved into enantiomers on acyclic G7 (**10**) (figure 4.5 a).

**Table 4.2.** Retention factor  $k_1$  (first eluted enantiomer), enantioseparation factor  $\alpha$  and resolution factor  $R_s$  for *N*-trifluoroacetyl-*O*-methyl esters of some  $\alpha$ -amino acids. Experimental condition: 85 °C (isothermal), 60 kPa (H<sub>2</sub>).

	CD7 ( <b>5</b> )			G7 ( <b>10</b> )		
	$k_1$	$\alpha$	$R_s$	$k_1$	$\alpha$	$R_s$
Ala	10.2	1.18	5.59	9.9	1.10	5.21
2-Abu	16.9	1.23	4.69	14.2	1.04	2.44
Val	28.4	1.09	1.75	15.6	1.04	2.02
Norval	34.1	1.14	2.65	15.9	1.05	2.75
<sup>t</sup> BuLeu	51.1	1.25	12.8	24.8	1.02	1.25

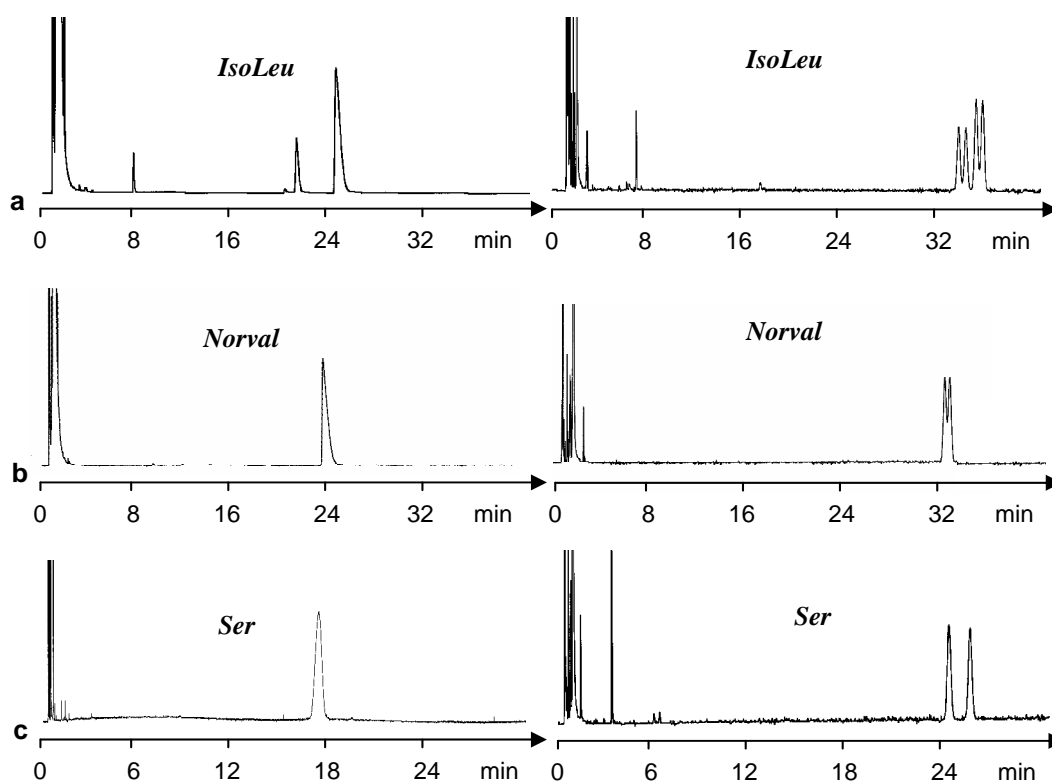


**Figure 4.5.** Gas-chromatographic separation of racemic *N*-trifluoroacetyl-*O*-ethyl esters of  $\alpha$ -amino acids on CD7 (**5**) (left) and on G7 (**10**) (right) (each 20 % (w/w) in PS 86). Columns: 20 m x 0.25 mm i.d. fused-silica capillary, film thickness 0.25  $\mu$ m. For other experimental conditions, cf. table 4.3.



Norvaline (**Norval**) (figure 4.5 b) and serine (**Ser**) (figure 4.5 c) can be separated on acyclic G7 (**10**) but not on cyclic G7 (**5**), while methionine (**Met**) does not show any enantioseparation on the acyclic G7 (**10**). Proline (**Pro**) shows the highest difference of the retention factors  $k_1$ . Further differences in the retention factor  $k$  and enantioseparation factor  $\alpha$  between CD7 (**5**) and G7 (**10**) are evident from table 4.3.

**Table 4.3.** Retention factor  $k_1$  (first eluted enantiomer), enantioseparation factor  $\alpha$  and resolution factor  $R_s$  for *N*-trifluoroacetyl-*O*-ethyl esters of some  $\alpha$ -amino acids. Experimental conditions: a) 90 °C (isothermal), 60 kPa (H<sub>2</sub>); b) 100 °C (isothermal), 80 kPa (H<sub>2</sub>); c) 110 °C (isothermal), 60 kPa (H<sub>2</sub>); d) 120 °C (isothermal), 60 kPa (H<sub>2</sub>).

	CD7 ( <b>5</b> )			G7 ( <b>10</b> )		
	$k_1$	$\alpha$	$R_s$	$k_1$	$\alpha$	$R_s$
Ala <sup>a</sup>	26.4	1.60	13.6	10.0	1.08	4.17
IsoLeu <sup>a</sup>	14.3	1.00	–	27.0	1.02	1.25
	16.7	1.00	–	28.3	1.02	1.04
Thr <sup>a</sup>	52.9	1.34	8.50	24.6	1.02	0.94
Norval <sup>a</sup>	21.7	1.00	–	24.9	1.01	0.84
Val <sup>a</sup>	11.7	1.08	1.60	16.6	1.03	1.70
Pro <sup>b</sup>	20.1	1.16	6.64	39.4	1.02	1.83
Ser <sup>b</sup>	27.3	1.00	–	25.3	1.06	3.03
Leu <sup>b</sup>	15.5	1.01	0.51	20.2	1.00	–
Asp <sup>c</sup>	37.8	1.03	1.15	44.2	1.03	2.08
Met <sup>d</sup>	143.8	1.04	1.66	45.7	1.00	–

As shown in figure 4.6, CD7 (**5**) exhibits the highest enantioselectivity in the optimized conditions for the enantioseparation of racemic *N*-trifluoroacetyl-*O*-ethyl ester derivative of serine (**Ser**) on the cyclic selectors with different cavity sizes [CD6 (**4**), CD7 (**5**) and CD8 (**6**)]. Yet, the most remarkable enantioseparation is still obtained on the linear dextrin G7 (**10**) as compared to the cyclic selectors **4-6**.

From these results it is evident that different and complementary enantiorecognition mechanisms occur with the *cyclic* vs. *acyclic* selectors CD7 (**5**) and G7 (**10**) and that an important role is played by the structure of the analytes (*methyl* vs. *ethyl* esters). This observation prevents the elucidation of a general and universal enantiorecognition model for enantioselective cyclodextrin derivatives.

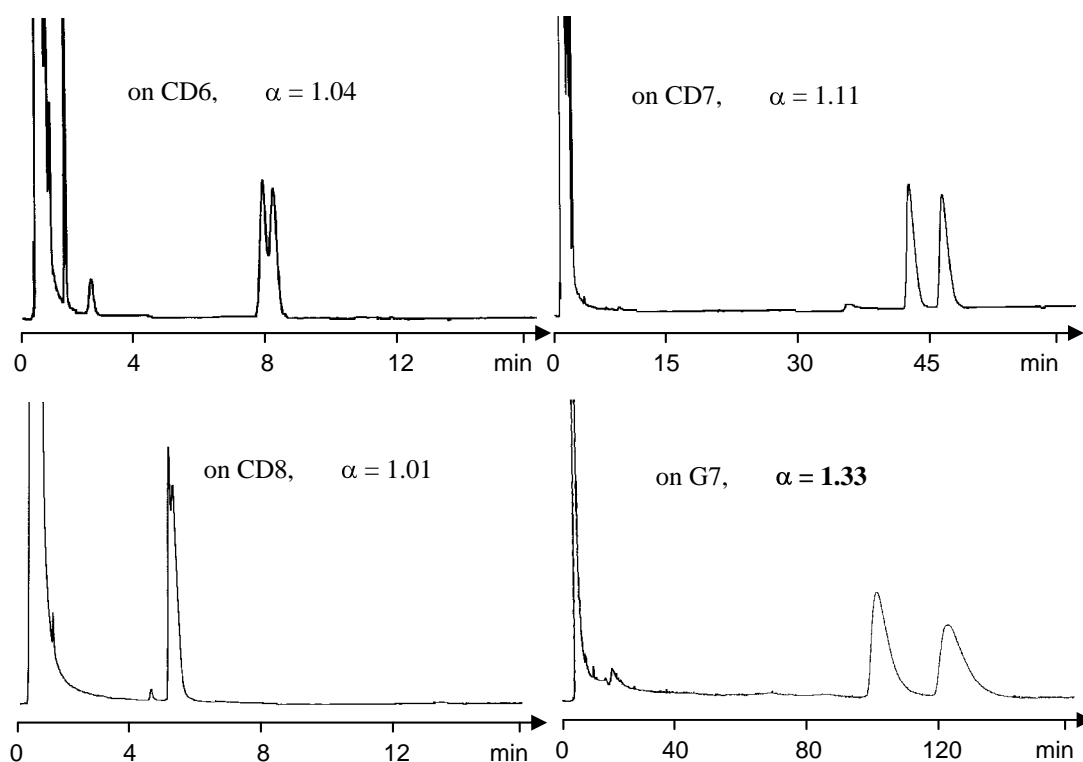


**Figure 4.6.** Gas-chromatographic separation of racemic *N*-trifluoroacetyl-*O*-ethyl ester of serine (**Ser**) on CD6 (**4**), CD7 (**5**), CD8 (**6**) and on G7 (**10**) (each 20 % (w/w) in PS 86). Columns: 10 m x 0.25 mm i.d. fused-silica capillary, film thickness 0.25  $\mu\text{m}$ . Carrier gas: 100 kPa He; oven temperature: 50  $^{\circ}\text{C}$  (for the structures of the selectors, see chapter II).

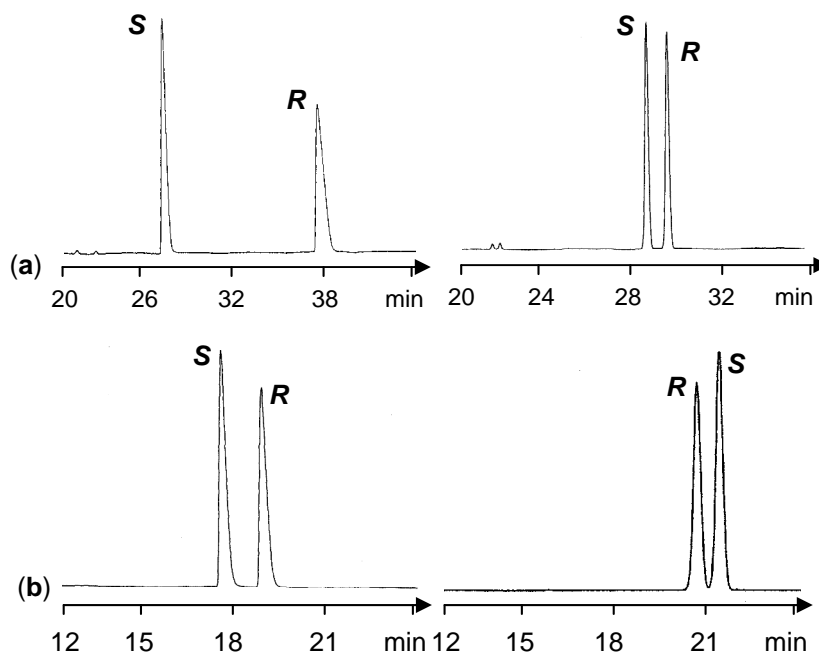
**Table 4.4.** Enantioseparation factor  $\alpha$  for *N*-trifluoroacetyl-*O*-ethyl ester of serine (**Ser**) enantioseparated on the cyclic (**4-6**) and acyclic chiral selectors (**10**) (for all the structures, see chapter II) at 50  $^{\circ}\text{C}$ .

	CD6 ( <b>4</b> )	CD7 ( <b>5</b> )	CD8 ( <b>6</b> )	G7 ( <b>10</b> )
<b>3e</b>	1.04	1.11	1.01	1.33

#### 4.4. Further enantioseparations of various derivatized and underivatized compounds

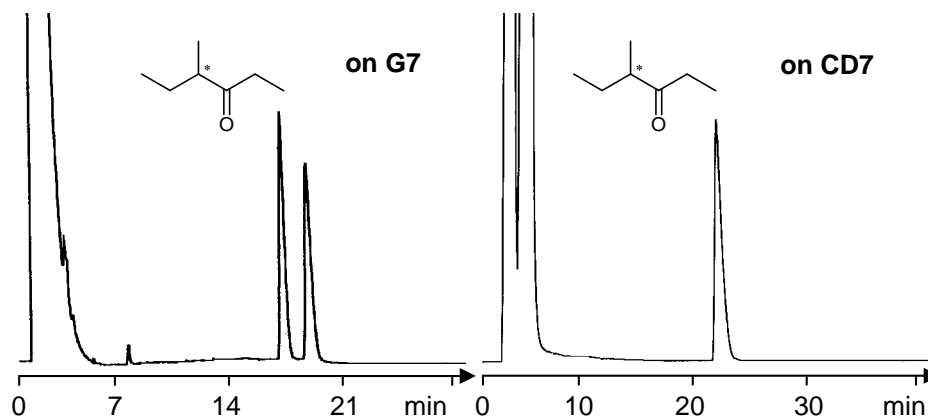
In addition to the amino acid derivatives, acyclic G7 (**10**) is capable to separate a broad spectrum of racemic compounds (table 4.5), especially fluorinated derivatives of aromatic and aliphatic amines and alcohols, but also some underivatized diols and ketones. Thus, the pentafluoropropionyl derivative of the aromatic 1-(phenyl)ethylamine **4a** as well as 1-(cyclohexyl)ethylamine **4b** are baseline separated on both the linear G7 (**10**) and cyclic CD7 (**5**). The heptafluorobutanoyl derivative of 2-octylamine **4d** is well separated on G7 (**10**) and on CD7 (**5**), while the 2-methyl-butylamine **4c** is not separated on both selectors. This shows that the two chiral stationary phases have a similar trend in their enantioselective ability towards some analytes.

Unexpectedly, whereas in the case of the amide **4a** the elution order is the same on both selectors, in the case of the amide **4b** the opposite elution order is observed (figure 4.7).



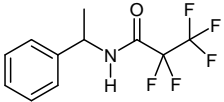
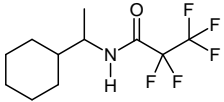
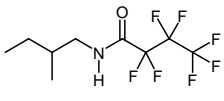
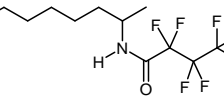
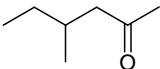
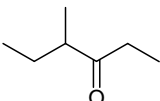
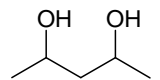
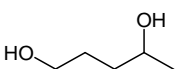
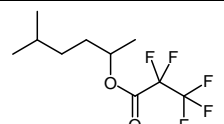
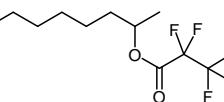
**Figure 4.7.** Gas-chromatographic separation of racemic pentafluoropropionyl derivatives of (a) 1-(phenyl)ethylamine **4a** and (b) 1-(cyclohexyl)ethylamine **4b** on CD7 (**5**) (left) and on G7 (**10**) (right) (each 20 % (w/w) in PS 86). Columns: 25 m x 0.25 mm i.d. fused-silica capillary, film thickness 0.25  $\mu\text{m}$ . For other experimental conditions, cf. table 4.5.

Both racemic ketones **4e** and **4f** are separated on acyclic G7 (**10**) but surprisingly the ketone **4f** is not separated on CD7 (**5**), although CD7 (**5**) and the G7 (**10**) display similar separation efficiency towards the ketone **4e** (figure 4.8 and table 4.5). This example represents a very important result where the enantioselectivity of a cyclodextrin derivative failed in contrast to the linear dextrin counterpart.



**Figure 4.8.** Gas-chromatographic separation of racemic 4-methyl-3-hexanone **4f** on CD7 (**5**) (right) and on G7 (**10**) (left) (each 20 % (w/w) in PS 86). Columns: 25 m x 0.25 mm i.d. fused-silica capillary, film thickness 0.25  $\mu\text{m}$ . For other experimental conditions, cf. table 4.5.

**Table 4.5.** Retention factor  $k_1$  (first eluted enantiomer), enantioseparation factor  $\alpha$  and resolution factor  $R_s$  for selected racemates on G7 (**10**). Column: 25 m x 0.25 mm i.d.; fused-silica capillary, film thickness 0.25  $\mu\text{m}$ , carrier gas  $\text{H}_2$ .

guest	$k_1$	$\alpha$	$R_s$	T ( $^\circ\text{C}$ )	P (kPa)
<b>4a</b> 	38.4	1.07	3.25	100	100
<b>4b</b> 	14.2	1.03	1.68	100	100
<b>4c</b> 	18.3	1.00	–	90	80
<b>4d</b> 	37.0	1.02	1.71	90	80
<b>4e</b> 	22.3	1.02	1.10	70	100
<b>4f</b> 	11.6	1.11	1.86	70	100
<b>4g</b> 	30.3 ( <i>meso</i> ) 31.6	1.03	1.74	60 60	50 50
<b>4h</b> 	24.7	1.01	1.05	60	50
<b>4i</b> 	4.12	1.00	–	60	100
<b>4l</b> 	12.6	1.00	–	60	100

Another interesting example of the inversion of the elution order of diastereomers comprises underivatized 2,4-pentanediol **4g**. The meso form of **4g** is eluted *before* the racemic form on the acyclic G7 (**10**) but *after* on the cyclic CD7 (**5**) (figure 4.9).

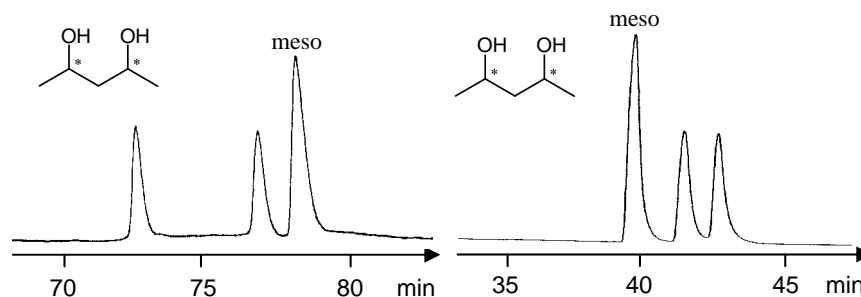


**Figure 4.9.** Gas-chromatographic separation of three stereoisomers of 2,4-pentanediol **4g** on CD7 **5** (*left*) and on G7 **10** (*right*) (each 20 % (w/w) in PS 86). Columns: 25 m x 0.25 mm i.d. fused-silica capillary, film thickness 0.25  $\mu\text{m}$ . For other experimental conditions, cf. table 4.5.

The importance of the cavity seems particularly apparent in the enantioseparation of aliphatic and aromatic alcohol derivatives. Thus the heptafluorobutanoyl derivatives of 5-methyl-2-hexanol **4i** and 2-octanol **4l** (table 4.5) are not separated on linear G7 (**10**), while they are very well separated on cyclic CD7 (**5**) with an enantioseparation factor of 1.17 and 1.12, respectively. Furthermore, it should be noted that although the derivatized aromatic amine derivative **4a** is baseline separated on linear G7 (**10**), the heptafluorobutanoyl derivative of phenylethanol and analogous fluorinated alcohols **4m-4q** (figure 4.10) are separated only on the cyclic CD7 (**5**), so that for these compounds there is probably a segment of their structure which is partially (or completely) included in the cyclodextrin cavity. Thus, for the overall structure of the analyte both contributions inside/outside from the selector may enhance the enantioselectivity.

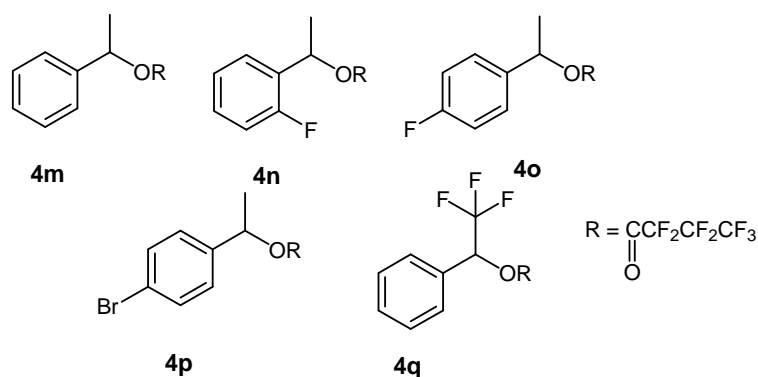


**Figure 4.10.** Structures of compounds **4m-4q**.

In figure 4.11 the enantioseparation of the mixture containing all the five alcohol derivatives on the cyclic CD7 (**5**) is shown.

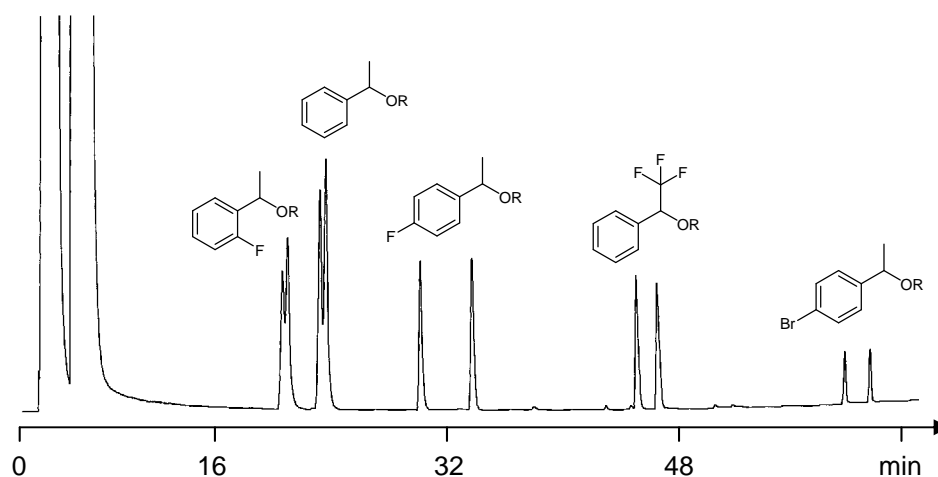


**Figure 4.11.** Gas-chromatographic separation of compounds **4m-4q** on CD7 (**5**) (20 % (w/w) in PS 86). Column: 20 m x 0.25 mm i.d. fused-silica capillary, film thickness 0.25  $\mu\text{m}$ . Carrier gas: 100 kPa  $\text{H}_2$ ; oven temperature: 80  $^\circ\text{C}$  (5 min), temperature program to 140  $^\circ\text{C}$ , 1  $^\circ\text{C}/\text{min}$ .

As mentioned in chapter I, the enantioselective gas-chromatographic analysis of chiral flavours and fragrances from various sources is of importance. For example, the typical flavour of the ripe peach (*Prunus persica-rosaceae*) is mainly due to  $\gamma$ -lactones (C10-C12, figure 4.12). The odour intensity of ordinary linear esters quickly declines with increasing C-number, whereas the odour of the higher  $\gamma$ -lactones, for example  $\gamma$ -dodecalactone, is very pronounced. A remarkable change in the odour character of the  $\gamma$ -lactones occurs with increasing length of the carbon side-chain.  $\gamma$ -Hexalactone for example has an intensively sweet-herbal, coumarinic odour. When the C-number increases, the odour becomes more fatty and coconut-like, but it suddenly changes into a peach-like odour from C-10 onwards, as mentioned above.



**Figure 4.12.** Peach flower and fruits and enantiomerically pure lactones responsible for their flavour.

These compounds (figure 4.13) are very well separated on the CD7 (5). Baseline enantioseparation of all members of the homologous series from  $\gamma$ -valerolactone (C5) to  $\gamma$ -dodecalactone (C12) is achieved as shown in figure 4.14.

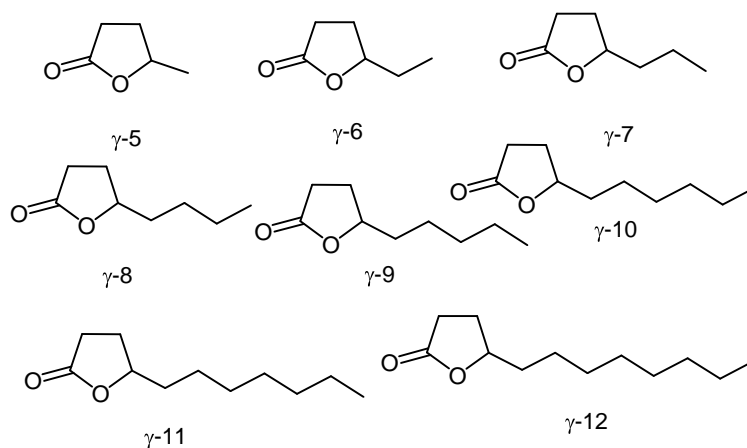


**Figure 4.13.** Structure of  $\gamma$ -lactones C5-C12.

In particular, in the region of the gas-chromatogram in which the  $\gamma$ -lactones C5-C8 elute (shown in figure 4.15), the particular enantioselectivity toward  $\gamma$ -valerolactone (C5), which then decreases with increasing length of the alkyl chain [(C8 > C7) < C6 < C5], should be noted.

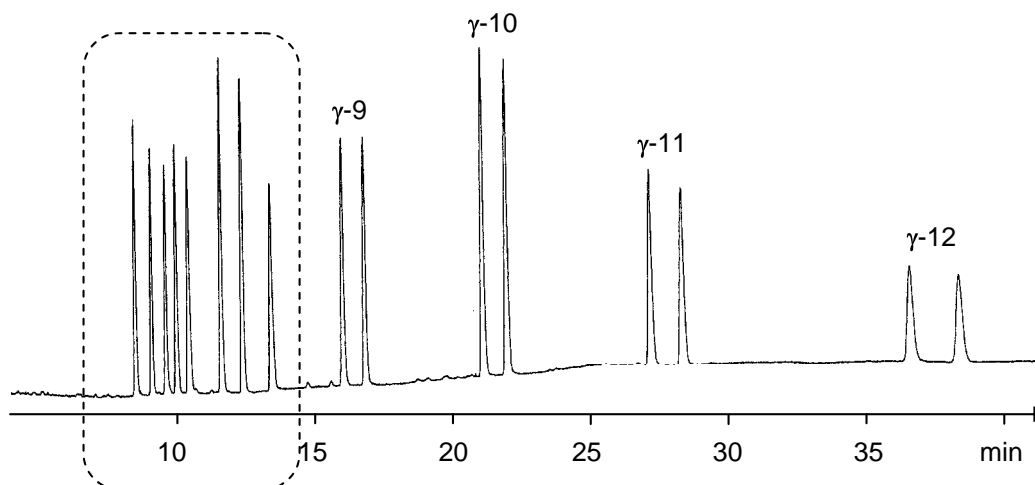


**Figure 4.14.** Gas-chromatographic separation of racemic  $\gamma$ -lactones (C5-C12) on CD7 (5) (20 % (w/w) in PS 86). Column: 20 m x 0.25 mm i.d. fused-silica capillary, film thickness 0.25  $\mu$ m. Carrier gas: 80 kPa H<sub>2</sub>; oven temperature: 90 °C (5 min), temperature program to 140 °C, 1 °C/min.

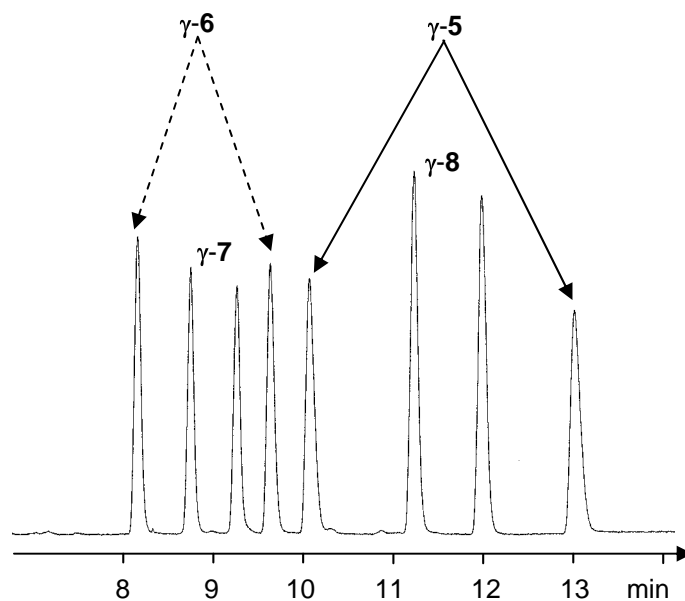


**Figure 4.15.** Region of the gas-chromatogram shown in figure 4.14, involving the  $\gamma$ -lactones C5-C8.

A completely different trend is observed using the linear G7 (**10**) as chiral selector. While  $\gamma$ -valerolactone (C5) is still baseline separated,  $\gamma$ -hexalactone (C6) is incompletely resolved and all lactones with longer chain length are not separated at all on acyclic G7 (**10**) (figure 4.16).

Furthermore, in those cases where enantioseparation was achieved, a considerably lower analysis temperature than with the cyclic CD7 (**5**) was necessary. No enantioseparation is observed, for example, by applying the temperature program described in figure 4.13 for the mixture of the  $\gamma$ -lactones (figure 4.15 for experimental details).

It seems reasonable to assume (as suggested by computational analysis)<sup>146</sup> that the alkyl chain is included in the cavity of the cyclodextrin selector and that this inclusion allows the stereogenic center to interact with the different parts (outside/inside) of CD7 (**5**), while inclusion is absent with G7 (**10**) (figure 4.14).<sup>147-148</sup>



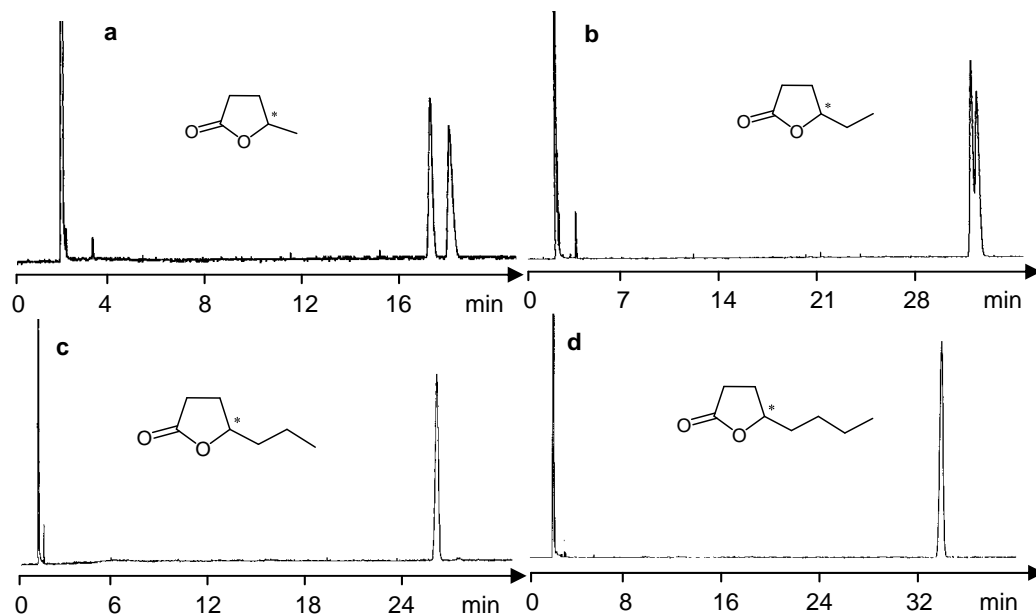


**Figure 4.16.** Gas-chromatographic separation of the  $\gamma$ -lactones (a) C5 (40 °C), (b) C6 (50 °C), (c) C7 (100 °C), (d) C8 (110 °C) on the acyclic selector G7 (10) (20 % (w/w) in PS 86). Column: 20 m x 0.25 mm i.d. fused-silica capillary, film thickness 0.25  $\mu$ m. Carrier gas: 80 kPa H<sub>2</sub>.

In figure 4.17 a schematic representation of the inclusion phenomenon which may occur between (*S*)- $\gamma$ -octalactone and CD7 (**5**) (C8) is shown. Two possible geometries can be expected; furthermore, considering the two enantiomeric forms of the analyte, a total of four possible geometries have to be considered. Because enantioseparation occurs solely on the cyclic CD7 (**5**), an inclusion mechanism may be considered in this case.

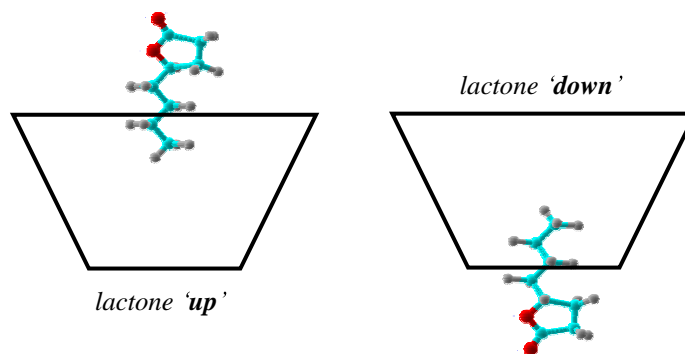


**Figure 4.17.** Possible geometries for the complexes formed between the CD7 (**5**) and the (*S*)- $\gamma$ -octalactone (C8).

As in the case of cyclic heptakis(2,3-di-*O*-acetyl-6-*O*-*tert*-butyldimethylsilyl)- $\beta$ -cyclodextrin CD7 (**5**), the chiral stationary phase based on G7 (**10**) is not able to separate apolar substrates such as racemic saturated hydrocarbons. These apolar compounds are usually enantioseparated on alkylated dextrins (see section 4.7).

#### 4.5. How does the degree of oligomerization in acyclic dextrins affect the enantioselectivity?

In order to evaluate the influence of the number of glucose units which form the acyclic chiral selectors on the enantioselectivity towards selected racemic compounds, the acyclic dextrins G8 (**12**), which derives from the cyclic CD8 (figure 4.18 and chapter II for further details) was screened as chiral stationary phases for enantioselective gas chromatography after suitable derivatization (chapter II).

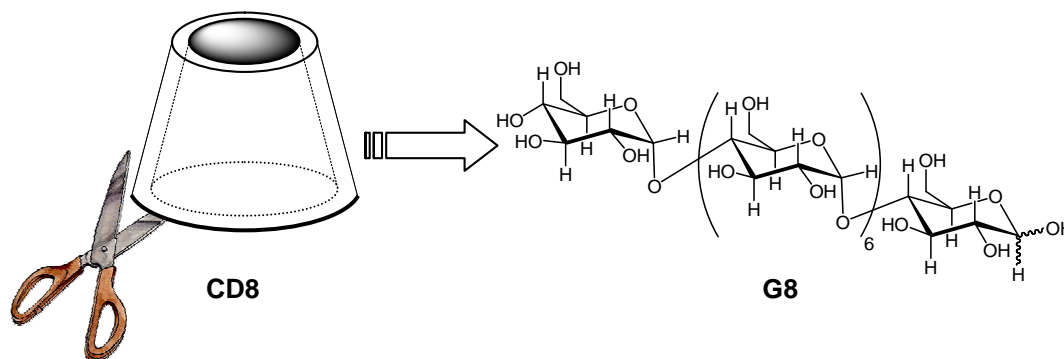


**Figure 4.18.** Schematic representation of the linear maltooctaose. The native cyclodextrin (CD8) is “cut” to obtain the corresponding linear system; for further details see reference 124.

The remarkable differences which are often observed turning from CD7 to CD8 derivatives as chiral selectors were not detected using linear G8 (**12**) compared with linear G7 (**10**). Thus, the enantioseparation factor of ‘compound B’ on G8 (**12**) is  $\alpha = 1.06$ , which is close to that obtained on G7 (**10**) ( $\alpha = 1.07$ ) and also for the mixture of five *N*-trifluoroacetyl-*O*-methyl esters of selected amino acids, the enantioseparation achieved on the selector with higher degree of oligomerization G8 (**12**) is similar to that on G7 (**10**) (figure 4.19).

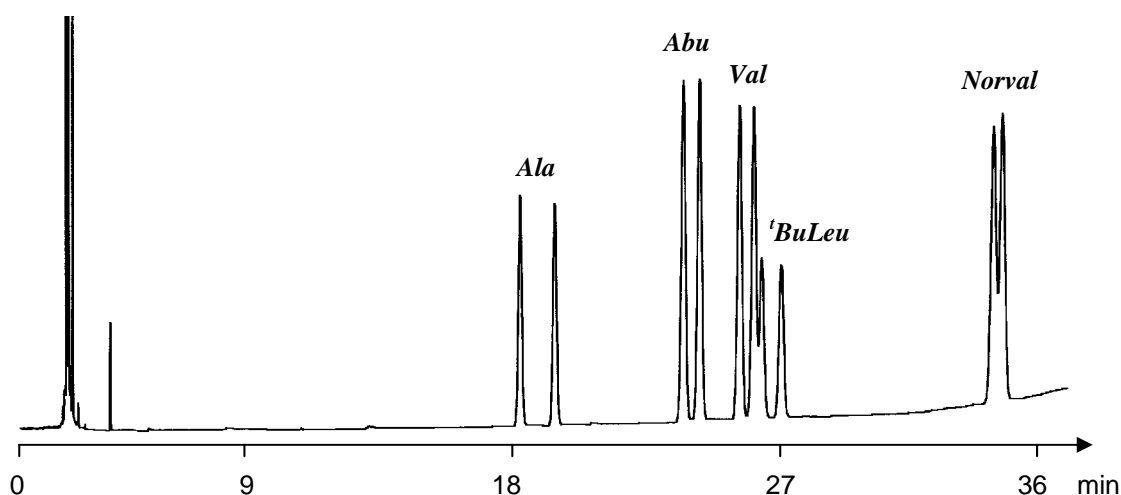


**Figure 4.19.** Gas-chromatographic separation of racemic *N*-trifluoroacetyl-*O*-methyl esters of  $\alpha$ -amino acids on G8 (**12**) (20 % (w/w) in PS 86). Column: 20 m x 0.25 mm i.d. fused-silica capillary, film thickness 0.25  $\mu$ m. Carrier gas: 50 kPa H<sub>2</sub>; oven temperature: 80 °C (5 min), temperature program to 120 °C, 0.5 °C/min.

On G8 (**12**), only the smaller enantioseparation of norvaline (**Norval**) and a slight difference in the elution order of *tert*-butyl leucine (**<sup>t</sup>BuLeu**) can be noted as compared to the enantioseparation on G7 (**10**) (figure 4.4).

The next important step related to test some acyclic smaller oligosaccharides consisted of the application as chiral selectors of maltotriose G3 (**14**) and *D*-G1 (**16**) and *L*-G1 (**18**) (figure 4.20; for further details see chapter II) which were derivatized as acetyl/TBDMS multifunctional systems.

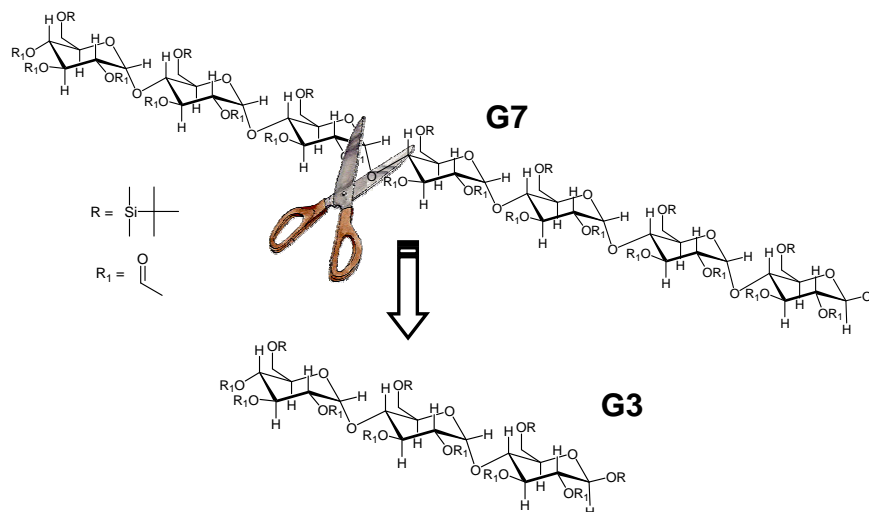


**Figure 4.20.** Structures of linear dextrin derivatives formed by seven and three glucose units.

Thus, the impact of outside interactions for cyclodextrin derivatives is indirectly confirmed using the above mentioned acyclic selectors with a lower degree of oligomerization. Even tris[(2,3-di-*O*,4''-*O*)-acetyl-(1'-*O*,6-*O*)-*tert*-butyldimethylsilyl]-maltotriose G3 (**14**), which is clearly devoid of a cavity, can be applied as chiral stationary phase in enantioselective gas chromatography. For instance, a slight enantioseparation of the *N*-trifluoroacetyl-*O*-methyl ester of selected amino acids shown in figure 4.21 is observed. In the case of the *tert*-butyl leucine derivative (**<sup>t</sup>BuLeu**), baseline separation is achieved (figure 4.21) on G3 (**14**). It can thus be concluded that the phenomenon of inclusion is not a requirement for enantiorecognition of this compound.

Moreover, on G3 (**14**) the enantiomers of the pentafluoropropionyl derivative of 1-(phenyl)ethylamine **4a** are also separated, whereby a reverse elution order compared to CD7 (**5**) and G7 (**10**) (figure 4.22 a) is observed.

Surprisingly, even the two enantiomers of the aliphatic amide **4l** derived from 2-octylamine are differentiated by linear G3 (**14**) (figure 4.22 b). Devoid of a cavity, in the case of G3 (**14**), only the acetyl groups (which can interact by strong dipolar interactions) and the *tert*-butyl

dimethylsilyl groups are responsible of enantiorecognition. It should also be noted that the first eluted peak has a broader peak width as compared with the second eluted peak which represents a rare phenomenon in enantioselective GC.

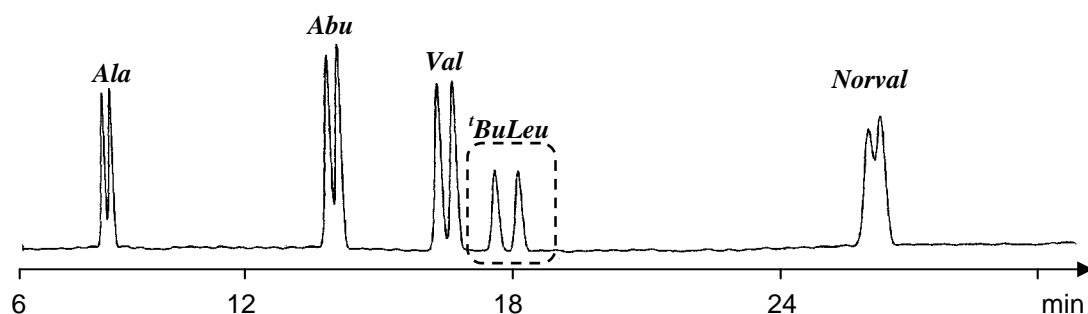


**Figure 4.21.** Gas-chromatographic enantioseparation of racemic *N*-trifluoroacetyl-*O*-methyl esters of  $\alpha$ -amino acids on G3 (**14**) (20 % (w/w) in PS 86). Column: 25 m x 0.25 mm I.D. fused-silica capillary, film thickness 0.25  $\mu$ m. Carrier gas: 50 kPa H<sub>2</sub>; oven temperature: 85 °C

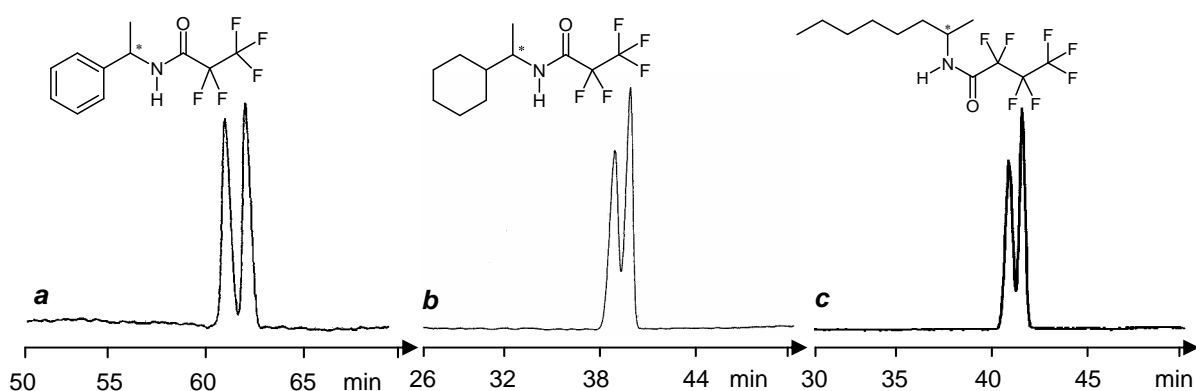


**Figure 4.22.** Gas-chromatographic separation of racemic **4a**, **4b** and **4d** on G3 (**14**) (20 % (w/w) in PS 86). Column: 25 m x 0.25 mm i.d. fused-silica capillary, film thickness 0.25  $\mu$ m. For **4a** and **4b**, carrier gas: 50 kPa bar dihydrogen; oven temperature: 90 °C; for **4d**, carrier gas: 80 kPa H<sub>2</sub>; oven temperature: 80 °C.

In figures 4.23 and 4.24 it is evident that even the single building block (2,3,4-tri-*O*-acetyl-1,6-di-*O*-*tert*-butyldimethylsilyl)-*D*-glucose (**16**), when mixed in a polysiloxane matrix, can be successfully used as chiral stationary phase for *N*-trifluoroacetyl-*O*-methyl ester of amino acids and also for the pentafluoropropionyl derivative of 1-(phenyl)ethylamine **4a**. However, on G1 (**16**) a lower temperature compared to that on both cyclic CD7 (**5**) and linear G7 (**10**) and G3 (**14**) is required (the *fronting* effect observed on chromatogram on *D*-G1 (**16**) is due to the low column temperature necessary for the separation of the amino acid derivatives).

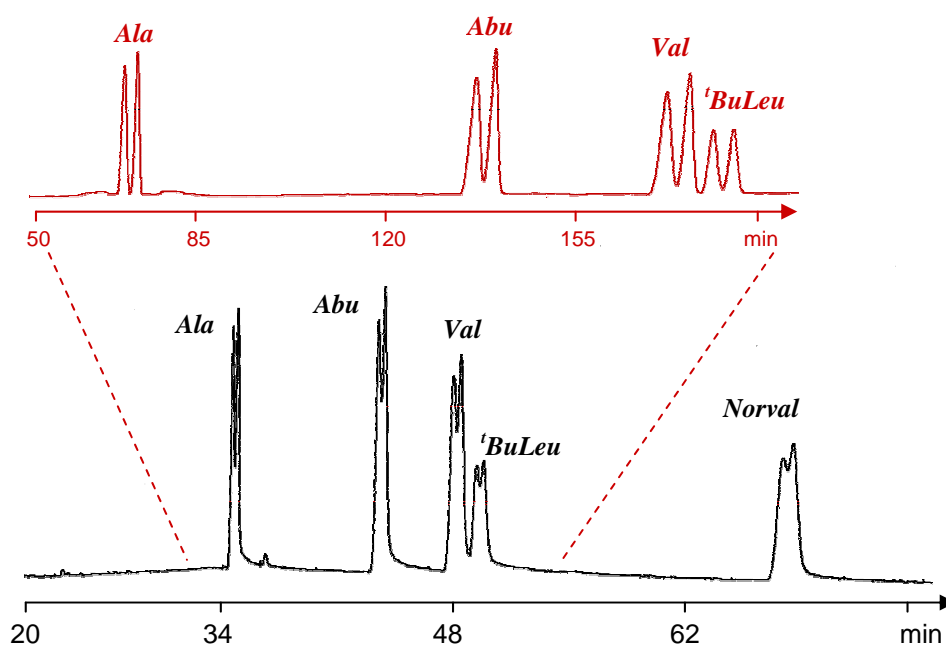


**Figure 4.23.** Gas-chromatographic separation of racemic *N*-trifluoroacetyl-*O*-methyl esters of  $\alpha$ -amino acids on *D*-G1 (**16**) (20 % (w/w) in PS 86). Column: 25 m x 0.25 mm i.d. fused-silica capillary, film thickness 0.25  $\mu$ m. Carrier gas: 90 kPa H<sub>2</sub>; oven temperature: 60 °C (5 min), temperature program to 85 °C, 0.5 °C/min (*bottom*). Gas-chromatographic separation of racemic *N*-trifluoroacetyl-*O*-methyl esters of  $\alpha$ -amino acids on *D*-G1 (**16**) (20 % (w/w) in PS 86). Column: 15 m x 0.25 mm i.d. fused-silica capillary, film thickness 0.25  $\mu$ m. Carrier gas: 100 kPa H<sub>2</sub>; oven temperature: 40 °C, isothermal (*top*, red line).

An analogous result is obtained in the case of oppositely configured selector (2,3,4-tri-*O*-acetyl-1,6-di-*O*-*tert*-butyldimethylsilyl)-*L*-glucose (**18**), leading to peak inversion which represents an unequivocal proof of an unexpected enantiomeric separation. This significant advantage to switch the elution order (compared to the cyclic selectors which are available only in the *D*-configuration) using the acyclic dextrans as *D*- or *L*-selector is well demonstrated by the enantioseparation of compound **4a**.

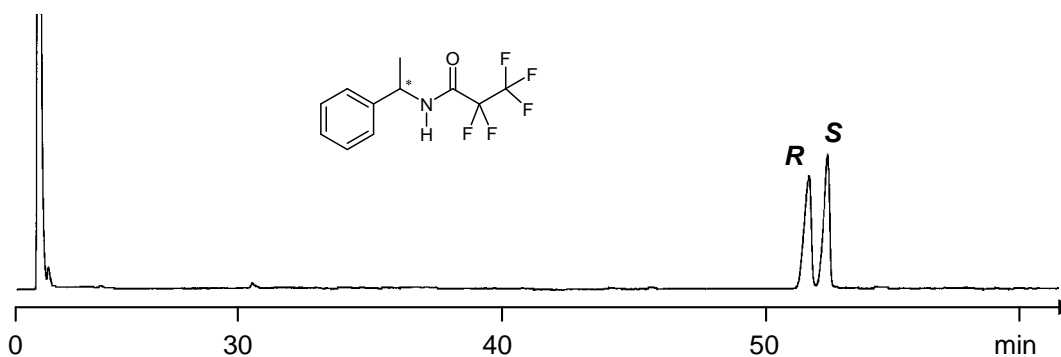


**Figure 4.24.** Gas-chromatographic enantioseparation of racemic **4a** on *D*-G1 (**16**) (20 % (w/w) in PS 86). Column: 25 m x 0.25 mm i.d. fused-silica capillary, film thickness 0.25  $\mu$ m. Carrier gas: 80 kPa H<sub>2</sub>; oven temperature: 100 °C.

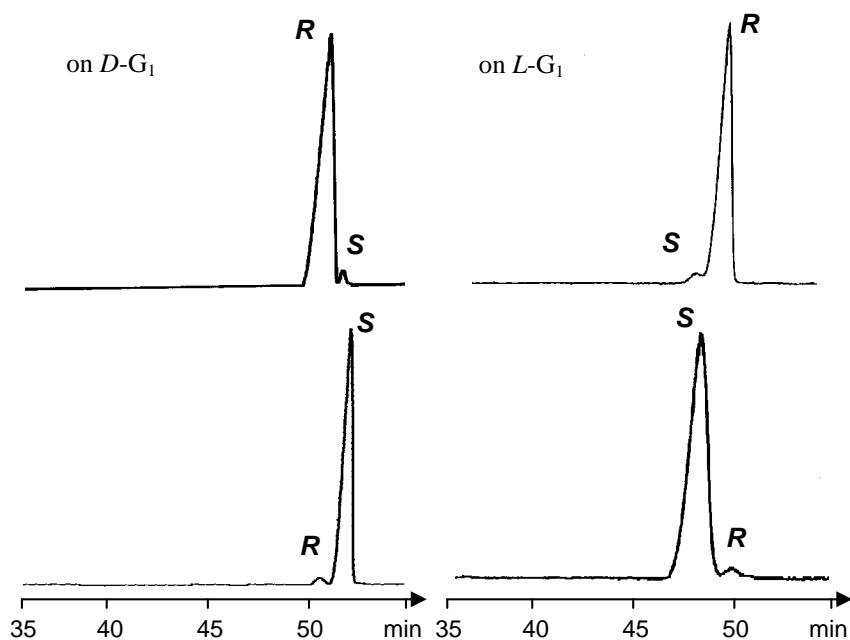


**Figure 4.25.** Gas-chromatographic separation of enantiomerically enriched samples of **4a** on the *D*-G1 (**16**) (left) and on the *L*-G1 (**18**) (right) (each 20 % (w/w) in PS 86). Columns: 25 m x 0.25 mm i.d. fused-silica capillary, film thickness 0.25  $\mu\text{m}$ . Carrier gas: 80 kPa  $\text{H}_2$ ; oven temperature: 100  $^\circ\text{C}$ .

Indeed, compound **4a** shows baseline separation on both monosaccharides phases *D*-G1 (**16**) and *L*-G1 (**18**) (figure 4.24), with the expected reversal of the elution order between the *D*- and *L*-glucose derivatives as shown in figure 4.25. In the case of the monosaccharide *D*-G1 (**16**) the elution order of **4a** is the same as on G3 (**14**), but opposite on G7 (**10**) and CD7 (**5**). *L*-G1 (**18**), on the other hand, shows the opposite elution to *D*-G1 (**16**), but the same as on the selectors with the highest degree of oligomerization, CD7 (**5**) and G7 (**10**), respectively. These unusual results are summarized in table 4.6.

**Table 4.6.** Elution order for the pentafluoropropionyl derivative of 1-(phenyl)ethylamine **4a** on the cyclic selector **5** and acyclic selectors **10**, **14**, **16**, **18**. Experimental condition: 100  $^\circ\text{C}$  (isothermal), 0.8 bar ( $\text{H}_2$ ).

<i>selector</i>	<i>elution order</i>	
<i>D</i> -CD7 ( <b>5</b> )	<i>S</i>	< <i>R</i>
<i>D</i> -G7 ( <b>10</b> )	<i>S</i>	< <i>R</i>
<i>D</i> -G3 ( <b>14</b> )	<i>R</i>	< <i>S</i>
<i>D</i> -G1 ( <b>16</b> )	<i>R</i>	< <i>S</i>
<i>L</i> -G1 ( <b>18</b> )	<i>S</i>	< <i>R</i>

#### 4.6. Preliminary study on acyclic dextrans with different derivatization patterns

For a further comparison between cyclic and acyclic dextrin derivatives employed as chiral selectors, linear dextrans analogous to well established cyclodextrin chiral stationary phases were investigated. Thus, the acyclic version G8 (**28**) of the versatile selector Lipodex E CD8 (**27**), diluted in a polysiloxane matrix PS 255 (30 % w/w) still maintains enantioselectivity. Although the very high enantioseparation for ‘compound B’ (see chapter I) on the cyclic CD8 (**27**) ( $\alpha = 10.6$  at 26 °C) is not achieved, enantioseparation is still present on the acyclic system G8 (**28**) ( $\alpha = 1.06$  at 26 °C, figure 4.26).

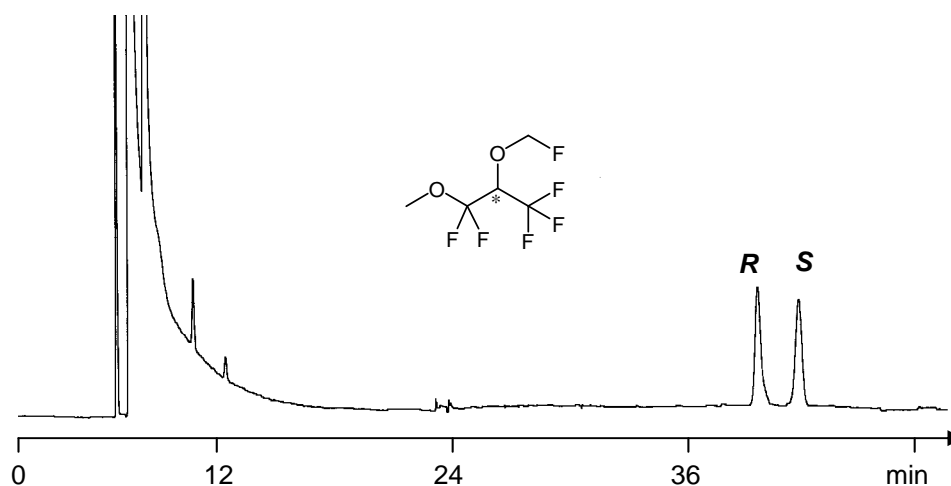


**Figure 4.26.** Gas-chromatographic separation of racemic 2-(fluoromethoxy)-3-methoxy-1,1,1,3,3-pentafluoropropane (‘compound B’) **4e** on octakis[3-*O*,-4''*O*]-butanoyl-(1'-*O*,2,6-di-*O*)-*n*-pentyl]-maltotriose **28**, 30 % (w/w) in PS 255. Column: 20 m x 0.25 mm i.d. fused-silica capillary, film thickness 0.25  $\mu$ m. Carrier gas: 30 kPa Helium; oven temperature: 30 °C.

It is interesting to note that the G8 (**28**) selector displays an enantioseparation factor ( $\alpha = 1.06$ ) which is similar to that obtained on the G7 (**10**) ( $\alpha = 1.07$ ), despite the presence of different functional groups, that is, acetyl/TBDMS for G7 (**10**) *versus* *n*-pentyl/butanoyl for G8 (**28**) and the same enantioseparation factor  $\alpha$  was obtained on G8 (**12**) (see chapter II for the structures). However, it seems reasonable to conclude that the enantioseparation of ‘compound B’ may require an inclusion-type association in order to justify the unusual high enantioseparation factors  $\alpha$  obtained on CD7 (**5**) and CD8 (**27**) respectively, in addition to the enantioselective outside interactions established for the acyclic selectors G7 (**10**) and G8 (**28**). In a mixture of five  $\alpha$ -amino acid derivatives, the enantiomers are also resolved on the acyclic counterpart of Lipodex E, G8 (**28**), and for the *tert*-butyl leucine derivative (<sup>t</sup>BuLeu) a partial enantioseparation is still achieved (figure 4.27)

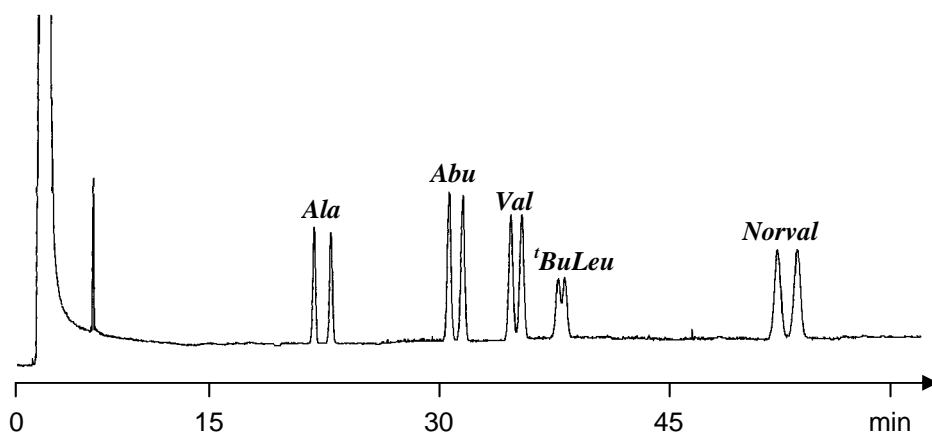


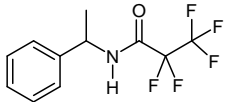
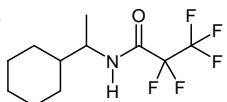
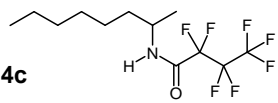
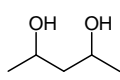
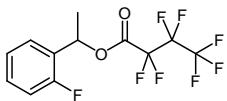
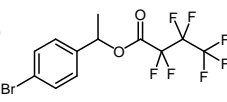
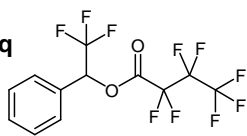
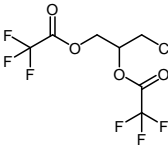
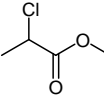
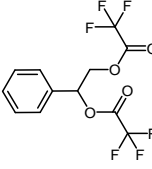
**Figure 4.27.** Gas-chromatographic enantioseparation of racemic *N*-trifluoroacetyl-*O*-methyl esters of  $\alpha$ -amino acids on octakis[(3-*O*,4'-*O*)-butanoyl-(1'-*O*,2,6-di-*O*)-*n*-pentyl]-maltooctaose G8 (**28**), 30 % (w/w) in PS 255. Column: 20 m x 0.25 mm i.d. fused-silica capillary, film thickness 0.25  $\mu$ m. Carrier gas: 50 kPa Helium; oven temperature: 90  $^{\circ}$ C.

As shown in table 4.7, the enantiomers of different classes of compounds can be separated on acyclic G8 (**28**), comprising amine and alcohol derivatives, in addition to the underivatized diol **4g**.

Furthermore, in this preliminary application of G8 (**28**) as linear counterpart of Lipodex E, some selected comparisons between the cyclic CD8 (**27**) and G8 (**28**) are reported in the tables 4.8 and 4.9. Thus, for *N*-trifluoroacetyl-*O*-methyl esters of  $\alpha$ -amino acids, the enantioseparation is achieved on the cyclic CD8 (**27**) and on the analogous linear dextrin counterpart G8 (**28**), although with significant reduced enantioselectivity (table 4.8).



**Table 4.7.** Retention factor  $k_1$  (first eluted enantiomer), enantioseparation factor  $\alpha$ , resolution factor  $R_s$ , for selected racemates on the linear octakis[(3-*O*,4''*O*)-butanoyl-(1'-*O*,2,6-di-*O*)-*n*-pentyl]-maltooctaose G8 (**28**). Column: 20 m x 0.25 mm i.d.; fused-silica capillary, film thickness 0.25  $\mu\text{m}$ , carrier gas: He.

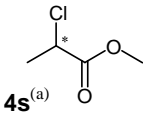
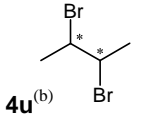
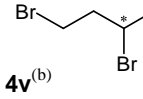
guest	$k_1$	$\alpha$	$R_s$	T ( $^{\circ}\text{C}$ )	P (kPa)
<b>4a</b> 	26.0	1.05	3.11	100	120
<b>4b</b> 	19.7	1.03	1.58	50	120
<b>4c</b> 	28.4	1.03	1.75	90	120
<b>4g</b> 	60.9 ( <i>meso</i> ) 63.5	1.04	2.59	45 45	120 120
<b>4n</b> 	50.1	1.01	1.08	60	120
<b>4p</b> 	59.9	1.01	0.98	60	120
<b>4q</b> 	19.6	1.03	1.57	50	120
<b>4r</b> 	11.0	1.02	1.05	75	120
<b>4s</b> 	12.4	1.05	2.75	60	120
<b>4t</b> 	30.8	1.08	4.45	100	120

**Table 4.8.** Retention factor  $k_1$  (first eluted enantiomer), enantioseparation factor  $\alpha$  and resolution factor  $R_s$  for *N*-trifluoroacetyl-*O*-methyl esters of some  $\alpha$ -amino acids. Experimental conditions: 100 °C, 50 kPa ( $H_2$ ). Columns: 25 m x 0.25 mm i.d. fused-silica capillary, film thickness 0.25  $\mu$ m.

	CD8 ( <b>27</b> )			G8 ( <b>28</b> )		
	$k_1$	$\alpha$	$R_s$	$k_1$	$\alpha$	$R_s$
Ala	5.02	1.09	3.28	2.28	1.04	1.56
IsoLeu	9.83	1.14	8.69	6.57	1.01	0.56
	10.3	1.15	9.57	6.87	1.01	0.56
Norval	9.86	1.28	11.4	5.99	1.02	0.88
Val	6.39	1.15	5.77	3.97	1.02	0.73
Ser	25.2	1.09	3.43	7.64	1.02	0.80
Leu	14.9	1.10	5.08	10.6	1.02	0.72
2-Abu	6.43	1.19	6.38	3.39	1.03	1.05

Particular attention was focused on halogenated compounds, such as the methyl ester of 2-chloro-propionic acid (**4s**), 2,3-dibromobutane (**4u**) and 2,4-dibromobutane (**4v**). The results for the enantioseparation of these compounds are summarized in the table 4.9.

**Table 4.9.** Retention factor  $k_1$  (first eluted enantiomer), enantioseparation factor  $\alpha$  and resolution factor  $R_s$  for racemic **4s**, **4u** and **4v**. Experimental conditions: a) 40 °C, 50 kPa ( $H_2$ ); b) 40 °C, 50 kPa ( $H_2$ ). Columns: 25 m x 0.25 mm i.d. fused-silica capillary, film thickness 0.25  $\mu$ m.

	CD8 ( <b>27</b> )			G8 ( <b>28</b> )		
	$k_1$	$\alpha$	$R_s$	$k_1$	$\alpha$	$R_s$
 <b>4s</b> <sup>(a)</sup>	39.8	2.38	25.3	22.7	1.18	3.89
 <b>4u</b> <sup>(b)</sup>	11.1	1.38	9.44	8.54	1.02	0.91
	11.6 (meso)	–	–	7.84 (meso)	–	–
 <b>4v</b> <sup>(b)</sup>	21.9	1.19	5.59	14.9	1.17	8.85

Although the enantioseparation on CD8 (**27**) is often higher than that on G8 (**28**), the remarkable enantioseparation of **4s** should be noted, in addition to different elution order for

the stereoisomers of compound **4u** and the comparable enantioseparation factor  $\alpha$  obtained for compound **4v** (figure 4.28).

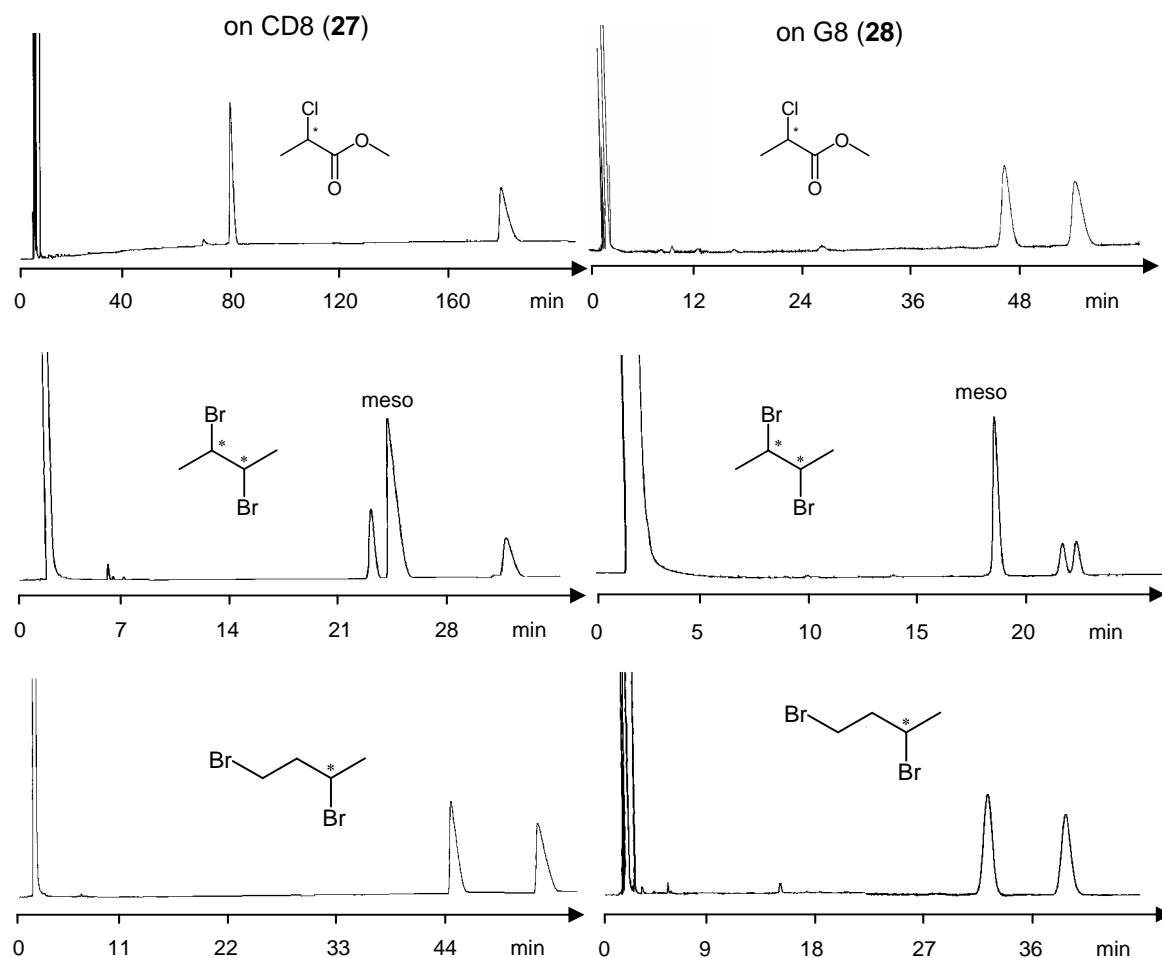


**Figure 4.28.** Gas-chromatographic enantioseparation of racemic **4s**, **4u** and **4v** on CD8 (**27**) (left) and on G8 (**28**) (right) (each 30 % (w/w) in PS 255). Columns: 25 m x 0.25 mm i.d. fused-silica capillary, film thickness 0.25  $\mu\text{m}$ . For other experimental conditions, cf. table 4.9.

Future studies will be focused on a comprehensive comparison between the acyclic/cyclic selectors, in addition to thermodynamic studies of selected enantioseparations displaying the highest enantioselectivity. It should be pointed out that the *n*-pentyl and butanoyl groups are suitable functionalities for the derivatization of acyclic dextrans and the anticipated influence of the degree of oligomerization of the new selectors (maltoheptaose vs. maltohexaose congeners) will be tested in the future.

In principle, an innumerable variety of acyclic dextrans derivatives are available in an effort to find a chiral stationary phase with an optimal derivatization pattern which may complement the enantioselectivity of the established cyclodextrin counterparts.

#### 4.7. Enantioseparation of saturated aliphatic hydrocarbons

Acyl groups represent strong dipoles which induce electron accepting interactions. This property makes them suitable for the separation of enantiomers of compounds with polar moieties close to the stereogenic center. However, it renders them unsuitable for the enantioseparation of chiral saturated hydrocarbons, devoid of any functionality, since these can not form association complexes by dipole-dipole interactions. On the contrary, the alkyl groups of peralkylated cyclodextrins will preferentially interact with analytes having long alkyl chains through Van der Waals' forces.

Previously, many efforts were undertaken to screen alkylated cyclodextrins or silylated cyclodextrins for the enantioseparation of the smallest hydrocarbons 3-methylhexane ( $C^*HMeEtPr$ ) and 2,3-dimethylpentane ( $C^*HMeEt^iPr$ ), containing only seven carbon atoms. It was found that among the different CDs tested the best results were obtained on Chirasil- $\beta$ -Dex **29** (per-*O*-methyl- $\beta$ -cyclodextrin, bonded to a polymer backbone, figure 4.29)<sup>84</sup> and heptakis(2,3-di-*O*-methyl-6-*O*-*tert*-butyldimethylsilyl)- $\beta$ -cyclodextrin CD7 (**7**) (30 % w/w in PS 86).

For these compounds generally better enantioseparations were achieved with **29**, but also the cyclic CD7 (**7**) constitutes a suitable CSP for the enantioseparation of these compounds (figures 4.30 and 4.31). The aim of the derivatization of the cyclic

CD7 (**7**) was to block the opening of the cavity at the primary side by bulky substituents (TBDMS) attached to the 6-positions of the CD ring and to direct the interactions with the analyte towards the secondary side.<sup>57</sup> In the case of the 3-methylhexane ( $C^*HMeEtPr$ ), baseline separation was achieved previously using a 50 m glass capillary column coated with undiluted octakis(2,3-di-*O*-pentyl-6-*O*-methyl)- $\gamma$ -cyclodextrin.<sup>102</sup> At present, no significantly higher enantioseparation factors are known for these compounds.

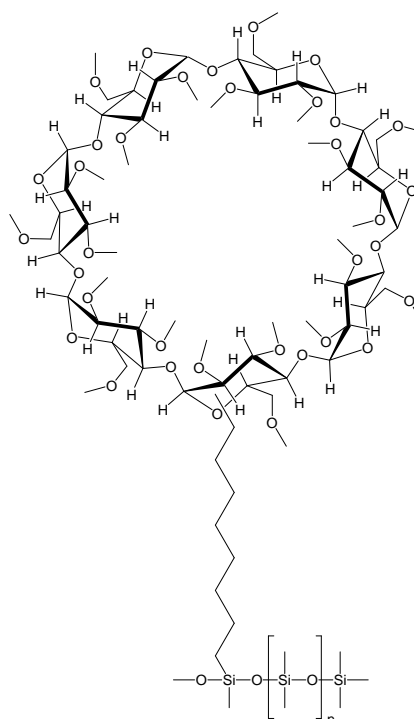


**Figure 4.29.** Structure of Chirasil- $\beta$ -Dex **29** (per-*O*-methyl- $\beta$ -cyclodextrin) bound to polydimethylsiloxane.<sup>84</sup>

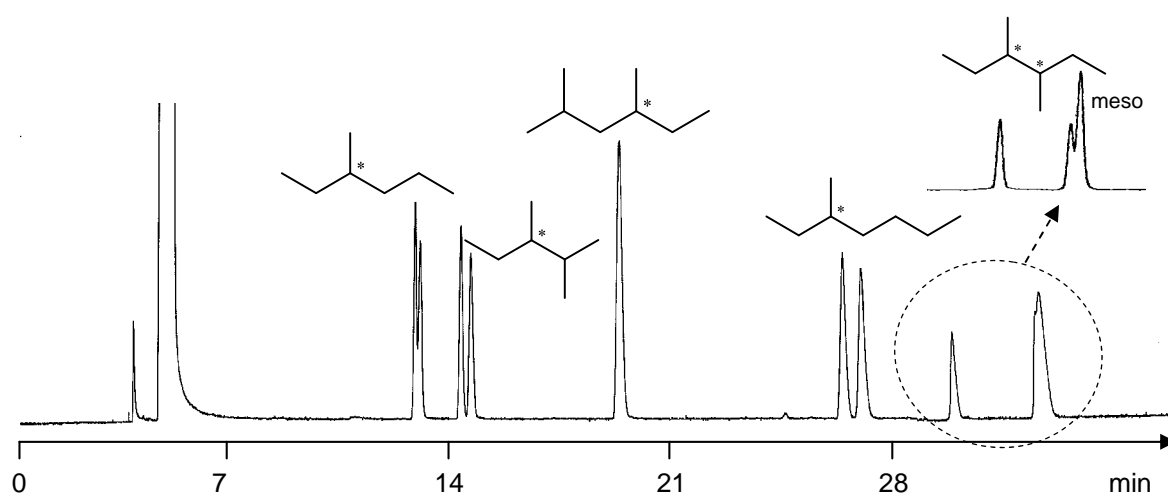


**Figure 4.30.** Gas-chromatographic enantioseparation of racemic 3-methylhexane, 2,3-dimethylpentane, 2,4-dimethylhexane, 3-methylheptane and 3,4-dimethylhexane on Chirasil- $\beta$ -Dex **29**, 25 m, T = 30 °C, carrier gas: 30 kPa H<sub>2</sub>.

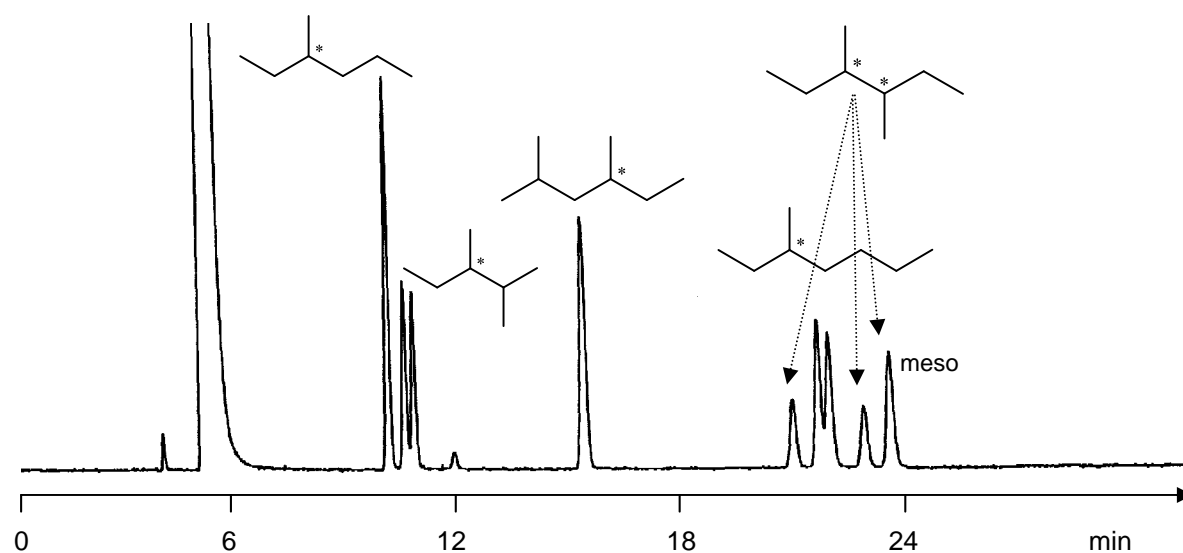


**Figure 4.31.** Gas-chromatographic enantioseparation of racemic 3-methylhexane, 2,3-dimethylpentane, 2,4-dimethylhexane, 3-methylheptane and 3,4-dimethylhexane on heptakis(2,3-di-O-methyl-6-O-tert-butyl-dimethylsilyl)- $\beta$ -cyclodextrin CD7 (**7**), (30 % (w/w) in PS 255). Column: 25 m x 0.25 mm i.d. fused-silica capillary, film thickness 0.25  $\mu$ m; T = 30 °C, carrier gas: 30 kPa H<sub>2</sub>

It is important to note that in the case of the enantioseparation of these small chiral hydrocarbons, no increase of the enantioseparation factor  $\alpha$  is obtained by decreasing the analysis temperature. For example, in the case of 3-methylhexane (C<sup>\*</sup>HMeEtPr) and 2,3-dimethylpentane (C<sup>\*</sup>HMeEt<sup>i</sup>Pr), the enantioseparation factor  $\alpha$  does not change over the range

30 °C to 15 °C and this behaviour reinforces the hypothesis that the enantioseparation of saturated hydrocarbons on alkylated cyclodextrins is mainly entropy controlled (figure 4.32).

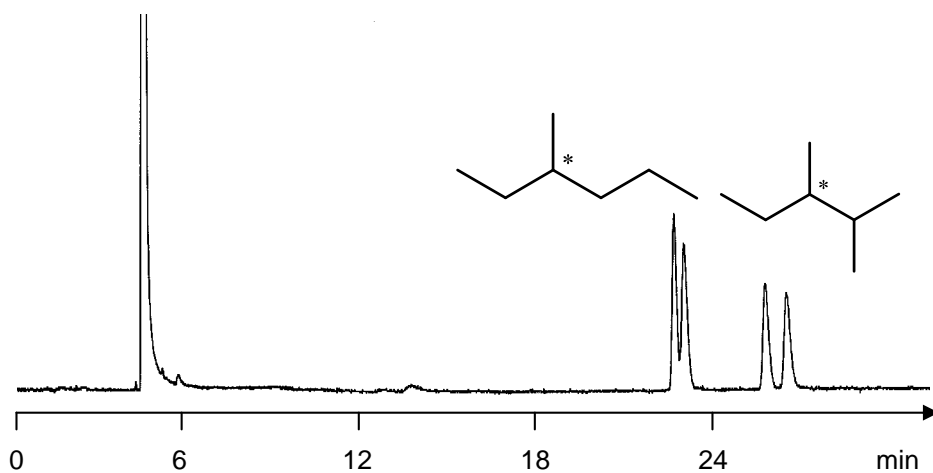


**Figure 4.32.** Gas-chromatographic enantioseparation of racemic 3-methylhexane, 2,3-dimethylpentane on Chirasil- $\beta$ -Dex **29**, 25 m, T = 15 °C, carrier gas: 30 kPa H<sub>2</sub>.

In order to check whether external interactions of peralkylated dextrin derivatives play a role in the enantio-recognition of saturated hydrocarbons, the permethylated G7 (**19**) diluted in polysiloxane OV-1701 and its bonded counterpart G7 (**26**) (for the synthesis and the structures of these selectors, see chapter II) were compared as CSPs for enantioselective gas chromatography. No enantioseparation (figure 4.33) is achieved on the acyclic dextrins G7 (**19**) and G7 (**26**), neither for the saturated hydrocarbons shown in figures 4.30 and 4.31, nor for several racemates which are usually separated on the per-*O*-methylated- $\beta$ -cyclodextrin (CD7).<sup>73, 78, 100</sup>

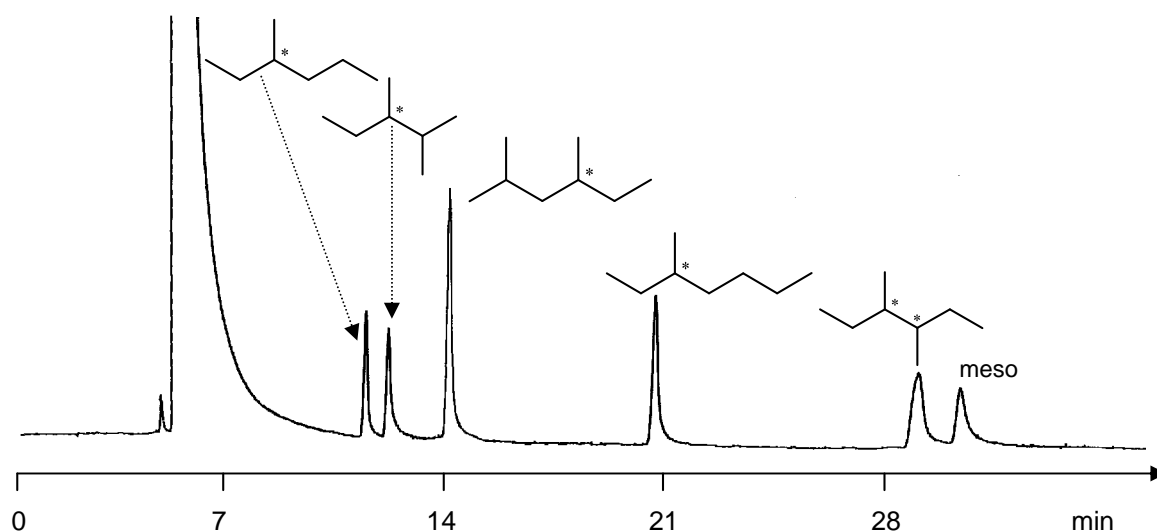


**Figure 4.33.** Gas-chromatographic enantioseparation of racemic 3-methylhexane, 2,3-dimethylpentane, 2,4-dimethylhexane, 3-methylheptane and 3,4-dimethylhexane on G7 (**19**), 25 m, T = 30 °C, carrier gas: 30 kPa H<sub>2</sub>.

In table 4.10 the enantioseparations of chiral saturated hydrocarbons on cyclic and acyclic CSPs are summarized.

**Table 4.10.** Retention factor  $k_1$  (first eluted enantiomer), enantioseparation factor  $\alpha$  and resolution factor  $R_s$  for racemic saturated hydrocarbons. Experimental condition: 30 °C (isothermal), 30 kPa ( $H_2$ ).

	Chirasil- $\beta$ -Dex ( <b>29</b> )			CD7 ( <b>7</b> )			G7 ( <b>19</b> )		
	$k_1$	$\alpha$	$R_s$	$k_1$	$\alpha$	$R_s$	$k_1$	$\alpha$	$R_s$
	1.09	1.02	0.87	0.98	1.00	–	1.03	1.00	–
	1.27	1.03	1.48	1.06	1.03	1.11	1.14	1.00	–
	1.88	1.00	–	1.83	1.00	–	1.32	1.00	–
	2.75	1.03	1.69	2.86	1.02	0.95	2.40	1.00	–
	3.14 3.55 (meso)	1.12 –	11.4 –	2.75 3.17 (meso)	1.11 –	6.01 –	3.63 3.85 (meso)	1.00 –	– –

Via comparative analysis of the enantioseparation on the cyclic and acyclic CSPs (table 4.10), the computational studies described by Lipkowitz and his “principle of maximum enantio-recognition” placed in the center of the cavity of the per-*O*-methylated- $\beta$ -cyclodextrin seems to be indirectly confirmed.<sup>55-56</sup>

In figure 4.34 a schematic representation of the complexes of (*S*)-2,3-dimethylpentane with the selector G7 (**19**) and CD7 (**29**) is shown (PCModel 6.0 program, MMx force field). In the case of the complex formed with the acyclic selector the degrees of freedom for the analyte are greater than those in the complex formed with the cyclic selector. This is due to the flexibility of the linear system which is unable to selectively bind the two enantiomers as the cyclic selector does. However, even assuming inclusion phenomena as the driving force of the enantio-recognition for these apolar substrates, a detailed mechanism for enantioselective interactions remains unclarified.

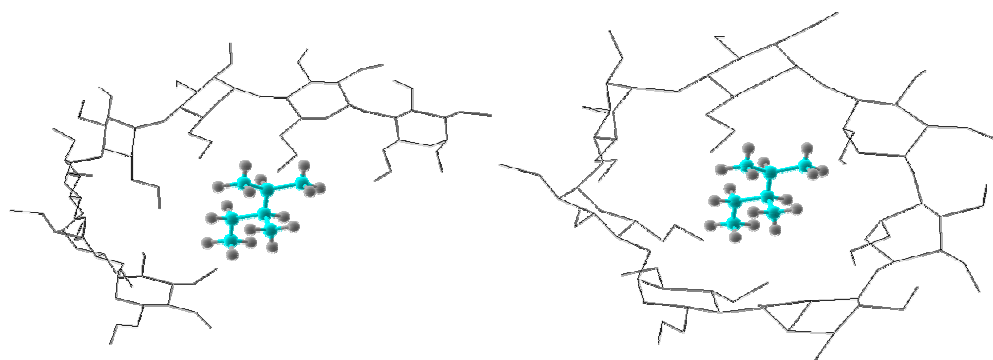


**Figure 4.34.** Schematic representation of the complexes formed by (*S*)-2,3-dimethylpentane and (*left*) linear permethylated G7 (**19**) and (*right*) per-*O*-methylated- $\beta$ -cyclodextrin.

#### 4.8. Thermodynamic data obtained from retention increment $R'$ analysis

Using the retention increment concept (for further details about  $R'$  see appendix), thermodynamic parameters were calculated for four pairs of enantiomers: the (*N*-trifluoroacetyl-*O*-ethyl ester) derivatives of proline (**Pro**) and aspartic acid (**Asp**),  $\gamma$ -valerolactone ( $\gamma$ -**5**) and pentafluoropropionyl derivative of 1-phenyl-ethylamine (**4a**). These data were measured at seven temperatures between 80 and 140 °C with intervals of 5 °C (table 4.8). These temperature-dependent measurements furnish the additional thermodynamic parameters  $\Delta_{R,S}(\Delta H)$  and  $\Delta_{R,S}(\Delta S)$ . The retention increment  $R'$ , from which  $-\Delta_{R,S}(\Delta G)$  is determined, was based on the relative retention  $r$  using *n*-tridecane ( $C_{13}H_{28}$ ) as standard.

The results are collected in table 4.8. The high enantioselectivity displayed for  $\gamma$ -valerolactone ( $\gamma$ -**5**) and 1-(phenyl)ethylamine derivative **4a** on cyclic CD7 (**5**) is reflected in significant thermodynamic parameters in comparison to those determined on acyclic G7 (**10**).

Furthermore, an interesting confirmation of the thermodynamic control of the separation is provided by the enantiorecognition of aspartic acid (**Asp**). The identical enantioseparation factor  $\alpha = 1.03$  is confirmed by comparable thermodynamic data on both CD7 (**5**) and G7 (**10**), as shown in table 4.8.

Moreover, this result implies that the two selectors exhibit a similar conformation or, in other words, the absence of a true cavity in G7 does not affect the enantiorecognition which is mainly due to the external interactions. In the case of the gas-chromatographic enantioseparation, the thermodynamic analysis is in good agreement with the enantioselectivity of the selectors, while in the NMR experiments solution it was demonstrated (chapter II) that the geometries of the complexes formed between the chiral selector and the analyte play a more determining role than the thermodynamic stability



differences, which are often significantly low. Yet, the novel multifunctional acyclic and the established cyclic dextrans represent complementary chiral selectors both as CSP in gas chromatography and CSA in NMR spectroscopy, due to the various interactions responsible for the enantioselectivity.

**Table 4.10.** Enantioselectivity  $-\Delta_{R,S}(\Delta G)$  ( $\text{kJ}\cdot\text{mol}^{-1}$ ),  $\Delta_{R,S}(\Delta H)$  ( $\text{kJ}\cdot\text{mol}^{-1}$ ) and  $\Delta_{R,S}(\Delta S)$  ( $\text{J}\cdot\text{mol}^{-1}\cdot\text{K}^{-1}$ ) of the complexation between the compounds (**Pro**), (**Asp**),  $\gamma$ -**5** and **4a** with the selector CD7 (**5**) and G7 (**10**) in polysiloxane PS 86 using *n*-tridecane as reference standard

Proline <i>N</i> -TFA- <i>O</i> -Ethyl ( <b>Pro</b> )			Aspartic acid <i>N</i> -TFA- <i>O</i> -Ethyl ( <b>Asp</b> )		
	$-\Delta_{R,S}(\Delta G)$ ( $\text{kJ}\cdot\text{mol}^{-1}$ )			$-\Delta_{R,S}(\Delta G)$ ( $\text{kJ}\cdot\text{mol}^{-1}$ )	
T ( $^{\circ}\text{K}$ )	CD7( <b>5</b> )	G7 ( <b>10</b> )	T ( $^{\circ}\text{K}$ )	CD7 ( <b>5</b> )	G7 ( <b>10</b> )
353.15	1.25	0.16	353.15	0.33	0.34
363.15	1.05	0.18	363.15	0.27	0.30
373.15	0.74	0.15	373.15	0.18	0.20
383.15	0.58	0.13	383.15	0.13	0.14
393.15	0.41	0.11	393.15	0.08	0.09
403.15	0.27	0.09	403.15	0.00	0.05
413.15	0.00	0.07	413.15	0.00	0.00
	$\Delta_{R,S}(\Delta H)$ ( $\text{kJ}\cdot\text{mol}^{-1}$ )			$\Delta_{R,S}(\Delta H)$ ( $\text{kJ}\cdot\text{mol}^{-1}$ )	
	-8.3	-0.9		-2.6	-2.4
	$\Delta_{R,S}(\Delta S)$ ( $\text{J}\cdot\text{mol}^{-1}\cdot\text{K}^{-1}$ )			$\Delta_{R,S}(\Delta S)$ ( $\text{J}\cdot\text{mol}^{-1}\cdot\text{K}^{-1}$ )	
	20.1	2.1		6.5	5.9
$\gamma$ - valerolactone ( $\gamma$ - <b>5</b> )			1-(phenyl)ethylamine-PFP derivative ( <b>4a</b> )		
	$-\Delta_{R,S}(\Delta G)$ ( $\text{kJ}\cdot\text{mol}^{-1}$ )			$-\Delta_{R,S}(\Delta G)$ ( $\text{kJ}\cdot\text{mol}^{-1}$ )	
T ( $^{\circ}\text{K}$ )	CD7 ( <b>5</b> )	G7 ( <b>10</b> )	T ( $^{\circ}\text{K}$ )	CD7 ( <b>5</b> )	G7 ( <b>10</b> )
353.15	1.85	2.75	353.15	2.31	0.31
363.15	1.84	2.53	363.15	1.90	0.29
373.15	1.64	2.10	373.15	1.61	0.26
383.15	1.55	1.57	383.15	1.50	0.21
393.15	1.51	0.00	393.15	1.34	0.16
403.15	1.46	0.00	403.15	1.18	0.13
413.15	1.49	0.00	413.15	1.00	0.09
	$\Delta_{R,S}(\Delta H)$ ( $\text{kJ}\cdot\text{mol}^{-1}$ )			$\Delta_{R,S}(\Delta H)$ ( $\text{kJ}\cdot\text{mol}^{-1}$ )	
	-16.1	-2.4		-8.1	-1.8
	$\Delta_{R,S}(\Delta S)$ ( $\text{J}\cdot\text{mol}^{-1}\cdot\text{K}^{-1}$ )			$\Delta_{R,S}(\Delta S)$ ( $\text{J}\cdot\text{mol}^{-1}\cdot\text{K}^{-1}$ )	
	37.8	5.9		17.1	4.2



## Conclusions



NMR spectroscopy and gas chromatography can contribute to elucidate the enantiorecognition mechanism by cyclodextrin derivatives. The results described in this work reveal the presence of at least two different mechanisms for the enantioselectivity of derivatized cyclodextrins when applied as chiral stationary phases (CSPs) in enantioselective gas chromatography and as chiral solvating agents (CSAs) in NMR spectroscopy. One involves a classical inclusion complex formation while the other envisions multimodal interactions with the cyclodextrin occurring externally on both the top and/or bottom side of the cavity. Chiral compounds can be differentiated by one or the other mechanism, or by the simultaneous contributions of both mechanisms.

Thus, for the first time, acyclic dextrans with different degrees of oligomerization were regioselectively derivatized, characterized and applied as chiral selectors. These derivatives exhibit the analogous derivatization pattern as the well known cyclodextrin derivatives,<sup>121</sup> obtained by the multistep synthetic procedure which involves selective protection/deprotection of the different hydroxyl groups.

A fundamental aspect of the linear dextrin derivatives, mainly in the case of the acyclic G7 (**10**), may be the presence of a segment similar to the “cavity section” of the cyclic analogue and another linear fragment of the selector. Consequently, both “pseudo-inclusion” and external interactions may occur simultaneously. In certain cases the presence of a cavity ( $\alpha$ -,  $\beta$ -,  $\gamma$ -congeners) proves not to be a prerequisite for enantiorecognition, as demonstrated in the case of the enantioseparation of selected substrates (chapter IV).

The versatility of the mixed acetylated/silylated cyclic and acyclic dextrans as promising selectors both as CSAs in NMR spectroscopic analysis and as CSPs for enantioselective gas chromatography is confirmed. Indeed, the rigidity which characterizes some cyclodextrin derivatives where dipole-dipole interactions between adjacent acyl residues stabilize the macrocycle can be complemented by the flexibility of acyclic dextrans in the enantioseparation field (size-fit concept). For this reason, depending on the structure of the analyte, enantioseparation can be obtained both by the cyclic and/or with the acyclic selector, but the enantiorecognition of these selectors is not predictable.

It should be pointed out that cyclodextrins have 30-40 ( $\alpha$ - $\gamma$ ) stereogenic centers in each molecule and the decisive enantioselective interaction can also take place externally on the outer surface of the selector when a suitable derivatization of hydroxyl groups allows the formation of the most stable enantioselective complex which is not necessarily an inclusion-type complex (figure C1).

## Conclusions

Thus, the inclusion process can not be regarded as a general requirement for the enantioselectivity. External interactions were indeed found to be the predominant mechanism for the enantioselectivity of some pentafluoropropionyl derivatives of aromatic and cyclic amines as well as for  $\alpha$ -amino acid derivatives and the viability of linear selectors consisting only of three (maltotriose derivative **14**) or even a single glucose (compound **16**) unit as CSPs is demonstrated in the results summarized in chapter IV.

Furthermore, in the present work, the external interactions were demonstrated in the case of the diastereomeric complexes formed by heptakis(2,3-di-*O*-acetyl-6-*O*-*tert*-butyldimethylsilyl)- $\beta$ -cyclodextrin (CD7) with the fluorinated diether 'compound B' by NMR spectroscopic studies in solution where the analyte was only partially accommodated in the cavity of the  $\beta$ -cyclodextrin derivative; thus, significant NOEs were detected (simultaneously) between the enantiomers of 'compound B' and both the different functional groups (acetyl/TBMDS) on the two rims of the CD7 (**5**). This NMR study represents also one of the few examples where only two geometries for the diastereomeric complexes were proposed. The enantiomers of 'compound B' seem to be placed in a limited region of the cyclodextrin derivative, in contrast to the multimodal geometries which are usually postulated in the literature.<sup>149</sup>

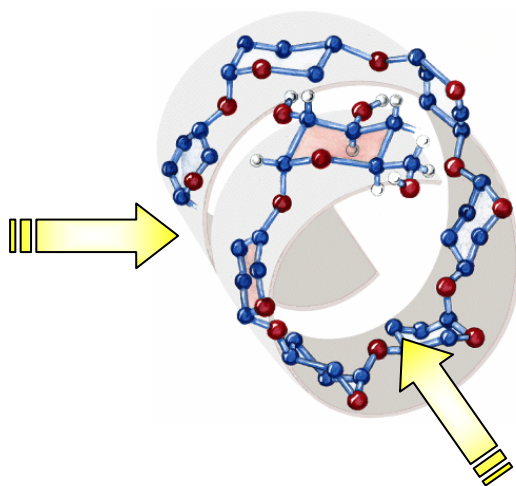


**Figure C1.** Helical structure of oligosaccharides formed by  $n$  glucose units.

In conclusion, the present work gives an answer to some key questions about the mechanism of enantioselectivity by cyclodextrins, differentiating between contributions of the cavity entity and the external surface of cyclodextrin derivatives.

Some examples in which the cavity does not represent the driving force for enantioselective complexation are presented, whereas in other cases inclusion phenomena (partial or complete inclusion) seem to be required for enantioselective interactions with the analyte. Thus, by considering the simultaneous contribution of outside/inside interactions with cyclodextrin derivatives it is possible to understand the present results. Furthermore, with this reappraisal it is possible to rationalize even some examples where the lack in the enantioselectivity of large ring cyclodextrin derivatives such as nonakis(2,3,6-tri-*O*-methyl)- $\delta$ -cyclodextrin and nonakis(2,3-di-*O*-methyl-6-*O*-*tert*-butyldimethylsilyl)- $\delta$ -cyclodextrin in enantioselective gas chromatography<sup>150</sup> and their weak interactions in solution as detected by capillary zone electrophoresis<sup>151</sup> were described.

Obviously, there are still many aspects which need to be investigated in order to understand and exploit the potential enantioselectivity of the acyclic dextrins selectors:

- a. the hydroxyl groups of the acyclic dextrins may be derivatized in many other ways; thus future attempts will be focused on the optimal combination of the suitable functional groups for the derivatization of the native acyclic dextrins;
- b. the analyte may be chemically modified in order to obtain more information about the mode of interaction with the selector.
- c. the use of mixed phases obtained by combining cyclic and acyclic dextrin derivatives may be tested. In this case, as well as in that one of the ‘Chiramix’ phase known in literature,<sup>152</sup> the two different selectors can be mixed and the effects of the various enantiorecognitions can be deduced.

The success obtained with the linear acetyl/TBDMS derivatives suggests several future applications in which the enantioseparation could be tuned and improved in comparison to that achieved by cyclodextrins.<sup>153</sup> For instance, in the case of saturated hydrocarbons, the inclusion phenomena were confirmed to be the driving-force of the enantio recognition, but a better combination of the alkyl chains on the hydroxyl groups of the native cyclodextrin might even improve the enantioseparation which are still not remarkable.

The use of *L*-glucose (which was tested in this work as monosaccharide derivative **16**, see chapter III for the structure) as a building block for the synthesis of oligosaccharides with a higher degree of oligomerization could indeed lead to the synthesis of *L*-maltoheptaose.<sup>154</sup> Important applications requiring a switch in the elution order of enantiomers would then be possible.

The selective modification of different acyclic oligosaccharides may find in the future interesting applications as chiral auxiliaries for enantioselective synthesis carried out in two-

## *Conclusions*

phase (organic-aqueous) media, in addition to their use as stationary phases for a myriad of chromatographic applications which are nowadays carried out with cyclodextrin derivatives. Thus, acyclic dextrans, after suitable derivatization, can be used in different applications where cyclodextrin derivatives failed in the enantiorecognition (due to the strong and non-selective interactions or due to unsuitable combination of the functional groups introduced on 2-, 3- and 6-OH sites).



Experimental section



*Materials and Methods.* The analytical GC was performed on an Agilent HP 5890A and on a Carlo Erba HRGC 5300 Mega Series equipped with a flame ionization detector (FID). Dihydrogen (99.999 %) or helium (99.999 %) was used as carrier gas.

Mass spectra were registered on a high-resolution ESI-(FT-ICR MS) Bruker Daltonics APEX II, 4.7 Tesla magnet.

NMR measurements were performed on a VARIAN INOVA 600 spectrometer operating at 600 and 150 MHz for  $^1\text{H}$  and  $^{13}\text{C}$ , respectively; on a VARIAN VXR 300 operating at 300 and 75 MHz for  $^1\text{H}$  and  $^{13}\text{C}$  and at 282 MHz for  $^{19}\text{F}$ ; on a BRUKER Advance W400 operating at 400 and 100 MHz for  $^1\text{H}$  and  $^{13}\text{C}$ .

The temperature was controlled to  $\pm 0.1$  °C.  $^1\text{H}$ -NMR chemical shifts are referenced to TMS as external standard. The 2D NMR spectra were obtained by using standard sequences. The ROESY (Rotating-frame Overhauser Enhancement Spectroscopy) spectra were recorded in the phase-sensitive mode, employing a mixing time of 0.3 s. The spectral width used was the minimum required in both dimensions. The pulse delay was maintained at 5 s; 512 hypercomplex increments of 8 scans and 2K data points each were collected. The data matrix was zero-filled to 2K x 1K and a Gaussian function was applied for processing in both dimensions. The gradient HMBC (Heteronuclear Multiple Bond Correlation) experiment was optimized for a long-range  $^1\text{H}$ - $^{13}\text{C}$  coupling constant of 8 Hz. The spectra were acquired with 512 time increments, 32 scans per  $t_1$  increment and a 3.5 ms delay period for suppression of one-bond correlation signals. No decoupling during acquisition was used. The selective relaxation rates were measured in the initial rate approximation by employing a selective  $\pi$  pulse at the selected frequency. After the delay  $\tau$ , a non-selective  $\pi/2$  pulse was employed to detect the longitudinal magnetization. For the biselective measurements, the two protons were inverted consecutively. Each selective relaxation rate experiment was repeated at least four times.

All solvents were dried according to standard procedures.<sup>155</sup> Native maltoheptaose was kindly provided by Dr. Laszlo Jicsinsky (Cyclolab, Hungary). Native maltotriose, *D*-glucose and *L*-glucose were purchased from Fluka.

Derivatization of amino acids, alcohols and amines was carried out according to the procedure described in literature.<sup>99b</sup> For the synthesis of the intermediates **3a-c**, synthesis and characterization of heptakis(2,3-di-*O*-methyl-6-*O*-*tert*-butyldimethylsilyl)- $\beta$ -cyclodextrin (**7**) and heptakis(2,3-di-*O*-*n*-pentyl-6-*O*-*tert*-butyldimethylsilyl)- $\beta$ -cyclodextrin (**8**), see reference 121. For the synthesis of Lipodex E **27**, see reference 75.

### Heptakis(2,3-di-*O*-acetyl-6-*O*-*tert*-butyldimethylsilyl)- $\beta$ -cyclodextrin (5)

To a solution of **3a** (1.86 g, 0.96 mmol) in pyridine (25 mL) acetic anhydride was added dropwise (22 mL) at room temperature. The mixture was heated for 4 hours at 100° C and further overnight at 60° C. After the removal of the solvent, the residue was dissolved in CH<sub>2</sub>Cl<sub>2</sub> and washed with brine and water. The organic layer was dried over MgSO<sub>4</sub>, the solvent was evaporated and the product purified by column chromatography on silica gel using a mixture toluene/*n*-hexane/ethanol (6:3:1) as eluant, to give 2.21 g (91 %) of **3b**.

ESI-MS *m/z* 1285 for [M + 2Na]<sup>+</sup>. Elemental analysis for C<sub>112</sub>H<sub>196</sub>O<sub>49</sub>Si<sub>7</sub>; calculated: C, 53.31%; H, 7.83%. Found: C, 53.01%; H, 7.98%. <sup>1</sup>H NMR (C<sub>6</sub>D<sub>12</sub>, 25 °C),  $\delta$ : 0.09 ((CH<sub>3</sub>)<sub>2</sub>Si, s, 42H), 0.93 ((CH<sub>3</sub>)<sub>3</sub>C, s, 63H), 1.99 (CH<sub>3</sub>, Ac-3, s, 21H), 2.01 (CH<sub>3</sub>, Ac-2, s, 21H), 3.79 (H<sub>6b</sub>, br. d, J<sub>6b6a</sub> = 10.0 Hz, 7H), 3.88 (H<sub>4</sub>, dd, J<sub>43</sub> = 8.6 Hz, J<sub>45</sub> = 9.6 Hz, 7H), 3.93 (H<sub>5</sub>, br. d, J<sub>54</sub> = 9.6 Hz, 7H), 4.10 (H<sub>6a</sub>, br. d, J<sub>6a6b</sub> = 10.0 Hz, 7H), 4.62 (H<sub>2</sub>, dd, J<sub>21</sub> = 3.7 Hz, J<sub>23</sub> = 9.9 Hz, 7H), 5.23 (H<sub>1</sub>, d, J<sub>12</sub> = 3.7 Hz, 7H), 5.43 (H<sub>3</sub>, dd, J<sub>32</sub> = 9.9 Hz, J<sub>34</sub> = 8.6 Hz, 7H) ppm; <sup>13</sup>C NMR (C<sub>6</sub>D<sub>12</sub>, 25 °C),  $\delta$ : -5.6 and -5.3 [(CH<sub>3</sub>)<sub>2</sub>Si], 18.2 [(CH<sub>3</sub>)<sub>3</sub>C], 20.0 (CH<sub>3</sub>, Ac-3), 20.3 (CH<sub>3</sub>, Ac-2), 25.7 [(CH<sub>3</sub>)<sub>3</sub>C], 62.3 (C<sub>6</sub>), 71.5 (C<sub>2</sub>+C<sub>3</sub>), 72.0 (C<sub>5</sub>), 75.6 (C<sub>4</sub>), 96.7 (C<sub>1</sub>), 168.9 (CO, Ac-2), 169.3 (CO, Ac-3) ppm.

### Hexakis(2,3-di-*O*-acetyl-6-*O*-*tert*-butyldimethylsilyl)- $\alpha$ -cyclodextrin (4)

The synthesis of the derivatized  $\alpha$ -cyclodextrin **4** was carried out in the same way as for compound **5**.<sup>120</sup>

<sup>1</sup>H NMR (C<sub>6</sub>D<sub>12</sub>, 25 °C),  $\delta$ : 0.09 ((CH<sub>3</sub>)<sub>2</sub>Si, s, 42H), 0.96 ((CH<sub>3</sub>)<sub>3</sub>C, s, 63H), 1.96 (CH<sub>3</sub>, Ac-3, s, 21H), 2.02 (CH<sub>3</sub>, Ac-3, s, 21H), 3.80 (H<sub>6b</sub>, br. d, J<sub>6b6a</sub> = 11.2 Hz, 7H), 3.83 (H<sub>4</sub> + H<sub>5</sub>, m, 14H), 4.12 (H<sub>6a</sub>, br. d, J<sub>6a6b</sub> = 11.2 Hz, 7H), 4.56 (H<sub>2</sub>, dd, J<sub>21</sub> = 3.5 Hz, J<sub>23</sub> = 10.4 Hz), 5.36 (H<sub>1</sub>, d, J<sub>12</sub> = 3.5 Hz, 7H), 5.41 (H<sub>3</sub>, br. t, 7H) ppm; <sup>13</sup>C NMR, C<sub>6</sub>D<sub>12</sub>,  $\delta$ : -5.7 and -5.4 [(CH<sub>3</sub>)<sub>2</sub>Si], 18.3 [(CH<sub>3</sub>)<sub>3</sub>C], 19.7 (CH<sub>3</sub>, Ac-3), 20.3 (CH<sub>3</sub>, Ac-2), 25.7 [(CH<sub>3</sub>)<sub>3</sub>C], 62.5 (C<sub>6</sub>), 71.5 (C<sub>2</sub>), 71.8 (C<sub>3</sub>), 72.1 (C<sub>5</sub>), 74.8 (C<sub>4</sub>), 95.9 (C<sub>1</sub>), 169.0 (CO, Ac-2), 169.2 (CO, Ac-3) ppm.

### Octakis(2,3-di-*O*-acetyl-6-*O*-*tert*-butyldimethylsilyl)- $\gamma$ -cyclodextrin (6)

The synthesis of the derivatized  $\gamma$ -cyclodextrin **6** was carried out in the same way as for compound **4**.<sup>120</sup>

<sup>1</sup>H NMR (C<sub>6</sub>D<sub>12</sub>, 25 °C),  $\delta$ : 0.09 ((CH<sub>3</sub>)<sub>2</sub>Si, s, 42H), 0.93 ((CH<sub>3</sub>)<sub>3</sub>C, s, 63H), 1.98 (CH<sub>3</sub>, Ac-2, s, 21H), 2.02 (CH<sub>3</sub>, Ac-2, s, 21H), 3.77 (H<sub>6b</sub>, br. d, J<sub>6b6a</sub> = 10.6 Hz, 7H), 3.96 (H<sub>4</sub>, dd, J<sub>43</sub> = 8.8 Hz, J<sub>45</sub> = 9.9 Hz, 7H), 4.00 (H<sub>5</sub>, br. d, J<sub>54</sub> = 9.9 Hz, 7H), 4.20 (H<sub>6a</sub>, br. d, J<sub>6a6b</sub> = 10.6 Hz, 7H), 4.52 (H<sub>2</sub>, dd, J<sub>21</sub> = 2.8 Hz, J<sub>23</sub> = 10.0 Hz), 5.20 (H<sub>1</sub>, d, J<sub>12</sub> = 2.8 Hz, 7H), 5.59 (H<sub>3</sub>, dd, J<sub>32</sub> = 10.0

Hz,  $J_{34} = 8.8$  Hz, 7H) ppm;  $^{13}\text{C}$  NMR,  $\text{C}_6\text{D}_{12}$ ,  $\delta$ : -5.3 and -5.6 [ $(\underline{\text{C}}\text{H}_3)_2\text{Si}$ ], 18.3 [ $(\text{CH}_3)_3\text{C}$ ], 19.9 ( $\text{CH}_3$ , Ac-3), 20.4 ( $\text{CH}_3$ , Ac-2), 25.7 [ $(\underline{\text{C}}\text{H}_3)\text{C}$ ], 62.1 ( $\text{C}_6$ ), 70.8 ( $\text{C}_2$ ), 71.9 ( $\text{C}_3$ ), 72.1 ( $\text{C}_5$ ), 74.4 ( $\text{C}_4$ ), 95.9 ( $\text{C}_1$ ), 169.0 (CO, Ac-2), 169.2 (CO, Ac-3) ppm.

**Heptakis[(1'-O,6-O)-tert-butyldimethylsilyl]-maltoheptaose (9):** 1 g (0.87 mmol) of native and dry maltoheptaose **G7** was dissolved under vigorous stirring in dry pyridine (15 mL). The solution was cooled on an ice bath. A solution of TBDMSCl (1.6 g, 10.6 mmol) in dry pyridine (20 mL) was then added dropwise to the cooled reaction vessel over 4 h. Cooling was continued for a further 2 h before the solution was allowed to warm to room temperature. After further 12 h at room temperature, the solvent was removed under reduced pressure to give a white solid, which was taken up in  $\text{CH}_2\text{Cl}_2$  (30 mL). The  $\text{CH}_2\text{Cl}_2$  phase was washed with aqueous solution of  $\text{KHSO}_4$  (20 mL, 1 M) to remove any residual pyridine, followed by saturated aqueous NaCl solution. The  $\text{CH}_2\text{Cl}_2$  layer was recovered and evaporated to dryness. Yield: 1.64 g (92 %, calculated on the main species). The product was used without further purification. A mixture of silylated linear dextrans was obtained (with 6 ( $\text{M}_1$ ), 7 ( $\text{M}_2$ ) and 8 ( $\text{M}_3$ ) *tert*-butyldimethylsilyl substituents), as confirmed by mass spectrometric analysis. ESI-MS  $m/z$  938 for  $[\text{M}_1 + 2\text{NH}_4]^{2+}$ , 994 for  $[\text{M}_2 + 2\text{NH}_4]^{2+}$ , 1052 for  $[\text{M}_3 + 2\text{NH}_4]^{2+}$ .

**Heptakis[(2,3-di-O,4'-O)-acetyl-(1'-O,6-O)-tert-butyldimethylsilyl]-maltoheptaose (10):** 1.5 g of crude heptakis[(1'-O, 6-O)-*tert*-butyldimethylsilyl]-maltoheptaose **G8** (**9**) were dissolved in dry pyridine (20 mL) and acetic anhydride (18 mL). The solution was stirred for 5 h at 100 °C and then concentrated. The remainder of the solvents were removed by coevaporation of toluene. The acetylation of the hydroxyl groups on the 2 and 3 position allowed the elucidation of the structure of the mixed acetyl/TBDMS selector by  $^1\text{H}$ - and  $^{13}\text{C}$ -NMR. The two main species with 7 or 8 TBDMS substituents having 16 ( $\text{M}_1$ ) and 15 ( $\text{M}_2$ ) acetyl groups respectively were obtained by column chromatography (toluene/*n*-hexane/ethanol, 5:4:1), to give 1.69 g (87 %) of ( $\text{M}_1 + \text{M}_2$ ).

ESI-MS  $m/z$  2647 for  $[\text{M}_1 + \text{Na}]^+$ , 2720  $[\text{M}_2 + \text{Na}]^+$ ; elemental analysis as calculated for  $\text{M}_1$  ( $\text{C}_{116}\text{H}_{202}\text{O}_{52}\text{Si}_7$ ): C 53.07 %, H 7.75 %; found: C 53.67 %, H 7.08 %. For  $\text{M}_2$  ( $\text{C}_{120}\text{H}_{214}\text{O}_{51}\text{Si}_8$ ), calculated: C 53.43 %, H 8.00 %. Found: C 53.35 %, H 8.17 %.

For  $\text{M}_1$ :  $^1\text{H}$  NMR ( $\text{CDCl}_3$ , 25 °C),  $\delta$ : -0.04 – 0.03 [ $(\underline{\text{C}}\text{H}_3)_2\text{Si}$ , s, 42H], 0.80 – 0.85 [ $(\underline{\text{C}}\text{H}_3)_3\text{C}$ , s, 63H], 1.92 – 2.06 ( $\underline{\text{C}}\text{H}_3$ , Ac, s, 48H), 3.30 – 4.21 ( $\text{H}_4$ ,  $\text{H}_5$ ,  $\text{H}_{6a}$ ,  $\text{H}_{6b}$ , m, 27H), 4.22 – 5.00 ( $\text{H}_2$ , m, 7H), 5.11 – 5.80 ( $\text{H}_1$ ,  $\text{H}_3$ ,  $\text{H}_{4'}$ , m, 14H), 6.19 ( $\text{H}_{1'}$ , d,  $J_{12} = 3.56$  Hz, 1H) ppm.  $^{13}\text{C}$  NMR ( $\text{CDCl}_3$ , 25 °C),  $\delta$ : -4.32 – -3.77 [ $(\underline{\text{C}}\text{H}_3)_2\text{Si}$ ], 19.6-19.7 [ $(\text{CH}_3)_3\text{C}$ ], 21.8-22.2 ( $\text{CH}_3$ , Ac), 27.1-

### Experimental section

27.3 [ $(\underline{\text{C}}\text{H}_3)\text{C}$ ], 62.5-62.7 ( $\text{C}_6$ ), 71.8-75.1 ( $\text{C}_2$ ,  $\text{C}_3$ ,  $\text{C}_5$ ,  $\text{C}_4$ ), 95.5-96.6 ( $\text{C}_1$ ), 170.2-171.9 ( $\text{CO}$ ,  $\text{Ac}$ ) ppm.

For  $\text{M}_2$ :  $^1\text{H}$  NMR ( $\text{CDCl}_3$ , 25 °C),  $\delta$ : -0.04 – 0.01 [ $(\underline{\text{C}}\text{H}_3)_2\text{Si}$ , s, 48H], 0.75 – 0.84 [ $(\underline{\text{C}}\text{H}_3)_3\text{C}$ , s, 72H], 1.92 – 2.01 ( $\underline{\text{C}}\text{H}_3$ ,  $\text{Ac}$ , s, 45H), 3.40 – 4.20 ( $\text{H}_4$ ,  $\text{H}_5$ ,  $\text{H}_{6a}$ ,  $\text{H}_{6b}$ , m, 27H), 4.20 – 4.96 ( $\text{H}_2$ , m, 7H), 5.11 – 5.80 ( $\text{H}_1$ ,  $\text{H}_3$ ,  $\text{H}_{4'}$ , m, 15H) ppm.  $^{13}\text{C}$  NMR ( $\text{CDCl}_3$ , 25 °C),  $\delta$ : -4.12 – -3.21 [ $(\underline{\text{C}}\text{H}_3)_2\text{Si}$ ], 17.6-19.9 [ $(\text{CH}_3)_3\underline{\text{C}}$ ], 23.9-24.6 ( $\text{CH}_3$ ,  $\text{Ac}$ ), 25.0-28.6 [ $(\underline{\text{C}}\text{H}_3)\text{C}$ ], 57.4 ( $\text{C}_6$ ), 60.2-60.7 ( $\text{C}_2$ ,  $\text{C}_3$ ,  $\text{C}_5$ ,  $\text{C}_4$ ), 94.1-95.5 ( $\text{C}_1$ ), 168.1-170.0 ( $\text{CO}$ ,  $\text{Ac}$ ) ppm.

**Octakis[(1'-*O*,6-*O*)-*tert*-butyldimethylsilyl]-maltooctaose (11).** The synthesis of this intermediate was carried out according to the procedure applied to the intermediate **9**. From 1 g (0.76 mmol) of native and dry maltoheptaose **G7**, 1.55 g (87 %) of the raw material was obtained after silylation. This product was used without further purification. A mixture of three silylated linear dextrans were isolated (with 8 ( $\text{M}_1$ ), 9 ( $\text{M}_2$ ) or 10 ( $\text{M}_3$ ) *tert*-butyldimethylsilyl substituents), as confirmed by mass spectrometry analysis.

ESI-MS  $m/z$  1137 for  $[\text{M}_1 + 2\text{NH}_4]^{2+}$ , 1194 for  $[\text{M}_2 + 2\text{NH}_4]^{2+}$ , 1250 for  $[\text{M}_3 + 2\text{NH}_4]^{2+}$ .

**Octakis[(2,3-di-*O*,4''-*O*)-acetyl-(1'-*O*,6-*O*)-*tert*-butyldimethylsilyl]-maltooctaose (12):** 1g of the crude octakis[(1'-*O*, 6-*O*)-*tert*-butyldimethylsilyl]-maltooctaose **11** were dissolved in dry pyridine (15 mL) and acetic anhydride (15 mL). The solution was stirred for 5 h at 100 °C and then concentrated. The acetylation of the hydroxyl groups on the 2 and 3 position allowed the elucidation of the structure of the mixed acetyl/TBDMS selector by  $^1\text{H}$ - and  $^{13}\text{C}$ -NMR. The two main species with 8 or 9 TBDMS substituents having 18 ( $\text{M}_1$ ) and 17 ( $\text{M}_2$ ) acetyl groups respectively were obtained by column chromatography (toluene/*n*-hexane/ethanol, 6:3:1), to give 1.18 g (91 %) of ( $\text{M}_1 + \text{M}_2$ ). After isolation of the two species the high ratio  $\text{M}_2/\text{M}_1$  (10:1) (where  $\text{M}_2$  shows an acetyl group on the anomeric center), only  $\text{M}_2$  were characterized by NMR spectroscopic analysis.

For  $\text{M}_2$ :  $^1\text{H}$  NMR ( $\text{CDCl}_3$ , 25 °C),  $\delta$ :  $^1\text{H}$  NMR ( $\text{CDCl}_3$ , 25 °C),  $\delta$ : -0.06 – 0.02 [ $(\underline{\text{C}}\text{H}_3)_2\text{Si}$ , s, 54H], 0.80 – 0.90 [ $(\underline{\text{C}}\text{H}_3)_3\text{C}$ , s, 81H], 1.86 – 2.05 ( $\underline{\text{C}}\text{H}_3$ ,  $\text{Ac}$ , s, 51H), 3.44 – 4.45 ( $\text{H}_4$ ,  $\text{H}_5$ ,  $\text{H}_{6a}$ ,  $\text{H}_{6b}$ , m, 31H), 4.6 – 4.98 ( $\text{H}_2$ , m, 8H), 5.15 – 5.85 ( $\text{H}_1$ ,  $\text{H}_3$ ,  $\text{H}_{4'}$ , m, 17H) ppm.  $^{13}\text{C}$  NMR ( $\text{CDCl}_3$ , 25 °C),  $\delta$ : -4.43 – -3.33 [ $(\underline{\text{C}}\text{H}_3)_2\text{Si}$ ], 18.2-19.6 [ $(\text{CH}_3)_3\underline{\text{C}}$ ], 22.1-24.8 ( $\text{CH}_3$ ,  $\text{Ac}$ ), 25.0-29.1 [ $(\underline{\text{C}}\text{H}_3)\text{C}$ ], 56.5-58.1 ( $\text{C}_6$ ), 60.1-61.2 ( $\text{C}_2$ ,  $\text{C}_3$ ,  $\text{C}_5$ ,  $\text{C}_4$ ), 92.2-96.3 ( $\text{C}_1$ ), 165.4-172.0 ( $\text{CO}$ ,  $\text{Ac}$ ) ppm.

**Tris[(1'-*O*,6-*O*)-*tert*-butyldimethylsilyl]-maltotriose (13)**

The same procedure described above for compounds **3a-c** and **9** was applied to maltotriose **G3** (1.02 g, 2.02 mmol) to obtain compound **13**. As with the maltoheptaose derivatives, a mixture of compounds, in this case with 3 ( $M_1$ ) or 4 ( $M_2$ ) TBDMS groups was obtained (1.58 g, 85%).

ESI-MS  $m/z$  865 for  $[M_1 + NH_4]^+$ , 980  $[M_2 + NH_4]^+$ . These intermediates were used without further purification and characterization.

**Tris[(2,3-di-*O*,4''-*O*)-acetyl-(1'-*O*,6-*O*)-*tert*-butyldimethylsilyl]-maltotriose (14)**

Compound **14** was synthesized according to the procedure employed for **5** and **10**. After column chromatography (*n*-hexane/ EtOAc, 6:4) the two species with three ( $M_1$ ) and four ( $M_2$ , main species) *tert*-butyldimethylsilyl groups and seven and eight acetyl groups, respectively, were obtained.

ESI-MS  $m/z$  1207 for  $[M_1 + Na]^+$ , 1279  $[M_2 + Na]^+$ ; elemental analysis calculated for  $M_1$  ( $C_{52}H_{90}O_{24}Si_3$ ), C 52.77 %, H 7.66 %; found: C 51.89 %, H 7.44 %. For  $M_2$  ( $C_{56}H_{102}O_{23}Si_4$ ), calculated: C 53.56 %, H 8.18 %; found: C 53.45 %, H 8.11 %.

For  $M_2$ :  $^1H$  NMR ( $CDCl_3$ , 25 °C),  $\delta$ : 0.01 – 0.07 [ $(\underline{CH}_3)_2Si$ , s, 24H], 0.76 – 0.89 [ $(\underline{CH}_3)_3C$ , s, 36H], 1.94 – 2.01 ( $\underline{CH}_3$ , Ac, s, 21H), 3.62– 4.05 ( $H_4$ ,  $H_5$ ,  $H_{6a}$ ,  $H_{6b}$ , m, 11H), 4.33 – 4.85 ( $H_2$ , m, 3H), 4.95 – 5.84 ( $H_1$ ,  $H_3$ ,  $H_{4''}$ , m, 7H) ppm.  $^{13}C$  NMR ( $CDCl_3$ , 25 °C),  $\delta$ : -4.85 – -4.51 [ $(\underline{CH}_3)_2Si$ ], 18.1-18.9 [ $(\underline{CH}_3)_3C$ ], 21.0-21.4 ( $CH_3$ , Ac), 25.8-26.4 [ $(\underline{CH}_3)C$ ], 60.2-62.5 ( $C_6$ ), 63.0-75.1 ( $C_2$ ,  $C_3$ ,  $C_5$ ,  $C_4$ ), 95.3, 95.5, 95.6 ( $C_1$ ), 169.6, 170.1, 170.2, 170.5, 170.8, 170.9, 171.0 (7  $\underline{CO}$ , Ac) ppm.

**1,6-di-*O*-*tert*-butyldimethylsilyl-*D*-glucose (15)**

TBDMSCl (2.5 g, 16.6 mmol) in pyridine (12 mL) was added dropwise to an ice-cold solution of *D*-glucose (1.03 g, 5.72 mmol) in pyridine (25 mL). The mixture was then stirred overnight at room temperature, after which the solvent was evaporated in vacuo with a rotary evaporator. The residue was dissolved in  $CH_2Cl_2$  and washed successively with aqueous solution of  $KHSO_4$  (1 M), brine and water. The organic layer was dried over anhydrous  $MgSO_4$  and the solvent evaporated to give a white solid containing two species with 2 ( $M_1$ ) and 3 ( $M_2$ ) TBDMS group, respectively.

ESI-MS  $m/z$  427 for  $[M_1 + NH_4]^+$ , 541  $[M_2 + NH_4]^+$ . The main species (as confirmed after acetylation, is the  $M_1$  intermediate).

**(2,3,4-tri-*O*-acetyl-1,6-di-*O*-*tert*-butyldimethylsilyl)-*D*-glucose (16)**

Acetic anhydride (13 mL) was added dropwise to a solution of **15** (1.10 g, 2.69 mmol) in pyridine (18 mL). The mixture was heated under reflux for 4 hours at 100° C, followed by overnight at 60° C. After removal of the solvent, the residue was dissolved in CH<sub>2</sub>Cl<sub>2</sub> and washed with brine and water. The organic layer was dried over MgSO<sub>4</sub> and, the solvent evaporated and the product purified by chromatography (*n*-hexane/ EtOAc 8:2) to give 0.81 g (57 %) of **16**.

ESI-MS *m/z* 558 for [M + Na]<sup>+</sup>. Elemental analysis, calculated for C<sub>24</sub>H<sub>46</sub>O<sub>9</sub>Si<sub>2</sub>: C 53.90 %, H 8.67 %; found: C 53.04 %, H 8.89 %.

<sup>1</sup>H NMR (CDCl<sub>3</sub>, 25 °C), δ: -0.01 – 0.08 [(CH<sub>3</sub>)<sub>2</sub>Si, s, 12H], 0.79 – 0.88 [(CH<sub>3</sub>)<sub>3</sub>C, s, 18H], 1.96 – 2.08 (CH<sub>3</sub>, Ac, s, 9H), 3.61– 4.01 (H<sub>5</sub>, H<sub>6a</sub>, H<sub>6b</sub>, m, 3H), 4.69 (H<sub>2</sub>, dd, J<sub>21</sub> = 8.1 Hz, J<sub>23</sub> = 7.6 Hz, 1H), 5.03 (H<sub>4</sub>, dd, J<sub>43</sub> = 8.0 Hz, J<sub>45</sub> = 9.4 Hz, 1H), 5.13 (H<sub>3</sub>, dd, J<sub>32</sub> = 7.6 Hz, J<sub>34</sub> = 8.0 Hz, 1H), 5.49 (H<sub>1</sub>, d, J<sub>12</sub> = 8.1 Hz, 1H).ppm. <sup>13</sup>C NMR (CDCl<sub>3</sub>, 25 °C), δ: -3.54 – -3.15 [(CH<sub>3</sub>)<sub>2</sub>Si], 19.6-20.2 [(CH<sub>3</sub>)<sub>3</sub>C], 22.6, 22.8, 22.9 (CH<sub>3</sub>, Ac), 27.2, 27.3 [(CH<sub>3</sub>)C], 63.8 (C<sub>6</sub>), 70.3, 71.7, 73.4, 74.2 (C<sub>2</sub>, C<sub>3</sub>, C<sub>5</sub>, C<sub>4</sub>), 95.7 (C<sub>1</sub>), 171.1, 171.5, 171.6 (CO, Ac) ppm.

**1,6-di-*O*-*tert*-butyldimethylsilyl-*L*-glucose (17)**

The same procedure applied to *D*-glucose was used for the synthesis of **17**, obtaining the same intermediates mentioned above.

ESI-MS *m/z* 427 for [M<sub>1</sub> + NH<sub>4</sub>]<sup>+</sup>, 541 [M<sub>2</sub> + NH<sub>4</sub>]<sup>+</sup>.

**(2,3,4-tri-*O*-acetyl-1,6-di-*O*-*tert*-butyldimethylsilyl)-*L*-glucose (18)**

To a solution of **13** (1.10 g, 2.69 mmol) in pyridine (20 mL), acetic anhydride (15 mL) was added dropwise. The mixture was heated under reflux for 4 hours at 100° C and then overnight at 60° C. After removal of the solvent, the residue was dissolved in CH<sub>2</sub>Cl<sub>2</sub> and washed with brine and water. The organic layer was dried over MgSO<sub>4</sub>, the solvent evaporated and the product was purified by chromatography (*n*-hexane/ EtOAc 8:2) to give 0.75 g (52 %) of **18**.

ESI-MS *m/z* 558 for [M + Na]<sup>+</sup>. Elemental analysis, calculated for C<sub>24</sub>H<sub>46</sub>O<sub>9</sub>Si<sub>2</sub>: C 53.90 %, H 8.67 %; found: C 53.23 %, H 8.21 %. (for the characterization, see compound **16**).



**Per-*O*-methyl-*D*-maltoheptaose (19)**

MeI (1.35 mL, 2.17 mmol) was added dropwise to a solution of maltoheptaose **G7** (417 mg, 0.36 mmol) and NaOH (750 mg, 18.8 mmol) in DMSO (18 mL). The reaction was stirred at room temperature, further NaOH (750 mg, 18.8 mmol) and MeI (1.35 mL, 2.17 mmol) were added twice after 24 hours each. The reaction was stopped after 72 hours, the excess of NaOH was neutralized by methanol (15 mL). After removal of solvent the residue was dissolved in CH<sub>2</sub>Cl<sub>2</sub>, washed with water and brine. The organic layer was dried over MgSO<sub>4</sub>, the solvent evaporated and the residue was purified by chromatography (AcOEt/ methanol 9:1) to give 475 mg (89 %) of **19**.

ESI-MS  $m/z$  1499 for [M + Na]<sup>+</sup>. Elemental analysis, calculated for C<sub>65</sub>H<sub>118</sub>O<sub>36</sub>: C 52.91 %, H 8.06 %; found: C 52.31 %, H 8.55 %. <sup>1</sup>H NMR (CDCl<sub>3</sub>, 25 °C),  $\delta$ : 2.85-4.18 (H<sub>2</sub>, H<sub>3</sub>, H<sub>4</sub>, H<sub>5</sub>, H<sub>6a</sub>, H<sub>6b</sub>, OCH<sub>3</sub>, m, 111H), 5.41-5.65 (H<sub>1</sub>, m, 7H) ppm. <sup>13</sup>C NMR (CDCl<sub>3</sub>, 25 °C),  $\delta$ : 57.1-61.2 (OCH<sub>3</sub>, C<sub>6</sub>), 70.4-71.2 (C<sub>5</sub>), 82.1-83.7 (C<sub>2</sub>, C<sub>3</sub>, C<sub>4</sub>), 96.5-97.2 (C<sub>1</sub>) ppm.

*Synthesis of D-maltoheptaose bonded to a polydimethylsiloxane via an undecenyl spacer*

***N*-(1-methanesulfonyl)-benzotriazole (21)**. To an ice-cold solution of benzotriazole **20** (2 g, 0.02 mmol) and pyridine (2.02 g, 0.03 mmol) in dry toluene (20 mL), methylsulfonyl chloride (1.56 mL) in toluene (5 mL) was added dropwise. The mixture was then stirred overnight at room temperature. AcOEt (26 mL) and H<sub>2</sub>O (17 mL) were added. The organic layer was separated, successively washed with water and brine, and dried over anhydrous MgSO<sub>4</sub>. Removal of solvents in vacuo gave a solid, which was recrystallized from benzene to afford *N*-(1-methanesulfonyl) benzotriazole **21** as colourless needles: mp 110-112 °C. Elemental analysis, calculated for C<sub>7</sub>H<sub>7</sub>N<sub>3</sub>O<sub>2</sub>S: C 42.63 %, H 3.58 %; found: C 42.03 %, H 3.41 %.

***N*-acylbenzotriazole (23)**. To a solution of the 10-undecenyl carboxylic acid **22** (920 mg, 5 mmol) and *N*-(1-methanesulfonyl)benzotriazole **21** (985 mg, 5 mmol) in THF (25 mL), triethylamine (1 mL, 7 mmol) was added dropwise at room temperature, and the mixture was heated under reflux overnight. After the removal of the solvent and excess triethylamine under reduced pressure, the residue was dissolved in EtOAc (75 mL). The organic layer was washed with water, dried over anhydrous MgSO<sub>4</sub> and evaporated. The resulting crude product was recrystallized from toluene to provide the desired compound **23**.

ESI-MS  $m/z$  303 for [M + NH<sub>4</sub>]<sup>+</sup>. Elemental analysis, calculated for C<sub>17</sub>H<sub>23</sub>N<sub>3</sub>O: C 71.55 %, H 8.12 %; found C 71.85 %, H 8.24 %. <sup>1</sup>H-NMR (CDCl<sub>3</sub>, 25 °C),  $\delta$ : 1.18 – 1.42 (m, 12H), 1.81 – 1.95 (m, 2H), 3.33 (dd, J = 7.5 Hz, J = 15.1, 2H), 4.84 (dd, J = 10.1 Hz, J = 17.1, 2H),

## Experimental section

5.68 – 5.83 (m, 1H), 7.40 – 8.24 (m, 4H) ppm.  $^{13}\text{C}$ -NMR ( $\text{CDCl}_3$ , 25 °C),  $\delta$ : 24.96, 29.41, 29.57, 29.62, 29.77, 29.80, 34.31, 36.05, 43.41, 114.71, 114.99, 120.64, 126.60, 130.65, 139.68, 173.24 (CO).

**10-Undecenoylhydrazide (24)**. To a solution of *N*-acylbenzotriazole **23** (1.4 g, 5 mmol) in THF (25 mL) a 1M solution (in THF) of anhydrous hydrazine (6 mL, 6 mmol) was added dropwise at room temperature. The reaction mixture was stirred at room temperature for about 4 h. Successively, THF was removed under reduced pressure, the residue was dissolved in EtOAc (75 mL). The organic layer was washed with saturated aqueous  $\text{Na}_2\text{CO}_3$ , water, dried over anhydrous  $\text{MgSO}_4$ , and evaporated to give a crude product, which was recrystallized from benzene, to obtain 0.88 g (91 %) of **24**.

ESI-MS  $m/z$  221  $[\text{M} + \text{Na}]^+$ ; mp 86–87 °C. Elemental analysis calculated for  $\text{C}_{11}\text{H}_{22}\text{N}_2\text{O}$ : C 66.62 %, H 11.18 %; found: C 67.04 %, H 12.03 %.  $^1\text{H}$  NMR ( $\text{CDCl}_3$ , 25 °C),  $\delta$ : 1.21 – 1.58 (m, 12 H), 1.93 – 2.21 (m, 6H), 4.87 (dd,  $J = 10.2$  Hz,  $J = 17.1$  Hz, 2H), 5.64 – 5.84 (m, 1H), 7.20 – 7.74 (s, broad, 1H, removed with  $\text{D}_2\text{O}$ ).  $^{13}\text{C}$ -NMR ( $\text{CDCl}_3$ , 25 °C),  $\delta$ : 24.81, 28.35, 28.49, 28.56, 28.59, 33.07, 33.44, 33.90, 113.47, 138.46, 173.47 (CO).

**D-maltoheptaosyl-10-undecenoylhydrazone (25)**. 0.5 g (0.434 mmol) of native maltoheptaose **G7** were dissolved in 5 mL of pyridine; 0.26 g (1.302 mmol) of 10-undecenoylhydrazide **24** were added and the mixture kept at 60 °C for 48 h. Solvent was removed and the solid residue was washed with EtOAc until pyridine-free, to give 0.51 g (88 %) of **25**.<sup>129</sup>

ESI-MS  $m/z$  1350  $[\text{M} + \text{NH}_4]^+$ . Elemental analysis, calculated for  $\text{C}_{53}\text{H}_{91}\text{N}_2\text{O}_{36}$ : C 47.78 %, H 6.88 %; found: C 47.02 %, H 6.53 %.

**Per-O-methyl-D-maltoheptaosyl-10-undecenoylhydrazone (26)**. Methylation of compound **25** was carried out according to the procedure described for the methylation of **19**. From 0.25 g (0.188 mmol) of **25**, after column chromatography (EtOAc/MeOH, 9:1), 0.28 g (89 %) of **26** were obtained.

ESI-MS  $m/z$  1691  $[\text{M} + \text{Na}]^+$ . Elemental analysis. calculated for  $\text{C}_{77}\text{H}_{137}\text{N}_2\text{O}_{36}$ : C 55.48 %, H 8.28 %; found: C 56.01 %, H 8.55 %.  $^1\text{H}$  NMR ( $\text{CDCl}_3$ , 25 °C),  $\delta$ : 1.22-2.20 ( $\text{CH}_2$ , m, 16H), 2.80-4.21 ( $\text{H}_2$ ,  $\text{H}_3$ ,  $\text{H}_4$ ,  $\text{H}_5$ ,  $\text{H}_6$ , OMe, m, 111H), 4.88 (m, 2H, double bond spacer), 5.46-5.55 ( $\text{H}_1$ , m, 7H), 5.73 (m, 1H, double bond spacer), 7.02 ( $\text{H}_1$ , d,  $J_{12} = 6.4$  Hz, 1H) ppm.

**Chemical bonding of per-*O*-methyl-*D*-maltoheptaosyl-10-undecenoylhydrazone **26** to hydridomethyldimethylsiloxane copolymer.**<sup>84</sup> A mixture of hydridomethyldimethylsiloxane copolymer (0.420 mg, ca. 0.33 mmol), hexachloroplatinic(IV) acid (0.1 mg, dissolved in THF (0.5 mL), added in several portions) toluene (10 mL) and per-*O*-methyl-*D*-maltoheptaosyl-10-undecenoylhydrazone **26** (0.25 g, 0.15 mmol) was stirred under reflux for 24 h. The solvent was evaporated in vacuo and the residue was taken up in anhydrous methanol (20 mL), separated from the catalyst and the solvent was removed under reduced pressure to give 612 mg of linear selector linked to the polymer. The disappearance of the double bond of the undecenyl spacer was confirmed by the absence of the characteristic double doublet at 5.51 ppm and the multiplet at 4.88 ppm of the double bond and the appearance of a singlet at -0.03 ppm, characteristic of the (CH<sub>3</sub>)<sub>2</sub>Si protons.

**Octakis[(3-*O*,-4''*O*)-butanoyl-(1'-*O*,2,6-di-*O*)-*n*-pentyl]-maltooctaose (**28**).** Native maltooctaose (0.5 g, 0.38 mmol) was dissolved in 14 mL of dry DMSO; 0.55 g (13.8 mmol) of pulverized NaOH and 1.7 mL (13.8 mmol) of 1-bromopentane were added and the mixture was stirred at room temperature. A white precipitate of NaBr was formed. After stirring for two days, another 0.55 g (13.8 mmol) of pulverized NaOH and 1.7 mL (13.8 mmol) of 1-bromopentane were added. After a total of 5 days, the mixture was poured on water and extracted twice with diethyl ether. The organic phase was washed with water, dried with Na<sub>2</sub>SO<sub>4</sub> and the solvent was evaporated. The raw product was characterized by maltooctaose bearing sixteen (M<sub>1</sub>), seventeen (M<sub>2</sub>) or eighteen (M<sub>3</sub>) *n*-pentyl functional groups, due to the excess of 1-bromopentane (1:1.4) used for the alkylation.

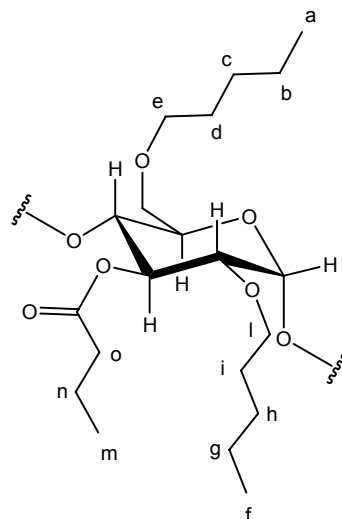
ESI-MS *m/z* 2348 [M<sub>1</sub> + H]<sup>+</sup>, 2508 [M<sub>2</sub> + H]<sup>+</sup>, 2578 [M<sub>3</sub> + H]<sup>+</sup>; this mixture was used for the subsequent acylation reaction without further purification.

0.1 g of this material and 1.7 mg (0.01 mmol) of 4-dimethylaminopyridine were dissolved in 3.5 mL of dry dichloromethane under nitrogen. After addition of triethylamine (0.09 mL, 0.63 mmol), 0.1 mL (0.56 mmol) of butyric anhydride was added. The mixture was stirred under reflux. After two days, another portion of 0.09 mL of triethylamine and 0.1 mL of butyric anhydride was added and the reflux continued. After another eight days, the excess of reagent and other volatiles were removed in a stream of nitrogen and the product was taken up in diethyl ether. The organic was washed with water, diluted NaHCO<sub>3</sub> solution, water, diluted NaH<sub>2</sub>PO<sub>4</sub> solution and lastly water. After drying with Na<sub>2</sub>SO<sub>4</sub>, removal of the solvent, the raw product was chromatographed over silica (toluene/ethyl acetate 9:1) to obtain 0.3 g (35 %) of **28**. The main species (as confirmed by <sup>1</sup>H-NMR analysis) is characterized by nineteen

## Experimental section

*n*-pentyl groups and seven butanoyl groups; only traces of the compound with seventeen pentyl groups and 9 butanoyl groups were isolated.

ESI-MS  $m/z$  1570  $[M + 2H]^{2+}$  (main species,  $C_{169}H_{306}O_{50}$ ).  $^1H$ -NMR (600 MHz,  $CDCl_3$ , 25 °C),  $\delta$ : 0.81-0.94 ( $CH_3$ , a-f-m, 78H), 1.11-1.38 ( $CH_2$ , b-c-g-h, 68H), 1.39-1.65 ( $CH_2$ , d-i-n 52H), 2.17-2.30 ( $CH_2$ , o, 18H), 2.91-4.22 ( $CH_2$ , e-l,  $H_2$ ,  $H_4$ ,  $H_5$ ,  $H_{6a}$ ,  $H_{6b}$ , 73 H), 4.52-5.75 ( $H_{4''}$ ,  $H_1$ ,  $H_3$ , 17H) ppm.



$^{13}C$ -NMR (150 MHz,  $CDCl_3$ , 25 °C),  $\delta$ : 13.4-22.5 ( $C_a$ ,  $C_f$ ,  $C_m$ ), 28.1-36.4 ( $C_b$ ,  $C_c$ ,  $C_d$ ,  $C_g$ ,  $C_h$ ,  $C_i$ ,  $C_n$ ), 62.8-82.2 ( $C_e$ ,  $C_l$ ,  $C_2$ ,  $C_3$ ,  $C_4$ ,  $C_5$ ,  $C_6$ ), 96.1-103.5 ( $C_1$ ) 128.2 ( $C_o$ ), 172.1-172.8 ( $C=O$ ).

## Appendix



A1. Synthesis of linear dextrin derivatives from cyclodextrins (alternative methods).....	145
A2. Diffusion Ordered Spectroscopy (DOSY).....	147
A3. The concept of retention increment R' .....	152

### **A1. Synthesis of linear dextrin derivatives from cyclodextrins (alternative methods)**

Since natural and modified oligosaccharides have found interest in cosmetic and pharmaceutical applications, there is a need of modified homologous oligosaccharides by more convenient and efficient routes. However, only few works are related to this demand due to: (i) the difficulty to achieve high regioselectivity by chemical modification of linear oligosaccharides; (ii) the extreme difficulty to obtain pure homologous linear oligosaccharides on a large scale.

Thus, the cost of obtaining the higher maltooligosaccharides with a degree of oligomerization 6 and 7 is prohibitive on a gram scale and those with a degree of oligomerization 8 are not yet commercially available. Moreover, their chemical synthesis is not suitable for operating at a preparative scale. Nevertheless, their acetylated and benzoylated derivatives can be obtained readily from cyclomaltooligosaccharides ( $\alpha$ -,  $\beta$ - and  $\gamma$ -cyclodextrins), respectively. The  $H_2SO_4$ -catalysed acetolysis of per-*O*-acetylated  $\alpha$ -,  $\beta$ - and  $\gamma$ -CDs has been reported by Farkas *et al.*<sup>125</sup> (this method is cited in chapter II) and Sakairi *et al.*<sup>156</sup> They obtained fully acetylated maltohexaose, maltoheptaose and maltooctaose from the corresponding cyclodextrins and after deacetylation the native dextrans are obtained. Similarly, Sakairi *et al.*<sup>157</sup> used acetolysis of per-*O*-benzoylated  $\alpha$ -,  $\beta$ - and  $\gamma$ -CDs to afford comparable yields of the corresponding linear derivatives. Recently, Lesur *et al.*<sup>158</sup> reported the selective modification at primary hydroxyl groups of maltooligosaccharides. Their work<sup>158</sup> and the mixed acetyl/TBDMS derivatives of this work,<sup>153</sup> represent the first regioselective modification of “acyclodextrins”. Since the selective halogenation of primary hydroxyl groups of CDs is now well established,<sup>121</sup> Lesur *et al.*<sup>158</sup> have chosen halogenated CDs as starting materials to explore routes to regioselectively derivatized maltooligosaccharides by acetolysis of appropriate CDs; this method is summarized in figure A1.

Unfortunately, the heptakis(2,3-di-*O*-acetyl-6-*O*-*tert*-butyldimethylsilyl)- $\beta$ -cyclodextrin CD7 (**5**) is not a suitable starting material for the acetolysis (figure A2) because the typical reaction conditions mentioned in figure A1 produce also the cleavage of the TBDMS, and consequently, a mixture of linear dextrin derivatives.

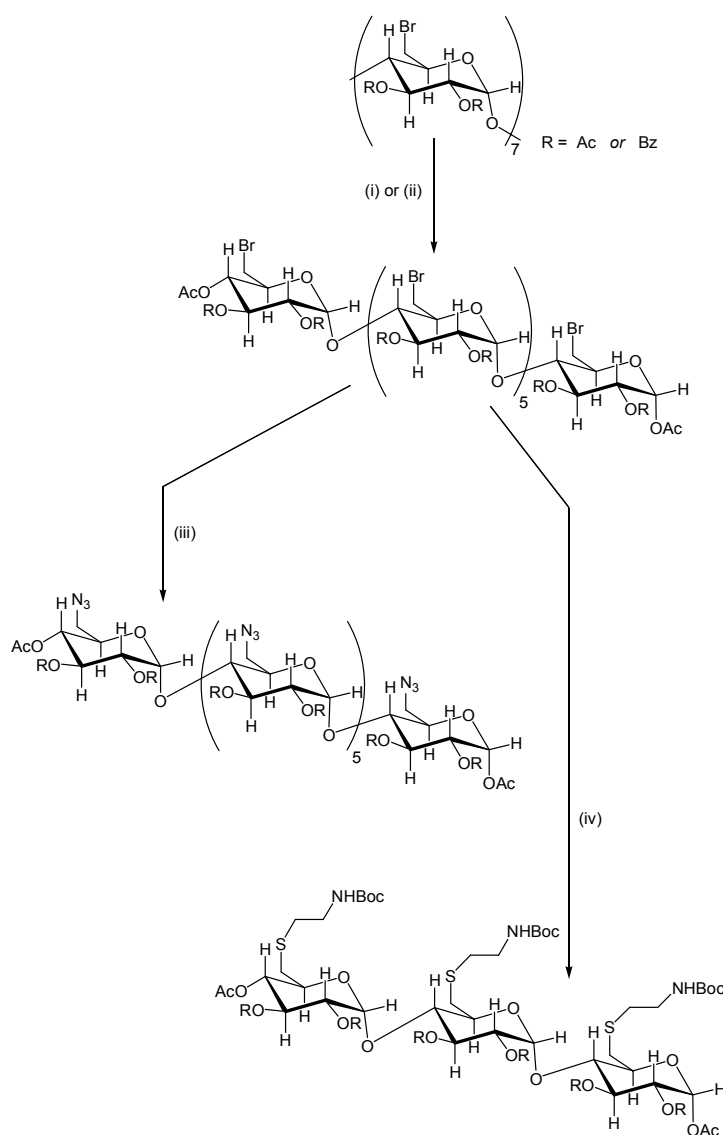


**Figure A1.** (i) 97:3 Ac<sub>2</sub>O-H<sub>2</sub>SO<sub>4</sub>, 57 °C, 28 h or 96:4 Ac<sub>2</sub>O-H<sub>2</sub>SO<sub>4</sub>, 57 °C, 30 h; (ii) Ac<sub>2</sub>O, 4.6 equiv. HClO<sub>4</sub>, 0 °C, 20 h then 36 °C, 20 h. (iii) LiN<sub>3</sub> (20 % in water), DMF, 48 h, rt. (iv) (Boc-amino)ethanethiol, Na<sub>2</sub>CO<sub>3</sub>, DMF, N<sub>2</sub>, rt, 4 days.

Thus per-6-*O*-TBDMS-2,3-di-*O*-acetyl CDs are more susceptible to acetolysis when subjected to such long reaction time mentioned in figure A1 (at shorter time the yield is very low).

It should be pointed out that the use of harsher conditions or longer reaction times lead to a depolymerization of the acyclic product rather than an increase of the amount of opened CDs. However, future applications for this synthetic step can be focused on the optimization of the cleavage of the TBDMS groups and/or on an additional step where the silylation of underivatized hydroxyl groups (produced by the acetolysis) is carried out.



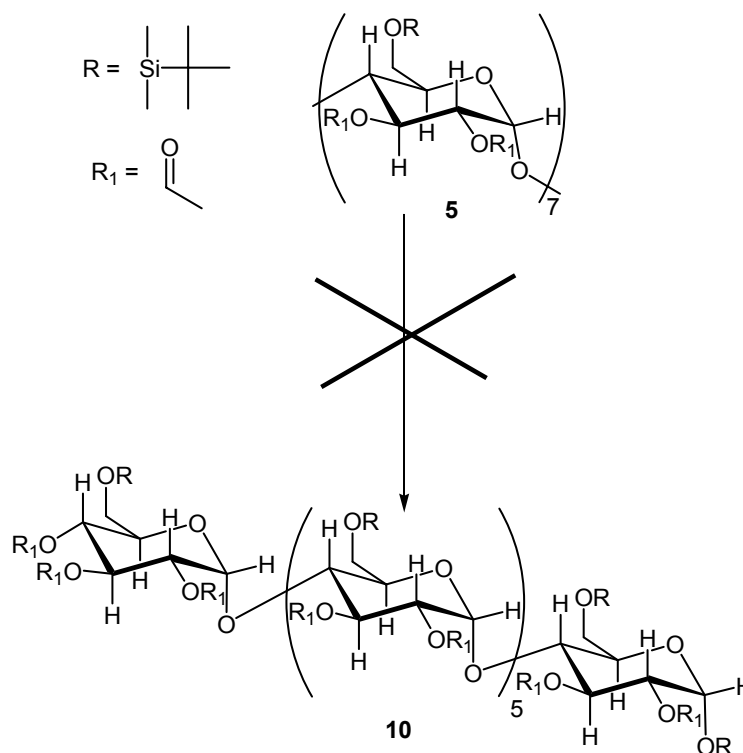


**Figure A2.** Schematic representation of the acetolysis of the  $\beta$ -cyclodextrin derivative **5** used in this work and its corresponding linear dextrin **10** (see chapter III for the alternative procedure).

By comparison with the different methods applied through several attempts carried out in this work, the two-step procedure for the acetyl/TBDMS derivative of maltoheptaose G7 (**10**) described in chapter II seems to be the most convenient route in order to achieve high yields by fast purification.

## A2. Diffusion Ordered Spectroscopy (DOSY)

Extensive information about the nuclear Overhauser effect (NOE) and the suitable pulse sequences applied in order to detect it are available in the literature.<sup>159-163</sup> In the subsequent context, further details are furnished on the DOSY technique.<sup>164</sup>

Diffusion NMR measurements are used in many different fields ranging from medical sciences to material sciences.<sup>164</sup> Recently, with the advent of high-resolution gradient enhanced spectroscopy, some general reviews dealing with the theoretical and practical aspects of gradient NMR spectroscopy have been published.<sup>165</sup> In addition, more-specific reviews on diffusion in polymers,<sup>164b</sup> zeolites and porous systems,<sup>164a</sup> surfactants,<sup>166</sup> and liquid crystals and membranes<sup>167</sup> have also been published. Since diffusion NMR spectroscopy is a totally non-invasive technique it is particularly suited to study molecular

dynamics and translational diffusion, and hence structural details in biological and physiological systems. Indeed, the application of diffusion NMR spectroscopy to membrane transport was recently reviewed,<sup>168</sup> and several reviews dealt with diffusion in restricted geometries.<sup>164</sup>

The basis for diffusion measurements is thus that magnetic field gradients can be used indirectly to label the position of NMR-active nuclei through their Larmor frequency. This is done by applying an external gradient of the magnetic field, which is described by equation 1, where  $\hat{i}$ ,  $\hat{j}$  and  $\hat{k}$  are the unit vectors in the  $x$ ,  $y$  and  $z$  directions, respectively.

$$G = \frac{\partial B_z}{\partial x} \hat{i} + \frac{\partial B_z}{\partial y} \hat{j} + \frac{\partial B_z}{\partial z} \hat{k} \quad (1)$$

Thus, the total external magnetic field at position  $r$  is given by equation 2. Spins precess with an angular frequency according to equation 3.

$$B_{(r)} = B_0 + G_{(r)} \quad (2)$$

$$\omega_{(r)} = -\gamma B_{(r)} \quad (3)$$

The acquired phase angle depends linearly on both  $B(r)$  and the duration of the gradient  $\delta$ . We assume that only a  $z$  gradient is present; hence the gradient produces the position-dependent phase angle  $\Phi(z)$  (equation 4). From this equation it is clear that the magnetic field gradient can be used to label the  $z$  position of the spins.

$$\Phi(z) = -\gamma B_{(z)} \delta \quad (4)$$

The most common approach to measure diffusion is to use the pulsed gradient spin echo (PGSE) NMR technique,<sup>169</sup> which is a modification of the Hahn spin echo pulse sequence.<sup>170</sup> In this sequence (figure A3 a), two identical gradient pulses are inserted, one into each period  $\tau$  of the spin-echo sequence. The net magnetization at the beginning of the experiment is oriented along the  $z$ -axis, which means that the ensemble of the spins are in thermal equilibrium. A  $90^\circ$  radiofrequency (RF) pulse is then applied and, as a consequence, the magnetization rotates from the  $z$ -axis to the  $x$ - $y$  plane. A pulse gradient of duration  $\delta$  and magnitude  $G$  is then

applied at a time point  $t_I$ . As a result, each spin experiences a phase shift according to the equation 5, at the end of the first period  $\tau$ , just before the application of the  $180^\circ$  RF pulse.

$$\Phi_i(\tau) = \gamma B_0 \tau + \gamma G \int_{t_I}^{t_I + \delta} z_i(t) dt \quad (5)$$

The left term in the equation 5 is the phase shift arising from the static magnetic field. The next step is the application of  $180^\circ$  RF pulse, which causes the reversal of the sign of the processing and the sign of the phase angle. A second gradient, equal in magnitude and duration to the first, is applied at time  $t_I + \Delta$ . In the first scenario (figure A3 b ) the spins do not undergo any translational motion along the  $z$ -axis, that is, the phase shift of each spin after the first period  $\tau$  is equal in magnitude to the phase shift of each spin after the second period  $\tau$ . Hence, the effects of the two pulsed gradients cancel out and all the spins refocus. In the presence of diffusion (the second scenario, figure A3 c), the phase shift of each spin after the first period  $\tau$  is different in magnitude from the phase shift after the second period  $\tau$ .

This effect occurs since, in the presence of diffusion, each species is located in a different position along the  $z$ -axis at time  $t_I$  and  $t_I + \Delta$ , and hence each species is situated in a different magnetic field (equation 2). Therefore, the spins precess with altered angular frequencies in these different periods of time (equation 3). Thus, the phase angle fans out (at least partially) in the presence of diffusion, and the echo signals is consequently smaller. It can be intuitively deduced that the larger diffusion is reflected by poorer refocusing of the spins and, consequently, by a smaller echo signal. From these equations it is apparent that the stronger and longer the phase of the pulsed gradients are, the poorer the refocusing of the spins and the smaller the recovered echo signal for diffusing spins are. In addition, it is clear that the larger the  $D$  value is (the duration between the pulsed gradients) the smaller the echo intensity will be.

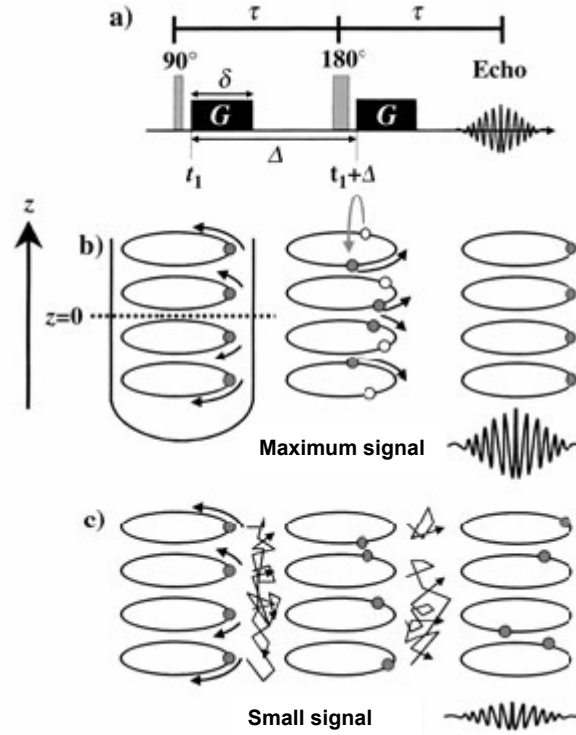


**Figure A3.** The PGSE pulse sequence.  $G$  is the amplitude of the pulsed gradient,  $\delta$  is its duration, and  $\Delta$  is the separation between the leading edges of the pulsed gradients. The effect of the absence (b) and presence (c) of diffusion on the phase shift and the signal intensity in a PGSE experiment is shown. In the sequence shown in (a) the term  $(\Delta - \delta/3)$  is the diffusion time.

Thus, without presenting the complete mathematical manipulations,<sup>165</sup> it is clear that the signal intensity should be described by the equation 6, where  $I_{(0,0)}$  and  $I_{(2\tau,0)}$  are the signal and echo intensity that would be observed immediately after the first  $90^\circ$  RF pulse and at  $2\tau$  respectively and  $f(\delta, G, \Delta, D)$  is a function that represents the signal attenuation as a result of diffusion.

$$I_{(2\tau,G)} = I_{(0,0)} \exp(-2\tau/T_2) f(\delta, G, \Delta, D) = I_{(2\tau,0)} f(\delta, G, \Delta, D) \quad (6)$$

Tanner *et. al.*<sup>169</sup> showed that the signal intensity for a single free-diffusing component is described by equation 7 and 8, where  $\gamma$  is the gyromagnetic ratio,  $G$  is the pulsed gradient strength,  $\Delta$  is the time separation between the pulsed-gradients,  $\delta$  is the duration of the pulse and  $D$  is the diffusion coefficient.

$$I_{(2\tau,G)} = I_{(0,0)} \exp(-2\tau/T_2) \exp(-\gamma^2 G^2 \delta^2 (\Delta - \delta/3) D) \quad (7)$$

$$\ln(I_{(2\tau,G)}/I_{(2\tau,0)}) = -\gamma^2 G^2 \delta^2 (\Delta - \delta/3) D = -bD \quad (8)$$

Thus, a plot of  $\ln(I_{(2\tau,G)}/I_{(2\tau,0)})$  versus the  $b$  values for an isotropic solution should give a straight line, the slope of which is equal to  $-D$ . If the sample of NMR includes multiple components differing in structure, since the spectral analysis is confusing, usually each component is measured after isolation or purification by means of re-crystallization or LC-NMR. DOSY provides a means for “virtual separation” of compounds; thus, the diffusion experiments can be processed and displayed as a 2D matrix with chemical shifts plotted along one axis and diffusion coefficients plotted along the perpendicular axis (figure A4).

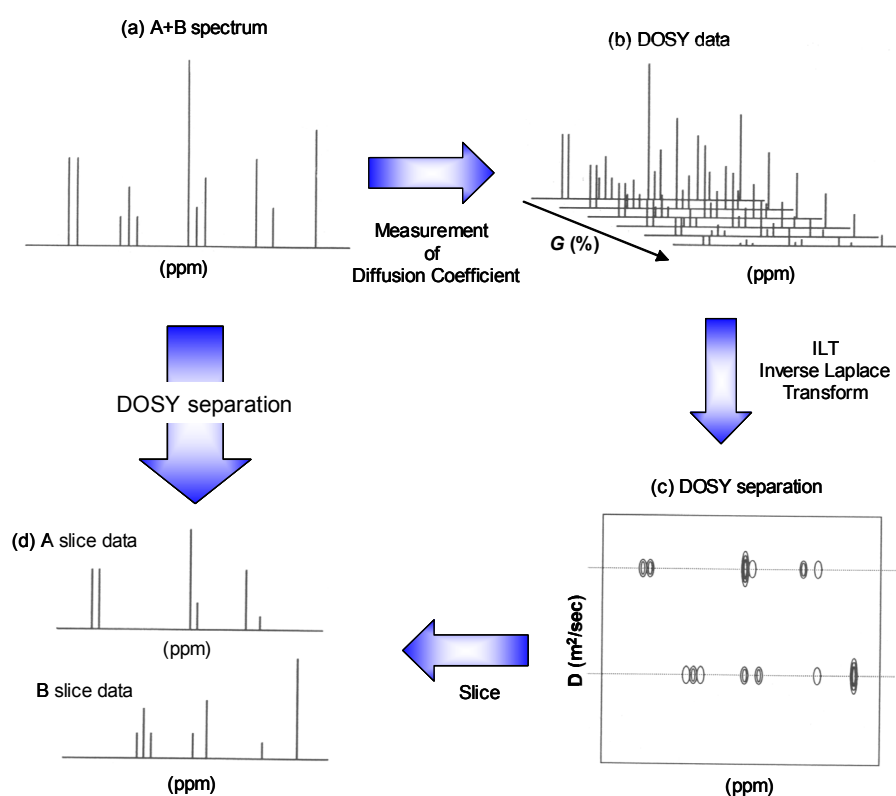


**Figure A4.** Schematic diagram of DOSY.

While the chemical shift information is obtained by fast Fourier transformation (FFT) of the time domain data, the diffusion information is obtained by an inverse Laplace transformation (ILT) of the signal decay data (figure A4). The goal of the DOSY experiment is to separate species spectroscopically (not physically) present in a mixture of compounds. In this sense,

the use of the DOSY experiment is reminiscent of the physical separation of compounds by chromatography. Thus, DOSY is also termed “NMR chromatography”.<sup>170</sup>

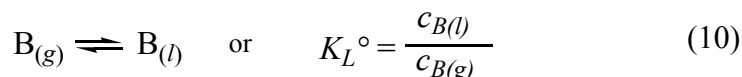
Applying Inverse Laplace Transform to the acquired decaying data (figure 6b), signals will be separated in the direction of indirect observation axis of multi dimension NMR, according to each diffusion coefficients of various components. Here, (figure 6c) is a schematic diagram of the most basic two-dimensional DOSY method outcome. X-axis ( $F_2$ ) of two dimensional NMR spectral DOSY corresponds to chemical shift as the same as that of usual COSY. On the other hand, Y-axis ( $F_1$ ) shows diffusion coefficient as an evolution parameter, in which the small diffusion coefficient signal is placed at the lower position of the spectrum and the large diffusion coefficient signal at the upper.

### A3. The concept of retention increment $R'$

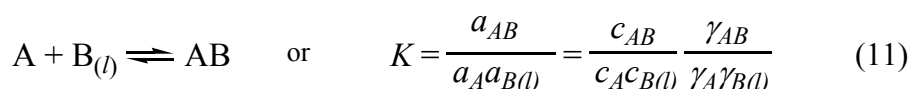
In enantioselective complexation GC, the concept of retention-increment  $R'$  can be used to quantitatively differentiate between physical contribution to retention arising from achiral gas-liquid partitioning and chemical contributions to retention arising from chiral molecular complexation whereby only the latter contribution leads to the separation of enantiomers:

$$-\Delta_{R,S}(\Delta G) = RT \ln(R'_R/R'_S) \quad (9)$$

It is even possible to extrapolate the achiral contribution to retention when a given pair of enantiomers is separated on two columns with different concentrations of the chiral selector. Consider a volatile selectand B migrating through a complexation column containing a dilute solution of the non-volatile selector A as an additive in the non-volatile solvent S (figure A5). When a complex is formed rapidly and reversibly between A and B, two equilibria can be distinguished

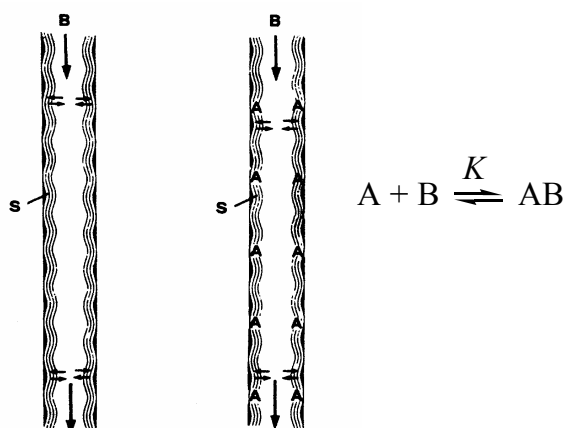


and



where the subscripts  $g$  and  $l$  refer to the gas and the liquid phase respectively.  $K_L^\circ$  is the distribution constant (partition coefficient) of B between the gas and the pure liquid phase S

neglecting the presence of A diluted in S (note that  $K_L^\circ$  quantifies the physical contribution to retention).



$$(17) \quad k'^{\circ} = \frac{t_R^{\circ}}{t_M^{\circ}} - 1 = K_L^{\circ} \frac{1}{\beta^{\circ}} \quad R' = \frac{K_L}{K_L^{\circ}} - 1 = K a_A \quad (18)$$

**Figure A5.** The principle of complexation GC. *Left:* reference column containing the pure solvent S. *Right:* complexation column containing the selector A in the solvent S. Retention parameters refer to the selectand B.<sup>84</sup>

$K$  is the thermodynamic complexation constant of A and B in S (note that  $K$  quantifies the chemical contribution to retention) and  $a_i$  is the activity of the species  $i$ , with the convention that  $a_i \rightarrow c_i$  at high dilution in the solvent S. As the amount of  $B_{(l)}$  injected (and therefore AB formed) is very low in the gas-chromatographic experiment, eq. (11) can be rewritten

$$K a_A = \frac{c_{AB}}{c_{B(l)}} \quad (12)$$

The total concentration of selectand B present in the liquid phase S is  $c_{B(l)} + c_{AB}$ . Hence, the apparent distribution constant  $K_L$  assuming no volume change on dissolution of B, is:

$$K_L = \frac{c_{B(l)} + c_{AB}}{c_{B(g)}} \quad (13)$$

Substituting (10) in (11), the expression (13) can be rewritten as

$$K_L = \frac{c_{B(l)}}{c_{B(g)}} + \frac{c_{AB}}{c_{B(g)}} = \frac{c_{B(l)}}{c_{B(g)}} + \frac{c_{B(l)}}{c_{B(g)}} \frac{c_{AB}}{c_{B(l)}} = K_L^\circ + K_L^\circ K a_A \quad (14)$$

or

$$K a_A = \frac{K_L}{K_L^\circ} - 1 \quad (15)$$

Thus the thermodynamic complexation constant  $K$  can be obtained from the plot of  $K_L$  versus  $a_A$  (eq. 6).<sup>171</sup> From eq. (15) a very useful relationship between  $K$  and chromatographic retention data can be developed when a reference column is employed containing the pure solvent S and when the inert non-complexing reference compound B\* (e.g. a saturated hydrocarbons) is co-injected with B.<sup>172</sup> The distribution constant of the selectand B between the gas and the pure liquid phase S in the reference column  $K_L^\circ$  is defined by

$$K_L^\circ = k'^\circ \beta^\circ \quad (16)$$

and the apparent distribution constant of the selectand B between the gas and the liquid phase S containing the selector A in the complexation column,  $K_L$ , is defined by

$$K_L = k' \beta \quad (17)$$

where  $k'^\circ$  is the retention factor of B in the pure solvent S in the reference column,  $k'$  is the reatention factor of B in the solution of A in S in the complexation column,  $\beta^\circ$  is the phase ratio of the reference column and  $\beta$  is the phase ratio of the complexation column. Eq. (12) can now be rewritten

$$K a_A = \frac{k'}{k'^\circ} \frac{\beta}{\beta^\circ} - 1 \quad (18)$$

For the non-complexing reference compound B\* (e.g. an inert saturated hydrocarbon) it is required that  $K^* = 0$  (symbols referring to the reference column are marked with a circle, e.g.  $K_L^\circ$ ,  $k'^\circ$ , whereas symbols referring to compound B\* are marked with an asterisk, e.g.  $k'^*$ ).

From eq. 10, it follows for B\* that



$$\frac{k'^*}{k'^{\circ*}} \frac{\beta}{\beta^{\circ}} = 1 \quad (19)$$

The ratio  $\beta/\beta^{\circ}$  is equal for B for co-injected B\* and Eq. (18) and (19) are combined to

$$K a_A = \frac{k'}{k'^{\circ}} \frac{k'^{\circ*}}{k'^*} - 1 \quad (20)$$

with

$$\frac{k'^*}{k'^{\circ*}} = \frac{t_R'^{\circ}}{t_R'^{\circ*}} = r^{\circ} \quad (21)$$

and

$$\frac{k'}{k'^*} = \frac{t_R'}{t_R'^*} = r \quad (22)$$

A relationship reminiscent of eq. (12) but referring now to relative retention data  $r^{\circ}$  and  $r$  is obtained

$$K a_A = \frac{r}{r^{\circ}} - 1 = \frac{r - r^{\circ}}{r^{\circ}} = R' \quad (23)$$

where  $r$  is the relative retention of the selectand B with respect to the inert reference compound B\* in a complexation column containing the selector A with the activity  $a_A$  in the inert solvent S, and  $r^{\circ}$  is the relative retention of the selectand B with respect to the same reference column containing the pure solvent S, devoid of the selector A.

The quantity  $R'$  is called the *retention-increment* of B.  $R'$  is a quantitative measure of complexation between A and B in S. Thus  $1/(1 + R')$  represents the fraction of the selectand B dissolved in the solvent S whereas  $R'/(1 + R')$  defines the fraction of the selectand B complexed with the selector A. Hence  $R'$  is proportional to the thermodynamic complexation constant  $K$ .

According to eq. (23) the retention increment  $R'$  is linearly related to  $a_A$  at a given temperature when a 1:1 complex is formed between A and B. The formal similarity between the basic equation of chromatography, eq. (17), describing the chromatographic process in the reference column and the derived equation of complexation chromatography eqs. (18) and

(23), describing the chromatographic process in the complexation should be noted. Consequently, the retention increment  $R'$  may also be called the chemical retention factor and  $r^\circ$  may be related to a physical hold-up time (figure A6).

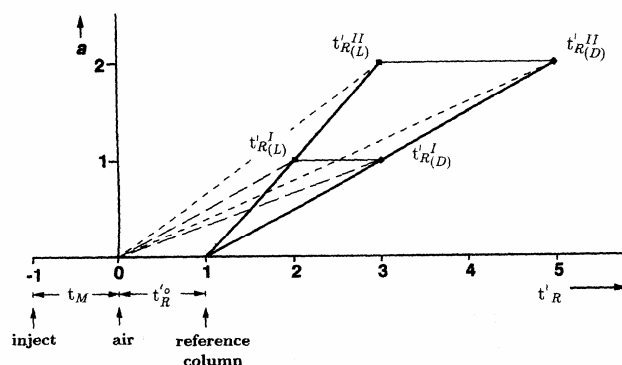


**Figure A6.** Schematic representation of the distinction between (i) non-enantioselective contributions to adjusted retention times of B,  $t_R'^\circ$ , and (ii) enantioselective contribution to adjusted retention times of Bi,  $t_{Ri}' - t_R'^\circ$  ( $i = L$  denoting enantiomers of B), leading to the constancy of the ratio  $R_D/R_L$ , as required by equation 16 (for simplification relative retentions  $r$  are replaced by adjusted retention time  $t_R'$ ,  $t_M$ ,  $t_R'^\circ$  were arbitrarily set unity, the ratio  $R_D/R_L$  represents arbitrary numbers).

The term selectivity  $S'$  is defined as the ratio of thermodynamic complexation constants  $K_D/K_L$ . According to eq. 38 the selectivity  $S'$  can be directly related by the ratio of the retention-increment  $R'$  of the selectand  $B_D$  and  $B_L$  competing for the same selector A in S. The selectivity  $S'$  is thus independent of the activity of A in S,  $a_A$ , and can be written as:

$$S'_{D,L} = \frac{K_D}{K_L} = \frac{R'_D}{R'_L} = \frac{r_D - r^\circ}{r_L - r^\circ} \quad (24)$$

An interesting application of the retention increment  $R'$  is the determination of the enantioselectivity in the complexation process, which is defined as the Gibbs energy (free enthalpy) difference  $-\Delta_{D,L}(\Delta G)$  of the transient diastereomeric complexes  $AB_D$  and  $AB_L$ . Thus eq. (9) can be rewritten in the following form

$$-\Delta_{D,L}(\Delta G) = RT \ln(R'_D/R'_L) = -\Delta_{D,L}(\Delta H) + T\Delta_{D,L}(\Delta S) \quad (25)$$

where  $R'_D/R'_L$  is defined in equation (24). The thermodynamic parameters  $-\Delta_{D,L}(\Delta G)$ ,  $-\Delta_{D,L}(\Delta H)$  and  $\Delta_{D,L}(\Delta S)$  of enantioselectivity can be obtained by van't Hoff plots when measurements are performed at different temperatures T according to:

$$R \ln \frac{R'_D}{R'_L} = \frac{-\Delta_{D,L}(\Delta G)}{T} = -\frac{\Delta_{D,L}(\Delta H)}{T} + \Delta_{D,L}(\Delta S) \quad (26)$$

In chapter IV selected enantioseparation experiments are complemented by the determination of thermodynamic data obtained according to the retention increment  $R'$  parameter mentioned above.



## References



## Introduction

1. [a] Villiers, A. *Compt. Rendu.* **1891**, *112*, 536. [b] Schardinger, F. *Z. Unters. Nahr. u. Genussm.* **1903**, *6*, 865. [c] Schardinger, F. *Wien. Klin. Wochenschr.* **1904**, *17*, 207. [d] Schardinger, F. *Zentralbl. Bakteriol. Parasitenk. Abt. 2* **1905**, *14*, 772. [e] Eastburn, S. D.; Tao, B. Y. *Biotechnol Adv* **1994**, *12*, 325.
2. Szejtli, J. *Chem. Rev.* **1998**, *98*, 1743.
3. Stella, V. J.; Rajewski, R. A. *Pharm. Res.* **1997**, *14*, 556.
4. Buschmann, H. J.; Schollmeyer, E. *J. Cosmet. Sci.* **2002**, *53*, 575.
5. Freudenberg, K.; Cramer, F. *Z. Naturforsch.* **1948**, *3b*, 464.
6. Hirose, T.; Yamamoto, Y. *Japanese Patent JP 55480*, **2001**.
7. Szejtli, J. *Cyclodextrin Technology*; Kluwer Academic Publishers: Dordrecht, **1988**, 450.
8. Yuan, D.-Q., Tahara, T.; Chen, W.-H.; Okabe, Y.; Yang, C.; Yagi, Y.; Nogami, Y.; Fukudome, M.; Fujita, K. *J. Org. Chem.* **2003**, *68*, 9456.
9. Khan, A. R.; Forgo, P.; Stine, K. J.; D'Souza, V. T. *Chem. Rev.* **1998**, *98*, 1977.
10. Nash, R. A. Cyclodextrins. In: Wade, A.; Weller, P. J. Editors. *Handbook of pharmaceutical excipients*. London: Pharm. Press & Am. Pharm. Assoc. **1994**, 145.
11. Hedges, R. A. *Chem. Rev.* **1998**, *98*, 2035.
12. Lu, X.; Chen, Y. *J. Chromatogr. A* **2002**, *955*, 133.
13. Muñoz-Botella, S.; del Castillo, B.; Martyn, M. A. *Ars Pharm.* **1995**, *36*, 187.
14. Loftsson, T.; Brewster, M. E. *J. Pharm. Sci.* **1996**, *85*, 1017.
15. Schneiderman, E.; Stalcup, A. M. *J. Chromatogr. B* **2000**, *745*, 83.
16. Fujishima, N.; Kusaka, K.; Umino, T.; Urushinata, T.; Terumi, K. *Japanese Patent JP 136,898*, **2001**.
17. Bhardwaj, R.; Dorr, R. T.; Blanchard, J. *J. Pharm. Sci. Technol.* **2000**, *54*, 233.
18. Dufosse, L.; Souchon, I.; Feron, G.; Latrasse, A.; Spinnler, H. E. *Biotechnol. Progr.* **1999**, *98*, 2035.
19. Lezcano, M.; Ai-Soufi, W.; Novo, M.; Rodriguez-Nunez, E.; Tato, J. V. *J. Agric. Food Chem.* **2002**, *50*, 108.
20. Holland, L.; Rizzi, G.; Malton, P. *PCT Int. Appl.* WO 67,716, **1999**.
21. [a] Altria, K. D.; Elder, D. *J. Chromatogr. A* **2004**, *1023*, 1. [b] Schurig, V.; Mayer, S. *J. Biochem. Biophys. Methods* **2001**, *48*, 117. [c] Fanali, S. *J. Chromatogr. A* **1997**, *792*, 227. [d] Verleysen, K.; Sandra, P. *Electrophoresis* **1998**, *19*, 2798.
22. [a] Waksmundzka-Hajnos, M. *J. Chromatogr. B* **1998**, *717*, 93. [b] Thuaud, N.; Sebillé, B.; Deratani, A.; Popping, B.; Pellet, C. *Chromatographia* **1993**, *36*, 373.

23. [a] Schurig, V. *J. Chromatogr. A* **2002**, *965*, 315. [b] Schurig, V. *J. Chromatogr. A* **2001**, *906*, 275. [c] He, L.; Beesley, T. E. *J. Liq. Chromatogr. Rel. Technol.* **2005**, *28*, 1075. [d] Schurig, V. *Trends Anal. Chem.* **2002**, *21*, 647. [e] Eiceman, G. A.; Gardea-Torresdey, J.; Overton, E.; Carney, K.; Dorman, F. *Anal. Chem.* **2002**, *74*, 2771. [f] Schurig, V. *Chirality* **2005**, *17*, S205.
24. [a] Macaudiere, P.; Caude, M.; Rosset, R.; Tambute, A. *J. Chromatogr.* **1987**, *405*, 135. [b] Macaudiere, P.; Caude, M.; Rosset, R.; Tambute, A. *J. Chromatogr. Sci.* **1989**, *27*, 383. [c] Kenichi, A. *Fragrance J.* **1999**, *27*, 28.
25. Evererts, F. M.; Beckers, J. L. In: *Isotachopheresis Theory, Instrumentation and Applications*, Elsevier, Amsterdam, **1984**.
26. Zaugg, S.; Caslavská, J.; Theurillat, R.; Thorman, W. *J. Chromatogr. A* **1999**, *838*, 337.
27. [a] Hinze, W. L.; Armstrong, D. W. *Anal. Lett.* **1980**, *13*, 1093. [b] Ward, T. J.; Armstrong, D. W. *J. Liq. Chromatogr.* **1986**, *9*, 407. [c] Han, S. M.; Armstrong, D. W. *Chem Anal.* **1990**, *108*, 81.
28. Breinholt, J.; Lehmann, S. V.; Varming, A. R. *Chirality* **1999**, *11*, 768.
29. Delgado, B.; Pérez, E.; Santano, M. C.; Minguillón, C. *J. Chromatogr. A* **2005**, *1092*, 36.
30. Hishiya, T.; Shibata, M.; Kakazu, M.; Asanuma, H.; Komiyama, M. *Macromolecules* **1999**, *32*, 2265.
31. Sreenivasan, K. *J. Appl. Polym. Sci.* **1998**, *70*, 15.
32. Kano, K. *J. Phys. Org. Chem.* **1997**, *10*, 286.

#### Chapter I

33. Dodziuk, H. *J. Mol. Struct.* **2002**, *614*, 33. Inoue, Y. *Ann. Rep. NMR Spectrosc.* **1993**, *27*, 59.
34. Davis, M. E.; Brewster, M. E. *Nature Rev.* **2004**, *3*, 1023.
35. Berthod, A.; Beesley, T. E.; Duncan, J. D.; Armstrong, D. W. *J. Pharm. Biomed. Anal.* **1990**, *8*, 123.
36. Han, S. M.; Han, Y. I., Armstrong, D. W. *J. Chromatogr. A* **1988**, *441*, 376.
37. Armstrong, D. W. *LC-GC Curr. Issues HPLC Technol.* **1997**, *15*, 20.
38. *Cyclobond Handbook* (Advanced Separation Technologies Inc., USA) **1992**.
39. Demarco, P. V.; Thakkar, A. L. *J. Chem. Soc. D* **1970**, *2*.
40. [a] Armstrong, D. W.; Ward, T. J.; Armstrong, R. D.; Beesley, T. E. *Science* **1986**, *232*, 1132. [b] Chankvetadze, B. *J. Chromatogr. A* **1997**, *792*, 269. [c] Chankvetadze, B.; Blaschke, G. *J. Chromatogr. A* **2001**, *906*, 309. [d] Chankvetadze, B. *Capillary*



- Electrophoresis in Chiral Analysis* **1997**, John Wiley & Sons, Chichester, UK, 555. [e] Schneider, H.-J.; Haket, F.; Rüdiger, V. *Chem. Rev.* **1998**, *98*, 1755. [f] Casy, A. F.; Mercer, A. D. *Magn. Res. Chem.* **1988**, *26*, 765. [g] Inoue, Y.; Hoshi, H.; Sakurai, M.; Chujo, R. *J. Am. Chem. Soc.* **1985**, *107*, 2319. [h] Inoue, Y. *J. Carbohydr. Chem.* **1989**, *8*, 29.
41. [a] Scriba, G. *J. Pharm. Biomed. Anal.* **2002**, *26*, 373. [b] Yamashoji, Y.; Ariga, T.; Asano, S.; Tanaka, M. *Anal. Chim. Acta* **1992**, *268*, 39. [c] Chankvetadze, B.; Burjanadze, N.; Maynard, K. D.; Bergander, D.; Bergenthal, D.; Blaschke, G. *Electrophoresis* **2002**, *23*, 3027.
42. Kano, K.; Kitae, T.; Takashima, H. *J. Inclusion Phenom. Mol. Recogn. Chem.* **1996**, *25*, 243.
43. Chankvetadze, B.; Endresz, G.; Bergenthal, D.; Blaschke, G. *J. Chromatogr. A* **1996**, *717*, 245.
44. [a] Zhou, L.; Thompson, R. A.; Reamer, R. A.; Miller, C.; Welch, C.; Ellison, D. K.; Wyvratt, J. *J. Chromatogr. A* **2003**, *987*, 409. [b] Zhou, L.; Thompson, R. A.; Reamer, R. A.; Lin, Z.; French, M.; Ellison, D. K.; Wyvratt, J. *Electrophoresis* **2003**, *24*, 2448.
45. [a] Chankvetadze, B.; Schulte, G.; Bergenthal, D.; Blaschke, G. *J. Chromatogr. A* **1998**, *798*, 149. [b] Chankvetadze, B.; Burjanadze, N.; Pintore, G.; Strickmann, D.; Bergenthal, G.; Blaschke, G. *Chirality* **1999**, *11*, 635. [c] Wedig, M.; Holzgrabe, U. *Electrophoresis* **1999**, *20*, 2698.
46. [a] Endresz, G.; Chankvetadze, B.; Bergenthal, D.; Blaschke, G. *J. Chromatogr. A* **1996**, *732*, 133. [b] Chankvetadze, B.; Endresz, G.; Schulte, G.; Bergenthal, D.; Blaschke, G. *J. Chromatogr. A* **1996**, *732*, 143.
47. [a] Galaverna, G.; Paganuzzi, M. C.; Corradini, R.; Dossena, A.; Marchelli, R. *Electrophoresis* **2001**, *22*, 3171. [b] Chankvetadze, B.; Kartoziya, I.; Burjanadze, N.; Bergenthal, D.; Luftmann, H.; Blaschke, G. *Chromatographia* **2001**, *53*, S290.
48. Chankvetadze, B. *Electrophoresis* **2002**, *23*, 4022.
49. Chankvetadze, B.; Fillet, M.; Burjanadze, N.; Bergenthal, D.; Bergander, K.; Luftmann, H.; Crommen, J.; Blaschke, G. *Enantiomer* **2000**, *5*, 313.
50. Pirkle, W. H. *J. Am. Chem. Soc.* **1966**, *88*, 1837.
51. [a] Rothchild, R. *Enantiomer* **2000**, *5*, 457. [b] Casy, A. F. *Trends Anal. Chem.* **1993**, *12*, 185. [c] Wenzel, T. J.; Wilcox, J. D. *Chirality* **2003**, *15*, 256. [d] Chi, Y.; Peelen, T. J.; Gellman, S. H. *Org. Lett.* **2005**, *7*, 3469. [e] Whitesides, G. M.; Lewis, D. W. *J. Am. Chem. Soc.* **1970**, *92*, 6979. [f] McCreary, M. D.; Lewis, D. W.; Wernick, D. L.; Whitesides, G. M. *J. Am. Chem. Soc.* **1974**, *96*, 1038.

52. [a] Seco, J. M.; Quinta, E.; Riguera, R. *Chem. Rev.* **2004**, *104*, 17. [b] Uccello-Barretta, G.; Balzano, F.; Caporusso, A. M.; Salvadori, P. *J. Org. Chem.* **1994**, *59*, 836. [c] Uccello-Barretta, G.; Balzano, F.; Caporusso, A. M.; Iodice, A.; Salvadori, P. *J. Org. Chem.* **1995**, *60*, 2227. [d] Uccello-Barretta, G.; Balzano, F.; Menicagli, R.; Salvadori, P. *J. Org. Chem.* **1996**, *61*, 363. [e]. Uccello-Barretta, G.; Cuzzola, A.; Balzano, F.; Menicagli, R.; Iuliano, A.; Salvadori, P. *J. Org. Chem.* **1997**, *62*, 827.
53. Uccello-Barretta, G.; Ferri, L.; Balzano, F.; Salvadori, P. *Eur. J. Org. Chem.* **2003**, 1741.
54. [a] Pirkle, W. H.; Welch, C. J. *J. Chromatogr. A* **1994**, *683*, 347. [b] Pirkle, W. H.; Selness, S. R. *J. Org. Chem.* **1995**, *60*, 3252. [c] Uccello-Barretta, G.; Balzano, F.; Sicoli, G.; Scarselli, A. *Eur. J. Org. Chem.*, in print.
55. Lipkowitz, K. B. *Chem. Rev.* **1998**, *98*, 1829.
56. Lipkowitz, K. B.; Coner, R.; Peterson, M. A.; Morreale, A.; Shackelford, J. *J. Org. Chem.* **1998**, *63*, 732.
57. Berthod, A.; Li, W.; Armstrong, D. W. *Anal. Chem.* **1992**, *64*, 873.
58. Cramer, F.; Dietsche, W. *Chem. Ber.* **1959**, *92*, 378.
59. Pirkle, W. H.; Pochapsky, T. C. *Chem. Rev.* **1989**, *89*, 347.
60. Ogston, A. G. *Nature* **1948**, *162*, 963.
61. Cramer, F. in *The Lock and Key Principle* ed. J.-P. Behr, Wiley, Chichester, 1-23, **1994**.
62. Schneider, H. J.; Blatter, T.; Cuber, U. In *Frontiers in Supramolecular Organic Chemistry and Photochemistry*, ed. H. J. Schneider and H. Dürr, VCH, Weinheim, 29-56, **1991**.
63. Kano, K.; Yoshiyasu, K.; Hashimoto, S. *J. Chem. Soc., Chem. Comm.* **1988**, 801.
64. Kano, K.; Minami, K.; Horiguchi, K.; Ishimura, T.; Kodera, M. *J. Chromatogr. A* **1995**, *694*, 307.
65. Kano, K.; Negi, S.; Takaoka, R.; Kamo, H.; Kitae, T.; Yamaguchi, M.; Okubo, H.; Hiramama, M. *Chem. Lett.* **1997**, 715.
66. Khaledi, M. G.; Quang, C. *J. High Resol. Chromatogr.* **1994**, *17*, 609.
67. Loos, K.; von Braunmühl, V.; Stadler, R. *Macromol Rap. Commun.* **1997**, *18*, 927.
67. Schurig, V.; Nowotny, H.-P.; Schleimer, M.; Schmalzing, D. *J. High Resol. Chromatogr.* **1989**, *12*, 549.
68. Schurig, V.; Zhu, J.; Muschalek, V. *Chromatographia* **1993**, *35*, 237.
69. Kano, K.; Tanaka, N.; Negi, S. *Eur. J. Org. Chem.* **2001**, 3689.
70. Gil-Av, E.; Feibush, B.; Charles-Sigler, R. *Tetrahedron Lett.* **1966**, *7*, 1009.
71. [a] Görög, S. *Fresenius' J. Anal. Chem.* **1998**, *1*, 4. [b] Srinivas, N. R.; Shyu, W. C.; Barbhaiya, R. H. *Biomed. Chromatogr.* **1995**, *9*, 1.

72. [a] Frank, H.; Nicholson, G. J.; Bayer, E. *J. Chromatogr. Sci.* **1977**, *15*, 174. [b] Frank, H.; Nicholson, G. J.; Bayer, E. *Angew. Chem. Int. Ed.* **1978**, *17*, 363.
73. [a] Schurig, V. *Angew. Chem. Int. Ed.* **1977**, *16*, 110. [b] Schurig, V.; Gil-Av, E. *J. Chem. Soc. D, Chem. Commun.* **1971**, 650. [c] Schurig, V.; Schmalzing, D.; Schleimer, M. *Angew. Chem. Int. Ed.* **1991**, *30*, 987.
74. [a] Kościelski, T.; Sybilska, D.; Jurczak, J. *J. Chromatogr.* **1983**, *261*, 357. [b] Kościelski, T.; Sybilska, D.; Jurczak, J. *J. Chromatogr.* **1983**, *280*, 131. [c] Juvancz, Z.; Alexander, G.; Szejtli, J. *J. High Resol. Chromatogr., Chromatogr. Commun.* **1987**, *10*, 105. [d] Juvancz, Z.; Alexander, G.; Szejtli, J. *J. High Resolut. Chromatogr., Chromatogr. Commun.* **1988**, *11*, 110. [e] Schurig, V.; Nowotny, H.-P. *J. Chromatogr.* **1988**, *441*, 155. [f] Schurig, V.; Jung, M.; Schmalzing, D.; Schleimer, M.; Duvokot, J.; Buyten, J. C.; Peene, J. A.; Mussche, P. *J. High Resolut. Chromatogr.* **1990**, *13*, 470.
75. [a] Juvancz, Z.; Markides, K. E.; Petersson, P.; Johnson, D. F.; Bradshaw, J. S.; Lee, M. L. *J. Chromatogr. A* **2002**, *982*, 119. [b] Abe, I.; Minami, H.; Nakao, Y.; Nakahara, T. *J. Sep. Sci.* **2002**, *25*, 661. [c] Abe, I.; Nagamatsu, D.; Nakahara, T.; Fabiany, G. *Chem. Lett.* **2004**, *33*, 260.
76. [a] Pfeiffer, J.; Schurig, V. *J. Chromatogr. A* **1999**, *840*, 145. [b] Ruderisch, A.; Pfeiffer, J.; Schurig, V. *Tetrahedron: Asymm.* **2001**, *12*, 2025.
77. [a] Kehraus, S.; König, G. M.; Wright, A. D. *J. Org. Chem.* **2002**, *67*, 4989. [b] König, W. A.; Krebber, R.; Mischnick, P. *J. High Resol. Chromatogr.* **1989**, *12*, 732. [c] Španik, I.; Oswald, P.; Krupčík, J.; Benička, E.; Sandra, P.; Armstrong, D. W. *J. Sep. Sci.* **2002**, *25*, 45. [d] Bayer, T.; Riemer, T.; Kessler, H. *J. Pept. Sci.* **2001**, *7*, 250.
78. König, W. A. *The Practice of Enantiomer Separation by Capillary Gas Chromatography*; Hüthig Verlag: Heidelberg, **1987**.
79. Jones, G. R.; Oldham, N. J. *J. Chromatogr. A* **1999**, *843*, 199.
80. Ahmed, F. E. *TrAC, Trends Anal. Chem.* **2003**, *22*, 170.
81. [a] Bicchi, C.; D'Amato, A.; Rubiolo, P. *J. Chromatogr. A* **1999**, *843*, 99. [b] Betts, T. J. *J. Chromatogr. A* **2001**, *936*, 33.
82. Juvancz, Z.; Petersson, P. *J. Microcol. Sep.* **1996**, *8*, 99.
83. Chena, G.; Shi, X. *Anal. Chim. Acta* **2003**, *498*, 39.
84. Cousin, H.; Trapp, O.; Peulon-Agasse, V.; Pannecoucke, X.; Banspach, L.; Trapp, G.; Jiang, Z.; Combret, J. C.; Schurig, V. *Eur. J. Org. Chem.* **2003**, 3273.
85. Cousin, H.; Cardinael, P.; Oulyadi, H.; Pannecoucke, X.; Combret, J. C. *Tetrahedron: Asymm.* **2001**, *12*, 81.

## References

86. Jaus, A.; Oehme, M. *J. Chromatogr. A* **2001**, *905*, 59.
87. [a] Takahisa, E.; Engel, K.-H. *J. Chromatogr. A* **2005**, *1063*, 181. [b] Junge, M.; König, W. A. *J. Sep. Sci.* **2003**, *26*, 1607.
88. Takahisa, E.; Engel, K.-H. *J. Chromatogr. A* **2005**, *1076*, 148.
89. Bada, J. L.; Glavin, D. P.; McDonald, G. D.; Becker, L. *Science* **1998**, *279*, 362.
90. Pizzarello, S.; Weber, A. L. *Science* **2004**, *303*, 1151.
91. Cronin, J. R.; Cooper, G. W.; Pizzarello, S. *Adv. Space Res.* **1995**, *15*, 91.
92. Crisma, M.; Moretto, A.; Formaggio, F.; Kaptein, B.; Broxterman, Q. B.; Toniolo, C. *Angew. Chem.* **2004**, *116*, 6863.
93. Cline, D. B. *Chirality* **2005**, *17*, S234.
94. Pizzarello, S.; Cronin, J. R. *Nature* **1998**, *394*, 236.
95. Glavin, D. P.; Bada, J. L.; Brinton, K. L. F.; McDonald, G. D. *Proc. Natl. Acad. Sci.* **1999**, *96*, 8835.
96. [a] Hazen, R. M.; Filley, T. R.; Goodfriend, G. A. *Proc. Natl. Acad. Sci.* **2001**, *98*, 5487. [b] Ehrenfreund, P.; Glavin, D. P.; Botta, O.; Cooper, G.; Bada, J. L. *Proc. Natl. Acad. Sci.* **2001**, *98*, 2138.
97. [a] Pizzarello, S.; Huang, Y.; Becker, L.; Poreda, R. J.; Nieman, R. A.; Cooper, G.; Williams, M. *Science* **2001**, *293*, 2236. [b] Munoz Caro, G. M.; Meierhenrich, U. J.; Schutte, W. A.; Barbier, B.; Segovia, A. A.; Rosenbauer, H.; Thiemann, H.-P.; Brack, A.; Greenberg, J. M. *Nature* **2002**, *416*, 403.
98. [a] Kobayashi, K.; Takano, Y.; Masuda, H.; Tonishi, H.; Kaneko, T.; Hashimoto, H.; Saito, T. *Adv. Space Res.* **2004**, *33*, 1277. [b] Szopa, C.; Meierhenrich, U. J.; Coscia, D.; Janin, L.; Goesmann, F.; Sternberg, R.; Brun, J.-F.; Israel, G.; Cabane, M.; Roll, R.; Raulin, F.; Thiemann, W.; Vidal-Madjar, C.; Rosenbauer, H. *J. Chromatogr. A* **2002**, *982*, 303. [c] Meierhenrich, U. J.; Munoz Caro, G. M.; Bredehöft, J. H.; Jessberger, E. K.; Thiemann, W. H.-P. *Proc. Natl. Acad. Sci.* **2004**, *101*, 9182. [d] Pietrogrande, M. C.; Zampolli, M. G.; Dondi, F.; Szopa, C.; Sternberg, R.; Buch, A.; Raulin, F. *J. Chromatogr. A* **2005**, *1071*, 255.
99. [a] Vandenabeele-Trambouze, O.; Rodier, C.; Dobrijevic, M.; Despois, D.; Sternberg, R.; Vidal-Madjar, C.; Grenier-Loustalot, M. F.; Raulin, F. *Chromatographia* **2001**, *53*, S-332. [b] Španik, I.; Krupčík, J.; Skačáni, I.; Sandra, P.; Armstrong, D. W. *J. Chromatogr. A* **2005**, *1071*, 59.
100. Schurig, V.; Juza, M.; Preschel, M.; Nicholson, G. J.; Bayer, E. *Enantiomer* **1999**, *4*, 297.
101. Abe, I.; Fujimoto, N.; Nakahara, T. *J. Chromatogr. A* **1994**, *676*, 469.

102. Meierhenrich, U. J.; Thiemann, W. H.-P.; Goesmann, F.; Roll, R.; Rosenbauer, H. *Chirality* **2001**, *13*, 454.
103. König, W. A.; Icheln, D.; Runge, T.; Pforr, I.; Krebs, A. *J. High. Resol. Chromatogr.* **1990**, *13*, 702.
104. Meierhenrich, U. J.; Nguyen, M.-J.; Barbier, B.; Brack, A.; Thiemann, W. H.-P. *Chirality* **2003**, *15*, S13.
105. Meierhenrich, U.; Thiemann, W. H.-P.; Rosenbauer, H. *Chirality* **1999**, *11*, 575.
106. Quack, M. *Angew. Chem. Int. Ed.* **2002**, *41*, 4618.
107. Crassous, J.; Chardonnet, C.; Saue, T.; Schwerdtfeger, P. *Org. Biomol. Chem.* **2005**, *3*, 2218.
108. Crassous, J.; Monier, F.; Dutasta, J.-P.; Ziskind, M.; Daussy, C.; Grain, C.; Chardonnet, C. *ChemPhysChem* **2003**, *4*, 541.
109. [a] Crassous, J.; Jiang, Z.; Schurig, V.; Polavarapu, P. L. *Tetrahedron: Asymm.* **2004**, *15*, 1995. [b] Jiang, Z.; Crassous, J.; Schurig, V. *Chirality* **2005**, *17*, 488.
110. Grosenick, H.; Schurig, V.; Costante, J.; Collet, A. *Tetrahedron: Asymm.* **1995**, *6*, 87.
111. Reichle, F. M.; Conzen, P. F. *Best Practice & Research Clinical Anaesthesiology* **2003**, *17*, 29.
112. Halpern, D. *J. Fluorine Chem.* **2002**, *118*, 47.
113. Franks, N. P.; Lieb, W. R. *Nature* **1982**, *300*, 487.
114. [a] Young, J. W. *US Pat.* **1992**, 5 114714. [b] Young, J. W. *US Pat.* **1992**, 5 114715.
115. [a] Juza, M.; Braun, E.; Schurig, V. *J. Chromatogr. A* **1997**, *769*, 119. [b] Schurig, V.; Grosenick, H. *J. Chromatogr. A* **1994**, *666*, 617.
116. [a] Wallin, R. F.; Regan, B. M.; Napoli, M. D.; Stern, I. J. *Anesth. Analg.* **1975**, *54*, 758. [b] Doi, M.; Ikeda, K. *Can. J. Anaesth.* **1993**, *40*, 122. [c] Funk, W.; Moldaschl, J.; Fujita, Y.; Taeger, K.; Hobbhahn, J. *Anaesthesist* **1996**, *45*, 22.
117. Cunningham, D. D.; Webster, J.; Nelson, D.; Williamson, B. *J. Chromatogr. B* **1995**, *668*, 41.
118. Schmidt, R.; Roeder, M.; Oeckler, O.; Simon, A.; Schurig, V. *Chirality* **2000**, *12*, 751.
119. Schurig, V.; Schmidt, R. *J. Chromatogr. A* **2003**, *1000*, 311.

## Chapter II

120. Ueno, A.; Breslow, R. *Tetrahedron Lett.* **1982**, *23*, 3451.

## References

121. [a] Fügedi, P.; Nanasi, P. *Carbohydr. Res.* **1988**, *175*, 173. [b] Takeo K.; Mitoh H.; Uemura K. *Carbohydrate Res.* **1989**, *187*, 203. [c] Miranda, E.; Sánchez, E.; Sanz, J.; Jimenez, M. I.; Martínez-Castro, I. *J. High Resol. Chromatogr.* **1998**, *21*, 225.
122. Fujita, K.; Ishizu, T.; Oshiro, K.; Obe, K. *Bull. Chem. Soc. Jpn.* **1989**, *62*, 2960.
123. Wenz, G. *Carbohydr. Res.* **1991**, *214*, 257.
124. [a] Jicsinszky, L. (Cyclolab R&D Laboratory, Hungary) Cyclodextrin Symposium **1992**, Chicago. [b] Jicsinszky, L. (Cyclolab R&B Laboratory, Hungary) Eurocarb **1995**, Sevilla.
125. Farkas, E.; Jánossy, L.; Harangi, J.; Kandra, L.; Lipták, A. *Carbohydr. Res.* **1997**, *303*, 407.
126. [a] Anibarro, M.; Gessler, K.; Usón, I.; Sheldrick, G. M.; Harata, K.; Uekama, K.; Hirayama, F.; Abe, Y.; Saenger, W. *J. Am. Chem. Soc.* **2001**, *123*, 11854. [b] Uccello Barretta, G.; Sicoli, G.; Balzano, F.; Salvadori, P. *Carbohydr. Res.* **2003**, *338*, 1103. [c] Laignel, B.; Bliard, C.; Massiot, G.; Nuzillard, J. M. *Carbohydr. Res.* **1997**, *298*, 251.
127. Ashton, P. R.; Königer, R.; Stoddart, J. F. *J. Org. Chem.* **1991**, *61*, 903.
128. [a] Ciucanu, I.; Kerek, F. *Carbohydr. Res.* **1984**, *131*, 209. [b] Irie, T.; Fukunaga, K.; Pitha, J.; Uekama, K.; Fales, H. M.; Sokolowski, E. A. *Carbohydr. Res.* **1989**, *192*, 167.
129. Breitinger, H.-G. *Tetrahedron Lett.* **2002**, *43*, 6127.
130. [a] Zhang, X.; Breslav, M.; Grimm, J.; Guan, K.; Huang, A.; Liu, F.; Maryanoff, C. A.; Palmer, D. Patel, M.; Qian, Y.; Shaw, C.; Sorgi, K.; Stefanick, S.; Xu, D. *J. Org. Chem.* **2002**, *67*, 9471. [b] Katritzky, A. R.; He, H.-Y.; Suzuki, K. *J. Org. Chem.* **2000**, *65*, 8210.
131. Katritzky, A. R.; Wang, M.; Zhang, S. *ARKIVOC* **2001**, *ix*, 19.
132. [a] Mele, A.; Raffaini, G.; Ganazzoli, F.; Juza, M.; Schurig, V. *Carbohydr. Res.* **2003**, *338*, 625. [b] Juza, M.; Di Giovanni, O.; Biressi, G.; Schurig, V.; Mazzotti, M.; Morbidelli, M. *J. Chromatogr. A* **1998**, *813*, 333. [c] Wenz, G.; Mischnick, P.; Krebber, R.; Richters, M.; König, W. A. *J. High Resol. Chromatogr.* **1990**, *13*, 724.
133. Schrodinger, Inc.: 1500 S. W. First Avenue, Suite 1180 Portland OR 97201/One Exchange Place, Suite 604, Jersey City, NJ 07302. [www.schrodinger.com](http://www.schrodinger.com)
134. Jorgensen, W. L.; Maxwell, D. S.; Tirado-Rives, J. *J. Am. Chem. Soc.* **1996**, *118*, 11225.
135. Halgren, T. A. *J. Comput. Chem.* **1996**, *17*, 490.

## Chapter III

136. Grosenick, H.; Juza, M.; Schurig, V.; Klein, J. *Enantiomer* **1996**, *1*, 337.
137. Fielding, L. *Tetrahedron* **2000**, *56*, 6151.

138. Connors, K. A. *Binding Constants: the Measurement of Molecular Complex Stability*, Wiley: New York, **1987**.
139. Wimmer, R.; Aachmann, F. L.; Larsen, K. L.; Peterson, S. B. *Carbohydr. Res.* **2002**, *337*, 841-849.
140. Cohen, Y.; Avram, L.; Frish, L. *Angew. Chem. Int. Ed.* **2005**, *44*, 520.
141. [a] Job, P. *Ann. Chim.* **1928**, *9*, 113. [b] Loukas, Y. L. *Analyst* **1997**, *122*, 377.
142. [a] Bom, A.; Bradley, M.; Cameron, K. S.; Clark, J. K.; van Egmond, J.; Feilden, H.; MacLean, E. J.; Muir, A. W.; Palin, R.; Rees, D. C., Zhang, M.-Q. *Angew. Chem. Int. Ed.* **2002**, *41*, 265. [b] Cameron, K. S.; Fletcher, D.; Fielding, L. *Magn. Res. Chem.* **2002**, *40*, 251.
143. Khajehpour, M.; Troxler, T.; Nanda, V.; Vanderkooi, J. M. *Proteins Struct. Funct. Bioinform.* **2004**, *55*, 275.
144. Tanner, J. E. *J. Chem. Phys.* **1970**, *52*, 2523.
145. Groneborg, A. M.; Clore, G. M. *Progr. NMR Spectrosc.* **1985**, *17*, 1.

#### Chapter IV

146. Schmarr, H. G.; Mosandl, A.; Kaunzinger, A. *J. Microcol. Sep.* **1991**, *3*, 395.
147. Cozzini, P.; Domiano, P.; Musini, P. C.; Zanardi, E. *J. Incl. Phenom. Macr. Chem.* **1996**, *26*, 295.
148. Bicchi, C.; Artuffo, G.; D'Amato, A.; Pellegrino, G.; Galli, A.; Galli, M. *J. High. Resol. Chromatogr.* **1991**, *14*, 701.

#### Conclusions

149. Sicoli, G.; Balzano, F.; Schurig, V.; Uccello-Barretta, G. *Chemistry, A European Journal.* **2005**, submitted, and references therein cited.
150. Wihstutz, K. *Ph. D. Dissertation* **2001**, Hamburg.
151. Larsen, K. L.; Endo, T.; Ueda, H.; Zimmermann, W. *Carbohydr. Res.* **1998**, *309*, 153.
152. Bayer, M.; Mosandl, A. *Flavour Fragr. J.* **2004**, *19*, 515.
153. [a] Sicoli, G.; Jiang, Z.; Jicsinsky, L.; Schurig, V. *Angew. Chem. Int. Ed.* **2005**, *44*, 4092. [b] Sicoli, G.; Jiang, Z.; Jicsinsky, L.; Schurig, V. *Angew. Chem.* **2005**, *117*, 4161.
154. Lipták, A.; Jodál, I.; Nánási, P. *Carbohydr. Res.* **1975**, *44*, 1.

#### Experimental section

155. Perrin, D.; Armarego, W. L.; Perrin, D. R. *Purification of Laboratory Chemicals*, Pergamon Press, Toronto, **1983**.

## Appendix

156. Sakairi, N.; Wang, L.-X.; Kuzuhara, H. *J. Chem. Soc., Chem. Commun.* **1991**, 289.
157. Sakairi, N.; Matsui, K.; Kuzuhara, H. *Carbohydr. Res.* **1995**, 266, 263.
158. Lesur, D.; Gassama, A.; Moreau, V.; Pilard, S.; Djedaini-Pilard, F. *Carbohydr. Res.* **2005**, 340, 1225.
159. [a] Johnson, M. A.; Pinto, B. M. *Carbohydr. Res.* **2004**, 339, 907. [b] Brand, T.; Cabrita, E. J.; Berger, S. *Prog. Nucl. Magn. Reson. Spectrosc.* **2005**, 46, 159.
160. Solomon, I. *Phys. Rev.* **1955**, 99, 559.
161. Neuhaus, D.; Williamson, M. P. *The Nuclear Overhauser Effect in Structural and Conformational Analysis*, 2nd ed.; Wiley-VHC: Weinheim, **2000**.
162. [a] Niccolai, N.; Valensin, G. *Advanced Magnetic Resonance Techniques in Systems of High Molecular Complexity*, Birkhauser: Boston, **1986**. [b] Girjesh, G.; Ramakrishna, V. H. *Conformation of Biological Molecules*, Springer-Verlag: New York, **1982**.
163. [a] Bothner-By, A. A.; Stephens, R. L.; Lee, J.; Warren, C. D.; Jeanloz, R. W. *J. Am. Chem. Soc.* **1984**, 106, 811. [b] Bax, A.; Davis, D. G. *J. Magn. Reson.* **1985**, 63, 207.
164. [a] Lauterbur, P. C. *Nature* **1973**, 242, 190. [b] Stark, D. D.; Bardley, W. G. *Magnetic Resonance Imaging*, 2nd ed., Mosby Company: St. Louis, **1992**. [c] Stark, D. D.; Bardley, W. G. *Methods of Magnetic Resonance Imaging and Spectroscopy*, Wiley: Chichester, **2000**. [d] Moseley, M. E.; Cohen, Y.; Mointorovitch, J.; Chileuitt, L.; Shimizu, H.; Kucharczyk, J.; Wendland, M. F.; Weinstein, P.R. *Magn. Res. Med.* **1990**, 16, 330. [e] Basser, P. J.; Mattiello, J.; Le Bihan, D. *Biophys. J.* **1994**, 66, 259.
165. [a] Kärger, J.; Ruthven, D. M. *Diffusion in Zeolites and Other Microporous Solids*, Wiley: New York, **1992**. [b] Nose, T. *Ann. Rep. NMR Spectrosc.* **1993**, 27, 218. [c] Price, W. S. *Concepts Magn. Res.* **1997**, 9, 299. [d] Callaghan, P. T.; Codd, S. L.; Seymour, J. D. *Concepts Magn. Res.* **1999**, 11, 181. [e] Price, W. S. *Concepts Magn. Res.* **1998**, 10, 197. [f] Kärger, J.; Pfeifer, H. *NMR and Catalysis*, Dekker: New York, **1994**. [g] Callaghan, P. T.; Coy, A. *NMR Probes and Molecular Dynamics*, Kluwer: Dordrecht, **1993**.
166. Söderman, O.; Stilbs, P. *Prog. Nucl. Magn. Reson. Spectrosc.* **1994**, 26, 445.
167. Lindblom, G.; Oradd, G. *Prog. Nucl. Magn. Reson. Spectrosc.* **1994**, 26, 483.
168. Waldeck, A. R.; Kuchel, P. W.; Lennon, A. J.; Chapman, B. E. *Prog. Nucl. Magn. Reson. Spectrosc.* **1997**, 30, 39.
169. Stejskal, O. E.; Tanner, J. E. *J. Chem. Phys.* **1965**, 42, 288.
170. Gounarides, J. S.; Chen, A.; Shapiro, M. J. *J. Chromatogr. B* **1999**, 725, 79.



171. [a] Gil-Av, E.; Herling, J. *J. Phys. Chem.* **1962**, *66*, 304. [b] Muhs, M. A.; Weiss, F. T. *J. Am. Chem. Soc.* **1962**, *84*, 4697. [c] Cvetanovič, R. J.; Duncan, F. J.; Falconer, W. F.; Irwin, R. S. *J. Am. Chem. Soc.* **1965**, *87*, 1827.
172. [a] Gil-Av, E.; Schurig, V. *Anal. Chem.* **1971**, *43*, 2030. [b] Schurig, V.; Chang, R. C.; Zlatkis, A.; Gil-Av, E.; Mikeš, F. *Chromatographia* **1973**, *6*, 115. [c] Schurig, V.; Chang, R. C.; Zlatkis, A.; Feibush, B. *J. Chromatogr.* **1974**, *99*, 147.



Meine akademischen Lehrer waren:

K. Albert, H. Bertagnolli, H.-J. Egelhaaf, G. Jung, E. Lindner, H. A. Mayer, K. Müller, U. Nagel, C. Ochsenfeld, D. Oelkrug, E. Plies, W. Rosenstiel, V. Schurig, B. Speiser, L. Weseman, K.-H. Wiesmüller.